Dissertation

Study on the Influence of Liquid Sloshing on FLNG Motion using Mechanical Model
(メカニカルモデルによる FLNG 運動に及ぼす液体スロッシングの影響に関する研究)

Department of Systems Integration
Specialization in Ocean and Space Engineering
Graduate School of Engineering
Yokohama National University

Akira Nakashima
(中島　晃)

A dissertation submitted for the degree of
Doctor of Engineering
2018.3

Abstract

This thesis presents the rational explanation on the influence of liquid sloshing on FLNG motion by means of a spring-mass type mechanical model representing the behaviour of liquid cargo and coupling effects on floating body motion.

The mechanical model to simulate sloshing was originally developed in the mid-1960s to represent the coupling effects on spacecraft motion for predicting and controlling its behaviour and stability. Author believes that the mechanical model is a useful tool for better understanding the interaction of liquid cargo and floating body motion and also an effective tool in collaborative works involving experts with various technical backgrounds.

Starting with the concept, the parameters of the mechanical model for a rectangular tank are determined analytically. Validity and limitation of the mechanical model are justified by comparing the results from experiment and calculation by other means.

The numerical analysis of coupled floating motion of barge with two (2) rectangular tanks and FLNG with six (6) rectangular tanks are performed and the results are compared with the ones obtained from the experiment and the calculation by others.

Next, rational explanation on the influence of liquid sloshing on barge and FLNG motion is presented, and transparency and accountability of the mechanical model are demonstrated.

Finally, the case studies for FLNG are performed and the effectiveness of the mechanical model in the basic design of FLNG is demonstrated.

Acknowledgements

This thesis would not have been possible without the help and guidance of my advisor, Professor Makoto Arai. His insights and comments have always helped me complete this thesis. I also deeply appreciate his continuous encouragement from the start.

I would like to thank Professor Kazuo Nishimoto, Dr. Liang Yee Cheng and Mr. Daniel Prata Vieira of University of São Paulo, and Dr. Xin Wang of Newcastle University for their continuous support as a research partner.

I would like to thank Mr. Tsuyoshi Kawahashi, Mr. Gustavo Massaki Karuka, Ms. Reina Hata, Mr. Takumi Harada and Mr. Ryohei Yoshioka who are my colleagues in the laboratory of Yokohama National University, for their kind support, fruitful discussion and advice.

I am grateful to Mr. Rajendran Ponnusamy of JGC UK for proofreading English and advice.

I would also like to thank JGC Corporation and colleagues in JGC for giving me such an opportunity.

Finally, I would like to express my special love and gratitude to my wife, Miwako and son, Shotaro. They have been a constant source of my energy.

Contents

Contents (Continued)

Contents (Continued)

List of Figures

List of Figures (Continued)

List of Figures (Continued)

List of Figures (Continued)

List of Tables

Nomenclature

a	Dimension along x axis of rectangular tank (m)
b	Dimension along y axis of rectangular tank (m)
g	Gravity constant (9.80665 m s^{-2})
h	Liquid height (m)
k	Wave number (rad m^{-1})
m_0	Fixed mass (kg)
m_n	Slosh mass (kg)
m_T	Total liquid mass (kg)
p	Fluid pressure (N m^{-2})
s	Relative location from tank bottom to the COG of floating body (m)
w_a	Incident wave amplitude (m)
x_n	Deflection of the slosh mass (m)
(x_G, y_G, z_G)	Centre of gravity of floating body including liquid cargo (m)
(x_{BG}, y_{BG}, z_{BG})	Centre of gravity of floating body excluding liquid cargo (m)
(x_{TG}, y_{TG}, z_{TG})	Centre of gravity of liquid cargo (m)
(x_b, y_b, z_b)	Centre of buoyancy of floating body (m)
(x_f, y_f, z_f)	Centre of floatation of floating body (m)

Nomenclature (Continued)

A_{wp}	Water plane area of floating body (m^2)
B	Breadth of floating body (m)
H	Tank height (m)
H_0	Fixed mass height (m)
H_n	Slosh mass height (m)
K_n	n-th spring constant ($N\ m^{-1}$)
I_0	Fixed mass inertia ($kg\ m^2$)
I_R	Mass inertia of rigid cargo ($kg\ m^2$)
I_d	Mass inertia of free rotating liquid ($kg\ m^2$)
M	Mass of floating body including liquid cargo (kg)
M_B	Mass of floating body excluding liquid cargo (kg)
V_w	Displaced volume of floating body (m^3)
X_0	Linear displacement along x axis (m)
α_0	Angular rotation about an axis through the COG of liquid cargo (rad)
γ_n	n-th fraction of critical damping (-)
ρ	Density of surrounding water ($kg\ m^{-3}$)
ρ_c	Density of cargo liquid ($kg\ m^{-3}$)
Φ	Velocity potential ($m^2\ s^{-1}$)
ω	Angular frequency ($rad\ s^{-1}$)
ω_n	n-th natural angular frequency ($rad\ s^{-1}$)

1. Introduction

1.1 Background

Over the past decade, the demand for liquefied natural gas (LNG) has increased sharply. LNG is the natural gas that is liquefied by cooling it to approximately −162 ˚C in order to reduce its volume by 1/600th. It is colourless, odourless, non-toxic, non-carcinogenic and in liquid form is about 46% of the density of water. It can be stored and transported in insulated tanks at standard atmospheric pressure. Its demand is expected to increase further in the near future, as LNG is considered "cleaner" than other fossil fuels (e.g. oil and coal) and supply of which is "more stable" than renewable energies (e.g. wind, solar, etc.).

The growing interest of governments and major oil and gas companies in LNG development has resulted in technical innovations in LNG supply chain, such as an increase in capacity of LNG tank systems, development of floating LNG production, storage and offloading units (FLNG), floating storage and regasification units (FSRU), etc. The advancement of FLNG system has created high expectations in development of offshore stranded gas fields and monetizing the gas from the existing offshore oil fields.

One of the major issues to be overcome in realization of FLNG is the motion prediction of floating bodies. This is essential to estimate the reliability and availability of FLNG. Research and development of motion prediction of floating body have been performed by a number of researchers and research groups over a long period of time. Thanks to the increased computing power, the study of motion prediction has achieved a sufficient level of sophistication for practical application—even though there are still technical issues in improving the accuracy, such as the need for methods to incorporate the viscous effect, gap resonance, wind and current load estimation, liquid cargo effects including sloshing, etc.

This thesis focuses on the effect of liquid cargo on the FLNG motion caused by the liquid movement including sloshing, free surface and free rotation. The tanks inside the FLNG contain a large amount of liquid product such as LNG, LPG, condensate, etc. Since the tanks in FLNG are used as a temporary storage of such liquid products, the liquid level in the tank will always change and never be filled completely. In such a condition with partially filled tank, the liquid in tanks is excited by the FLNG motion, and the movement of the liquid may be intense at a certain frequency. This intense liquid movement is called sloshing, and the damage to the tank due to sloshing and its influence on the FLNG motion are major concerns regarding safety, operability, productivity and cost. [1), 2), 3), 4), 5)]

1.2 Literature Review

The researches focusing on the coupling of liquid movement in tanks and floating body motion are ongoing since long ago. As early as 1880, there was an idea to install "water chambers" in a ship to

reduce the roll motion [6), 7)]. In the mid-1960s, Bosch and Vugts [8), 9)] rediscovered this almost forgotten idea, and performed systematic measurements to gather necessary information to understand why the tank performed as an anti-rolling device and to apply them to design tanks for practical applications.

Also in the mid-1960s, the research works in "sloshing" were compiled and published in the United States for the spacecraft application [10), 11)]. The monograph published in 1966 as NASA SP-106, "The Dynamic Behavior of Liquids in Moving Containers" has been widely used by the community researching on sloshing effects. As the main purpose was to control spacecraft behavior and stability, emphasis was placed on frequencies and total forces at small excitation amplitudes. The NASA SP-106 is unfortunately out of print now; however, a revised edition issued by Dodge [10)] is available now.

Since the 1970s, the advent of large vessels such as oil tankers, LPG carriers, LNG carriers, etc. carrying large quantities of liquid, damage to integrity of tank and hull structures due to violent sloshing of liquid cargo has begun to attract attention. Thanks to the increased computing power and development of CFD, it has now become possible to simulate a complicated fluid behaviour and local pressure to some extent with high accuracy. Meanwhile, the interaction between liquid movement in tanks and floating body motion continued to be an important concern, and the interest shifted from the development of anti-rolling device to the improvement of accuracy in motion prediction of floating body.

The barge motion in beam waves influenced by the rectangular tanks partially filled with water was investigated by Yamashita [12)] and Molin et al [13)] by means of numerical calculation and test conducted on an experimental model. Malenica et al [14)] presented the calculation method for the dynamic coupling between sloshing and seakeeping and validated it against the results from Molin et al [13)]. Their calculation method was based on the linear potential theory in the frequency domain. Many other researchers also studied the coupling of liquid movement in tanks and floating body motion using the linear potential theory [15), 16), 17), 18)].

The floating body motion affected by non-linear sloshing in tanks partially filled with water was investigated by Journée [19)], Rognebakke and Faltinsen [20)], Lee et al [21), 22), 23)], Wang and Arai [24), 25), 26), 27)], Kawahashi, Arai et al [28), 29)], Kim et al [30)] and Rocha et al [31)]. The behavior of liquid in tanks was represented by the fluid dynamic methods such as boundary element method, finite difference method, particle method, etc. and it was coupled with the floating body motion.

1.3 Objectives

The objective of this thesis is to provide a rational explanation on the complex phenomena of the FLNG motion affected by liquid sloshing.

As a result of past research efforts, it has now become possible to simulate accurately the complex phenomena of sloshing itself and its influence on floating body motion using numerical calculation. Despite the improvement in accuracy of the simulation the correctness of results from such a highly

elaborate numerical calculation is difficult to verify. The proven calculation methods available so far do not guarantee the correctness of the calculation results. There are many factors such as incorrect input parameters, incorrect analysis settings, etc. that provide erroneous results.
Comparison of results from experiments conducted on physical models is the most reliable verification method; however, this is time consuming and expensive. An alternate approach is to confirm whether the major characteristic indicator such as the natural period or the period corresponding to the peak response is close to the one predicted by other means. Although this approach only provides partial reliability, it can be done easily. Another benefit of this approach is that it is possible to identify the fundamental mechanism of the phenomenon of interest. Lee et al [22] used the "simplified mass-spring sloshing model" to explain the mechanism of the two peaks of roll motion in his Doctorate thesis.
The mass-spring type mathematical model, in other words "mechanical model", prescribes the mechanism of the phenomena of interest [10), 11)]. This method can only realize the phenomena of the prescribed mechanism, but its calculation process is simple, transparent and easy to trace the link between the input parameters and the output.
For the purpose of explaining the complex phenomena of floating body motion influenced by sloshing, this approach is the preferred choice over CFD based numerical calculation method.

1.4 Applications for Basic Design of FLNG

In author's opinion, the CFD based numerical calculation method, especially capable of simulating the non-linear liquid behaviour is suitable to simulate the phenomenon as accurately as possible; however, this is not suitable for seeking an optimal solution.
It is not practical to use the CFD based numerical calculations that predicts the floating body motion taking into account of liquid cargo effects and determine important FLNG design parameters such as tank type and tank arrangement. Instead, simpler calculation methods are necessary at the initial design stage.
The calculation method based on the linear potential theory in the frequency domain could be used. However, calculation method based on the mechanical model is a better option.
The most noteworthy benefit of the mechanical model is that the link between input parameters and output is easy to trace. The author demonstrates this benefit in the thesis.
The transparent traceability and accountability are particularly important in FLNG application to demonstrate its credibility to the experts with various technical backgrounds such as project management, natural gas processing, electrical, instrument, structure, etc. who are involved in FLNG design.
Since mechanical model is capable of explaining the complex phenomena of floating body motion influenced by the sloshing effect and satisfying the above mentioned criteria in sharing the knowledge with other experts, it is a better choice than the numerical calculation based on CFD.

2. Mechanical Model of Liquid Cargo

2.1 General

The effect of lateral sloshing, which is dynamic in nature, is mainly due to a horizontal oscillation of centre of liquid mass relative to the tank. This can be well represented by an equivalent mechanical model.

The mechanical model of sloshing was originally developed in the mid-1960s to represent the coupling effects with spacecraft motion for predicting and controlling its behaviour and stability as shown in Figure 2.1. The pendulum model was adopted in spacecraft application since the gravity acceleration was treated explicitly as a variable parameter. The spring-mass model is another way to represent the mechanical model, which does not treat the gravity acceleration explicitly, for which deriving the equation of motion is more straightforward than the pendulum model.

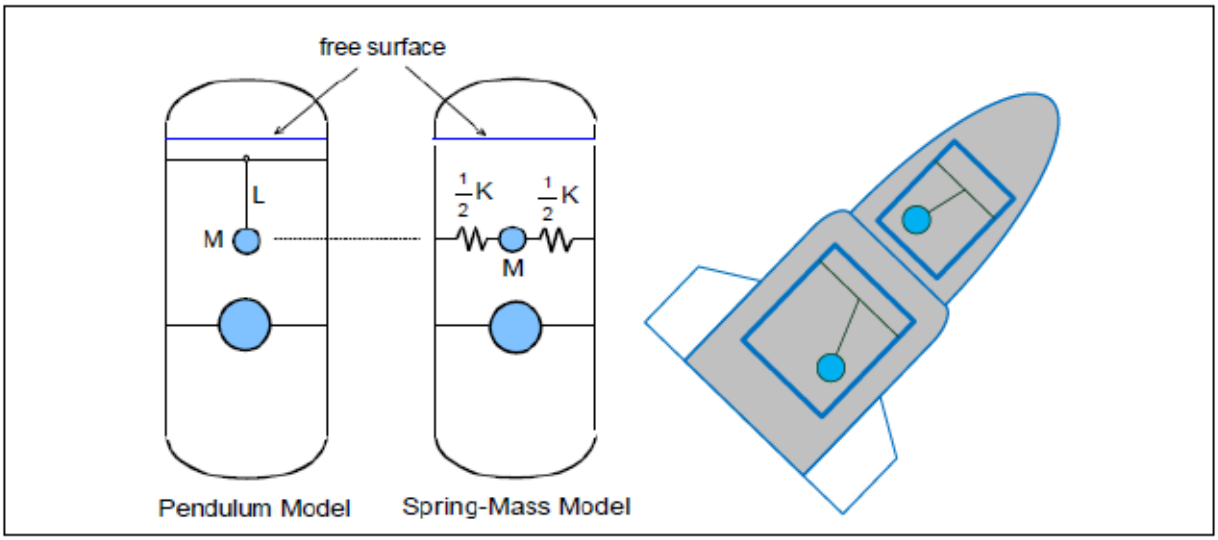

Figure 2.1. Mechanical Model Application for Spacecraft

The spring-mass type mechanical model is a better choice for marine and offshore industrial applications as it is not necessary to consider the change in gravity acceleration.

Author adopted the spring-mass type mechanical model for analysing the influence of liquid cargo on FLNG motion and predicting the FLNG motion considering the liquid cargo effect as shown in Figure 2.2.

The details of mathematical expression are provided in Appendices 1, 2 and 3.

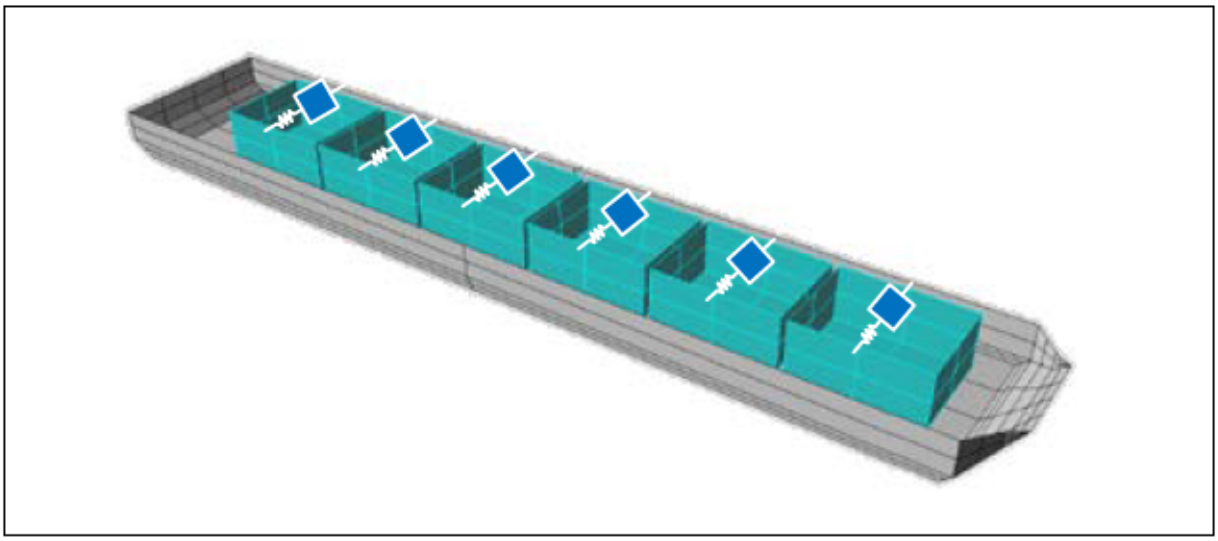

Figure 2.2. Mechanical Model Application for FLNG

2.2 Description of Mechanical Model

The dynamic behaviour of liquid in a tank is represented by the mechanical model as shown in Figure 2.3. The liquid inside the tank is replaced by masses, springs, dampers and a disk.

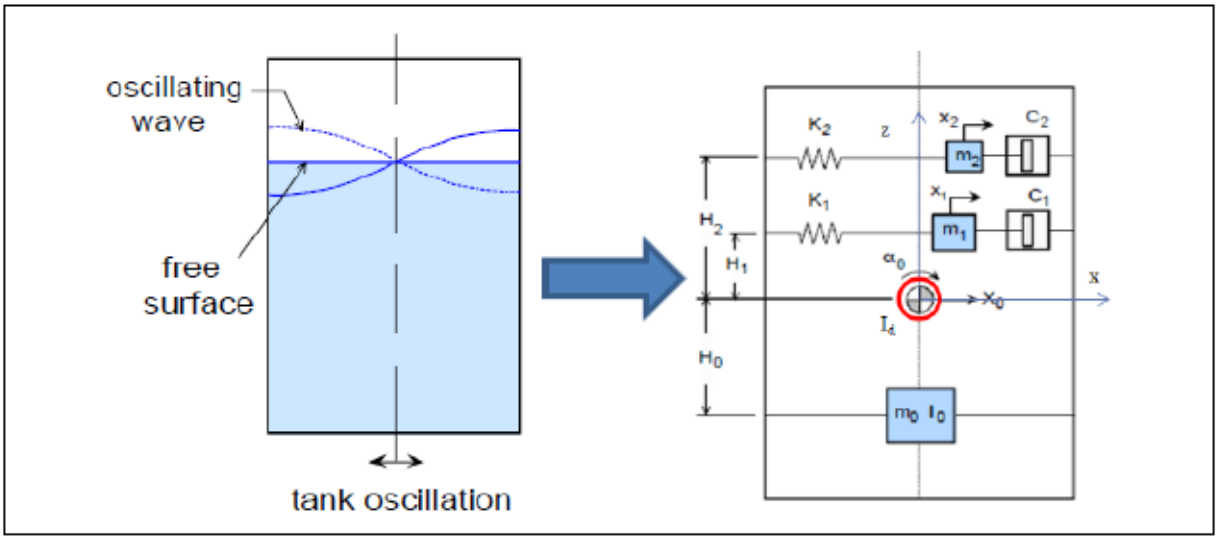

Figure 2.3. Spring-Mass Mechanical Model of Liquid in Tank

The fixed mass and mass inertia are represented by m_0 and I_0, respectively. Each of slosh modes corresponding to the sloshing natural frequencies is represented by the spring-mass and damper system. Only two systems are shown in Figure 2.3 for clarity, but there are theoretically infinite systems and slosh modes. The mass for each slosh mode is located at H_n which is the height from the centre of gravity of the liquid. Throughout this thesis, the positive direction of H_0 is taken opposite to the height of slosh masses. H_n, i. e., the height of m_n, is positive when the n-th mode

mass is located above the COG, but H_0 is positive when it is located below the COG. The damping is neglected. In addition, a disk I_d is introduced as the mass inertia of free rotating liquid which does not contribute to the mass inertia of the liquid.

When the tank is excited at angular frequency ω by a small time-varying linear displacement X_0 along the x axis and angular rotation α_0 about an axis through the COG, the amplitude of the horizontal force and moment exerted by X_0 and α_0 are obtained as follows:

$$\frac{F_{x\_amp}}{m_T\omega^2} = X_0\left\{1+\sum_{n=1}^{\infty}\frac{m_n}{m_T}\frac{\omega^2}{\omega_n^2-\omega^2}\right\} + h\alpha_0\left\{\sum_{n=1}^{\infty}\frac{m_n}{m_T}\frac{g}{h\omega_n^2}+\sum_{n=1}^{\infty}\frac{m_n}{m_T}\left(\frac{H_n}{h}+\frac{g}{h\omega_n^2}\right)\frac{\omega^2}{\omega_n^2-\omega^2}\right\}$$

$$\frac{M_{y\_amp}}{m_T h\omega^2} = X_0\left\{\sum_{n=1}^{\infty}\frac{m_n}{m_T}\frac{g}{h\omega_n^2}+\sum_{n=1}^{\infty}\frac{m_n}{m_T}\left(\frac{H_n}{h}+\frac{g}{h\omega_n^2}\right)\frac{\omega^2}{\omega_n^2-\omega^2}\right\}$$
$$+h\alpha_0\left\{\begin{array}{r}\dfrac{I_y}{m_T h^2}+\displaystyle\sum_{n=1}^{\infty}\frac{m_n}{m_T}\frac{g}{h\omega_n^2}\frac{g}{h\omega^2}+\sum_{n=1}^{\infty}\frac{m_n}{m_T}\frac{g}{h\omega_n^2}\left(\frac{2H_n}{h}+\frac{g}{h\omega_n^2}\right)\\ +\displaystyle\sum_{n=1}^{\infty}\frac{m_n}{m_T}\left(\frac{H_n}{h}+\frac{g}{h\omega_n^2}\right)^2\frac{\omega^2}{\omega_n^2-\omega^2}\end{array}\right\}$$

$$I_y = I_R - I_d$$

where m_T, ω_n, h, g and I_R are total liquid mass, n-th natural angular frequency, liquid height, gravity constant and mass inertia of rigid cargo, respectively.

2.3 Vertical and Yaw Oscillation

When the tank is exited horizontally, it is assumed that the COG of the liquid in tank does not move up and down. Therefore, linear vertical sloshing does not occur.

When the tank is exited vertically, the vertical sloshing will occur. The vertical sloshing is a non-linear parametric vibration due to parametric instability since waves are not excited directly by vibration normal to the free surface. The vertical sloshing is created more easily when the excitation frequency is close to twice the sloshing natural frequency of the fundamental mode.

In this thesis, the vertical motion of the liquid and sloshing are omitted since it is a non-linear, high frequency and insignificant phenomena.

The vertical motion and sloshing affect the heave and pitch motion of the floating body, however, the experimental measurements and numerical calculations by other researchers showed that the influence is negligible.

When the tank is exited rotationally about the vertical axis, no net force is generated, but it creates moment about vertical axis. In this thesis, the moment about vertical axis is also omitted, since its magnitude is small.

2.4 Determination of Parameters for Rectangular Tank Model

To determine the parameters of a mechanical model, horizontal force and moment could be obtained by analytical, numerical or experimental means. For simple tank geometry such as a rectangular tank as shown in Figure 2.4, an analytical solution is possible. Appendices 4 and 5 provide additional consideration for other tank geometry.

Two coordinate systems, global and local to the tank are defined. The global coordinate system OXYZ is right handed inertial coordinate system with the Z-axis pointing vertically upwards. The local coordinate system oxyz to the tank is right handed with the origin fixed at the liquid centre of gravity, and moves with the tank. The axes of coordinate system local to the tank are parallel to the global coordinate system.

The tank is rectangular with plan dimensions of a and b, and internal liquid height as h.

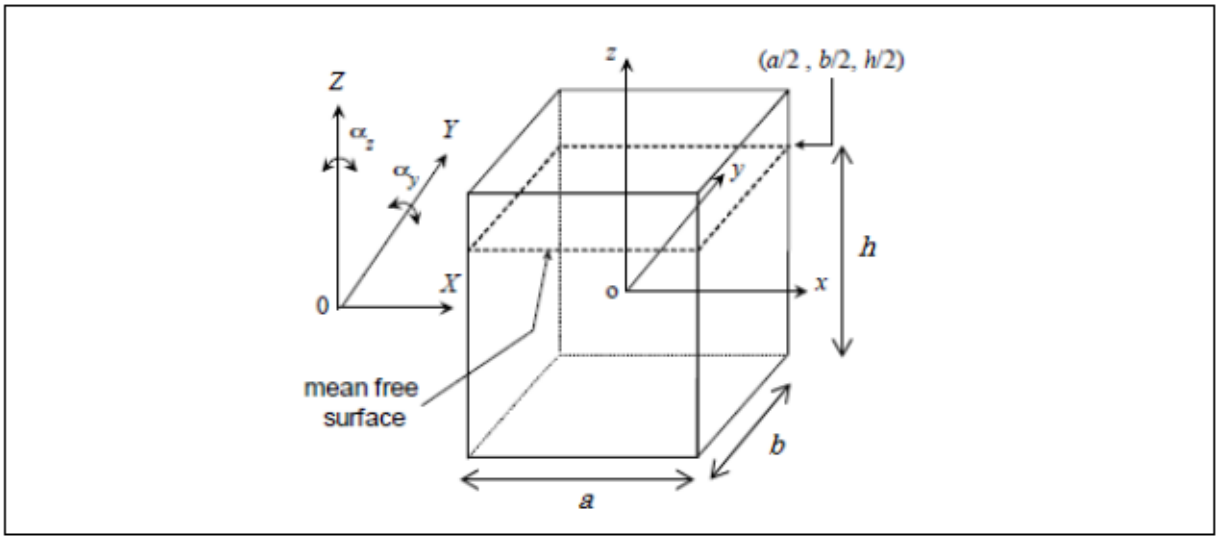

Figure 2.4. Rectangular Tank

Assuming the liquid in the tank is incompressible, inviscid and irrotational, liquid motion can be described by velocity potential, Φ which satisfies the following basic equations:

$$\nabla^2\Phi = \frac{\partial^2\Phi}{\partial x^2} + \frac{\partial^2\Phi}{\partial y^2} + \frac{\partial^2\Phi}{\partial z^2} = 0$$

$$\frac{\partial\Phi}{\partial t} + \frac{p}{\rho_c} + gz = 0$$

where p and ρ_c are fluid pressure and fluid density, respectively.

When the tank is excited at an angular frequency ω by a small time-varying linear displacement X_0 along x axis the boundary conditions are specified as follows:

$$\left[\frac{\partial^2\Phi}{\partial t^2}+g\frac{\partial\Phi}{\partial z}\right]_{z=\frac{h}{2}}=0 \qquad \text{at free surface}$$

$$\left[\frac{\partial\Phi}{\partial z}\right]_{z=-\frac{h}{2}}=0 \qquad \text{at tank bottom}$$

$$\left[\frac{\partial\Phi}{\partial x}\right]_{x=\pm\frac{a}{2}}=X_0\omega\exp(i\omega t), \quad \left[\frac{\partial\Phi}{\partial y}\right]_{y=\pm\frac{b}{2}}=0 \qquad \text{at tank walls}$$

First, by solving the eigenvalue problem, natural frequencies are determined as follows:

$$\omega_n^2=g\lambda_n\tanh(\lambda_n h), \quad \lambda_n=\frac{(2n-1)\pi}{a}$$

Then, solving the basic differential equation to satisfy the boundary conditions, the velocity potential of liquid in the rectangular tank excited horizontally is obtained as follows:

$$\Phi=X_0\omega\exp(i\omega t)\left\{x+\sum_{n=1}^{\infty}\frac{\omega^2}{\omega_n^2-\omega^2}\frac{4a(-1)^{n-1}}{\pi^2(2n-1)^2}\frac{\cosh\left[\lambda_n\left(z+h/2\right)\right]}{\cosh(\lambda_n h)}\sin(\lambda_n x)\right\}$$

The unsteady liquid pressure is:

$$p=-\rho\frac{\partial\Phi}{\partial t}$$

$$=-i\rho X_0\omega^2\exp(i\omega t)\left\{x+\sum_{n=1}^{\infty}\frac{\omega^2}{\omega_n^2-\omega^2}\frac{4a(-1)^{n-1}}{\pi^2(2n-1)^2}\frac{\cosh\left[\lambda_n\left(z+h/2\right)\right]}{\cosh(\lambda_n h)}\sin(\lambda_n x)\right\}$$

The free surface elevation is:

$$\eta=-\frac{1}{g}\frac{\partial\Phi}{\partial t}\bigg|_{z=\frac{h}{2}}=-i\frac{X_0\omega^2}{g}\exp(i\omega t)\left\{x+\sum_{n=1}^{\infty}\frac{\omega^2}{\omega_n^2-\omega^2}\frac{4a(-1)^{n-1}}{\pi^2(2n-1)^2}\sin(\lambda_n x)\right\}$$

The horizontal force and moment in the rectangular tank excited horizontally are obtained by integrating the liquid pressure over the tank wall area.

$$F_x = -im_T X_0 \omega^2 \exp(i\omega t) \times \left\{ 1 + \sum_{n=1}^{\infty} \frac{8\,(a/h)\tanh(\lambda_n h)}{\pi^3 (2n-1)^3} \frac{\omega^2}{\omega_n^2 - \omega^2} \right\}$$

$$M_y = -im_T h X_0 \omega^2 \exp(i\omega t) \times \left[\frac{1}{12}\left(\frac{a}{h}\right)^2 + \sum_{n=1}^{\infty} \left\{ \frac{8\,(a/h)\tanh(\lambda_n h)}{\pi^3 (2n-1)^3} \left[\frac{1}{2} - \frac{2\,(a/h)}{\pi(2n-1)} \tanh\left(\frac{\lambda_n h}{2}\right) + \frac{g}{h\omega_n^2} \right] \frac{\omega^2}{\omega_n^2 - \omega^2} \right\} \right]$$

When the tank is excited at an angular frequency ω by a small time-varying angular rotation α_0 about an axis through the COG, the boundary conditions are specified as follows:

$$\left[\frac{\partial^2 \Phi}{\partial t^2} + g \frac{\partial \Phi}{\partial z} \right]_{z=-\frac{h}{2}} = 0 \qquad \text{at free surface}$$

$$\left[\frac{\partial \Phi}{\partial z} \right]_{z=-\frac{h}{2}} = -\alpha_0 x \omega \exp(i\omega t) \qquad \text{at tank bottom}$$

$$\left[\frac{\partial \Phi}{\partial x} \right]_{x=\pm\frac{a}{2}} = \alpha_0 z \omega \exp(i\omega t), \quad \left[\frac{\partial \Phi}{\partial y} \right]_{y=\pm\frac{b}{2}} = 0 \qquad \text{at tank walls}$$

Solving the basic differential equation to satisfy the boundary conditions, the velocity potential of liquid in the rectangular tank excited rotationally about Y axis is obtained as follows:

$$\Phi = h^2 \alpha_0 \omega \exp(i\omega t) \times \left\{ \begin{array}{l} \displaystyle\sum_{n=1}^{\infty} \frac{4\,(-1)^n}{\pi^3 (2n-1)^3} \left(\frac{\sin(\lambda_n a z/h)\sinh(\lambda_n a x/h)}{\cosh(\lambda_n a^2/2h)} + \left(\frac{a}{h}\right)^2 \frac{\sin(\lambda_n x)\cosh[\lambda_n (z - h/2)]}{\sinh(\lambda_n h)} \right) \\ \displaystyle + \sum_{n=1}^{\infty} \frac{\omega^2}{\omega_n^2 - \omega^2} \frac{4\,(-1)^n}{\pi^2 (2n-1)^2} \frac{a}{h} \left(\frac{1}{2} - \frac{2\,(a/h)}{\pi(2n-1)} \tanh\left(\frac{\lambda_n h}{2}\right) + \frac{g}{h\omega_n^2} \right) \frac{\sin(\lambda_n x)\cosh[\lambda_n (z + h/2)]}{\cosh(\lambda_n h)} \end{array} \right\}$$

The horizontal force and moment in the rectangular tank excited rotationally are obtained by integrating the liquid pressure over the tank wall area.

$$F_x = -im_T h\alpha_0\omega^2 \exp(i\omega t)\times \left[\frac{1}{12}\left(\frac{a}{h}\right)^2 + \sum_{n=1}^{\infty}\left\{\frac{8\,(a/h)\tanh(\lambda_n h)}{\pi^3(2n-1)^3}\left[\frac{1}{2} - \frac{2\,(a/h)}{\pi(2n-1)}\tanh\left(\frac{\lambda_n h}{2}\right) + \frac{g}{h\omega_n^2}\right]\frac{\omega^2}{\omega_n^2-\omega^2}\right\}\right]$$

$$M_y = -im_T h^2\alpha_0\omega^2 \exp(i\omega t)\times \left[\begin{array}{l}\dfrac{I_y}{m_T h^2} + \dfrac{1}{12}\left(\dfrac{a}{h}\right)^2\dfrac{g}{h\omega^2} + \displaystyle\sum_{n=1}^{\infty}\frac{16\,(a/h)\tanh(\lambda_n h)}{\pi^3(2n-1)^3}\frac{g}{h\omega_n^2}\left(\frac{1}{2} - \frac{2\,(a/h)}{\pi(2n-1)}\tanh\left(\frac{\lambda_n h}{2}\right) + \frac{g}{2h\omega_n^2}\right) \\ \quad + \displaystyle\sum_{n=1}^{\infty}\frac{8\,(a/h)\tanh(\lambda_n h)}{\pi^3(2n-1)^3}\left[\frac{1}{2} - \frac{2\,(a/h)}{\pi(2n-1)}\tanh\left(\frac{\lambda_n h}{2}\right) + \frac{g}{h\omega_n^2}\right]^2\frac{\omega^2}{\omega_n^2-\omega^2}\end{array}\right]$$

The amplitude of the horizontal force and moment in the rectangular tank excited horizontally and rotationally is obtained as follows:

$$\frac{F_{x\_amp}}{m_T\omega^2} = X_0\left\{1 + \sum_{n=1}^{\infty}\frac{8\,(a/h)\tanh(\lambda_n h)}{\pi^3(2n-1)^3}\frac{\omega^2}{\omega_n^2-\omega^2}\right\} + h\alpha_0\left[\frac{1}{12}\left(\frac{a}{h}\right)^2 + \sum_{n=1}^{\infty}\left\{\frac{8\,(a/h)\tanh(\lambda_n h)}{\pi^3(2n-1)^3}\left[\frac{1}{2} - \frac{2\,(a/h)}{\pi(2n-1)}\tanh\left(\frac{\lambda_n h}{2}\right) + \frac{g}{h\omega_n^2}\right]\frac{\omega^2}{\omega_n^2-\omega^2}\right\}\right]$$

$$\frac{M_{y\_amp}}{m_T h\omega^2} = X_0\left[\frac{1}{12}\left(\frac{a}{h}\right)^2 + \sum_{n=1}^{\infty}\left\{\frac{8\,(a/h)\tanh(\lambda_n h)}{\pi^3(2n-1)^3}\left[\frac{1}{2} - \frac{2\,(a/h)}{\pi(2n-1)}\tanh\left(\frac{\lambda_n h}{2}\right) + \frac{g}{h\omega_n^2}\right]\frac{\omega^2}{\omega_n^2-\omega^2}\right\}\right] + h\alpha_0\left[\begin{array}{l}\dfrac{I_y}{m_T h^2} + \dfrac{1}{12}\left(\dfrac{a}{h}\right)^2\dfrac{g}{h\omega^2} \\ \quad + \displaystyle\sum_{n=1}^{\infty}\frac{16\,(a/h)\tanh(\lambda_n h)}{\pi^3(2n-1)^3}\frac{g}{h\omega_n^2}\left(\frac{1}{2} - \frac{2\,(a/h)}{\pi(2n-1)}\tanh\left(\frac{\lambda_n h}{2}\right) + \frac{g}{2h\omega_n^2}\right) \\ \quad + \displaystyle\sum_{n=1}^{\infty}\frac{8\,(a/h)\tanh(\lambda_n h)}{\pi^3(2n-1)^3}\left[\frac{1}{2} - \frac{2\,(a/h)}{\pi(2n-1)}\tanh\left(\frac{\lambda_n h}{2}\right) + \frac{g}{h\omega_n^2}\right]^2\frac{\omega^2}{\omega_n^2-\omega^2}\end{array}\right]$$

When the force and moment obtained by the spring-mass system and the velocity potential equal to each other, slosh mass, associated height and mass inertia of the disk are determined as follows:

$$\frac{m_n}{m_T} = \frac{8a}{h}\frac{\tanh(\lambda_n h)}{\pi^3(2n-1)^3}$$

$$\frac{H_n}{h}=\frac{1}{2}-\frac{2\,(a/h)}{\pi(2n-1)}\tanh\left(\frac{\lambda_n h}{2}\right)$$

Note that following relationship is considered.

$$\sum_{n=1}^{\infty}\frac{m_n}{m_T}\frac{g}{h\omega_n^2}=\sum_{n=1}^{\infty}\frac{8a}{h}\frac{\tanh(\lambda_n h)}{\pi^3(2n-1)^3}\frac{g}{h\omega_n^2}=\sum_{n=1}^{\infty}\frac{8a}{h}\frac{\tanh(\lambda_n h)}{\pi^3(2n-1)^3}\frac{1}{h\lambda_n\tanh(\lambda_n h)}$$

$$=\sum_{n=1}^{\infty}\frac{8a}{h}\frac{1}{\pi^4(2n-1)^4}\frac{a}{h}=\sum_{n=1}^{\infty}\frac{8}{\pi^4(2n-1)^4}\left(\frac{a}{h}\right)^2=\frac{1}{12}\left(\frac{a}{h}\right)^2$$

Remaining parameters, spring constant, fixed mass and its height are determined as below:

$$K_n=m_n\omega_n^2=m_T\frac{8a}{h}\frac{\tanh(\lambda_n h)}{\pi^3(2n-1)^3}g\lambda_n\tanh(\lambda_n h)=m_T\frac{8g}{h}\frac{\tanh^2(\lambda_n h)}{\pi^2(2n-1)^2}$$

$$m_0=m_T-\sum_{n=1}^{\infty}m_n,\quad H_0=\sum_{n=1}^{\infty}\frac{m_n}{m_0}H_n$$

The moment of inertia of liquid cargo is smaller than that of rigid, solid or frozen liquid cargo since the liquid rotates freely. The effective moment of inertia of rectangular tank is formulated as below:

$$I_y=\frac{1}{12}m_T\left(a^2+h^2\right)\left\{1-\frac{4}{1+(h/a)^2}+\frac{768\,a/h}{\pi^5\left[1+(h/a)^2\right]}\sum_{n=1}^{\infty}\frac{\tanh\left[(2n-1)\pi h/2a\right]}{(2n-1)^5}\right\}$$

For around y-axis

$$I_R=\frac{1}{12}m_T\left(a^2+h^2\right),\quad I_d=I_R\left\{\frac{4}{1+(h/a)^2}-\frac{768\,a/h}{\pi^5\left[1+(h/a)^2\right]}\sum_{n=1}^{\infty}\frac{\tanh\left[(2n-1)\pi h/2a\right]}{(2n-1)^5}\right\}$$

For around x-axis

$$I_R=\frac{1}{12}m_T\left(b^2+h^2\right),\quad I_d=I_R\left\{\frac{4}{1+(h/b)^2}-\frac{768\,b/h}{\pi^5\left[1+(h/b)^2\right]}\sum_{n=1}^{\infty}\frac{\tanh\left[(2n-1)\pi h/2b\right]}{(2n-1)^5}\right\}$$

3. Validation of Mechanical Model

3.1 General

In order to demonstrate the credibility of the author's method presented in this thesis, the moment generated by the rotational oscillation of rectangular tank is calculated and compared with the results obtained by the experiment or calculation by other means.

3.2 Moment for Rotational Oscillation

One of the targets for comparison, the moment for rotational oscillation of the rectangular tank was obtained by Bosch et al [8), 9)] experimentally. Another was calculated by the 3D finite difference method (FDM) developed by Arai et al [32)].
The parameters of rectangular tank with water for the validation are shown in Table 3.1. The results are presented using a non-dimensional form used by Bosch et al.

$$M_{nd\_amp} = \frac{M_{amp}}{\rho_c g a^3 b}$$

$$\sigma = \omega\sqrt{\frac{a}{g}}$$

where M_{amp}, ρ_c, g and ω are the moment amplitude, fluid density, gravity constant and angular frequency, respectively.

Table 3.1. Parameters of Rectangular Tank for Validation

	Case 1	Case 2	Case 3
h/a	0.04	0.32	0.58
h/H	0.06	0.50	0.90
s/a	0.00	0.00	0.00

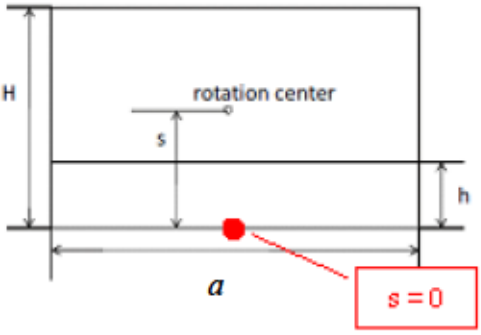

The force amplitude along x-axis and the moment amplitude about y-axis that coincides with the liquid centre of gravity are obtained by the following formulas:

$$\frac{F_{x\_amp}}{m_T \omega^2} = X_0\{1 + A\} + h\alpha_0\{B\}$$

$$\frac{M_{y\_amp}}{m_T h\omega^2} = X_0\{B\} + h\alpha_0\left\{\frac{I_y}{m_T h^2} + C + D\frac{1}{\omega^2}\right\}$$

where,

$$A = \sum_{n=1}^{\infty}\frac{m_n}{m_T}\frac{\omega^2}{\omega_n^2 - \omega^2}$$

$$B = \sum_{n=1}^{\infty}\frac{m_n}{m_T}\frac{g}{h\omega_n^2} + \sum_{n=1}^{\infty}\frac{m_n}{m_T}\left(\frac{H_n}{h} + \frac{g}{h\omega_n^2}\right)\frac{\omega^2}{\omega_n^2 - \omega^2}$$

$$C = \sum_{n=1}^{\infty}\frac{m_n}{m_T}\frac{g}{h\omega_n^2}\left(\frac{2H_n}{h} + \frac{g}{h\omega_n^2}\right) + \sum_{n=1}^{\infty}\frac{m_n}{m_T}\left(\frac{H_n}{h} + \frac{g}{h\omega_n^2}\right)^2\frac{\omega^2}{\omega_n^2 - \omega^2}$$

$$D = \sum_{n=1}^{\infty}\frac{m_n}{m_T}\frac{g^2}{h^2\omega_n^2}$$

When the rotation axis does not coincide with the liquid centre of gravity, coordinate conversion is performed to calculate the moment around the rotation axis.

$$\frac{M_{y\_amp}'}{m_T h\omega^2} = X_0\left\{(1+A)\frac{(z_{TG} - z_0)}{h} + B\right\} + h\alpha_0\left\{(1+A)\frac{(z_{TG} - z_0)^2}{h^2} + 2B\frac{(z_{TG} - z_0)}{h} + \frac{I_y}{m_T h^2} + C + D\frac{1}{\omega^2}\right\}$$

where, z_{TG} is the liquid centre of gravity along the z-axis and z_0 is the location of the rotation axis along the z-axis.

3.2.1 Accuracy of Calculation

The analytical solution of sloshing in the rectangular tank is represented by the sum of infinite series; however, only the first, i.e., the lowest, frequency slosh mass can practically be used when the mechanical model parameters are derived by other than analytical solution.
It is commonly accepted that higher order modes (n > 2) can usually be ignored since the magnitudes of the slosh mass for those modes are very small compared to the fundamental mode. Table 3.2 shows the ratio of the calculated moment amplitude adding up to n modes to the calculated moment considering 100 modes. The convergence is quick and the summation up to 100 modes is sufficiently accurate as the analytical solution. The error of calculated moment amplitude considering only the 1st mode (n=1) in the range from quasi-static region to resonant region is

within 2%. In high frequency region, the accuracy becomes worse; however, the moment in this frequency region is small and not so important for practical application.

Table 3.2. Accuracy of Calculation for Cut-Off Mode in Case 1 (h/a=0.04) for 1.9 deg

	Non-dimensional frequency, σ				
	0.032	0.255	0.511	0.766	0.990
n = 1	0.9856	0.9876	0.9946	1.0095	1.0364
n = 5	0.9998	0.9999	0.9999	1.0001	1.0003
n = 20	1.0000	1.0000	1.0000	1.0000	1.0000
n = 100	1.0000	1.0000	1.0000	1.0000	1.0000

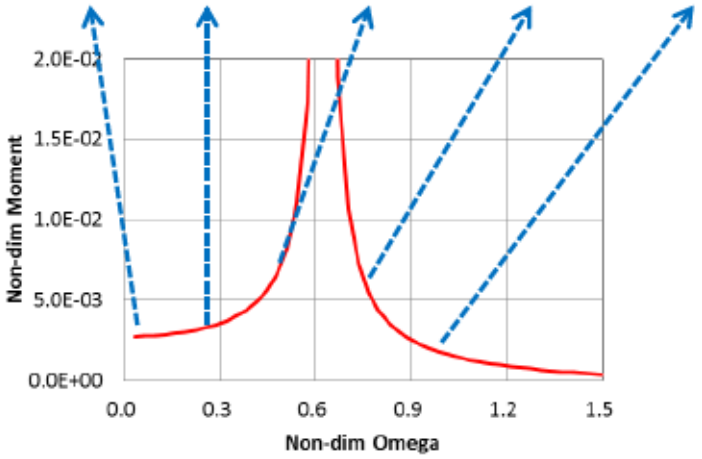

3.2.2 Comparisons

Comparisons of moments for the rotational oscillation of rectangular tank are shown in Figure 3.1. The moment in the vicinity of the sloshing natural frequency does not become as large as predicted by linear theory due to non-linear liquid motion such as a train of small waves, hydraulic jump, etc. Figure 3.1 (a) shows that the author's method presented in this thesis overestimates the moment in the vicinity of the sloshing natural frequency and the 3D FDM reproduces the experimental measurement. In Figure 3.1 (b), the author's method shows good agreement with the moment calculated by the 3D FDM when the rotational oscillation is small.
Figure 3.1 (c) shows that for case of the intermediate water level, the author's method replicates the 3D FDM calculation better than that of low water level shown in Figure 3.1 (a).
Figure 3.1 (d) and (e) show that for case of the high water level, the author's method does not replicate moment in the vicinity or higher region of the sloshing natural frequency when the rotational oscillation is large. In addition, the moment is limited due to the phenomenon that the water level reaches to the tank ceiling which is not prescribed by this method. However, this method replicates the 3D FDM calculation well when the rotational oscillation is small.

Actually, the simulation by the 3D FDM shows that even in the low and high frequency range apart from the sloshing natural frequency, the non-linear liquid motion especially multi-modal behaviour is observed. Therefore the moment calculated by the 3D FDM does not match exactly with the one

calculated by the author's method presented in this thesis. However, it is also confirmed that the linear liquid motion is the major contributor.

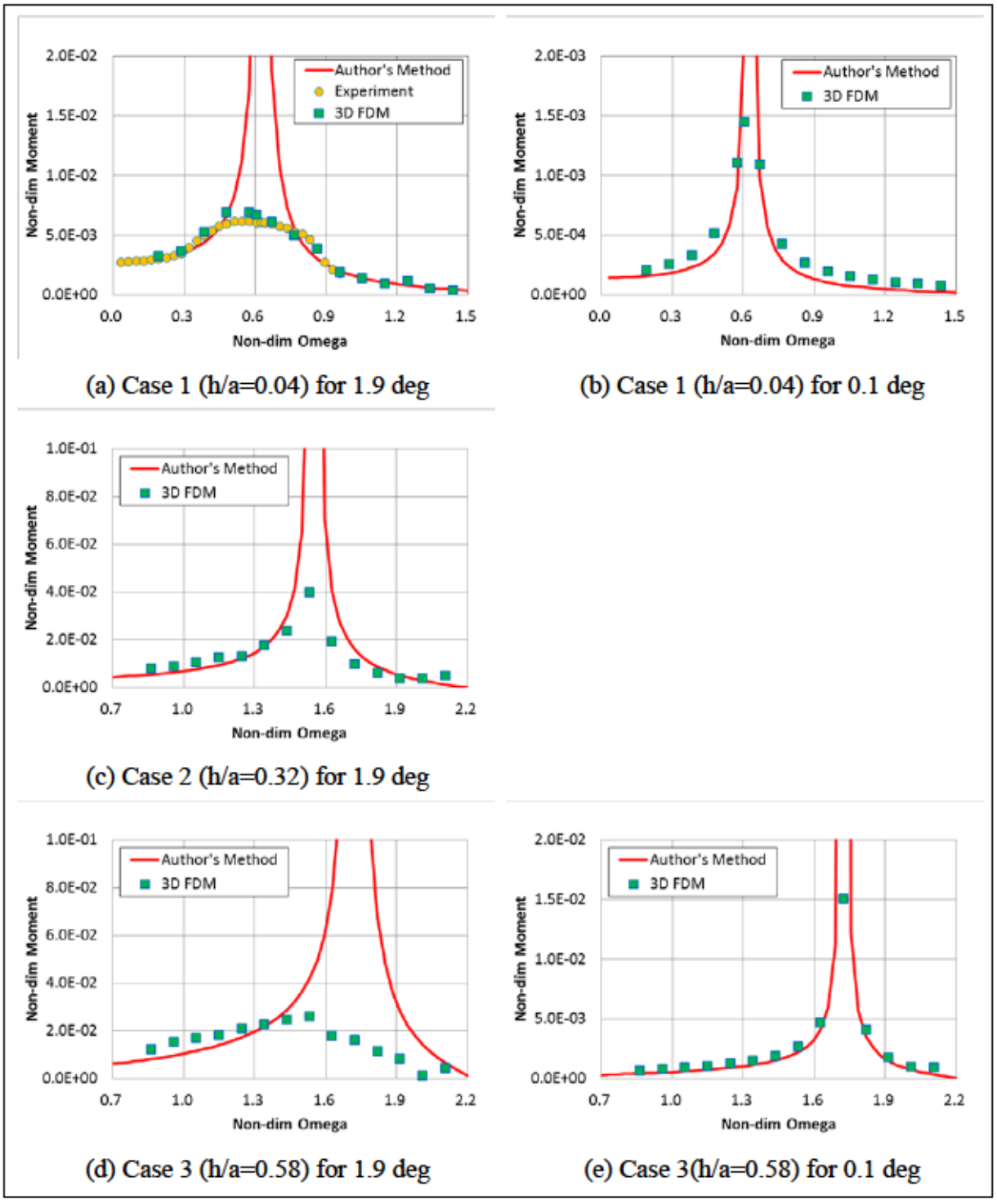

(a) Case 1 (h/a=0.04) for 1.9 deg

(b) Case 1 (h/a=0.04) for 0.1 deg

(c) Case 2 (h/a=0.32) for 1.9 deg

(d) Case 3 (h/a=0.58) for 1.9 deg

(e) Case 3(h/a=0.58) for 0.1 deg

Figure 3.1. Moment for Rotational Oscillation of Rectangular Tank

3.3 Validity and Limitation

Based on the validation performed on the mechanical model, its validity and limitation are concluded as follows:

- Sloshing behaviour in small oscillation is well predicted.
- The fundamental sloshing mode represents the sloshing behaviour sufficiently and the higher order modes can be ignored as commonly accepted.
- Resonant response in large oscillation is over predicted.
- Nonlinear behaviour that is not prescribed in the mechanical model limits the magnitude of sloshing moment.
- Ceiling effect that is not prescribed in the mechanical model limits the magnitude of sloshing moment.

4. Coupled Equation of Floating Body Motion and Liquid Cargo Effects

4.1 Floating Body Motion without Liquid Cargo

The floating body motion relative to its COG is described by the following equation in frequency domain.

$$\left[-\omega^2\left(\mathbf{M_G}+\mathbf{M_{A\_G}}\right)+i\omega\mathbf{B_G}+\mathbf{C_G}\right]\cdot\mathbf{X_G}=\mathbf{F_G^{DI}}$$

where $\mathbf{X_G}$ is the floating body motion matrix, $\mathbf{M_G}$ is the mass matrix of the floating body, $\mathbf{M_{A\_G}}$ is the hydrodynamic added mass matrix, $\mathbf{B_G}$ is the hydrodynamic potential and quadratic damping matrix, $\mathbf{C_G}$ is the hydrostatic restoring matrix, and $\mathbf{F_G^{DI}}$ is the hydrodynamic excitation force matrix due to incoming and diffraction waves. All matrices are obtained relative to the COG of the floating body. The mass matrix of the floating body relative to its COG, $\mathbf{M_G}$ is described below:

M ... Mass of floating body

$\mathrm{COG}=(x_G,y_G,z_G)$ ... COG of floating body

$$\mathbf{M_G}=\begin{pmatrix} M & 0 & 0 & 0 & 0 & 0 \\ 0 & M & 0 & 0 & 0 & 0 \\ 0 & 0 & M & 0 & 0 & 0 \\ 0 & 0 & 0 & I_{11}^G & I_{12}^G & I_{13}^G \\ 0 & 0 & 0 & I_{21}^G & I_{22}^G & I_{23}^G \\ 0 & 0 & 0 & I_{31}^G & I_{32}^G & I_{33}^G \end{pmatrix}$$

$$I_{11}^G=\iiint_M\left[(y-y_G)^2+(z-z_G)^2\right]dm \qquad I_{12}^G=I_{21}^G=-\iiint_M(x-x_G)(y-y_G)\,dm$$
$$I_{22}^G=\iiint_M\left[(x-x_G)^2+(z-z_G)^2\right]dm \qquad I_{13}^G=I_{31}^G=-\iiint_M(x-x_G)(z-z_G)\,dm$$
$$I_{33}^G=\iiint_M\left[(x-x_G)^2+(y-y_G)^2\right]dm \qquad I_{23}^G=I_{32}^G=-\iiint_M(y-y_G)(z-z_G)\,dm$$

Radius of Gyration and Specific product of inertia are expressed below:

$$R_{11}^G=\sqrt{\frac{I_{11}^G}{M}} \quad R_{22}^G=\sqrt{\frac{I_{22}^G}{M}} \quad R_{33}^G=\sqrt{\frac{I_{33}^G}{M}}$$

$$R_{12}^G=R_{21}^G=-\sqrt{\frac{\left|I_{12}^G\right|}{M}}\times\mathrm{sgn}\left(I_{12}^G\right) \quad R_{13}^G=R_{31}^G=-\sqrt{\frac{\left|I_{13}^G\right|}{M}}\times\mathrm{sgn}\left(I_{13}^G\right) \quad R_{23}^G=R_{32}^G=-\sqrt{\frac{\left|I_{23}^G\right|}{M}}\times\mathrm{sgn}\left(I_{23}^G\right)$$

The hydrostatic restoring matrix of the floating body relative to its COG, $\mathbf{C_G}$ is described below:

$$\mathbf{C_G} = g \times \begin{pmatrix} 0 & 0 & 0 & 0 & 0 & 0 \\ 0 & 0 & 0 & 0 & 0 & 0 \\ 0 & 0 & \rho A_{wp} & \rho A_{wp}(y_f - y_G) & -\rho A_{wp}(x_f - x_G) & 0 \\ 0 & 0 & \rho A_{wp}(y_f - y_G) & \rho(S_{11}^G + V_w z_b) - M z_G & \rho S_{12}^G & -\rho V_w x_b + M x_G \\ 0 & 0 & -\rho A_{wp}(x_f - x_G) & \rho S_{21}^G & \rho(S_{22}^G + V_w z_b) - M z_G & -\rho V_w y_b + M y_G \\ 0 & 0 & 0 & 0 & 0 & 0 \end{pmatrix}$$

$$S_{11}^G = \iint_{A_{wp}} (y - y_G)^2 \, da \quad S_{22}^G = \iint_{A_{wp}} (x - x_G)^2 \, da \quad S_{12}^G = S_{21}^G = -\iint_{A_{wp}} (x - x_G)(y - y_G) \, da$$

$\rho V_w = M$

A_{wp} ... Water Plane Area

$\mathrm{COB} = (x_b, y_b, z_b)$ ... Center of Buoyancy of floating body

$\mathrm{COF} = (x_f, y_f, z_f)$ ... Center of Floatation on waterplane

$$\rho g(S_{11}^G + V_w z_b) - M g z_G = \rho g V_w \left(\frac{S_{11}^G}{V_w} + z_b - z_G \right) = Mg \cdot GM_t$$

$$\rho g(S_{22}^G + V_w z_b) - M g z_G = \rho g V_w \left(\frac{S_{22}^G}{V_w} + z_b - z_G \right) = Mg \cdot GM_l$$

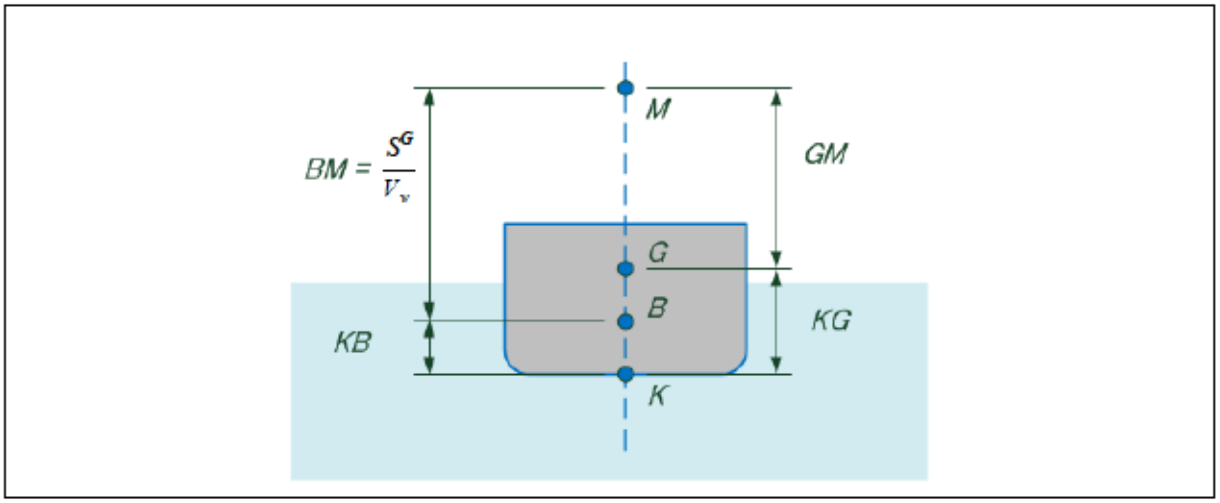

Figure 4.1. Static Properties of Floating Body

4.2 Coupled Floating Body Motion with Liquid Cargo

To obtain the equation of coupled motion of the floating body and the effects due to liquid cargo, the forces induced by the liquid cargo are added to the equation of the floating body motion. When there are multiple tanks, liquid forces from all the tanks are added together.

$$\left[-\omega^2\left(\mathbf{M}_{\mathbf{B\_G}}+\mathbf{M}_{\mathbf{A\_G}}\right)+i\omega\mathbf{B}_{\mathbf{G}}+\mathbf{C}_{\mathbf{G}}\right]\cdot\mathbf{X}_{\mathbf{G}}=\mathbf{F}_{\mathbf{G}}^{\mathbf{DI}}+\sum\left[\mathbf{F}_{\mathbf{T}}^{\mathbf{L}}+\mathbf{F}_{\mathbf{TG}}\right]\cdot\mathbf{X}_{\mathbf{G}}$$

where $\mathbf{M}_{\mathbf{B\_G}}$ is the mass matrix of the floating body (excluding liquid cargo) relative to its COG (including liquid cargo), $\mathbf{F}_{\mathbf{T}}^{\mathbf{L}}$ is the tank liquid force matrix relative to the local tank origin and $\mathbf{F}_{\mathbf{TG}}$ is the matrix transferring the coordinate of the tank liquid force from the local tank origin to the COG. Note that the mass matrix, $\mathbf{M}_{\mathbf{B\_G}}$ excludes the liquid mass, but mass inertia is calculated relative to the COG of the floating body including liquid cargo.

M ... Mass of floating body **including liquid cargo**

M_B ... Mass of floating body **excluding liquid cargo**

$\mathrm{COG}=(x_G,y_G,z_G)$ ... COG of floating body **including liquid cargo**

$\mathrm{COG_B}=(x_{BG},y_{BG},z_{BG})$ ... COG of floating body **excluding liquid cargo**

$\mathrm{COG_T}=(x_{TG},y_{TG},z_{TG})$ ... COG of liquid cargo

The mass matrix of the floating body (excluding liquid cargo) relative to its COG (including liquid cargo) is described below:

$$\mathbf{M}_{\mathbf{B\_G}}=\begin{pmatrix} M_B & 0 & 0 & 0 & M_B(z_{BG}-z_G) & -M_B(y_{BG}-y_G) \\ 0 & M_B & 0 & -M_B(z_{BG}-z_G) & 0 & M_B(x_{BG}-x_G) \\ 0 & 0 & M_B & M_B(y_{BG}-y_G) & -M_B(x_{BG}-x_G) & 0 \\ 0 & -M_B(z_{BG}-z_G) & M_B(y_{BG}-y_G) & I_{B11}^G & I_{B12}^G & I_{B13}^G \\ M_B(z_{BG}-z_G) & 0 & -M_B(x_{BG}-x_G) & I_{B21}^G & I_{B22}^G & I_{B23}^G \\ -M_B(y_{BG}-y_G) & M_B(x_{BG}-x_G) & 0 & I_{B31}^G & I_{B32}^G & I_{B33}^G \end{pmatrix}$$

$$I_{B11}^G=\iiint_{M_B}\left[(y-y_{BG})^2+(z-z_{BG})^2\right]dm+M_B\left[(y_{BG}-y_G)^2+(z_{BG}-z_G)^2\right]$$

$$I_{B22}^G=\iiint_{M_B}\left[(x-x_{BG})^2+(z-z_{BG})^2\right]dm+M_B\left[(x_{BG}-x_G)^2+(z_{BG}-z_G)^2\right]$$

$$I_{B33}^G=\iiint_{M_B}\left[(x-x_{BG})^2+(y-y_{BG})^2\right]dm+M_B\left[(x_{BG}-x_G)^2+(y_{BG}-y_G)^2\right]$$

$$I_{B12}^G=I_{B21}^G=-\iiint_{M_B}(x-x_{BG})(y-y_{BG})\,dm-M_B\left[(x_{BG}-x_G)(y_{BG}-y_G)\right]$$

$$I_{B13}^G=I_{B31}^G=-\iiint_{M_B}(x-x_{BG})(z-z_{BG})\,dm-M_B\left[(x_{BG}-x_G)(z_{BG}-z_G)\right]$$

$$I_{B23}^G=I_{B32}^G=-\iiint_{M_B}(y-y_{BG})(z-z_{BG})\,dm-M_B\left[(y_{BG}-y_G)(z_{BG}-z_G)\right]$$

$\mathbf{F_T^L}$ is tank liquid force matrix relative to local tank origin.

$$\mathbf{F_T^L} = m_T\omega^2 \times \begin{pmatrix} 1+A_x & 0 & 0 & 0 & hB_x & 0 \\ 0 & 1+A_y & 0 & -hB_y & 0 & 0 \\ 0 & 0 & 1 & 0 & 0 & 0 \\ 0 & -hB_y & 0 & \frac{I_x}{m_T}+h^2C_y+D_y\frac{h^2}{\omega^2} & 0 & 0 \\ hB_x & 0 & 0 & 0 & \frac{I_y}{m_T}+h^2C_x+D_x\frac{h^2}{\omega^2} & 0 \\ 0 & 0 & 0 & 0 & 0 & 0 \end{pmatrix}$$

where,

$$A_x = \sum_{n=1}^{\infty}\frac{m_{xn}}{m_T}\frac{\omega^2}{\omega_{xn}^2-\omega^2} \qquad A_y = \sum_{n=1}^{\infty}\frac{m_{yn}}{m_T}\frac{\omega^2}{\omega_{yn}^2-\omega^2}$$

$$B_x = \sum_{n=1}^{\infty}\frac{m_{xn}}{m_T}\frac{g}{h\omega_{xn}^2}+\sum_{n=1}^{\infty}\frac{m_{xn}}{m_T}\left(\frac{H_{xn}}{h}+\frac{g}{h\omega_{xn}^2}\right)\frac{\omega^2}{\omega_{xn}^2-\omega^2}$$

$$B_y = \sum_{n=1}^{\infty}\frac{m_{yn}}{m_T}\frac{g}{h\omega_{yn}^2}+\sum_{n=1}^{\infty}\frac{m_{yn}}{m_T}\left(\frac{H_{yn}}{h}+\frac{g}{h\omega_{yn}^2}\right)\frac{\omega^2}{\omega_{yn}^2-\omega^2}$$

$$C_x = \sum_{n=1}^{\infty}\frac{m_{xn}}{m_T}\frac{g}{h\omega_{xn}^2}\left(\frac{2H_{xn}}{h}+\frac{g}{h\omega_{xn}^2}\right)+\sum_{n=1}^{\infty}\frac{m_{xn}}{m_T}\left(\frac{H_{xn}}{h}+\frac{g}{h\omega_{xn}^2}\right)^2\frac{\omega^2}{\omega_{xn}^2-\omega^2}$$

$$C_y = \sum_{n=1}^{\infty}\frac{m_{yn}}{m_T}\frac{g}{h\omega_{yn}^2}\left(\frac{2H_{yn}}{h}+\frac{g}{h\omega_{yn}^2}\right)+\sum_{n=1}^{\infty}\frac{m_{yn}}{m_T}\left(\frac{H_{yn}}{h}+\frac{g}{h\omega_{yn}^2}\right)^2\frac{\omega^2}{\omega_{yn}^2-\omega^2}$$

$$D_x = \sum_{n=1}^{\infty}\frac{m_{xn}}{m_T}\frac{g^2}{h^2\omega_{xn}^2} \qquad D_y = \sum_{n=1}^{\infty}\frac{m_{yn}}{m_T}\frac{g^2}{h^2\omega_{yn}^2}$$

$$I_x = I_{xR} - I_{xd} \qquad I_y = I_{yR} - I_{yd}$$

$\mathbf{F_{TG}}$ is the matrix transferring the coordinate of the tank liquid force from local tank origin to COG.

$$\mathbf{F_{TG}} = \begin{bmatrix} 0 & -\mathbf{F_T^{L11}V} \\ \mathbf{VF_T^{L11}} & \mathbf{VF_T^{L12}} - \mathbf{F_T^{L21}V} - \mathbf{VF_T^{L11}V} \end{bmatrix}$$

where,

$$\mathbf{F_T^L} = \begin{bmatrix} \mathbf{F_T^{L11}} & \mathbf{F_T^{L12}} \\ \mathbf{F_T^{L21}} & \mathbf{F_T^{L22}} \end{bmatrix} \qquad \mathbf{V} = \begin{bmatrix} 0 & -(z_{TG} - z_G) & y_{TG} - y_G \\ z_{TG} - z_G & 0 & -(x_{TG} - x_G) \\ -(y_{TG} - y_G) & x_{TG} - x_G & 0 \end{bmatrix}$$

$$\mathbf{F_T^{L11}} = m_T\omega^2 \times \begin{pmatrix} 1+A_x & 0 & 0 \\ 0 & 1+A_y & 0 \\ 0 & 0 & 1 \end{pmatrix} \qquad \mathbf{F_T^{L12}} = m_T\omega^2 \times \begin{pmatrix} 0 & hB_x & 0 \\ -hB_y & 0 & 0 \\ 0 & 0 & 0 \end{pmatrix}$$

$$\mathbf{F_T^{L21}} = m_T\omega^2 \times \begin{pmatrix} 0 & -hB_y & 0 \\ hB_x & 0 & 0 \\ 0 & 0 & 0 \end{pmatrix}$$

$$\mathbf{F_T^{L22}} = m_T\omega^2 \times \begin{pmatrix} \frac{I_x}{m_T} + h^2C_y + D_y\frac{h^2}{\omega^2} & 0 & 0 \\ 0 & \frac{I_y}{m_T} + h^2C_x + D_x\frac{h^2}{\omega^2} & 0 \\ 0 & 0 & 0 \end{pmatrix}$$

The forces induced by liquid cargo are finally divided into added mass part and hydrostatic restoring part. The hydrostatic restoring part represents the free surface effect. Details of the tank liquid force matrix are provided in Appendix 6.

$$\mathbf{F_T^L} + \mathbf{F_{TG}} = \omega^2\mathbf{M_{LA\_G}} + \mathbf{C_{L\_G}}$$

And the equation of the floating body motion coupled with the liquid cargo effects is obtained as follows:

$$\left[-\omega^2\left(\mathbf{M_{B\_G}} + \mathbf{M_{A\_G}} + \sum\mathbf{M_{LA\_G}}\right) + i\omega\mathbf{B_G} + \mathbf{C_G} - \sum\mathbf{C_{L\_G}}\right]\cdot\mathbf{X_G} = \mathbf{F_G^{DI}}$$

or

$$\left[-\omega^2\left(\mathbf{M_G} + \mathbf{M_{A\_G}} + \sum\mathbf{M_{L\_G}}\right) + i\omega\mathbf{B_G} + \mathbf{C_G} - \sum\mathbf{C_{L\_G}}\right]\cdot\mathbf{X_G} = \mathbf{F_G^{DI}}$$

4.3 Hydrodynamic Matrix

The hydrodynamic matrices, $\mathbf{M}_{\mathbf{A\_G}}$, $\mathbf{B}_{\mathbf{G}}$ and $\mathbf{F}_{\mathbf{G}}^{\mathbf{DI}}$ are provided by the radiation and diffraction calculation. ANSYS AQWA[33] program is utilized for this purpose in this thesis.
The reference point of the hydrodynamic matrices in ANSYS AQWA coincides with the COG of the floating body; hence, the output from ANSYS AQWA is directly used.

The velocity potential of incoming wave and phase definition are described in Appendix 7.

The hydrodynamic matrices obtained by radiation and diffraction calculation from other programs such as WAMIT [34], WADAM, etc., the reference point of the hydrodynamic matrices and the floating body motion are not at the COG of the floating body, but the points are on the still water surface.
In such a case, the hydrodynamic matrices relative to the reference point shall be transformed relative to the COG or the other matrices, $\mathbf{M}_{\mathbf{G}}$, $\mathbf{M}_{\mathbf{B\_G}}$, $\mathbf{C}_{\mathbf{G}}$ and $\mathbf{F}_{\mathbf{T}}^{\mathbf{L}}$ shall be transformed relative to the reference point.
The matrix transformation relative to the reference point adopted in WAMIT and WADAM is provided in Appendix 8.

5. Validation of Coupled Floating Body Motion

5.1 General

In order to demonstrate the credibility of the author's method presented in this thesis, the RAO of sway and roll motion with and without the liquid cargo effects are calculated and compared with the results obtained from the literature, experiment or calculation by other means.

5.2 Barge with Rectangular Tanks

Molin et al [13] proposed a theoretical model for predicting the floating body motion coupled with a sloshing in internal tanks, based on the linear potential theory. They performed a model test aimed at providing data to validate the theoretical model.

Their experimental model was a rectangular barge with two (2) rectangular tanks located on the barge deck as shown in Figure 5.1. The sway and roll motion of the barge for beam waves were measured and calculated with the tanks filled to different levels with water.

The principal particulars of the barge and tanks are presented in Tables 5.1, 5.2 and 5.3, and calculated natural frequency is presented in Table 5.4.

The comparison of the sway and roll motion of the barge measured and calculated by Molin et al and the author's method presented in this thesis is shown in Figure 5.2 which confirms that the results are in good agreement.

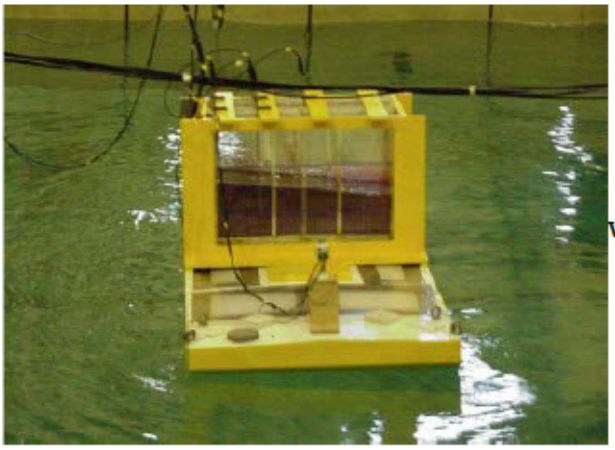

wo

Figure 5.1. Barge Model with Two Rectangular Tanks

Table 5.1. Principal Particulars of Empty Barge

Length BP	3.000 m
Breadth	1.000 m
Depth	0.267 m
Mass	0.169 kg
KG	0.240 m
Roll radius of gyration relative to COG of empty barge	0.414 m

Table 5.2. Principal Particulars of Tank

Length	0.250 m
Width	0.800 m
Depth	0.600 m
Bottom elevation from barge keel	0.300 m

Table 5.3. Principal Particulars of Floating Barge with Water Filled Tanks

	Case 1	Case 2
Draft	0.108 m	0.108 m
Water level in tank 1	0.190 m	0.190 m
Water level in tank 2	0.190 m	0.390 m
Displacement	0.285 m^3	0.285 m^3
KG	0.287 m	0.330 m
Roll radius of gyration relative to COG of floating barge	0.372 m	0.373 m
GMt	0.638 m	0.594 m

Table 5.4. Calculated Natural Frequency

	Case 1	Case 2
Roll natural frequency without liquid cargo effects (solid cargo)	4.74 rad/s	4.55 rad/s
Sloshing natural frequency of tank 1	4.94 rad/s	4.94 rad/s
Sloshing natural frequency of tank 2	4.94 rad/s	5.92 rad/s

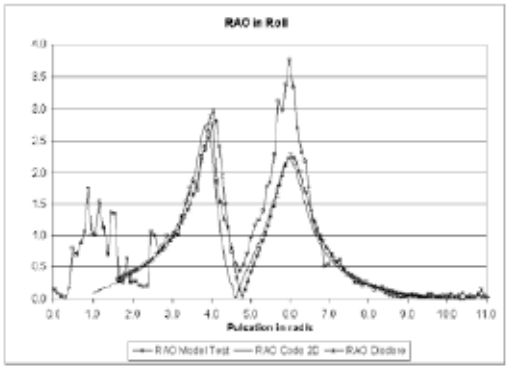

Figure 5: 19 cm + 19 cm. Smooth walls. RAO of the roll motion (rd/m).

(a) Case 1 Roll (Molin et al.)

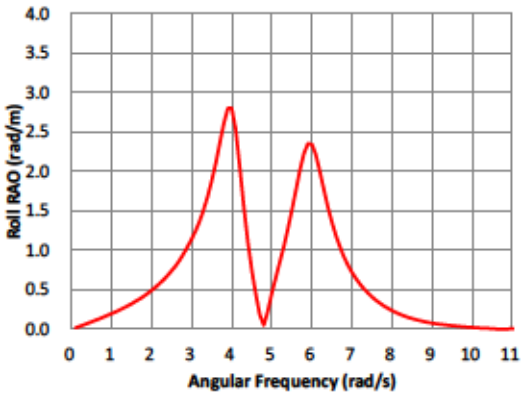

(b) Case 1 Roll (present method)

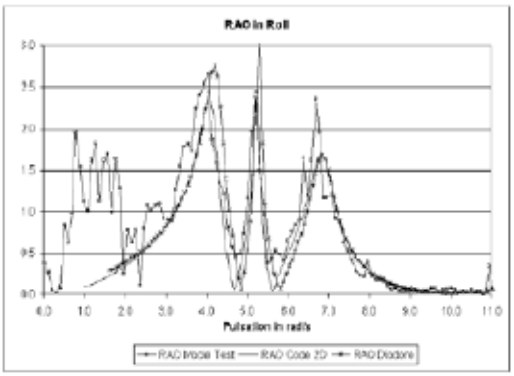

Figure 9: 19 cm + 39 cm. Smooth walls. RAO of the roll motion (rd/m).

(c) Case 2 Roll (Molin et al.)

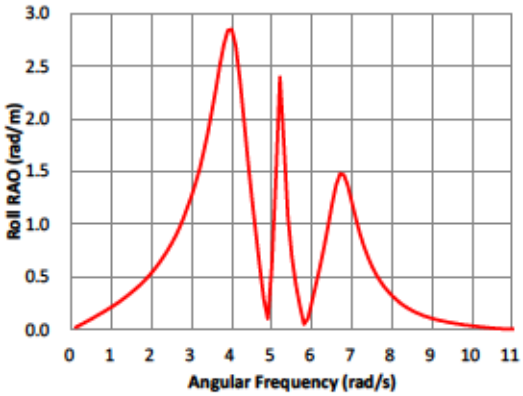

(d) Case 2 Roll (present method)

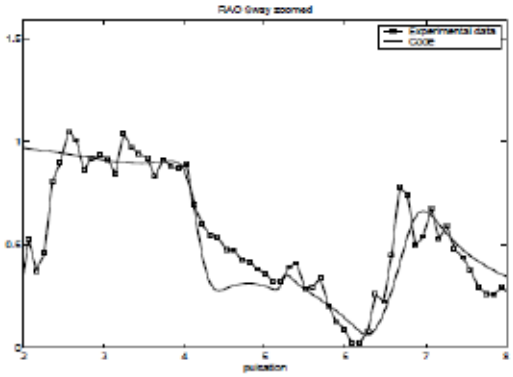

Figure 10: 19 cm + 39 cm. Smooth walls. RAO of the sway motion.

(e) Case 2 Sway (Molin et al.)

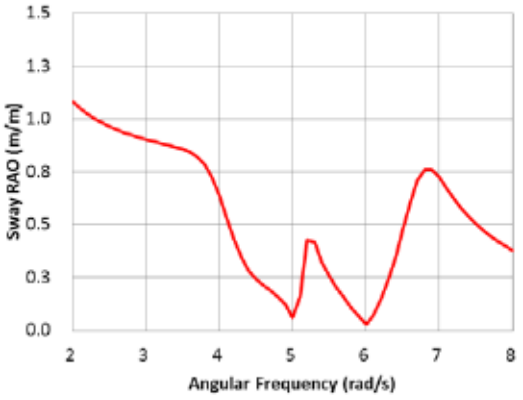

(f) Case 2 Sway (present method)

Figure 5.2. RAO of Sway and Roll motion with Liquid Cargo Effects

5.3 FLNG with Rectangular Tanks

Rocha et al [31] measured the 6-DOF FLNG motion coupled with and without the liquid cargo effects and calculated them by numerical method based on linear potential theory (WAMIT). Their FLNG model was a barge type hull equipped with six (6) rectangular tanks located inside the hull as shown in Figures 5.3 and 5.4. The loading conditions corresponded to that all the six (6) tanks were filled with water up to 15%, 50% and 90% of the tank height.

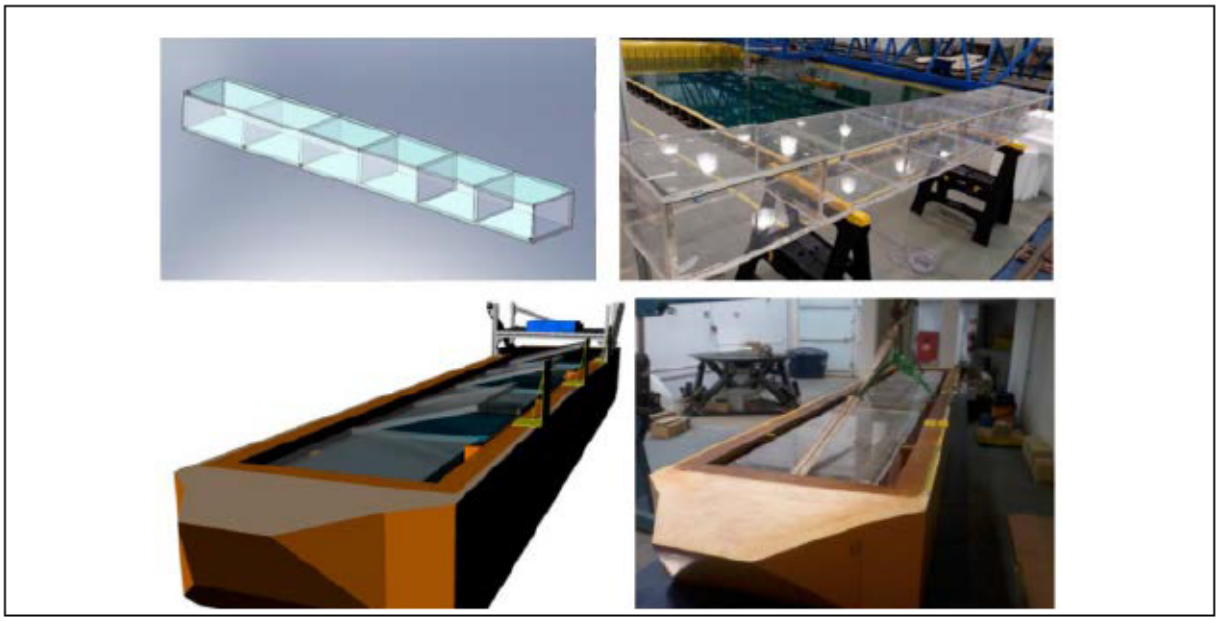

Figure 5.3. FLNG Model with Six Rectangular Tanks

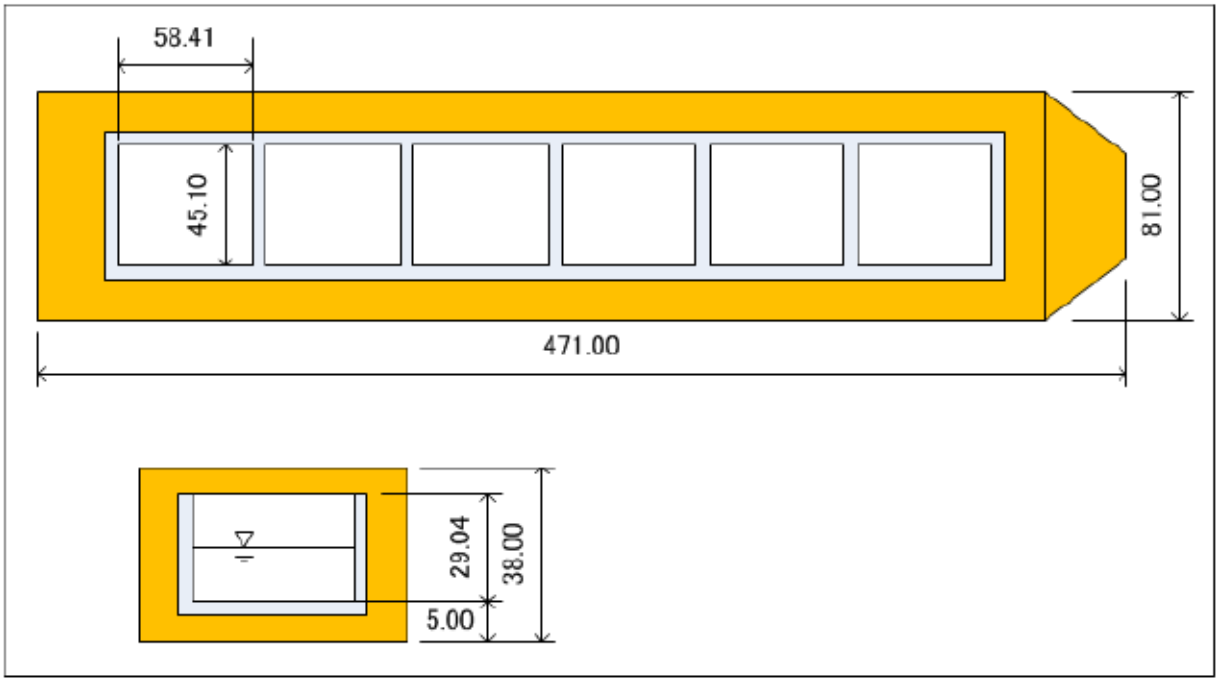

Figure 5.4. Tank Arrangement of FLNG Model (unit: m)

For validation, the sway and roll motion for beam waves with two (2) loading conditions of 15% and 50% are selected. The principal particulars and properties of the loading condition are presented in Tables 5.5, 5.6 and 5.7.

Table 5.5. Principal Particulars of FLNG

Length Overall	471 m
Length BP	450 m
Breadth	81 m
Depth	38 m

Table 5.6. Principal Particulars of Tank

Length	58.41 m
Width	45.10 m
Depth	29.04 m
Bottom elevation from FLNG keel	5.00 m

Table 5.7. Loading Conditions

Draft	12.22 m	16.60 m
Water level in tanks	4.36 m (15%)	14.52 m (50%)
Displacement volume	432,364 m^3	591,683 m^3
KG	22.99 m	18.53 m
Roll radius of gyration relative to COG of FLNG	31.86 m	26.02 m
GMt	28.62 m	23.19 m
Roll natural period without liquid cargo effects (solid cargo)	15.2 s	14.0 s
Sloshing natural period of tank	14.0 s	8.7 s

As shown in Figures 5.5 and 5.6, the numerical calculation of the author's method presented in this thesis is compared with the FLNG motion measured and calculated by Rocha et al. The RAO calculated by the author's method is very close to the one calculated by WAMIT.

While comparing the experimental measurement, for the loading condition of 15%, the sway and roll motion around the sloshing natural period [Fig. 5.5 (c) and (d)] are not well replicated by either the author's method or WAMIT. As Rocha et al pointed out in their paper, this is due to non-linear sloshing in the tanks and the limitation of the calculation method based on the linear potential theory. For the loading condition of 50%, the calculations results match well with the experimental measurements.

It is concluded that the sway and roll motion affected by the liquid cargo effects are reasonably evaluated by the author's method presented in this thesis and WAMIT, except for the case in which the effect of the non-linear sloshing is significant [Fig. 5.5 (c) and (d)].

One important observation is that the roll motion for the loading condition of 50% seems to be not affected much by the liquid cargo effects.

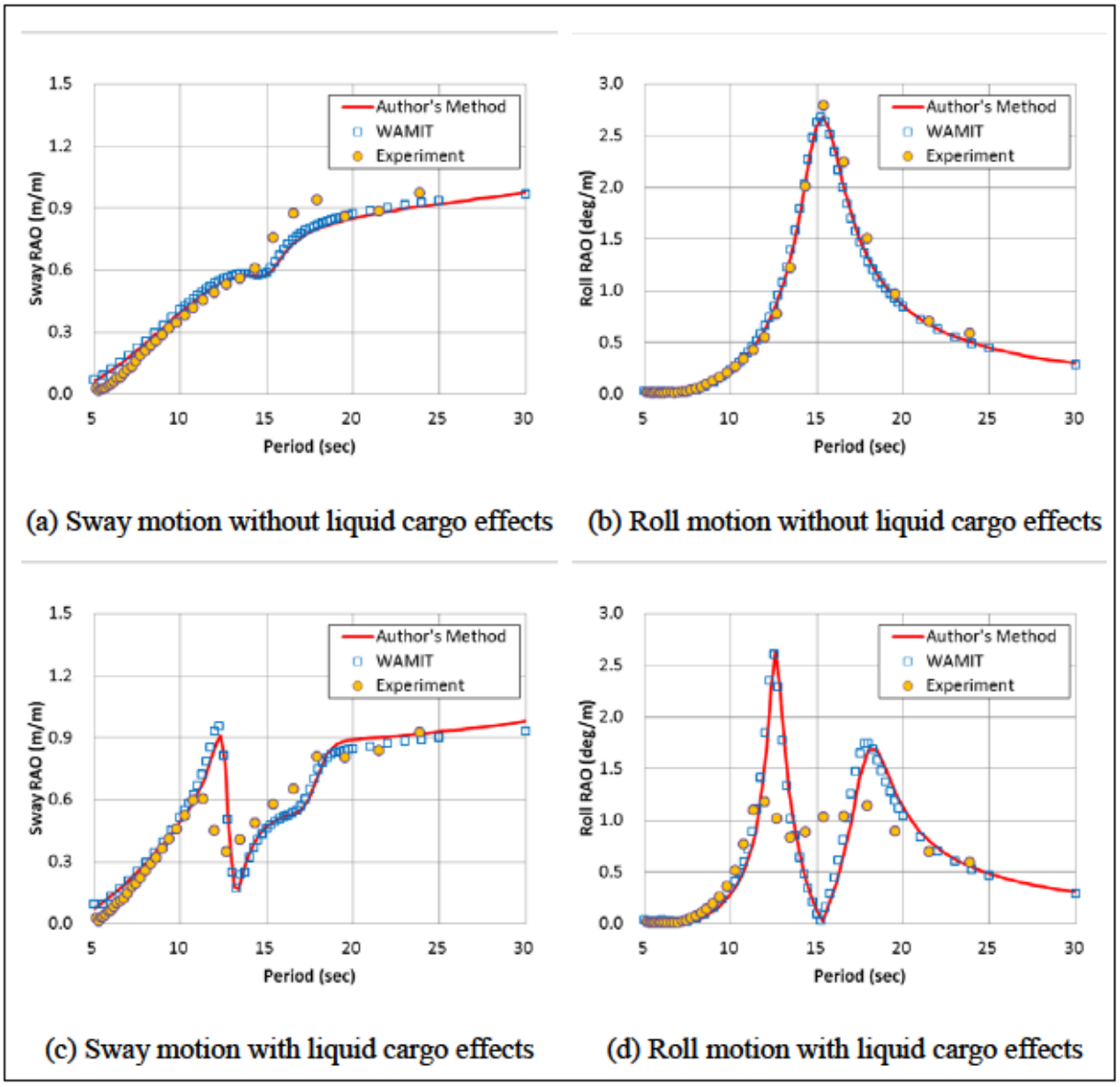

Figure 5.5. RAO of Sway and Roll motion for Loading Condition of 15%

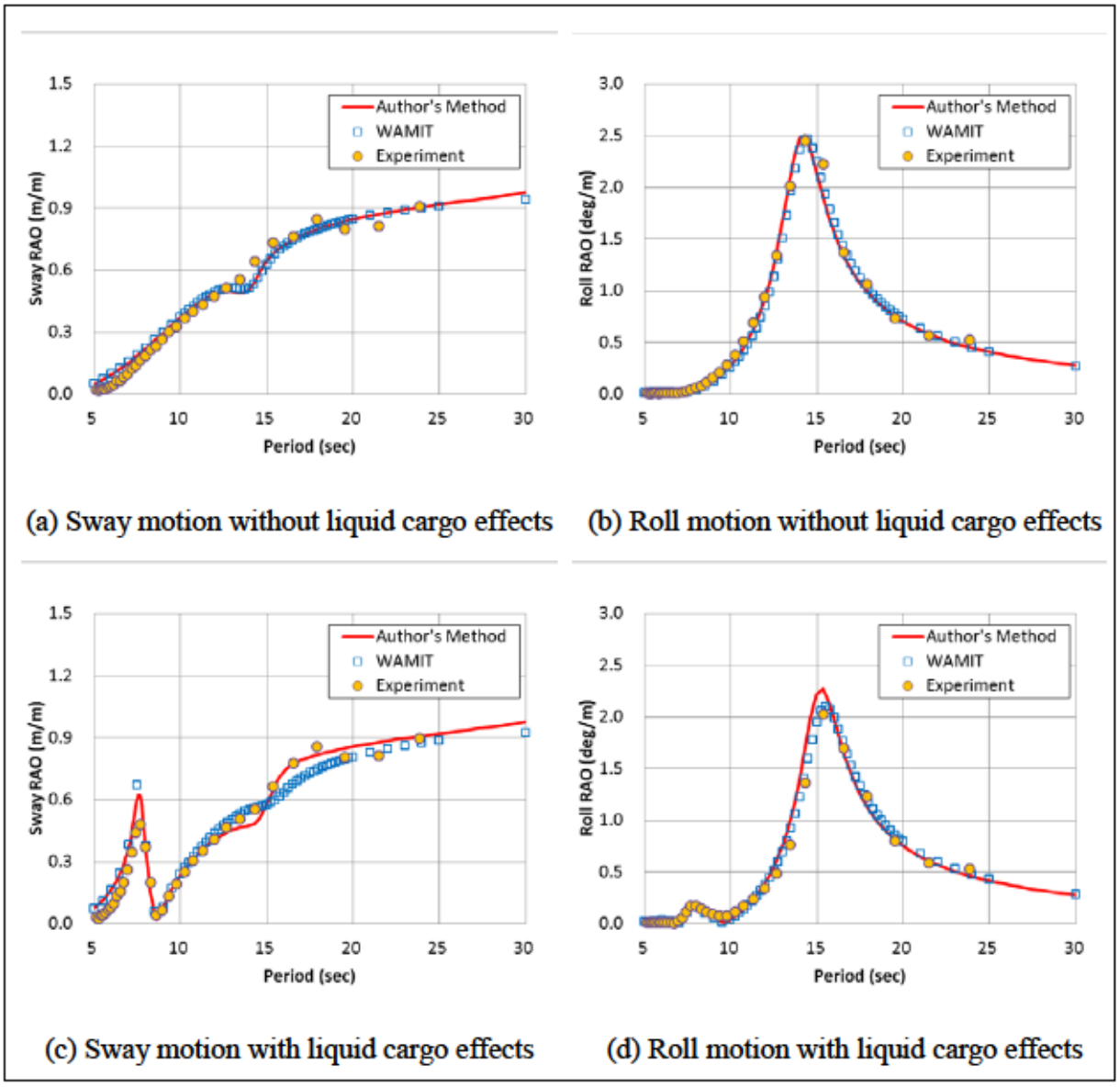

Figure 5.6. RAO of Sway and Roll motion for Loading Condition of 50%

5.4 Validity and Limitation

Based on the comparisons presented in this chapter, validity and limitation of the coupling of floating body motion and mechanical model are concluded as follows:

- The sway and roll motion influenced by the sloshing is reasonably well predicted.
- The frequency characteristics of sway and roll motion fluctuate greatly at around the first sloshing natural frequency/period.
- When the effect of the non-linear sloshing is significant, the author's method overestimates the peak response and the local minimum response.

6. Rational Explanation of Liquid Cargo Effects on Floating Body Motion

6.1 General

In order to identify effect of the liquid cargo on the sway and roll motion of the floating body, the equation of sway and roll motion is extracted and presented below from the matrix form of the equation obtained in chapter 4.2.

$$\left[-\omega^2\left(M+m_{A\_G}^{22}+\sum_{j=1}^{N}m_{Tj}A_{yj}\right)+i\omega b_G^{22}\right]x_{G2}+\left[-\omega^2\left(m_{A\_G}^{24}-\sum_{j=1}^{N}m_{Tj}\left[A_{yj}\left(z_{TGj}-z_G\right)+h_jB_{yj}\right]\right)+i\omega b_G^{24}\right]x_{G4}=F_{G2}^{DI}$$

$$\left[-\omega^2\left(m_{A\_G}^{42}-\sum_{j=1}^{N}m_{Tj}\left[A_{yj}\left(z_{TGj}-z_G\right)+h_jB_{yj}\right]\right)+i\omega b_G^{42}\right]x_{G2}$$
$$+\left[-\omega^2\left(I_{11}^G+m_{A\_G}^{44}+\sum_{j=1}^{N}\left\{-I_{xdj}+m_{Tj}\left[A_{yj}\left(z_{TGj}-z_G\right)^2+2h_jB_{yj}\left(z_{TGj}-z_G\right)+h_j^2C_{yj}\right]\right\}\right)+i\omega b_G^{44}+\left(\rho gV_w\cdot GM_t-\sum_{j=1}^{N}m_{Tj}h_j^2D_{yj}\right)\right]x_{G4}=F_{G4}^{DI}$$

where, M is the mass of the floating body including the liquid cargo and is equal to ρV_w, ρ is the density of the surrounding water, V_w is the displaced volume, I_{11}^G and GM_t are the mass inertia and the transverse metacentric height of the floating body including the liquid cargo relative to its COG, $m_{A\_G}^{kl}$, b_G^{kl} and F_{Gk}^{DI} are the hydrodynamic added mass, damping and wave forces for k and l components, respectively. The characters x_{G2} and x_{G4} are the sway and roll motion of the COG of the floating body, j is the number of tanks, and N is the total number of tanks. The term $-\sum_{j=1}^{N}m_{Tj}h_j^2D_{yj}$ represents the free surface effect of the liquid cargo.
Further, the equation of sway is divided by $\rho V_w w_a \omega^2$ and the equation of roll is divided by $\rho V_w B w_a \omega^2$, and the non-dimensional equations of motion are obtained.

$$\left[-\left(1+a^{22}{}'\right)+ib^{22}{}'\right]x_2'+\left[-a^{24}{}'+ib^{24}{}'\right]x_4'=F_2'$$

$$\left[-a^{42}{}'+ib^{42}{}'\right]x_2'+\left[-\left\{\left(\frac{R_{11}^G}{B}\right)^2+a^{44}{}'\right\}+ib^{44}{}'+c^{44}{}'\right]x_4'=F_4'$$

The non-dimensional hydrodynamic coefficients in the equations are as follows:

$$a^{22}{}'=\frac{m_{A\_G}^{22}+\sum_{j=1}^{N}m_{Tj}A_{yj}}{\rho V_w}$$

$$a^{24}{}' = \frac{m_{A\_G}^{24} - \sum_{j=1}^{N} m_{Tj}\left[A_{yj}\left(z_{TGj} - z_G\right) + h_j B_{yj}\right]}{\rho V_w B} \qquad a^{42}{}' = \frac{m_{A\_G}^{42} - \sum_{j=1}^{N} m_{Tj}\left[A_{yj}\left(z_{TGj} - z_G\right) + h_j B_{yj}\right]}{\rho V_w B}$$

$$a^{44}{}' = \frac{m_{A\_G}^{44} + \sum_{j=1}^{N}\left\{-I_{xdj} + m_{Tj}\left[A_{yj}\left(z_{TGj} - z_G\right)^2 + 2h_j B_{yj}\left(z_{TGj} - z_G\right) + h_j^2 C_{yj}\right]\right\}}{\rho V_w B^2}$$

$$b^{22}{}' = \frac{b_G^{22}}{\rho V_w \omega} \quad b^{24}{}' = \frac{b_G^{24}}{\rho V_w B\omega} \quad b^{42}{}' = \frac{b_G^{42}}{\rho V_w B\omega} \quad b^{44}{}' = \frac{b_G^{44}}{\rho V_w B^2 \omega}$$

$$c^{44}{}' = \frac{g \cdot GM_t}{B^2\omega^2} - \frac{\sum_{j=1}^{N} m_{Tj} h_j^2 D_{yj}}{\rho V_w B^2 \omega^2}$$

$$x_2{}' = \frac{x_{G2}}{w_a} \quad x_4{}' = \frac{Bx_{G4}}{w_a} \quad F_2{}' = \frac{F_{G2}^{DI}}{\rho V_w w_a \omega^2} \quad F_4{}' = \frac{F_{G4}^{DI}}{\rho V_w B w_a \omega^2}$$

where, w_a is the incident wave amplitude, B is the breadth of the floating body, R_{11}^G is the roll radius of gyration.

The absolute values of non-dimensional terms and the real part of the terms (2, 2) and (4, 4) expressed as below are used in the following chapters.

$$A^{22} = \sqrt{\left(1 + a^{22}{}'\right)^2 + \left(b^{22}{}'\right)^2} \qquad \left|R^{22}\right| = \left|1 + a^{22}{}'\right|$$

$$A^{24} = \sqrt{\left(a^{24}{}'\right)^2 + \left(b^{24}{}'\right)^2}$$

$$A^{42} = \sqrt{\left(a^{42}{}'\right)^2 + \left(b^{42}{}'\right)^2}$$

$$A^{44} = \sqrt{\left\{-\left(\frac{R_{11}^G}{B}\right)^2 - a^{44}{}' + c^{44}{}'\right\}^2 + \left(b^{44}{}'\right)^2} \qquad \left|R^{44}\right| = \left|-\left(\frac{R_{11}^G}{B}\right)^2 - a^{44}{}' + c^{44}{}'\right|$$

6.2 Barge with Rectangular Tanks

This chapter addresses the effect of the liquid cargo on the sway and roll motion of the barge stated in the chapter 5.2.

The first point of consideration is the sway-roll coupling affected by the liquid cargo effects. The sway and roll affect each other and the degree of sway-roll coupling is represented by the terms, A^{24} and A^{42}.

Figures 6.1 and 6.2 show the non-dimensional absolute of the terms, A^{22}, A^{24}, $A^{42}$and A^{44}, non-dimensional exciting forces, $F_2{}'$ and $F_4{}'$, RAOs of sway and roll excluding and including the liquid cargo effects in tanks for case 1 barge, respectively. Two (2) RAOs are presented: one is obtained with the sway-roll coupling and the other is without the coupling.

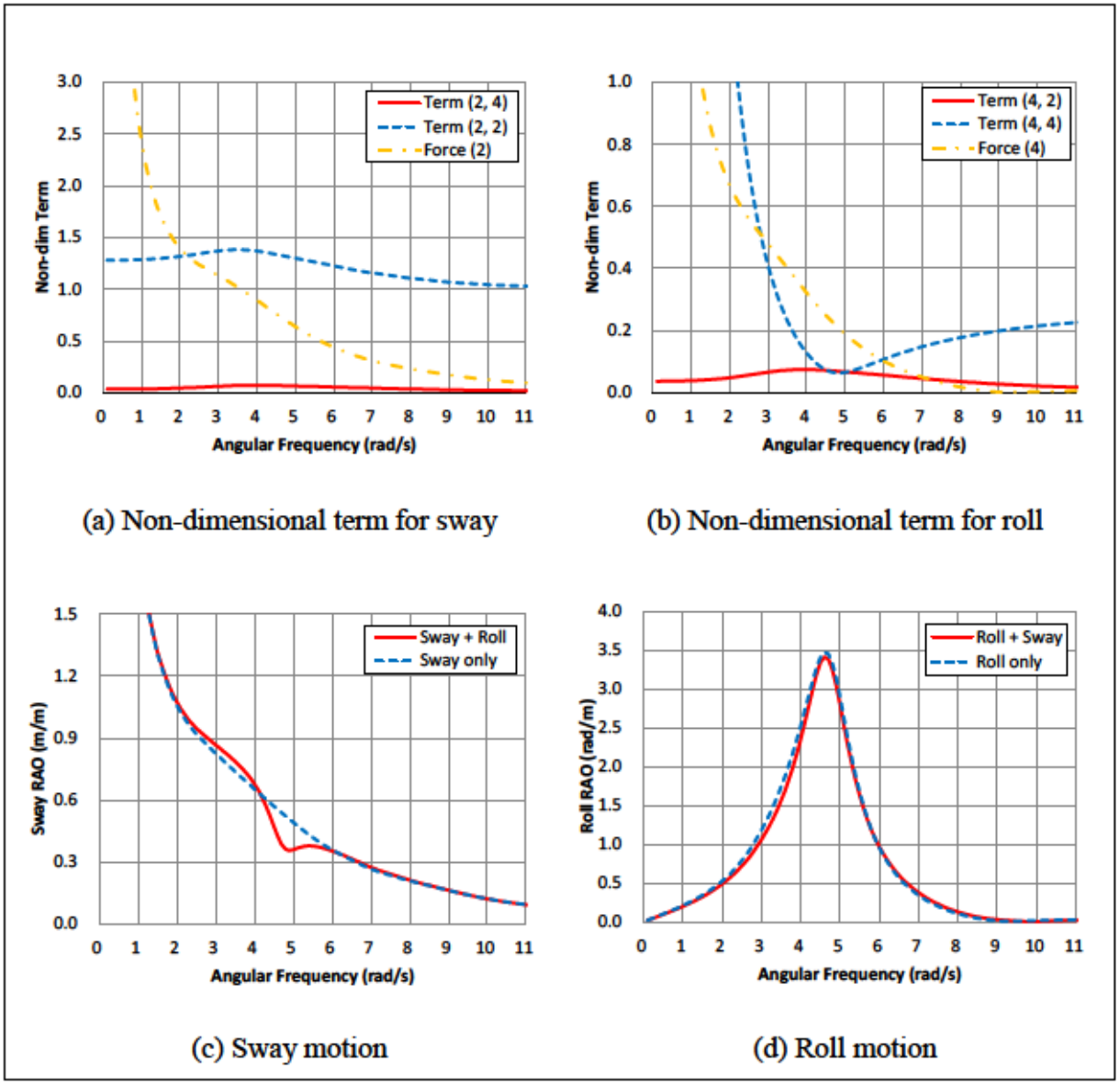

Figure 6.1. Sway and Roll motion without Liquid Cargo Effects for Case 1

For the barge motion without the liquid cargo effects in tanks, the sway-roll coupling is not significant as shown in Figure 6.1. The $A^{24}$and A^{42} terms [solid line in (a) and (b)] are kept small relative to the other terms in all the frequency range and the RAOs of sway and roll are almost the same regardless of the sway-roll coupling [(c) and (d)].

When the liquid cargo effects in tanks are added as shown in Figure 6.2, the $A^{24}$and A^{42} terms [solid line in (a) and (b)] become large in the whole frequency range, especially around the sloshing natural frequency. As a result, the sway-roll coupling is enhanced. Appreciation of this fact is necessary in order to understand the coupled sway and roll motion with the liquid cargo effects.

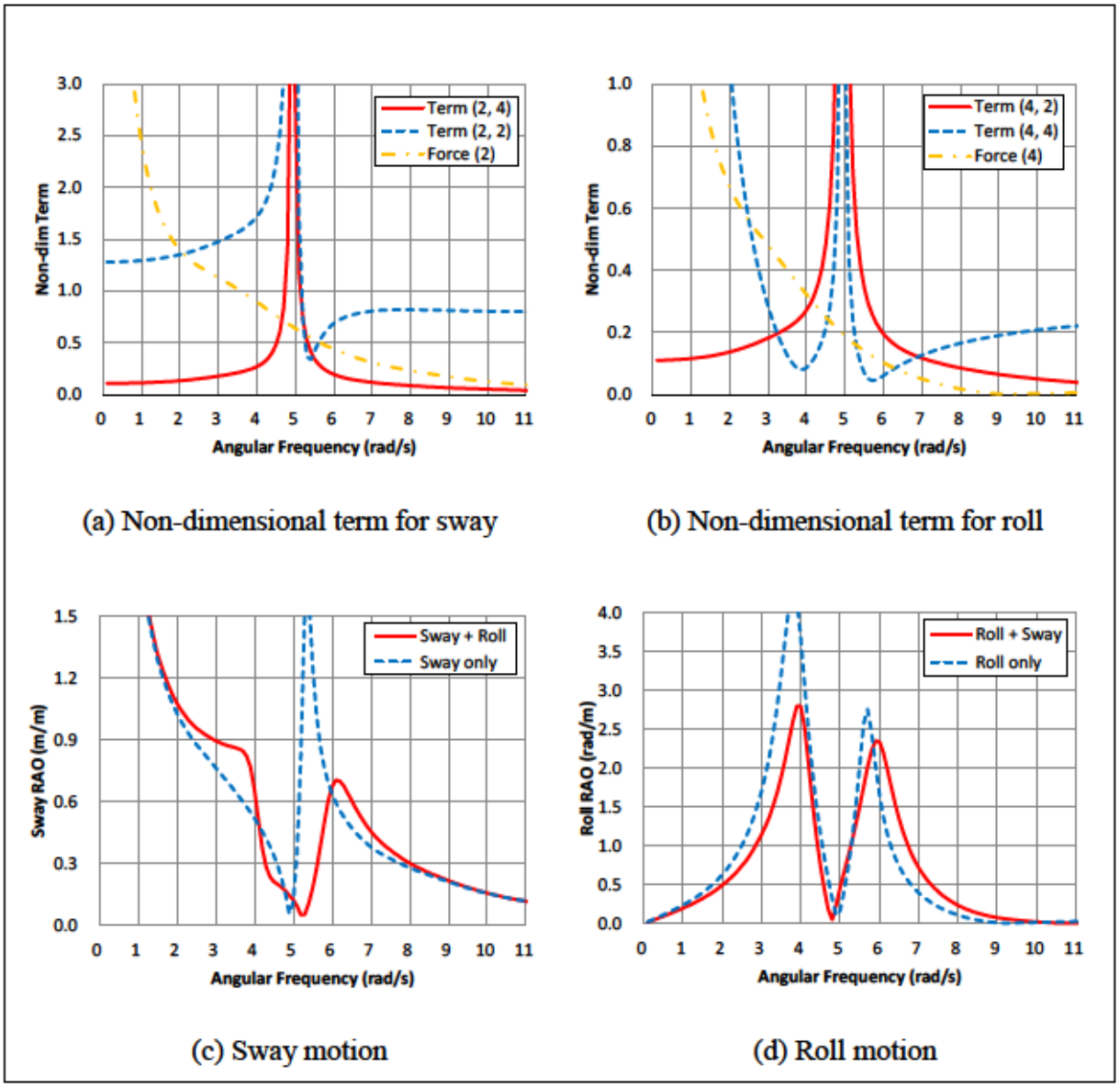

Figure 6.2. Sway and Roll motion with Liquid Cargo Effects for Case 1

The second point of consideration is on the terms which provide major contribution towards sway and roll motions.

The term R^{22}, having major contribution towards the sway motion is characterized by the mass. As shown in Figure 6.3 (a), the term R^{22} without liquid [dotted line in (a)] does not vary significantly. When the liquid cargo effects are considered, it varies significantly due to sloshing in tanks [solid line in (a)]. It becomes extremely large at the sloshing natural frequency, 4.94 rad/s; the decoupled sway motion becomes very small [dotted line in (e)]. In frequency greater than the sloshing natural frequency, it changes rapidly from the extremely large value to zero (0) at 5.35 rad/s [The reason why the solid line in (a) does not reach to zero (0) is due to resolution of the horizontal axis of the graph], where the local peak of the decoupled sway motion is observed [dotted line in (e)].
Due to strong coupling with roll motion as shown in Figure 6.2 (a), these extreme sway motions are moderated and the corresponding frequency is shifted [solid line in (e)].

The term R^{44}, having major contribution towards the roll motion is characterized by the mass inertia and the restoring moment. As shown in Figure 6.3 (b), the term R^{44} without liquid [dotted line in (b)] takes zero (0) at the frequency, 4.74 rad/s and a roll resonant peak is observed [dotted line in (d)].
When the liquid cargo effects are considered, it becomes zero (0) at 3.86 rad/s and 5.70 rad/s [solid line in (b)]. In addition, it has a peak value at sloshing natural frequency, 4.94 rad/s. Accordingly, the two peaks at 3.86 rad/s and 5.70 rad/s and local minimum at 4.94 rad/s are observed in roll motion decoupled from sway motion [dotted line in (f)].
When coupling with sway motion is considered, the frequency corresponding to the peaks and the local minimum are shifted [solid line in (f)].
At this point, it is essential to understand that due to free surface effect, the restoring moment is smaller and as a result, roll motion which decoupled from sway motion becomes larger. And then the sway coupling reduces the roll motion.

The consideration and explanation for case 1 barge are valid for the case 2 barge as well. Figures 6.4, 6.5 and 6.6 show the graphs corresponding to Figures 6.1, 6.2 and 6.3, respectively.

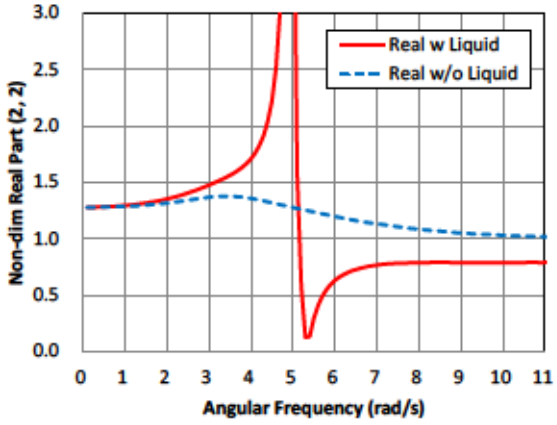

(a) Real part of the term (2, 2)

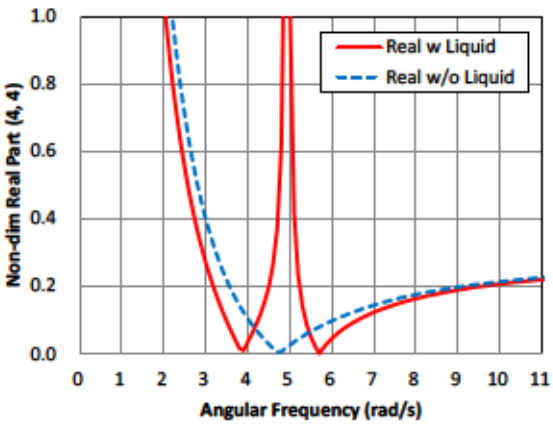

(b) Real part of the term (4, 4)

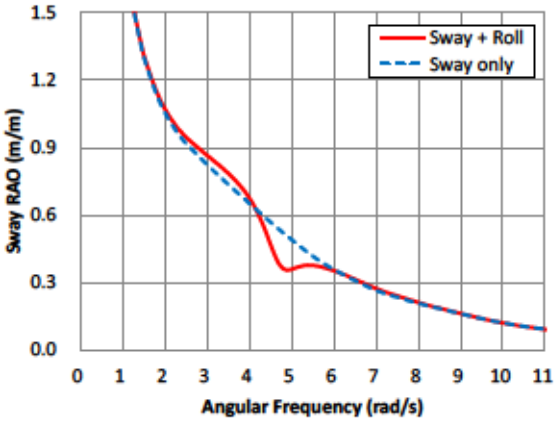

(c) Sway motion without liquid cargo effects

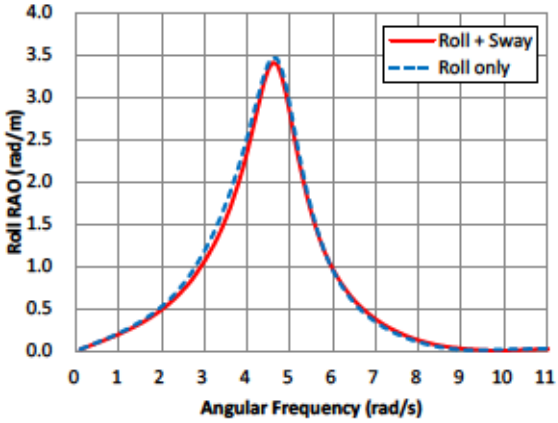

(d) Roll motion without liquid cargo effects

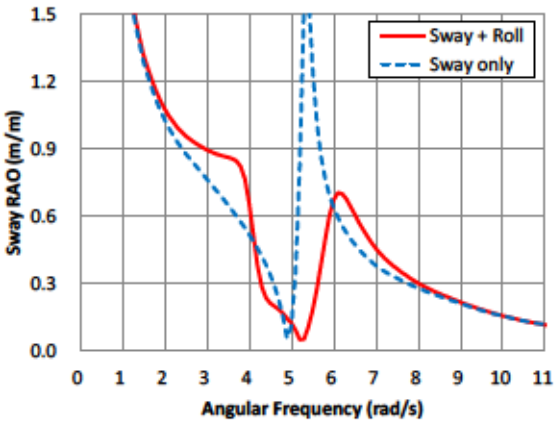

(e) Sway motion with liquid cargo effects

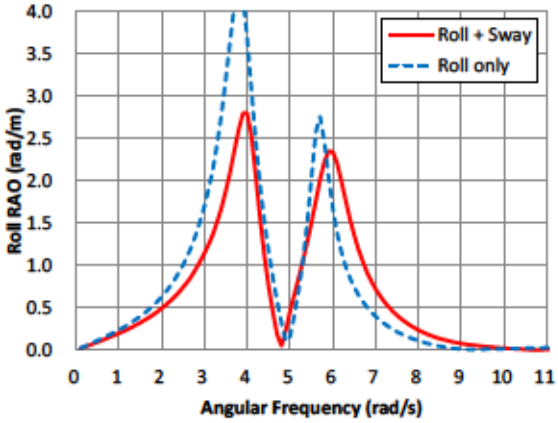

(f) Roll motion with liquid cargo effects

Figure 6.3. Sway and Roll motion with and without Liquid Cargo Effects for Case 1

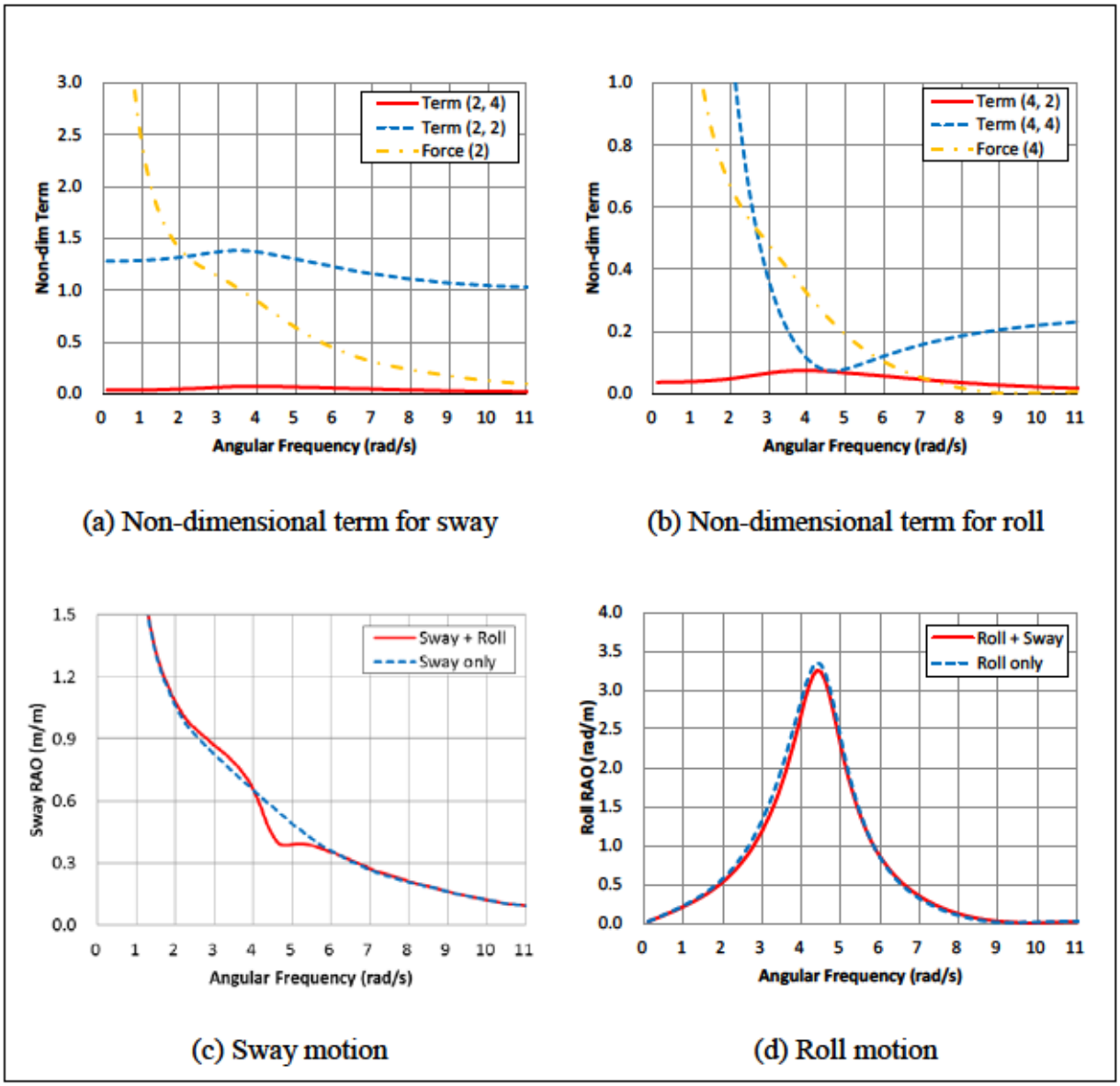

Figure 6.4. Sway and Roll motion without Liquid Cargo Effects for Case 2

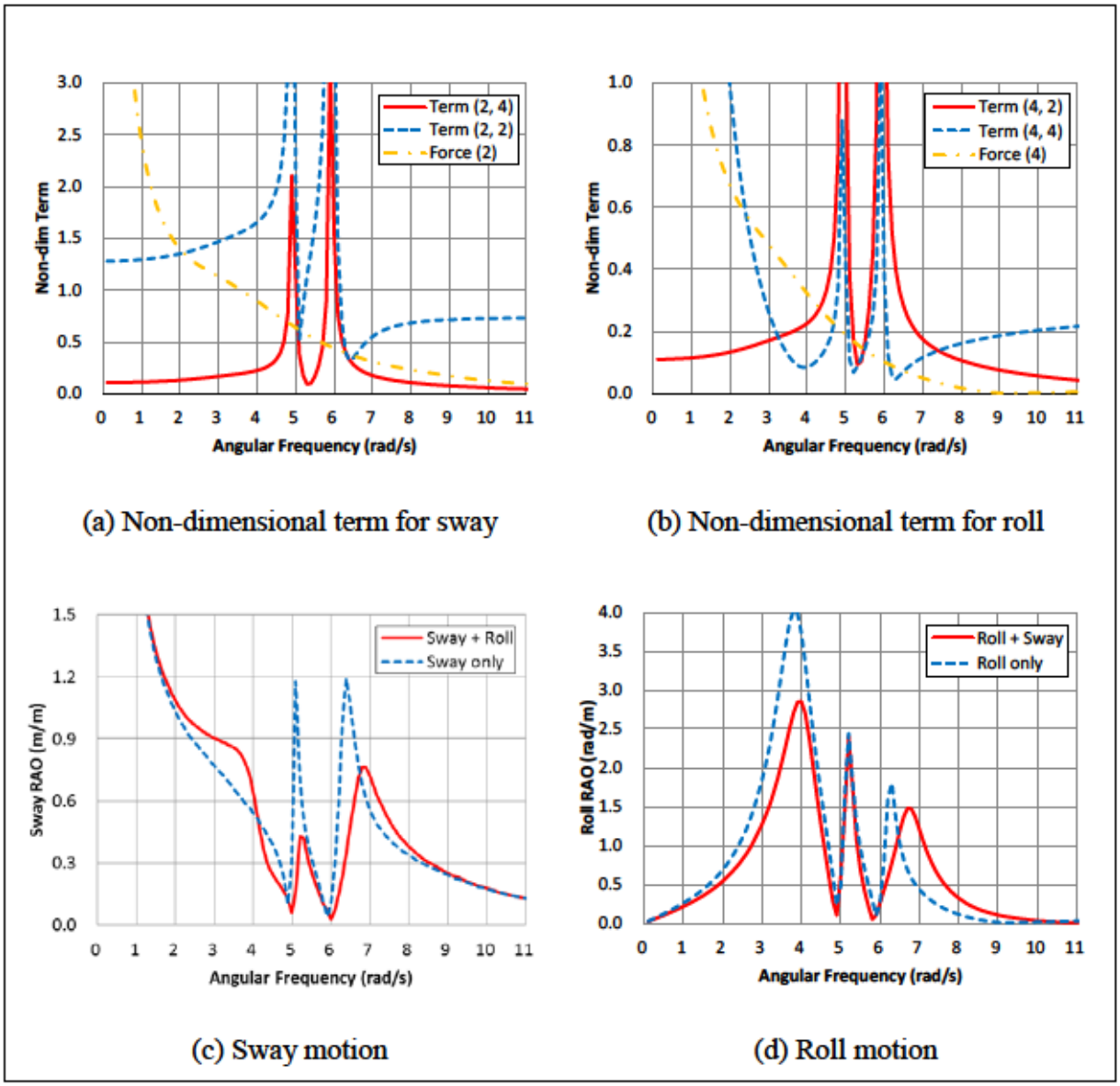

Figure 6.5. Sway and Roll motion with Liquid Cargo Effects for Case 2

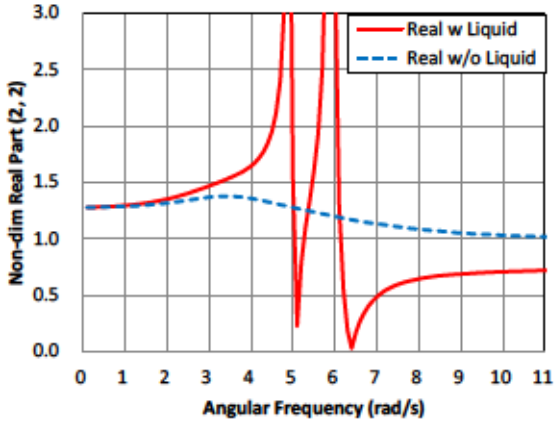

(a) Real part of the term (2, 2)

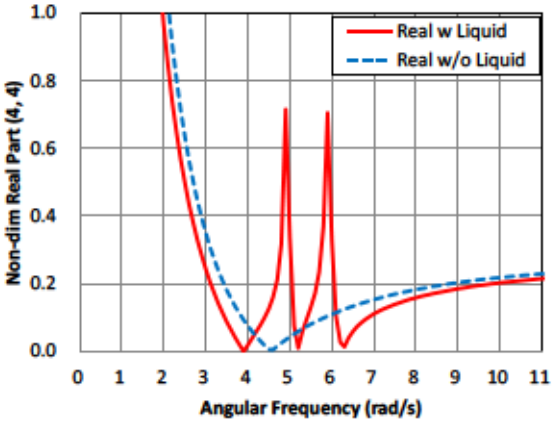

(b) Real part of the term (4, 4)

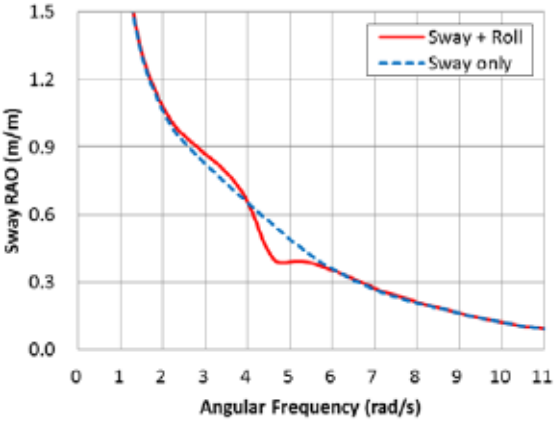

(c) Sway motion without liquid cargo effects

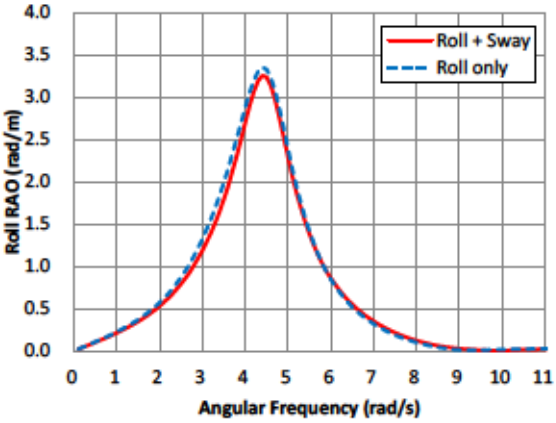

(d) Roll motion without liquid cargo effects

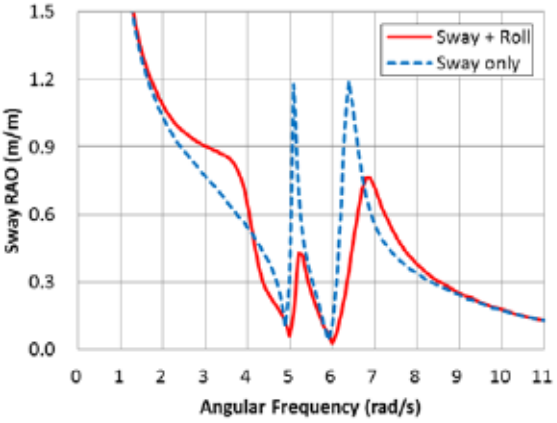

(e) Sway motion with liquid cargo effects

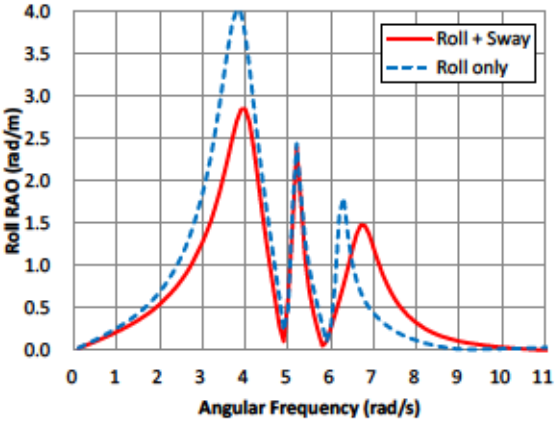

(f) Roll motion with liquid cargo effects

Figure 6.6. Sway and Roll motion with and without Liquid Cargo Effects for Case 2

6.3 FLNG with Rectangular Tanks

This chapter addresses the effect of the liquid cargo on the sway and roll motion of the FLNG stated in the chapter 5.3.

The first point of consideration is the sway-roll coupling affected by the liquid cargo effects. The sway and roll affect each other and the degree of sway-roll coupling is represented by the terms, A^{24} and A^{42}.

Figures 6.7 and 6.8 show the non-dimensional absolute of the terms, A^{22}, A^{24}, $A^{42}$and A^{44}, non-dimensional exciting forces, $F_2{}'$ and $F_4{}'$, RAOs of sway and roll excluding and including the liquid cargo effects in tanks for the loading condition of 15%, respectively. Two (2) RAOs are presented: one is obtained with the sway-roll coupling and the other is obtained without the coupling.

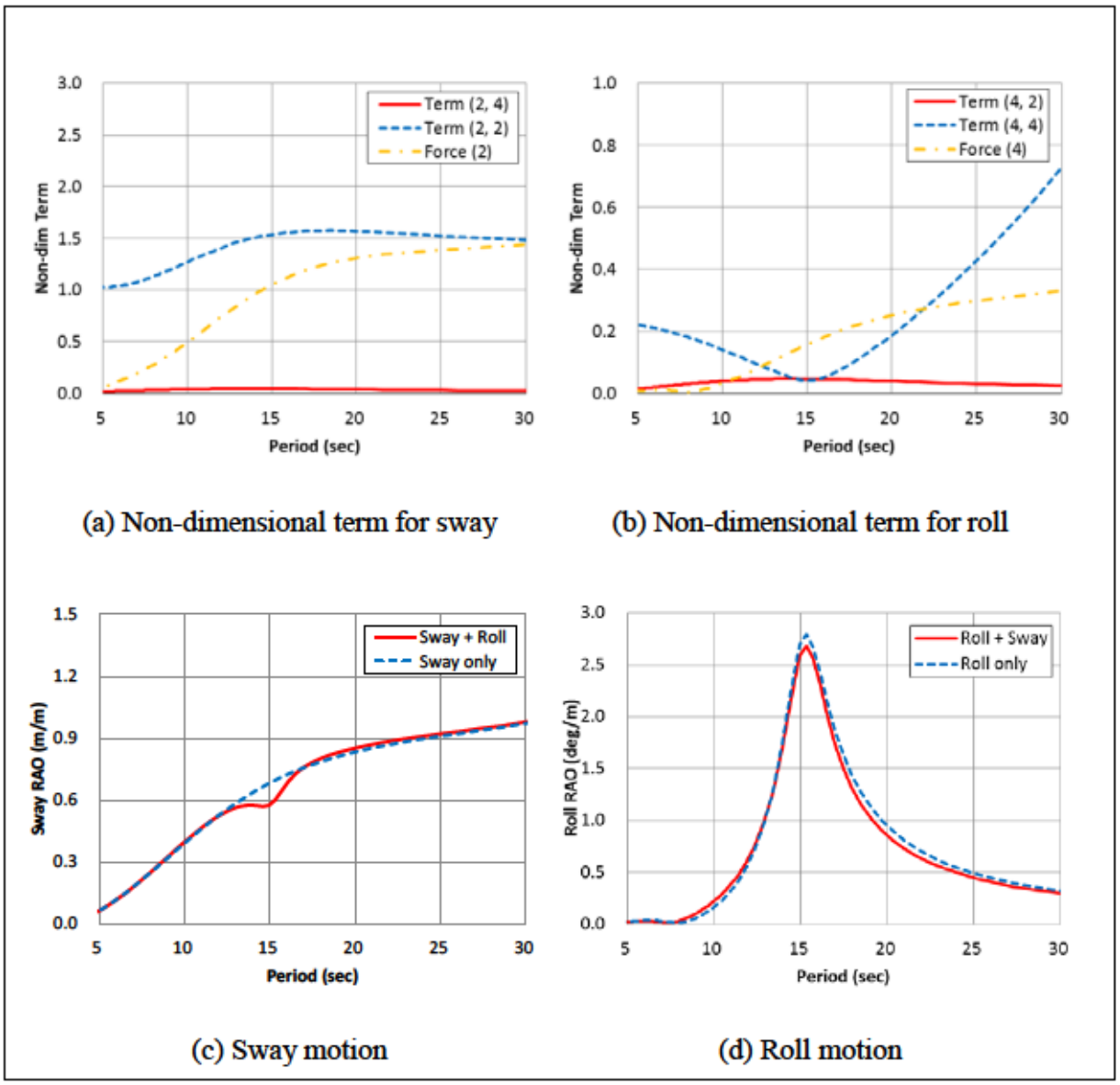

Figure 6.7. Sway and Roll motion without Liquid Cargo Effects for Loading Condition of 15%

For the FLNG motion without the liquid cargo effects in tanks, the sway-roll coupling is not significant as shown in Figure 6.7. The $A^{24}$and A^{42} terms [solid line in (a) and (b)] are kept small relative to the other terms in all the period range and the RAOs of sway and roll are almost the same regardless of the sway-roll coupling [(c) and (d)].

When the liquid cargo effects in tanks are added as shown in Figure 6.8, the $A^{24}$and A^{42} terms [solid line in (a) and (b)] become large in the whole period range, especially around the sloshing natural period. As a result, the sway-roll coupling is enhanced. It is essential to appreciate this fact in order to understand the coupled sway and roll motion with the liquid cargo effects.

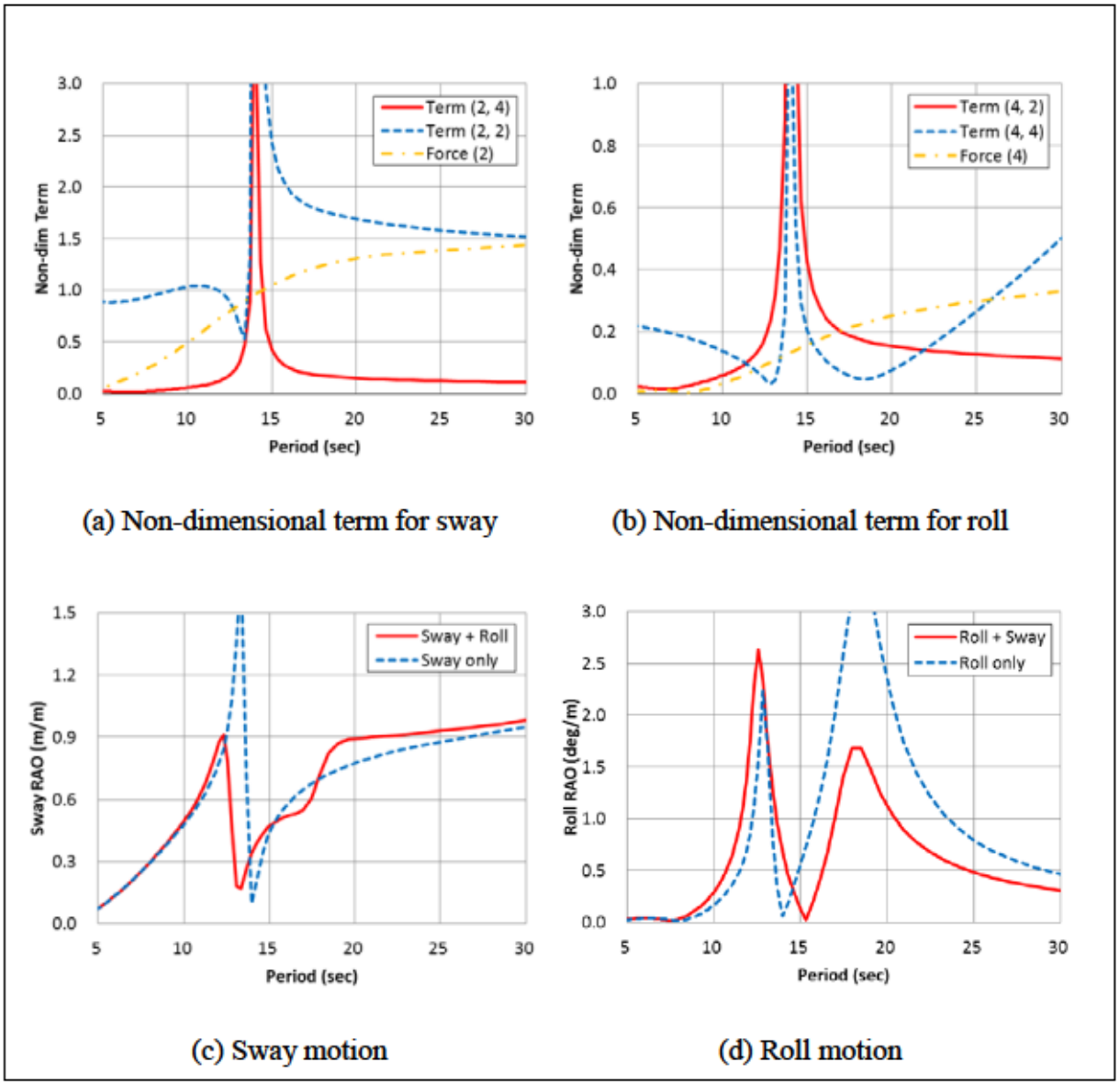

Figure 6.8. Sway and Roll motion with Liquid Cargo Effects for Loading Condition of 15%

The second point of consideration is on the terms which provide major contribution towards sway and roll motions.

The term R^{22}, having major contribution towards the sway motion, is characterized by the mass. As shown in Figure 6.9 (a), the term R^{22} without liquid [dotted line in (a)] does not varies significantly. When the liquid cargo effects are considered, it varies significantly due to sloshing in tanks [solid line in (a)]. It becomes extremely large at the sloshing natural period, 14.0 sec; the decoupled sway motion becomes very small [dotted line in (e)]. In the period shorter than the sloshing natural period, the term R^{22} changes rapidly from the extremely large value to zero (0) at 13.4 sec, where the local peak of the decoupled sway motion is observed [dotted line in (e)].
Due to strong coupling with roll motion as shown in Figure 6.8 (a), these extreme sway motions are moderated and the corresponding period is shifted [solid line in (e)].

The term R^{44}, having major contribution towards the roll motion is characterized by the mass inertia and the restoring moment. As shown in Figure 6.9 (b), the term R^{44} without liquid [dotted line in (b)] takes zero (0) at the period, 15.2 sec and a roll resonant peak is observed [dotted line in (d)].
When the liquid cargo effects are considered, it has zero (0) twice, at 13.0 sec and 18.4 sec [solid line in (b)]. In addition, it has a peak value at the sloshing natural period, 14.0 sec. Accordingly, the two peaks at 13.0 sec and 18.4 sec and local minimum at 14.0 sec are observed in roll motion decoupled from sway motion [dotted line in (f)].
When the coupling with sway motion is considered, the period corresponding to the peaks and the local minimum are shifted [solid line in (f)].
At this point, it is essential to appreciate that due to free surface effect, the restoring moment is smaller and as a result; roll motion decoupled from sway motion becomes larger. And then the sway coupling reduces the roll motion.

For the loading condition of 50% shown in Figures 6.10, 6.11 and 6.12, exactly the same reasoning holds; however the shape is different due to difference in the natural period and degree of influence from sloshing on roll motion. Since the degree of influence of sloshing on roll motion is not so strong, the influence of roll motion on sway motion is not significant. However, the roll motion is still affected significantly by the liquid cargo effects such as free surface effect and enhancement of the sway-roll coupling.

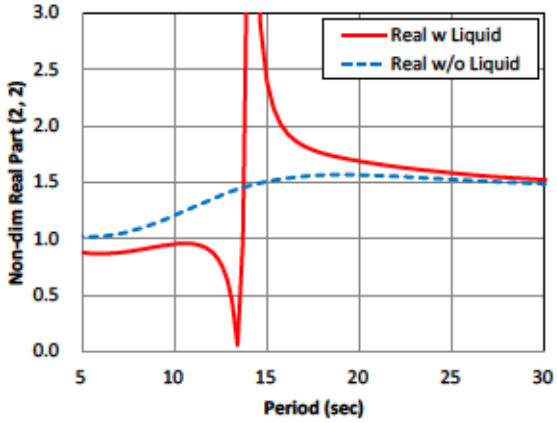

(a) Real part of the term (2, 2)

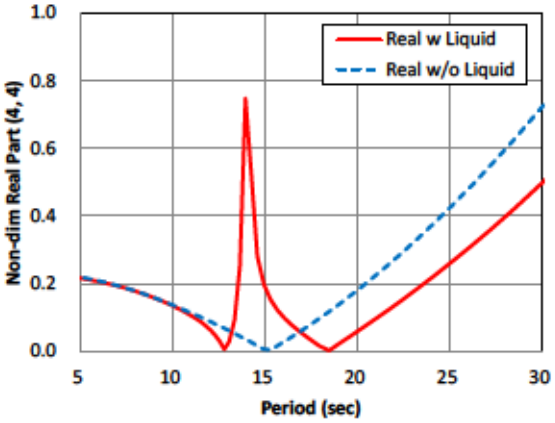

(b) Real part of the term (4, 4)

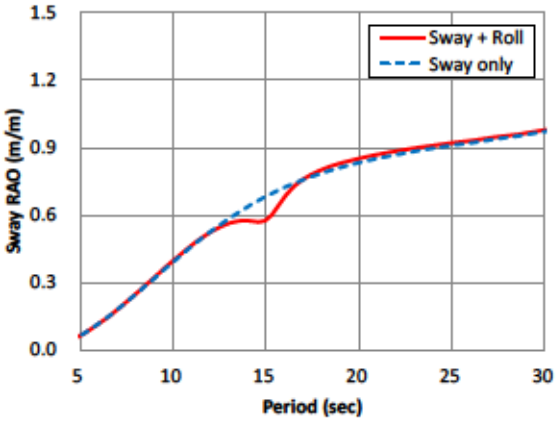

(c) Sway motion without liquid cargo effects

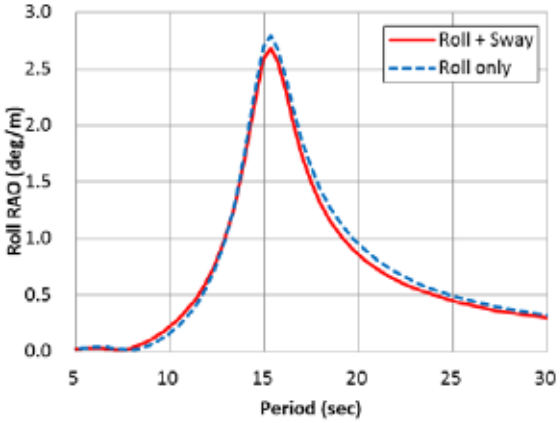

(d) Roll motion without liquid cargo effects

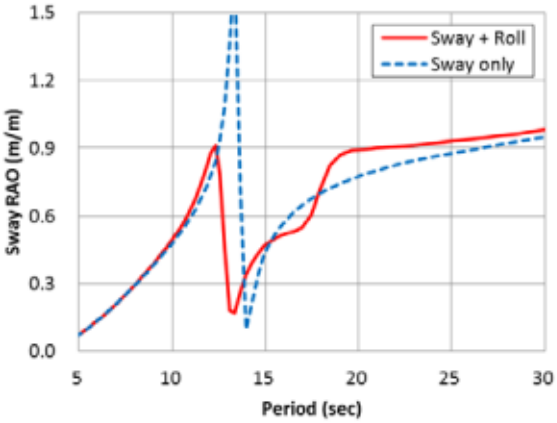

(e) Sway motion with liquid cargo effects

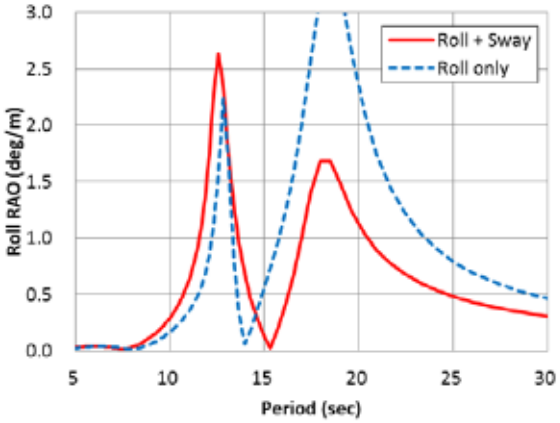

(f) Roll motion with liquid cargo effects

Figure 6.9. Sway and Roll motion with and without Liquid Cargo Effects for LC of 15%

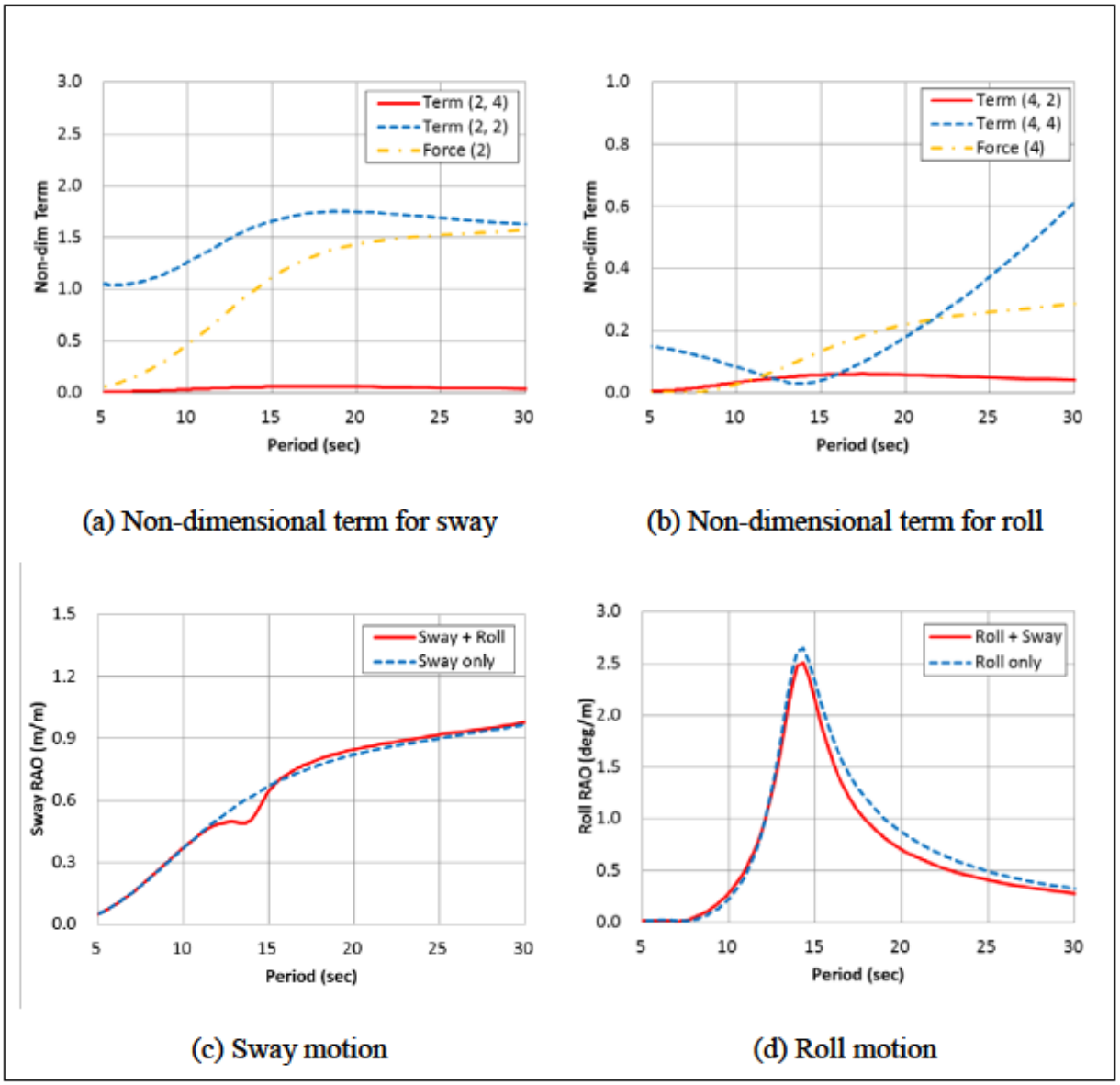

Figure 6.10. Sway and Roll motion without Liquid Cargo Effects for Loading Condition of 50%

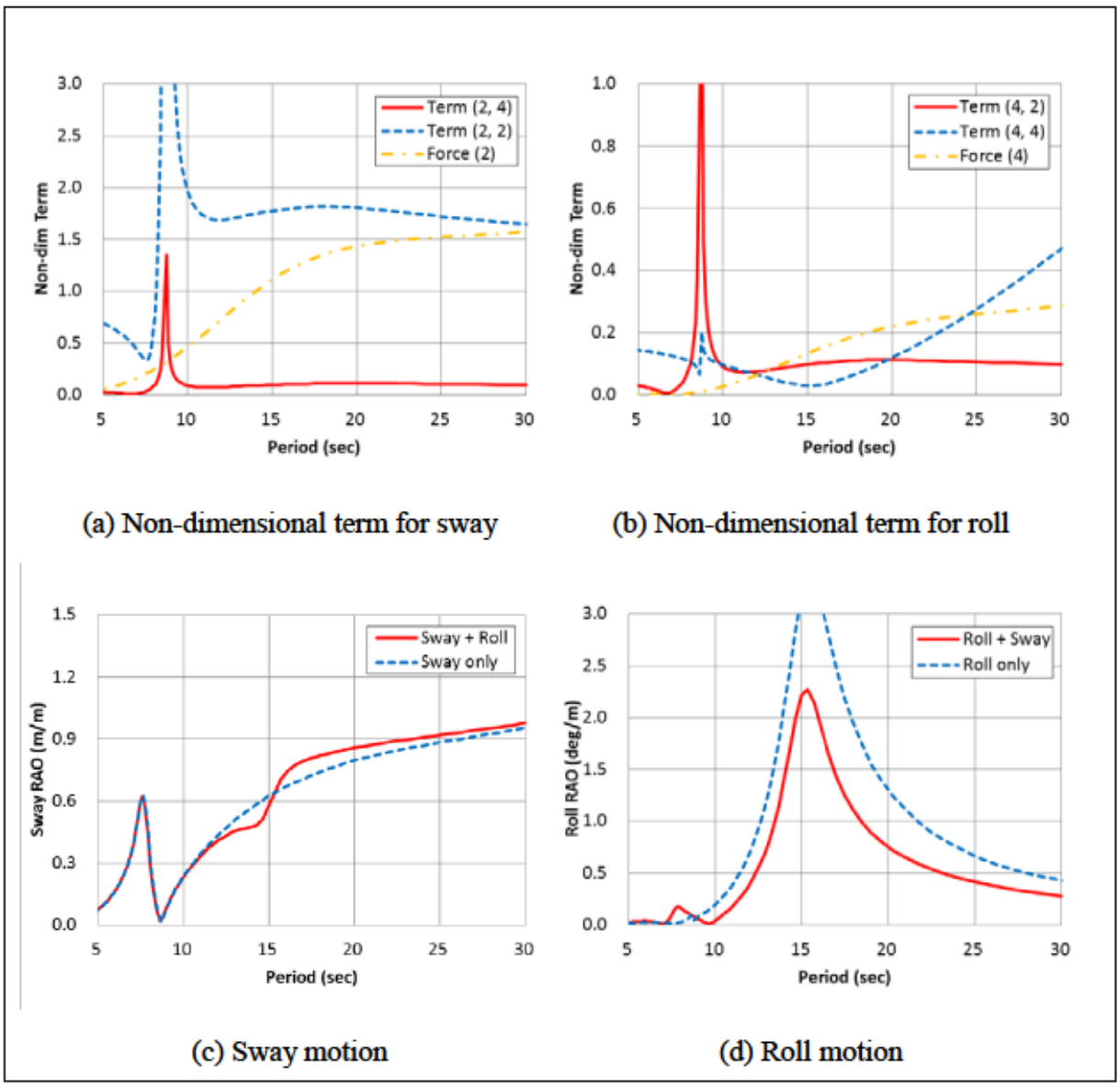

Figure 6.11. Sway and Roll motion with Liquid Cargo Effects for Loading Condition of 50%

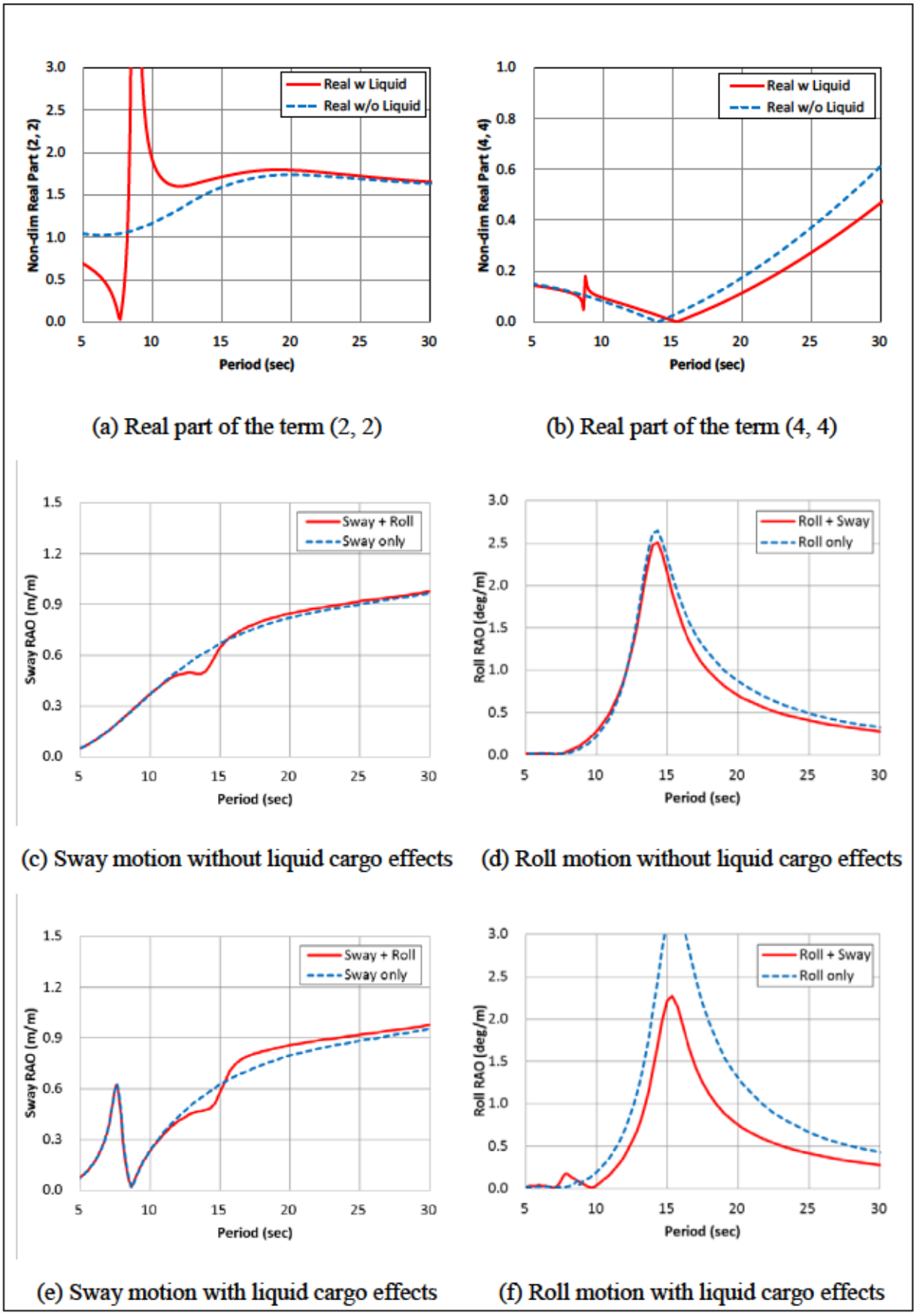

(a) Real part of the term (2, 2)

(b) Real part of the term (4, 4)

(c) Sway motion without liquid cargo effects

(d) Roll motion without liquid cargo effects

(e) Sway motion with liquid cargo effects

(f) Roll motion with liquid cargo effects

Figure 6.12. Sway and Roll motion with and without Liquid Cargo Effects for LC of 50%

The third point of consideration is the degree of influence of sloshing on roll motion.

In order to understand the different behaviour of roll motion between the loading conditions of 15% and 50%, the degree of influence of sloshing on roll motion should be investigated.
Figure 6.13 shows that the peak period of the term R^{22} [solid line in (a) and (c)] is shifted according to the sloshing natural period of the liquid cargo in tanks but the magnitude of it is at the same level in both the loading conditions of 15% and 50%. As a result, the peak and the local minimum of the sway motion is shifted but appeared significantly in both the loading conditions [dotted and solid lines in (b) and (d)].

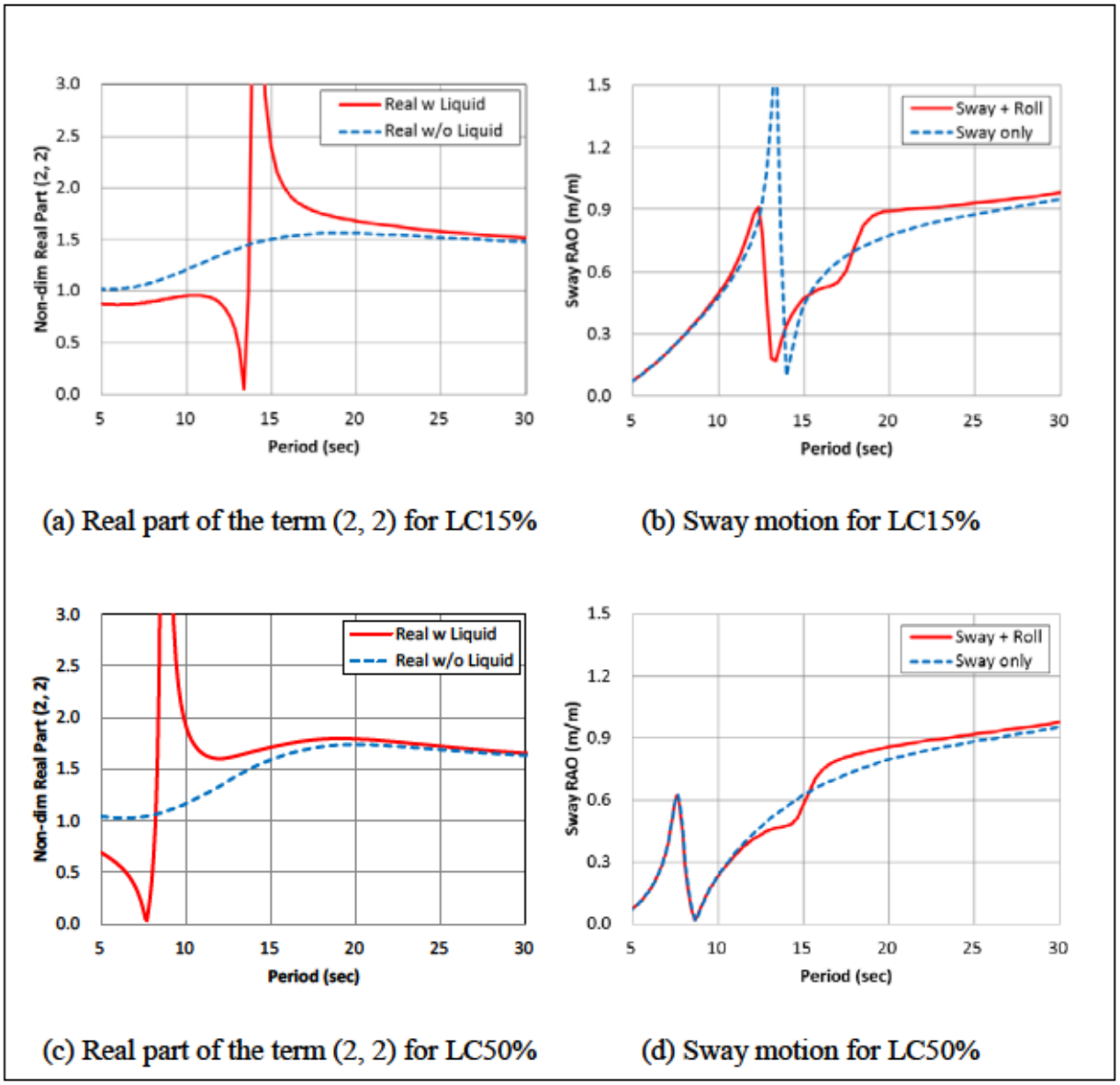

Figure 6.13. Sway motion with Liquid Cargo Effects

On the other hand, Figure 6.14 shows that the magnitude of the term R^{44} [solid line in (a) and (c)] is significantly reduced in the loading condition of 50%, and as a result the influence of sloshing on roll motion is reduced [dotted and solid lines in (d)].

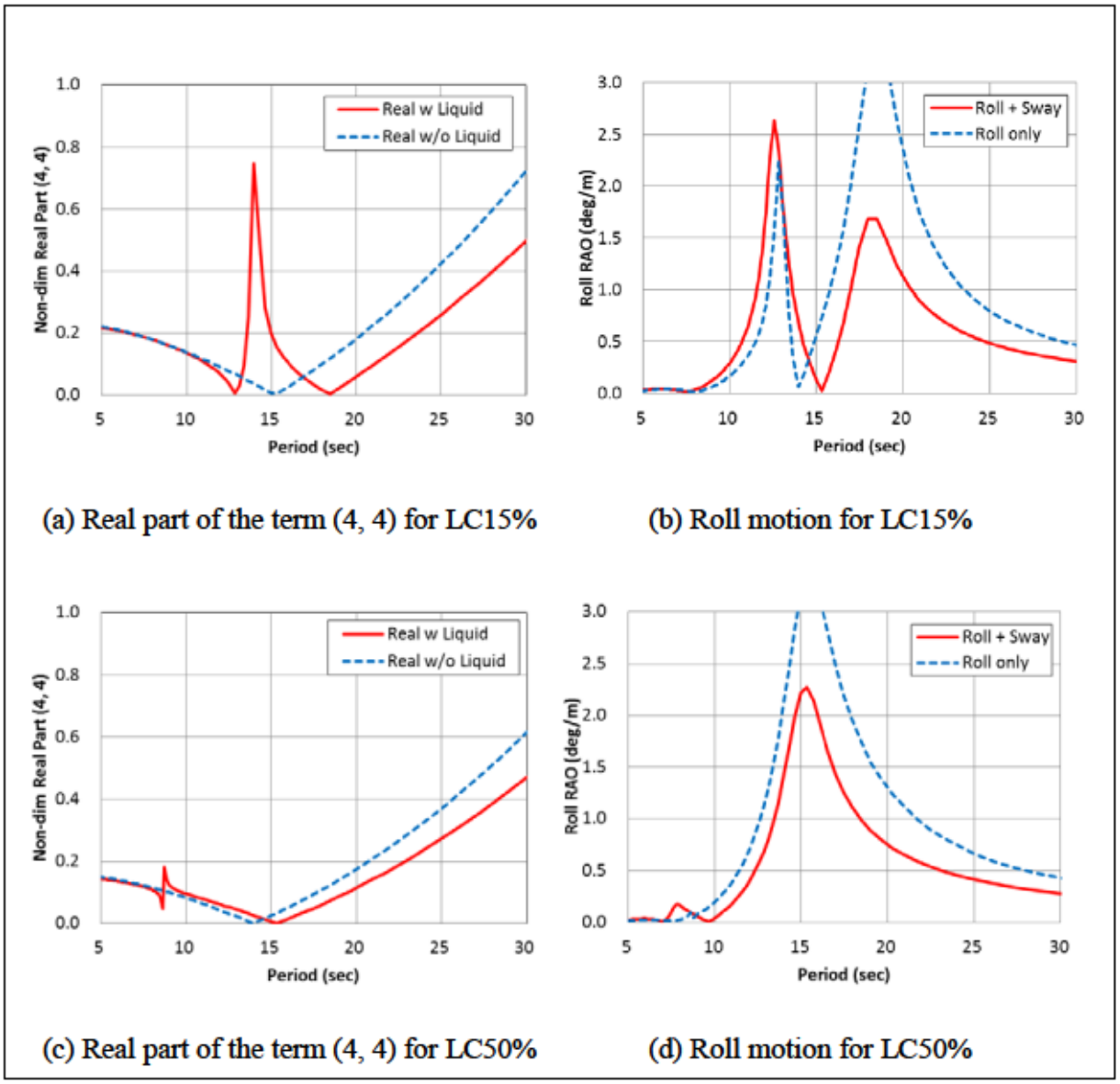

(a) Real part of the term (4, 4) for LC15%

(b) Roll motion for LC15%

(c) Real part of the term (4, 4) for LC50%

(d) Roll motion for LC50%

Figure 6.14. Roll motion with Liquid Cargo Effects

The degree of influence of sloshing on roll motion for the different loading condition can be explained using the mechanical model.

The vertical distance of the liquid slosh mass to COG of the floating body affects the degree of influence of sloshing on roll motion. Figure 6.15 shows the vertical position of the COG of floating body, liquid in tank and liquid slosh mass. The first slosh mass height from the tank bottom, H_1' the vertical distance between COGs of the floating body and tank liquid, Z_0 and the vertical distance from COG of the floating body to the first slosh mass, Z_1 are expressed as below:

$$H_1^{'} = \frac{h}{2} + H_1$$

$$Z_0 = z_{TG} - z_G$$

$$Z_1 = z_{TG} - z_G + H_1$$

where, s, h, H_1, z_{TG} and z_G are the relative location from tank bottom to the COG of floating body, liquid height, the first slosh mass height relative to the COG of liquid in tank, the vertical location of the COG of liquid in tank and floating body, respectively.

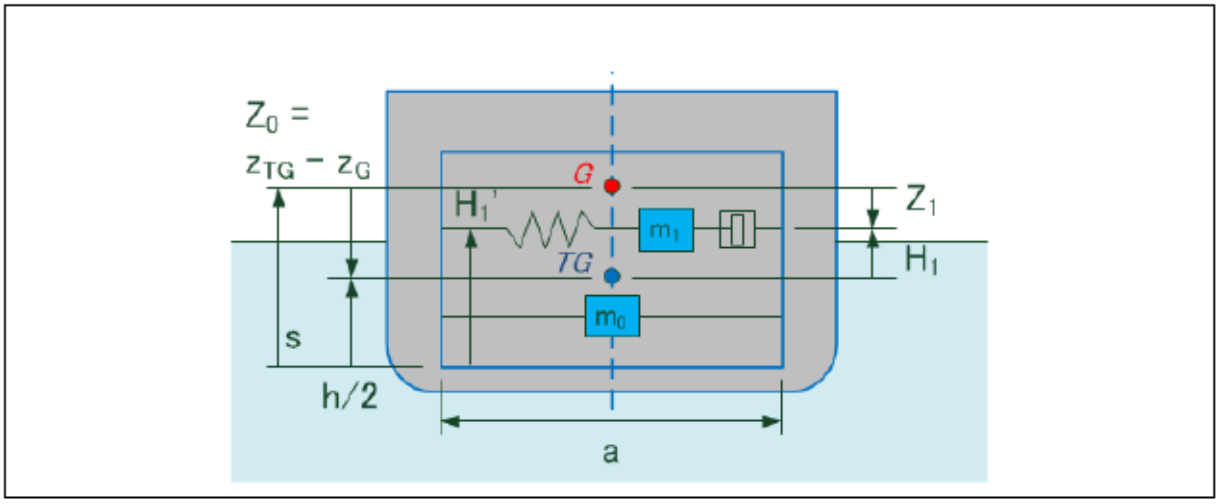

Figure 6.15. Vertical Position of COGs and Liquid Mass

The sloshing influence factor (SIF) for the tank is defined as follows:

$$SIF = -I_{xd} + m_T\left[A_y\left(z_{TG} - z_G\right)^2 + 2hB_y\left(z_{TG} - z_G\right) + h^2 C_y\right]$$

The SIF indicates the degree of influence of sloshing on roll motion considering the difference in the term R^{44} with and without liquid cargo effect and eliminating the free surface effect that is independent of vertical position and the liquid filling level.
The SIF is divided into two parts, frequency independent and frequency dependent.

$$SIF_{FI} = -I_{xd} + m_T\left[2h\frac{m_{y1}}{m_T}\frac{g}{h\omega_{y1}^2}\left(z_{TG}-z_G\right)+h^2\frac{m_{y1}}{m_T}\frac{g}{h\omega_{y1}^2}\left(\frac{2H_{y1}}{h}+\frac{g}{h\omega_{y1}^2}\right)\right]$$

$$= -I_{xd} + \frac{2m_{y1}g}{\omega_{y1}^2}\left(z_{TG}-z_G+H_{y1}+\frac{g}{2\omega_{y1}^2}\right)$$

$$SIF_{FD} = m_T\left[\frac{m_{y1}}{m_T}\left(z_{TG}-z_G\right)^2+2h\frac{m_{y1}}{m_T}\left(\frac{H_{y1}}{h}+\frac{g}{h\omega_{y1}^2}\right)\left(z_{TG}-z_G\right)+h^2\frac{m_{y1}}{m_T}\left(\frac{H_{y1}}{h}+\frac{g}{h\omega_{y1}^2}\right)^2\right]\frac{\omega^2}{\omega_{y1}^2-\omega^2}$$

$$= m_{y1}\left[\left(z_{TG}-z_G\right)^2+2\left(H_{y1}+\frac{g}{\omega_{y1}^2}\right)\left(z_{TG}-z_G\right)+\left(H_{y1}+\frac{g}{\omega_{y1}^2}\right)^2\right]\frac{\omega^2}{\omega_{y1}^2-\omega^2}$$

$$= m_{y1}\left(z_{TG}-z_G+H_{y1}+\frac{g}{\omega_{y1}^2}\right)^2\frac{\omega^2}{\omega_{y1}^2-\omega^2}$$

The non-dimensional coefficient of frequency dependent part of SIF expressed below is used for the discussion hereafter. Since the term $\frac{\omega^2}{\omega_{y1}^2-\omega^2}$ is significantly large at around resonance, SIF_{FD} part becomes dominant in SIF.

$$SIF_{FD\_non-dim\_coefficient} = \frac{m_{y1}\left(z_{TG}-z_G+H_{y1}+\frac{g}{\omega_{y1}^2}\right)^2}{\rho_c a^4 b}$$

where ρ_c and b are fluid density of the liquid in tank and tank length, respectively.

The non-dimensional coefficient of frequency dependent part of SIF is plotted in Figure 6.16 with Z_1/a in abscissa for graphs (a) to (e) and Z_0/a for graph (f).Solid blue dots in Figure 6.16 represent FLNG loading conditions of 15% and 50%. The non-dimensional coefficient SIF for LC15% is larger than that of LC50%, which represents that the degree of influence of sloshing on roll motion is significant in LC15%, but not in LC50%.

As shown in graph (c) of Figure 6.16, single polynomial relationship is observed for the cases where h/a is greater than 0.15. This means that the degree of influence of sloshing on roll motion depends solely on the relative location of slosh mass and COG of the floating body where the liquid filling level is intermediate or deep.

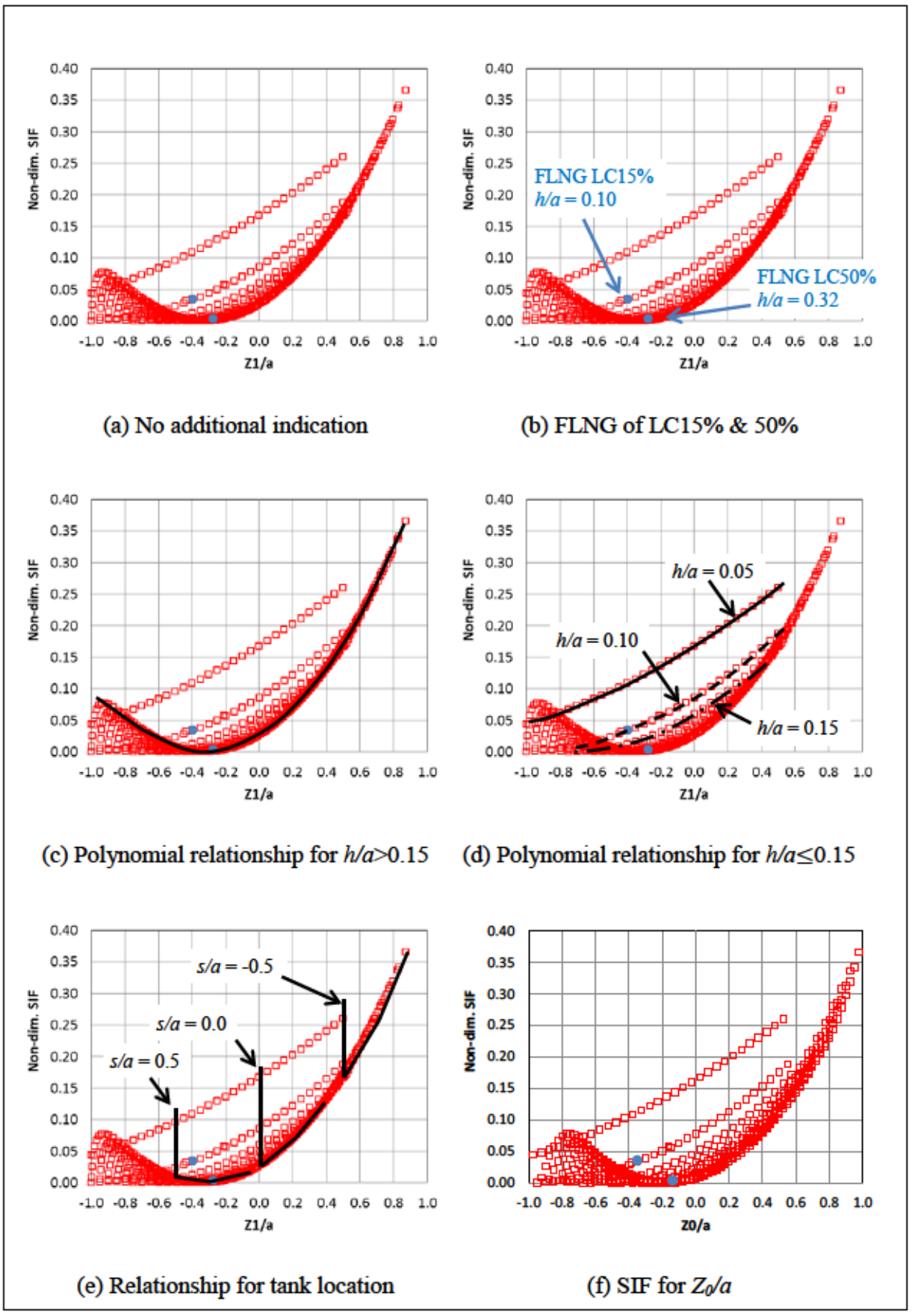

(a) No additional indication

(b) FLNG of LC15% & 50%

(c) Polynomial relationship for $h/a>0.15$

(d) Polynomial relationship for $h/a\leq0.15$

(e) Relationship for tank location

(f) SIF for Z_0/a

Figure 6.16. Sloshing Influence Factor

As shown in graph (d) of Figure 6.16, the polynomial relationship is still observed but strongly dependent on the liquid filling level for the cases where h/a is equal to or less than 0.15.
The graph (e) of Figure 6.16 indicates the series of $s/a = 0.5$, $s/a = 0.0$ and $s/a = -0.5$ with different liquid filling level. The positive values of s/a indicates that the COG of floating body is above the tank bottom whereas the negative values indicates that the COG is below the tank bottom. This graph shows that greater influence of sloshing on roll motion is expected when the tank is located above the COG of floating body like Molin barge.
When Z_1/a is in the range between -0.5 and -0.2 and h/a is greater than 0.15, the degree of sloshing on roll motion is negligible or small.
When Z_1/a is out of the range between -0.5 and -0.2 or h/a is equal to or less than 0.15, the degree of sloshing on roll motion is significant.
It is to be noted that the magnitude of the non-dimensional coefficient SIF has no effect on the magnitude of the roll motion affected by sloshing. The large SIF does not cause large roll motion. The magnitude of the roll motion depends on mass inertia, restoring, potential and viscous damping and moment due to incident wave.

According to this investigation, the tank location typically adopted in FLNG (the tank is located below the COG of floating body) is found to be good in reducing the influence of sloshing on roll motion. It is expected that the significant influence on roll motion is observed only when the liquid in the tank is low.

For preliminary assessment of influence of sloshing on roll motion, Z_0/a instead of Z_1/a can be used as shown in Figure 6.16 (f). Z_0/a does not include slosh mass height, H_1 and it can be calculated by using only the COG of floating body and liquid height in tank.
When Z_0/a is in the range between -0.4 and -0.1 and h/a is greater than 0.15, the degree of sloshing on roll motion is negligible or small.

6.4 Summary of Liquid Cargo Effects on Floating Body Motion

Based on the materials presented in this chapter, the influence of liquid sloshing on the barge and FLNG motion is concluded as follows:

- The liquid cargo effects enhance the sway-roll coupling. The absolute of the non-dimensional terms $A^{24}$and A^{42} represents the degree of the sway-roll coupling.
- The sway motion affected by liquid cargo effects is analysed focusing on the non-dimensional term R^{22} and sway-roll coupling. An explanation on observation of the peak and the local minimum in sway RAO due to the effect of liquid cargo is provided rationally.
- The roll motion affected by liquid cargo effects is analysed focusing on non-dimensional term R^{44} and sway-roll coupling. An explanation on observation of the peaks and the local minimum in roll RAO due to the effect of liquid cargo is provided rationally.
- The degree of influence of sloshing on roll motion corresponding to the relative vertical location of tank and the fraction of liquid level in tank is investigated. The mechanical model provides quantitative estimates of the influence.
- The analysis is performed for two independent research results, the barge motion by Molin et al and the FLNG motion by Rocha et al. The influence of liquid sloshing observed in both of them can be explained using the same approach with the mechanical model.

7. Case Study for FLNG

7.1 General

In order to demonstrate the usefulness of the mechanical model in the FLNG development and basic design, case study for FLNG stated in the chapter 5.3 is performed.

7.2 Double-row Tank Arrangement

The "double-row" tank arrangement is adopted in FLNG in order to reduce the influence of sloshing [3] and its effect on FLNG sway and roll motions is addressed in this chapter.

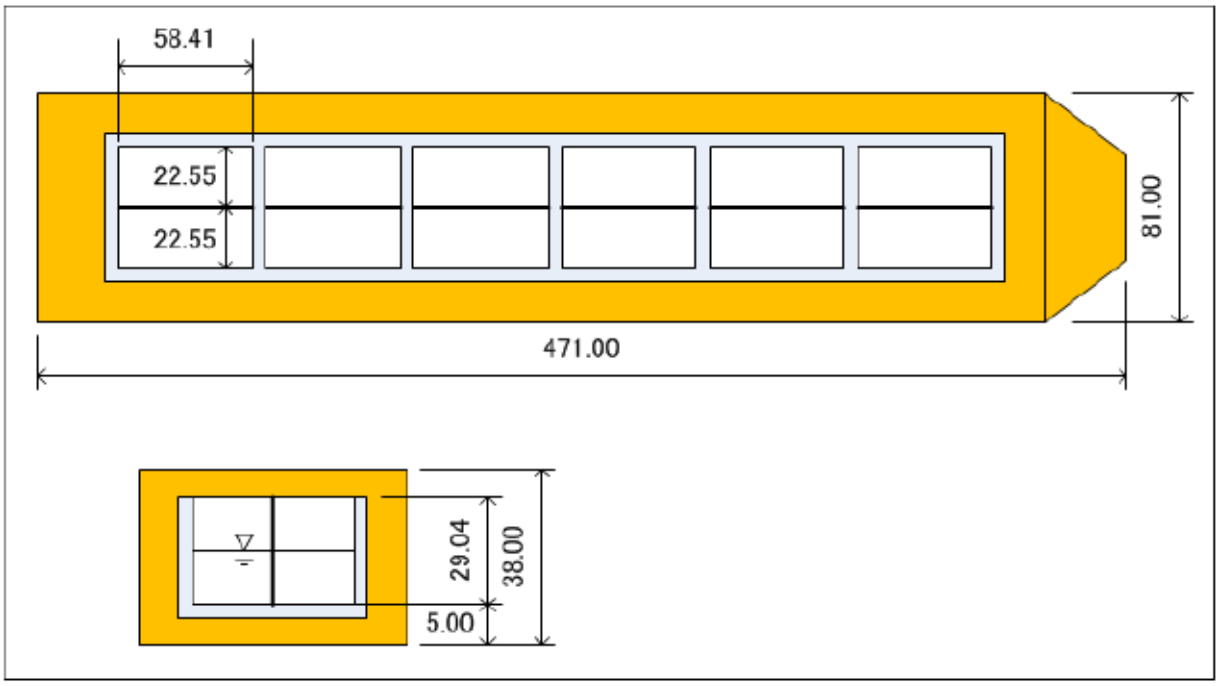

Figure 7.1. Tank Arrangement of FLNG Model for Double-row Case (unit: m)

Table 7.1. Loading Conditions for Double-row Case

Draft	12.22 m	16.60 m
Water level in tanks	4.36 m (15%)	14.52 m (50%)
Displacement volume	432,364 m^3	591,683 m^3
KG	22.99 m	18.53 m
Roll radius of gyration relative to COG of FLNG	31.86 m	26.02 m
GMt	28.62 m	23.19 m
Roll natural period without liquid cargo effects (solid cargo)	15.2 s	14.0 s
Sloshing natural period of tank	7.3 s	5.5 s

For this case, the six (6) tanks split into two as shown in Figure 7.1 are considered. As shown in Table 7.1, the displacement, KG, roll radius of gyration and GMt are same as the original in Table 5.7, but the sloshing natural period of tank becomes shorter since the tank width becomes shorter.

Figures 7.2 and 7.3 show the results of sway and roll motion. Corresponding to the change in sloshing natural period of tank, the peak and the local minimum of the sway motions are shifted. For the roll motion, the influence of sloshing on roll motion is reduced significantly.

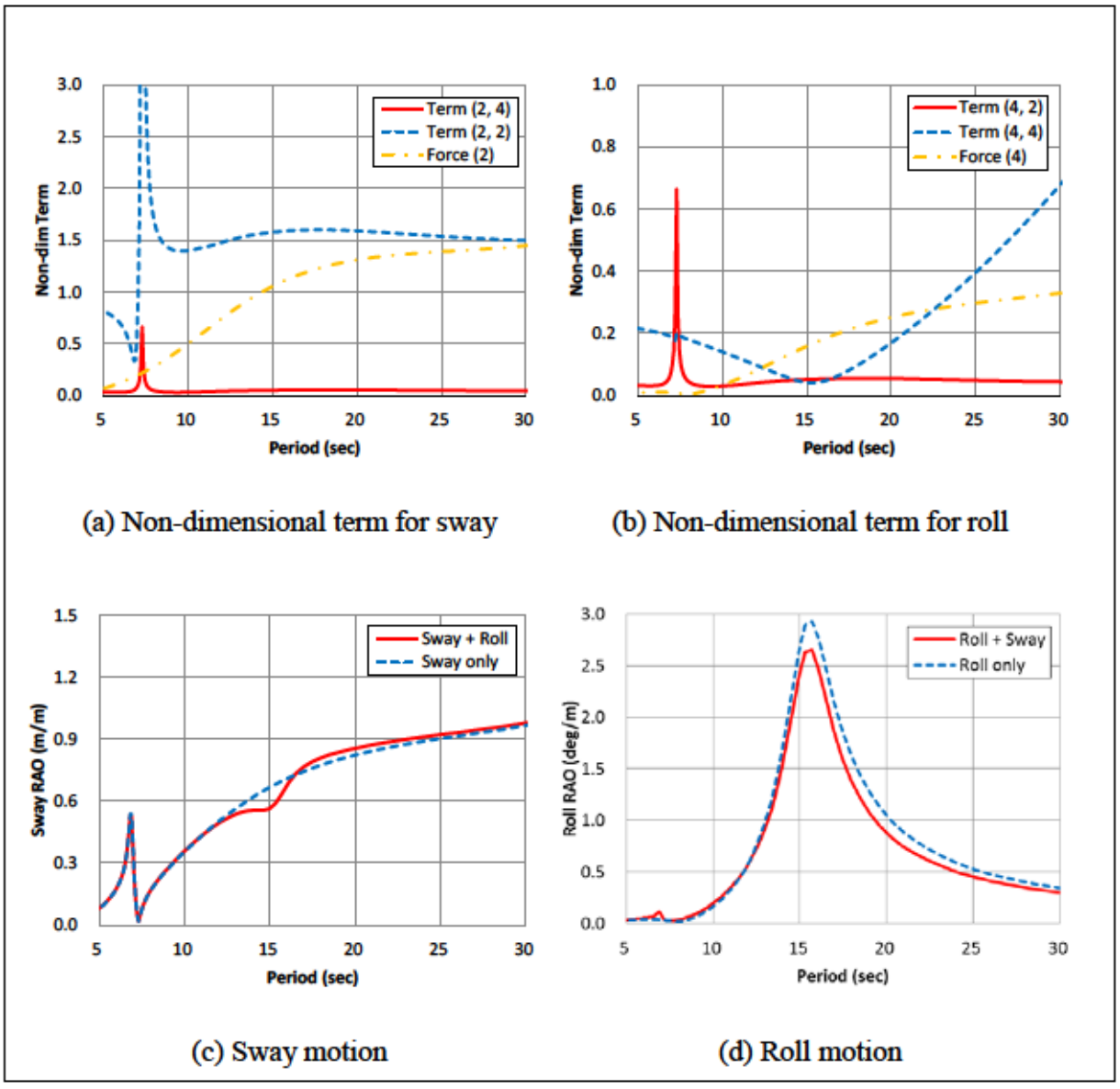

Figure 7.2. Sway and Roll motion with Liquid Cargo Effects for LC of 15% Double-row Case

As shown in Figure 7.4, the sloshing influence factor is changed corresponding to changing *a* from 45.10 m to 22.55 m.

For the loading condition of 15%, SIF becomes small and as a result, the influence of sloshing on roll motion is reduced significantly. For the loading condition of 50%, SIF and the influence of sloshing on roll motion are kept small.

According to this study, it is confirmed that the double-row tank arrangement is quite effective in reducing the influence of sloshing on motion.

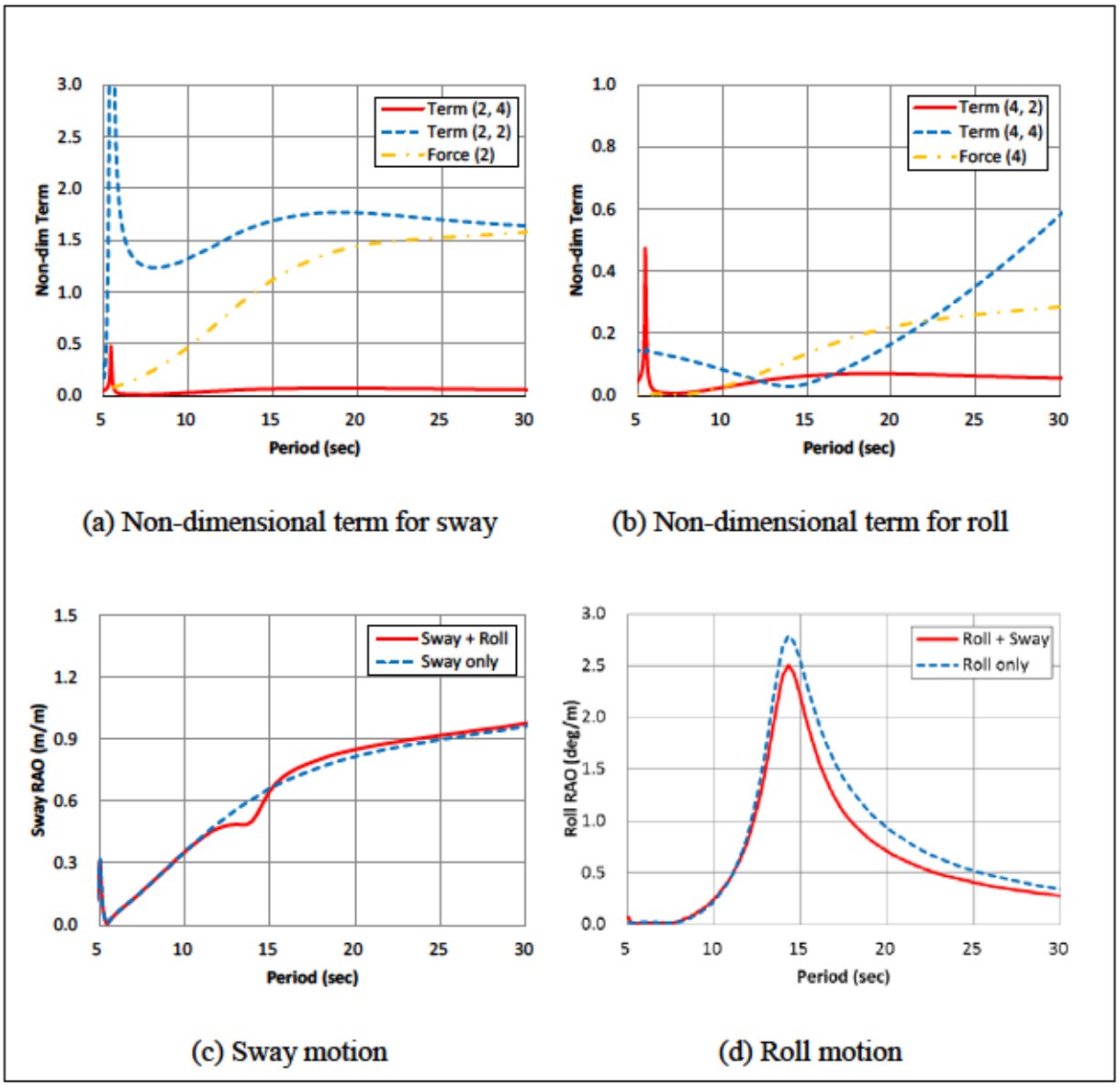

Figure 7.3. Sway and Roll motion with Liquid Cargo Effects for LC of 50% Double-row Case

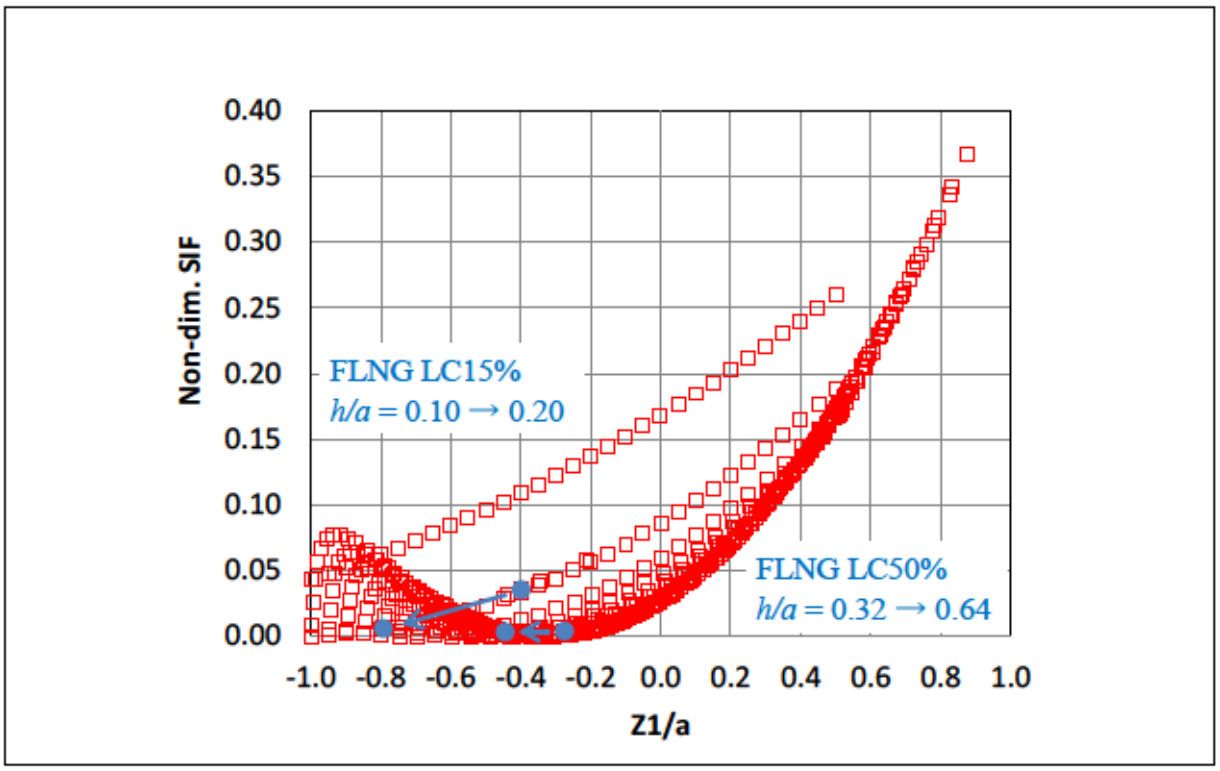

Figure 7.4. Sloshing Influence Factor for Double-row Tank Arrangement

7.3 Vertical Position of Tanks

According to the third point of consideration in chapter 6.3, vertical position of tanks affects the influence of sloshing on roll motion.

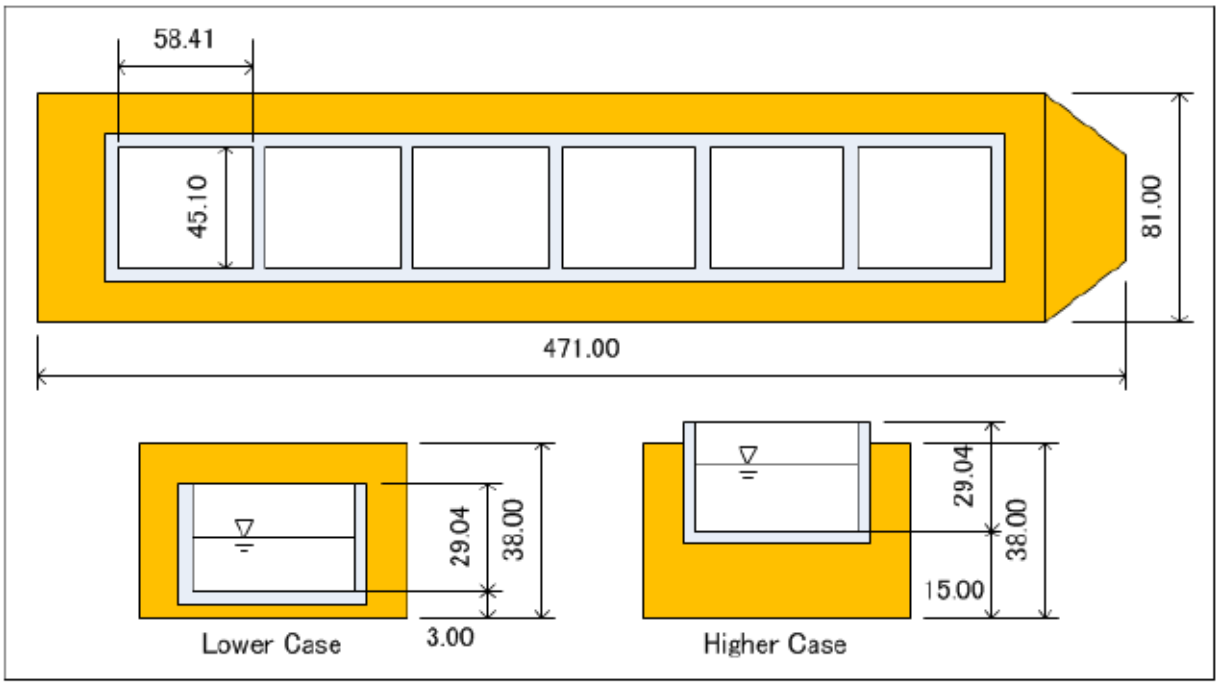

Figure 7.5. Tank Arrangement of FLNG Model Tank Vertical Position Case (unit: m)

To demonstrate this, lower and higher case loading conditions are studied. The tanks are positioned at 2 m below and 10 m above the position considered in the original case for lower and higher case respectively.
As shown in Tables 7.2 and 7.3, the displacement is same as the original in Table 5.7, but KG, roll radius of gyration and GMt are slightly changed due to change in tank's vertical position.

Firstly, change of the sloshing influence factor is investigated as shown in Figure 7.6. As the vertical position of the tank changes, Z_1/a and SIF change accordingly. Since SIF variation is not so large, the influence of sloshing on roll motion is expected to be small.

Table 7.2. Loading Conditions for Lower Case

Draft	12.22 m	16.60 m
Water level in tanks	4.36 m (15%)	14.52 m (50%)
Displacement volume	432,364 m^3	591,683 m^3
KG	22.68 m	17.75 m
Roll radius of gyration relative to COG of FLNG	32.02 m	26.22 m
GMt	28.94 m	23.97 m
Roll natural period without liquid cargo effects (solid cargo)	15.1 s	13.8 s
Sloshing natural period of tank	14.0 s	8.7 s

Table 7.3. Loading Conditions for Higher Case

Draft	12.22 m	16.60 m
Water level in tanks	4.36 m (15%)	14.52 m (50%)
Displacement volume	432,364 m^3	591,683 m^3
KG	24.59 m	22.41 m
Roll radius of gyration relative to COG of FLNG	31.27 m	25.53 m
GMt	27.03 m	19.32 m
Roll natural period without liquid cargo effects (solid cargo)	15.4 s	15.2 s
Sloshing natural period of tank	14.0 s	8.7 s

Figures 7.7 thru 7.10 show the results of sway and roll motion. Comparing the Figures 6.8 and 6.11 of the original case, no remarkable difference is observed. For the cases with the loading condition of 15%, sloshing affected the floating body motion obviously. The magnitude of the roll motion affected by sloshing, however, is not changed since the magnitude of the roll motion depends on the mass inertia, restoring, potential and viscous damping and moment due to incident wave which are not changed largely.
For the higher case with the loading condition of 50%, the influence of sloshing on roll motion can be observed [(d) in Figure 7.10]. In this case, a peak response of roll motion is observed due to greater influence of sloshing on roll motion, but it is not large due to small external force [dotted

line in (d)]. The peak response of roll motion at the period within the range of 7 to 10 second is mainly due to sway-roll coupling enhanced by sloshing.
Note that this higher case is not realistic in FLNG. The unrealistic tank position is adopted in this case study in order to highlight the degree of influence of sloshing.

According to this study, the tank location typically adopted in FLNG is found to be a good arrangement with sufficient margin in deducing the influence of sloshing on roll motion.

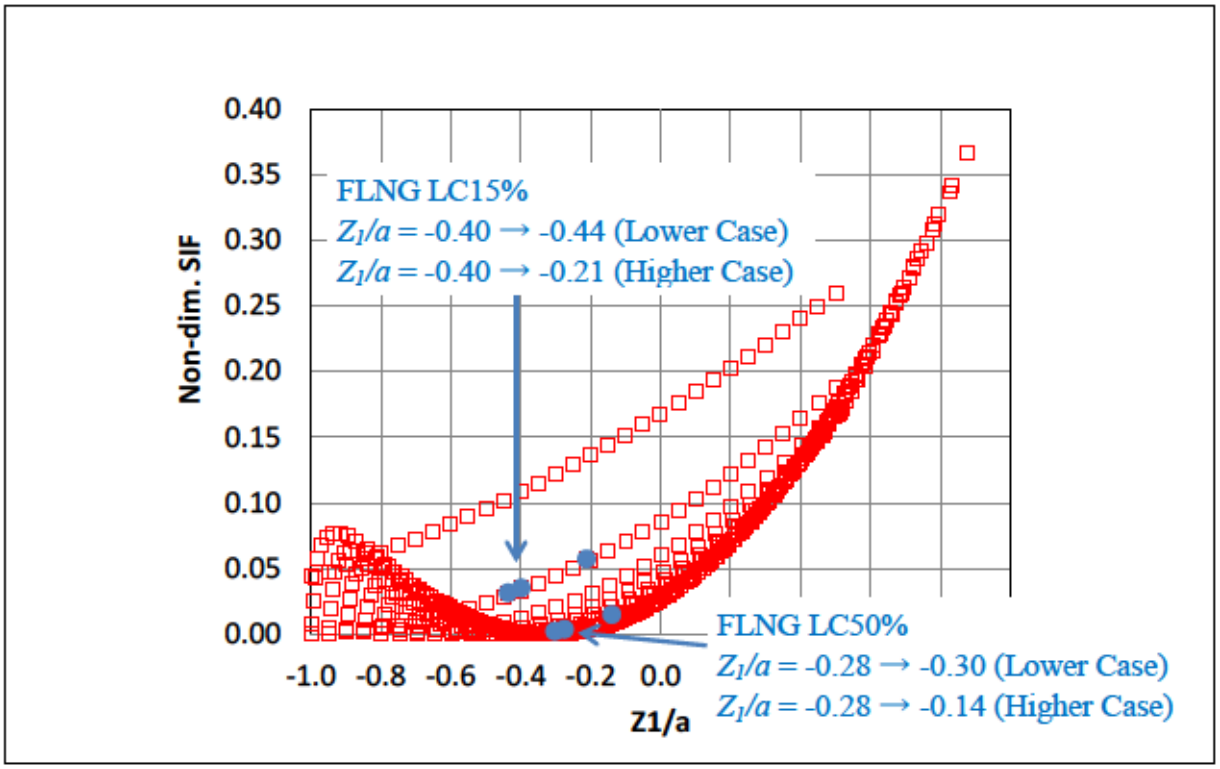

Figure 7.6. Sloshing Influence Factor for Tank Vertical Position Case

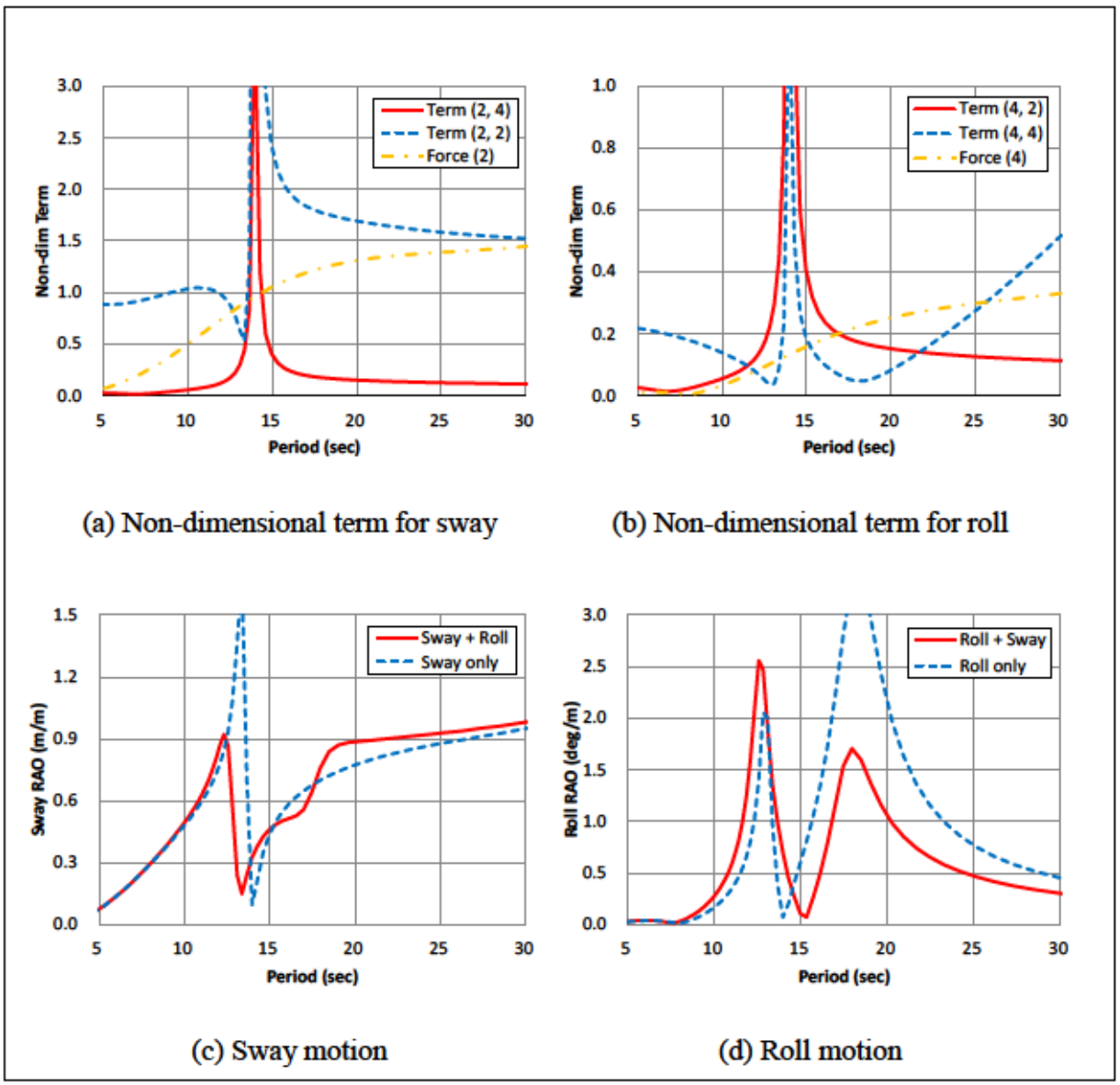

Figure 7.7. Sway and Roll motion with Liquid Cargo Effects for LC of 15% Lower Case

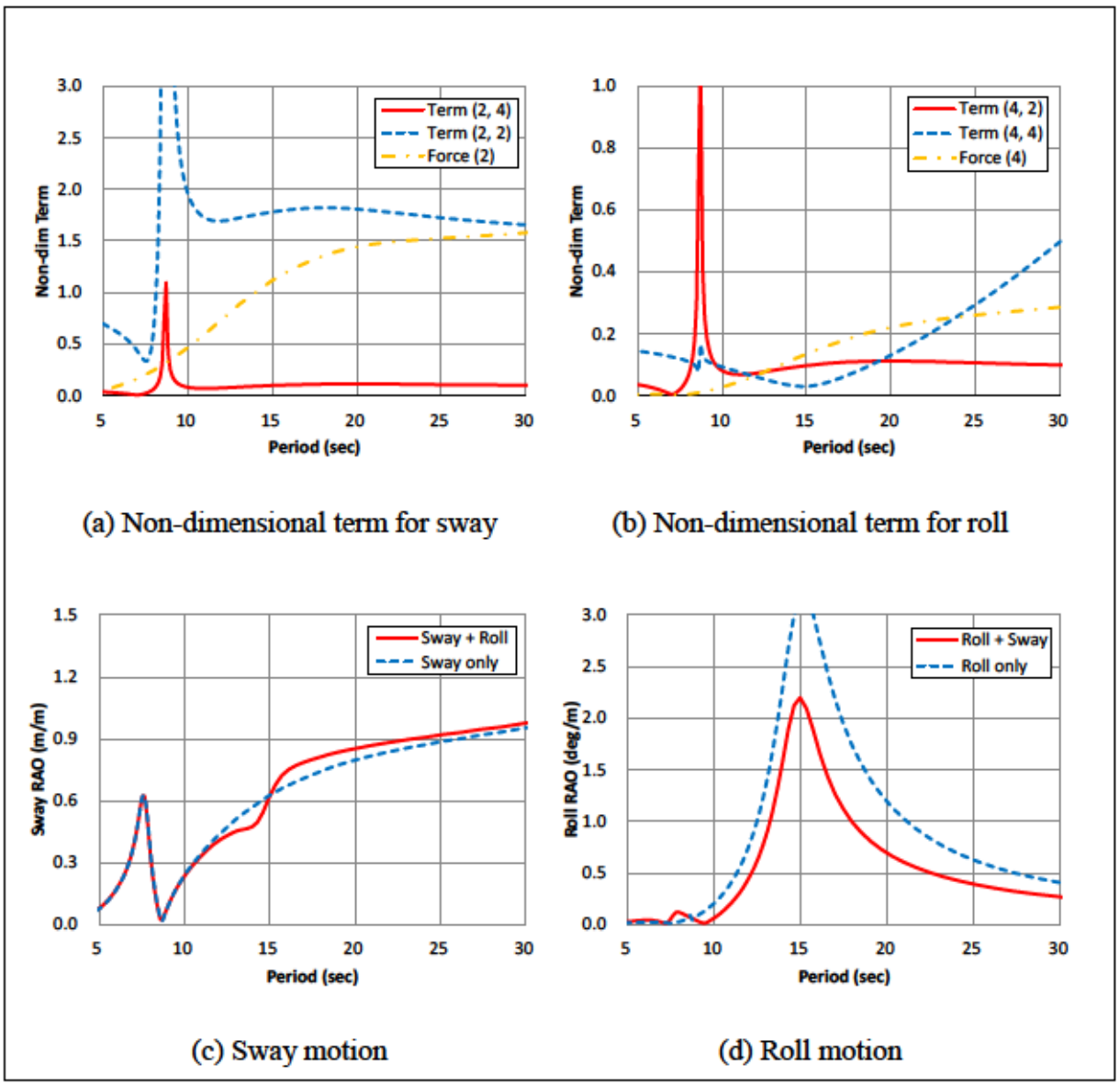

Figure 7.8. Sway and Roll motion with Liquid Cargo Effects for LC of 50% Lower Case

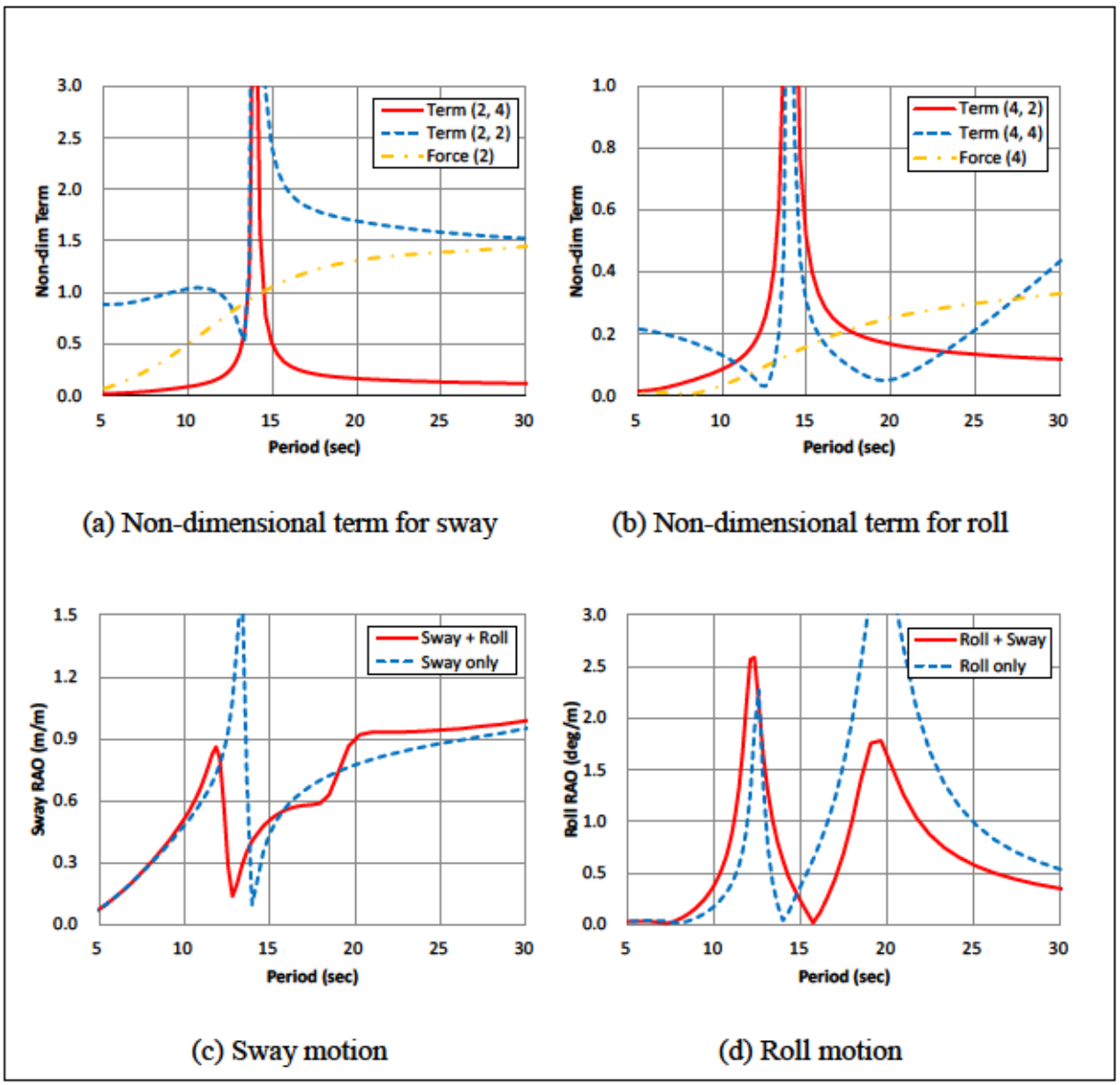

Figure 7.9. Sway and Roll motion with Liquid Cargo Effects for LC of 15% Higher Case

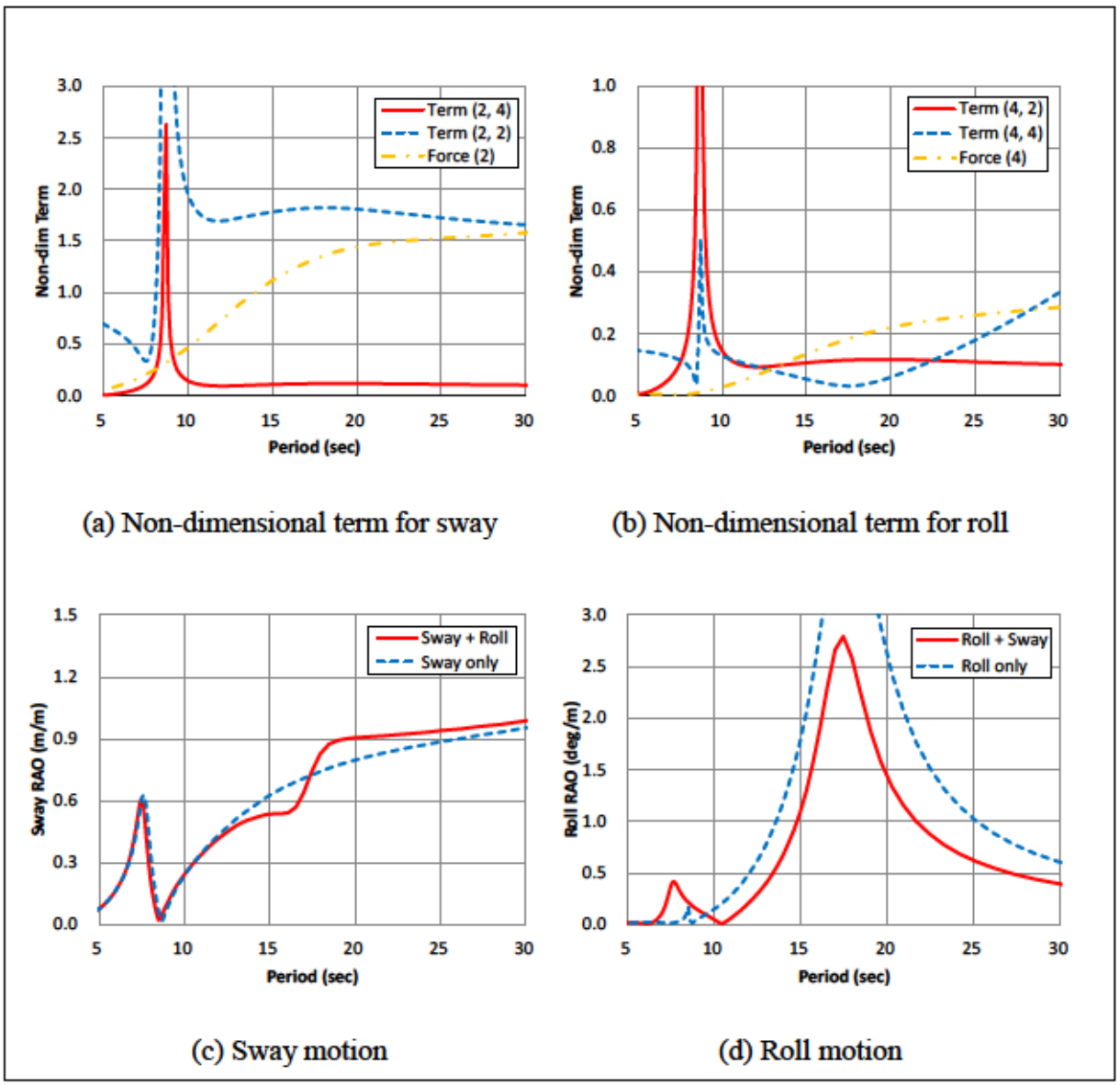

Figure 7.10. Sway and Roll motion with Liquid Cargo Effects for LC of 50% Higher Case

7.4 Storage Tank Operation

In this thesis, for the FLNG study so far, the liquid filling level considered is the same for all six (6) tanks. However, it is common in actual operation that the liquid filling level for each tank is different, and it can also be controlled.

For storage tank operation case, multiple liquid filling levels for each tank are modelled as shown in Figures 7.11 and 7.12. For each case, the draft is kept same as that of the loading conditions of 15% and 50%.

The tank operation case 1 is the case where filling of storage tanks is done as evenly as possible but with different filling levels. The tank operation case 2 is the case where filling of the storage tank is performed two by two in order.

As shown in Tables 7.4 and 7.5, the displacement is same as the original in Table 5.7, but KG, roll radius of gyration and GMt are slightly changed due to the change of the tank filling.

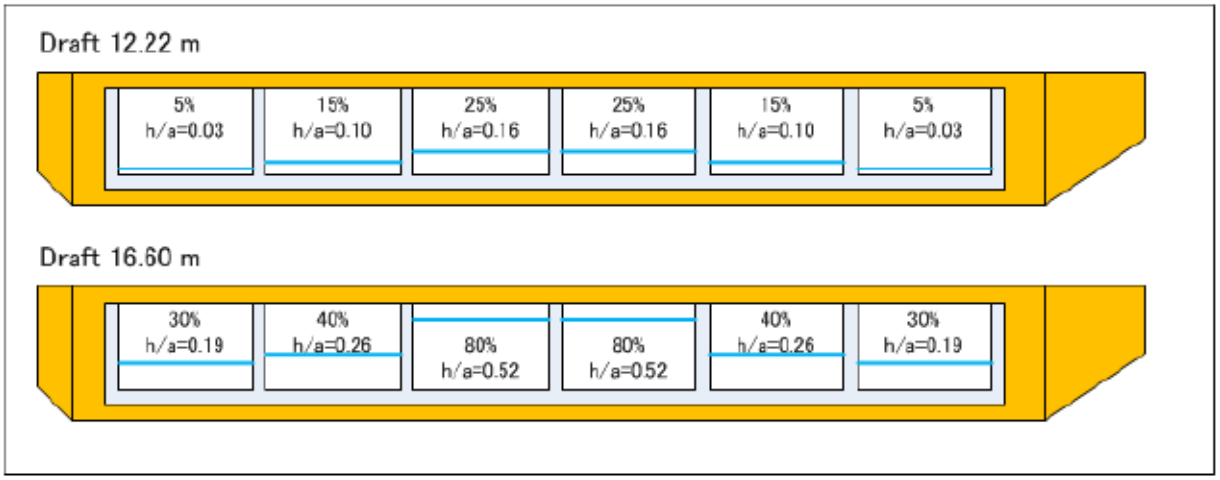

Figure 7.11. Multiple Liquid Filling for Tank Operation Case 1

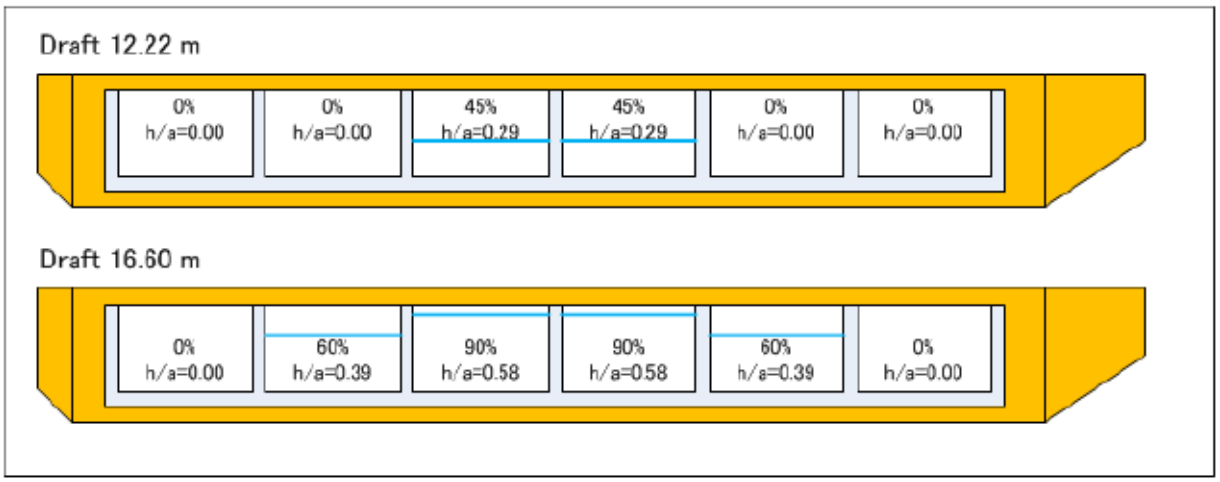

Figure 7.12. Multiple Liquid Filling for Tank Operation Case 2

For the tank operation case 1 as shown in Figures 7.13 and 7.14, three (3) peak responses are observed corresponding to the 3 different filling levels of tanks. Interestingly, the response peaks of sway and roll at the wave period around 25 second cancel each other [(c) and (d) in Figure 7.13].
For the tank operation case 2 as shown in Figures 7.15 and 7.16, due to the high filling level, remarkable influence of sloshing is observed only in the sway motion for the short period wave.

According to this study, the tank operation case 2 where filling of the storage tank is performed two by two in order is the preferred operation to reduce the influence of sloshing on motion.
It is also noted that this operation will minimize the duration of the low filling level in tank, and reduce the influence of sloshing on motion.

Table 7.4. Loading Conditions for Tank Operation Case 1

Draft	12.22 m	16.60 m
Water level in tanks	Figure 7.11	Figure 7.11
Displacement volume	432,364 m^3	591,683 m^3
KG	23.10 m	19.05 m
Roll radius of gyration relative to COG of FLNG	31.81 m	25.98 m
GMt	28.52 m	22.67 m
Roll natural period without liquid cargo effects (solid cargo)	15.2 s	14.1 s

Table 7.5. Loading Conditions for Tank Operation Case 2

Draft	12.22 m	16.60 m
Water level in tanks	Figure 7.12	Figure 7.12
Displacement volume	432,364 m^3	591,683 m^3
KG	23.69 m	20.11 m
Roll radius of gyration relative to COG of FLNG	31.58 m	25.91 m
GMt	27.93 m	21.62 m
Roll natural period without liquid cargo effects (solid cargo)	15.3 s	14.4 s

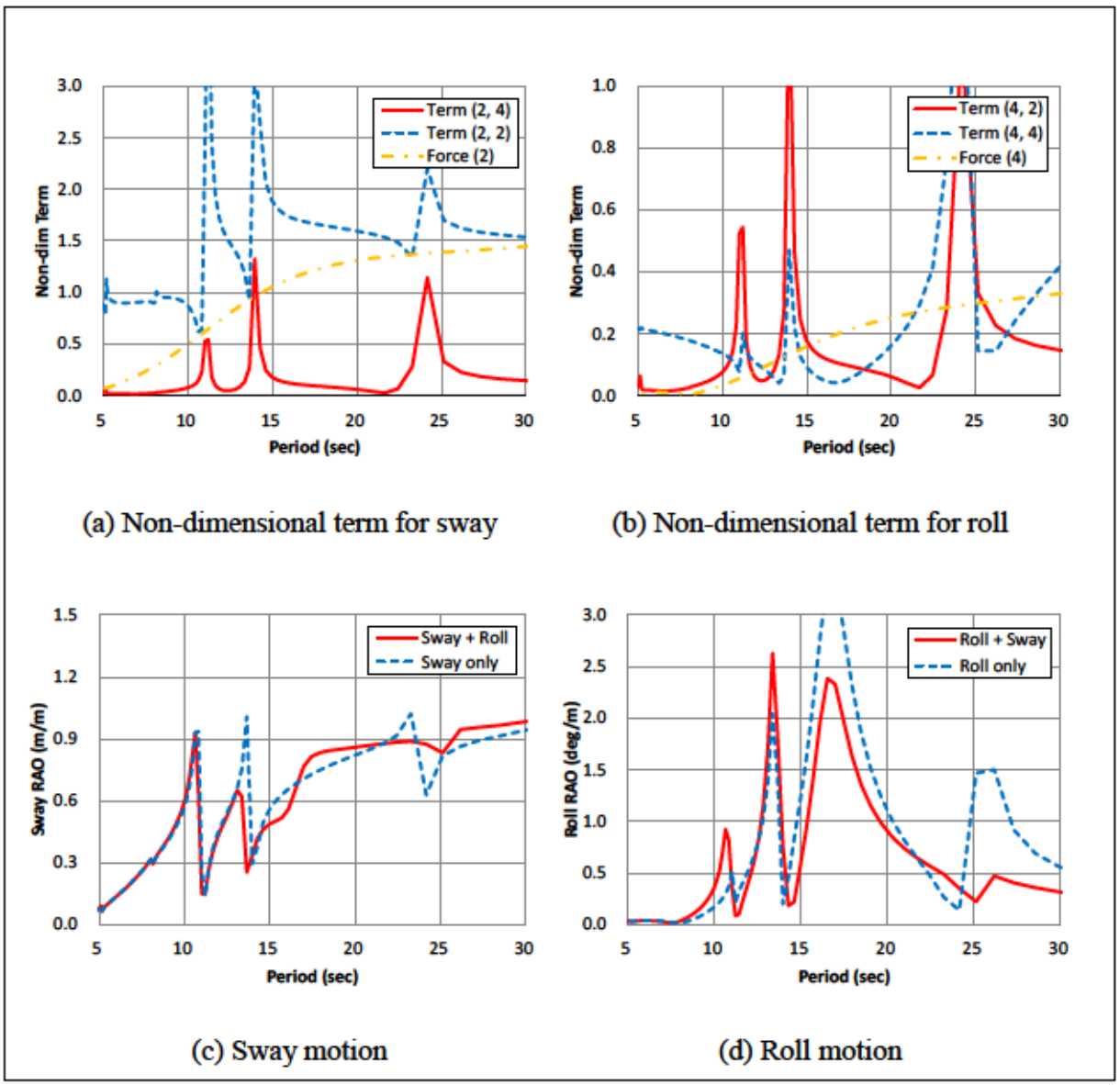

Figure 7.13. Sway and Roll motion with Liquid Cargo Effects for Draft 12.22 m Tank Operation Case 1

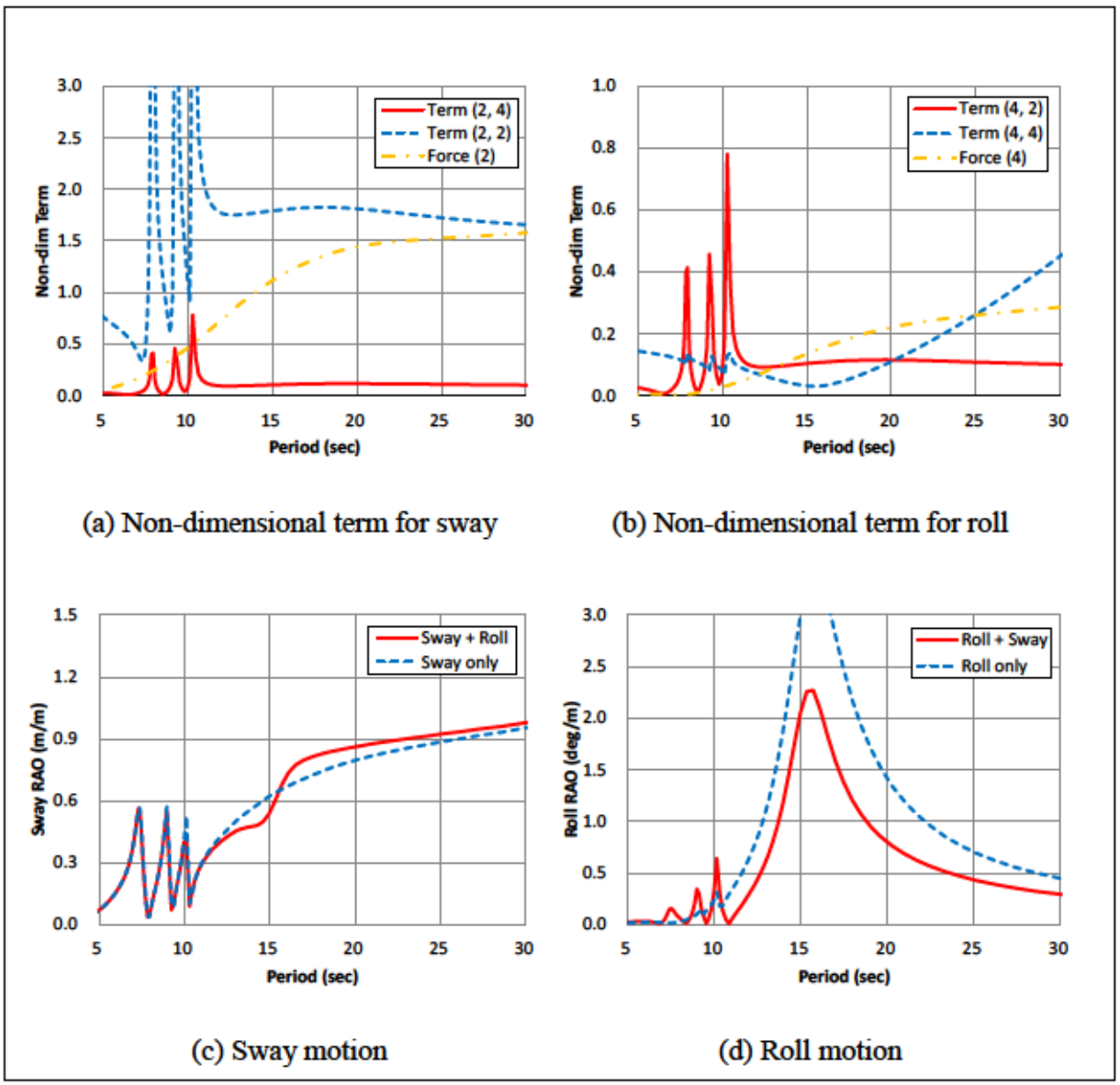

Figure 7.14. Sway and Roll motion with Liquid Cargo Effects for Draft 16.60 m Tank Operation Case 1

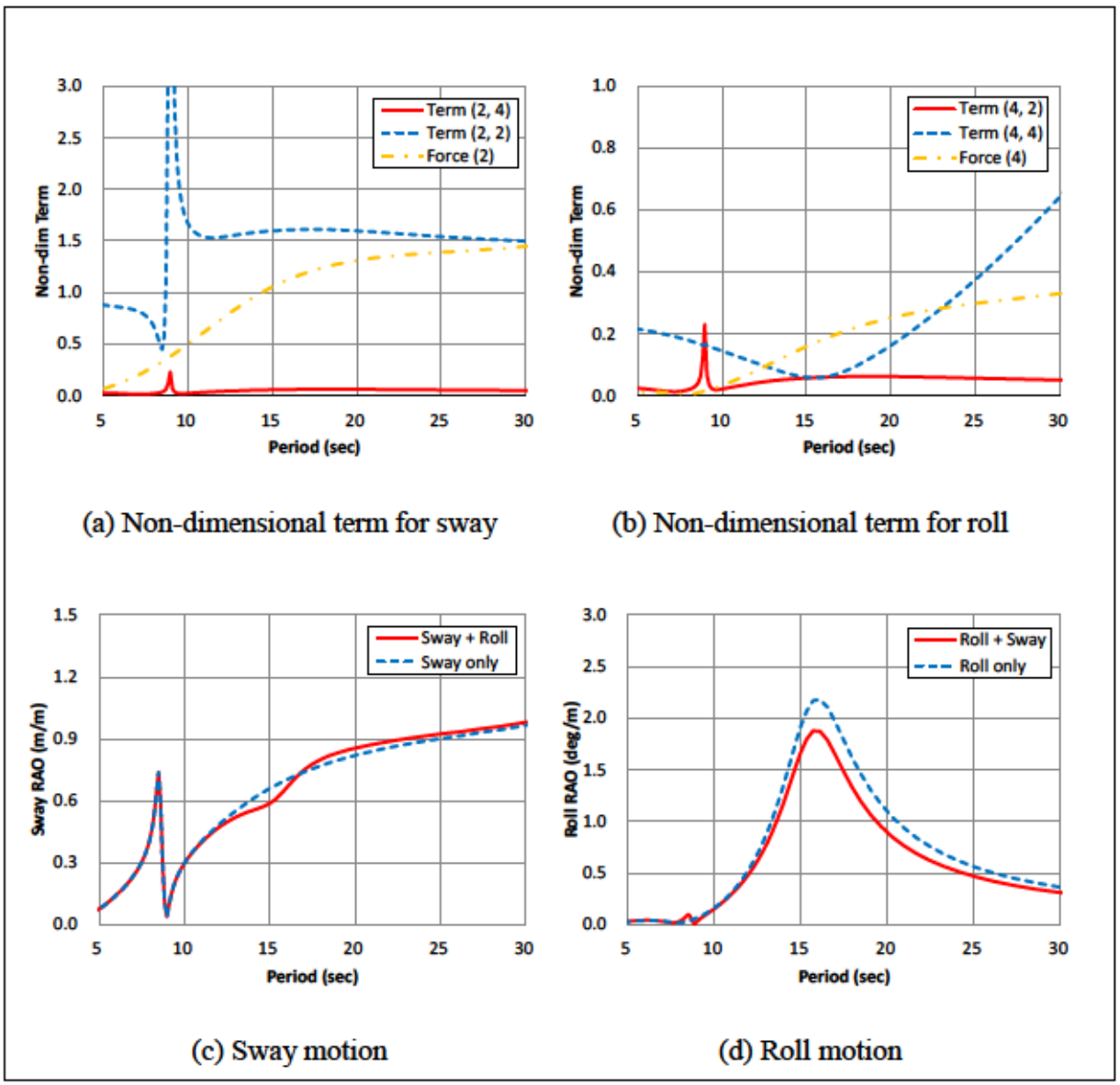

Figure 7.15. Sway and Roll motion with Liquid Cargo Effects for Draft 12.22 m Tank Operation Case 2

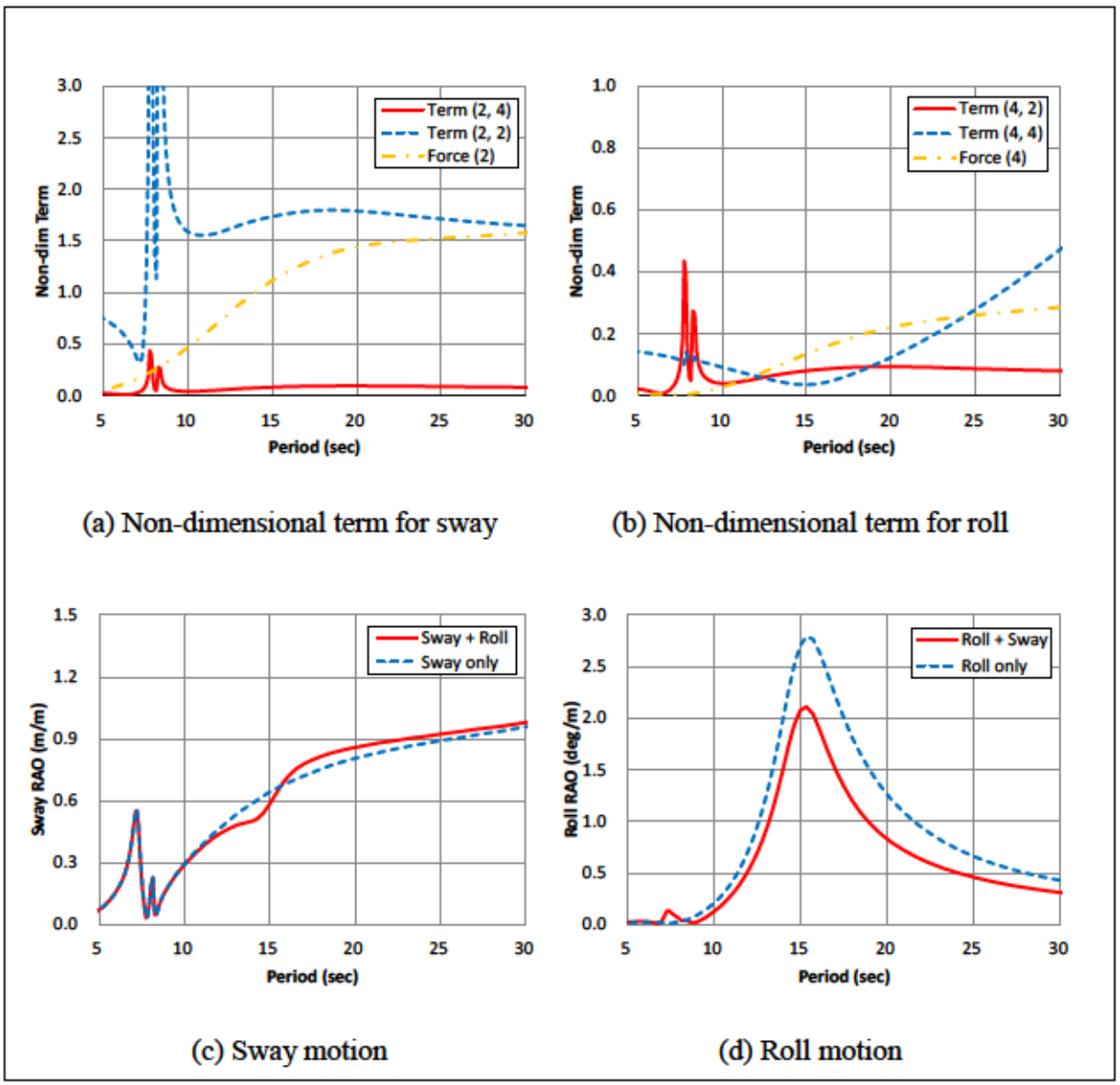

Figure 7.16. Sway and Roll motion with Liquid Cargo Effects for Draft 16.60 m Tank Operation Case 2

7.5 Summary of Case Study

Three (3) case studies are performed and the usefulness of the mechanical model in the FLNG development and basic design are demonstrated. Findings from these case studies for reducing the influence of sloshing on FLNG motion are as follows:

- The double-row tank arrangement is quite effective measure.
- The standard tank location adopted in FLNG is the preferred arrangement which is robust.
- The tank operation where filling of the storage tank is performed two by two in order is the preferred choice of operations.

8. Conclusions

The calculation method based on the mechanical model is presented in this thesis in order to estimate and understand the influence of the liquid cargo effects on the floating body motion. The conclusions drawn from the study undertaken are presented below.

- The liquid cargo effects are represented by the spring-mass type mechanical model and they are coupled with motion of floating body.
- The parameters of a mechanical model for the liquid in a rectangular tank are determined analytically.
- The method presented in this thesis is validated by comparing with the moment for the rotational oscillation of a rectangular tank measured by Bosch et al and the one calculated by 3D FDM program.
- The method presented is validated also by comparing the barge motion measured and calculated by Molin et al.
- The method presented is again validated by comparing the FLNG motion measured and calculated by Rocha et al.
- The sway and roll motion affected by the liquid cargo effects are reasonably evaluated, except in the case where the effect of the non-linear sloshing is significant.
- The liquid cargo effects enhance the sway-roll coupling. This shall be paid attention in order to understand the coupled sway and roll motion with the liquid cargo effects.
- A rational explanation on observation of peak and local minimum in sway RAO due to the effect of liquid cargo is provided by taking into account of the effect of the mass and sway-roll coupling.
- A rational explanation for observation of peak and local minimum in roll RAO due to the effect of liquid cargo is provided by taking into account of the effect of mass inertia, restoring moment, and sway-roll coupling.
- The mechanical model provides quantitative estimates of degree of influence of sloshing on roll motion corresponding to the relative vertical location of tank and the fraction of liquid level in tank.
- The influence of liquid sloshing observed in two independent research results, the barge motion by Molin et al. and the FLNG motion by Rocha et al. both can be explained by a single method using the mechanical model.
- Three (3) case studies are performed and the effectiveness of the mechanical model in the FLNG development and basic design is demonstrated.

In the future, further investigations on the followings will enhance the completeness of this research work.

- Investigation on influence of non-linear sloshing at low filling level
  The method of Verhagen and van Wijngaarden was a simple analytical solution which predicted the non-linear roll moment at low filling level of the tank fairly well. This method was coupled with the floating body motion by Journée [19].
  Incorporating principles from this method would eliminate some of the weaknesses in the method suggested by the author using the mechanical model.
  Considering the anti-roll tank and the experimental result of FLNG with loading condition of 15%, it is expected that the low filling of liquid reduces the roll motion.
- Investigation of surge and pitch motion
  The characteristics of surge and pitch motion affected by the liquid cargo effects are similar to that of the sway and roll motion, but not complex due to reduced influence of sloshing on pitch motion.
- Investigation of yaw motion
  The influence of sloshing on yaw motion is expected to be insignificant; however, it is worth quantifying the effect.
- Investigation of floating body motion in quartering sea
  The influence of sloshing investigated in the past only for the beam sea is the most significant sea for sway and roll. The influence of sloshing to this motion is expected to be less significant; however, it is worth quantifying the effect.
- Investigation of floating body motion in irregular sea in short and long term sea states
  This investigation would quantify whether the floating body motion is amplified by sloshing, and identify sea states that should have been taken into account.
- Investigation using the prismatic tanks instead of the rectangular tanks
  According to the Appendix 4 of this thesis, parameters for the prismatic tank model can be obtained easily. This investigation would yield more realistic results since the tank shape actually adopted for FLNG and LNGC is prismatic.

This thesis covers the influence of sloshing on sway and roll motion of FLNG based on linear potential theory, and considerations and conclusions are presented provided based on the results obtained only from by the quantitative examination. However, the author is in possession of a lot of useful findings and knowledge.

Hence, the author would like to add additional notes which are not mentioned in the preceding chapters of this thesis and some of which are not yet undergone quantitative inspection. Author hopes that these notes would be verified by research in the future.

1. The influence of sloshing on pitch, heave and yaw motion is not significant and practically negligible.
2. When the liquid height in tank is very low, the sloshing natural period is long and the sloshing affects sway, roll and surge motions. However the enlarged motion is balanced and becomes smaller due to sway-roll coupling and surge-pitch coupling.
3. When the liquid height in tank is low, the sloshing affects sway, roll and surge motions. However, the motions are not be enlarged a lot due to non-linearity of the sloshing.
4. When the liquid height in tank is intermediate or deep, roll motion will not enlarge a lot due to large mass inertia effect and the small external roll moment.
5. When the liquid height in tank is intermediate or deep, sway and surge motions will be enlarged. In addition, the corresponding short period wave appears frequently.
6. Considering above mentioned facts, due attention shall be paid to sway and surge motions affected by sloshing of liquid at intermediate or deep height in the tank. This may worsen the FLNG performance in the normal environmental condition; e.g. fatigue, offloading operation, although it does not get affected in the harsh environmental condition; e.g. ultimate strength, safety.

Table 8.1. Influence of sloshing on FLNG motion

Liquid height in tank	Very low ($h/a \leq 0.05$)	Low ($0.05 < h/a \leq 0.15$)	Intermediate Deep
Sloshing natural period	Long	Middle	Short
Sway	NP [2]	NP [3]	Attention [3,6]
Roll	NP [2]	NP [3]	NP [4]
Surge	NP [2]	NP [3]	Attention [3,6]
Pitch	NP [1]	NP [1]	NP [1]
Heave	NP [1]	NP [1]	NP [1]
Yaw	NP [1]	NP [1]	NP [1]

NP: No problem

9. References

9.1 Cited in the Thesis

1) A Nakamura. New technology for offshore natural gas development －LNG-FPSO－, Journal of the Japanese Association for Petroleum Technology, Vol. 74, No. 2, pp. 152-161, 2009. (in Japanese)
2) K Nagai. Expectations and recent trends for floating LNG, JOGMEC Oil and natural gas review, Vol. 47, No. 5, pp. 73-82, 2013. (in Japanese)
3) D H Lee, M K Ha, S Y Kim and S C Shin. Research of design challenges and new technologies for floating LNG, International Journal of Naval Architecture and Ocean Engineering, 6, pp. 307-322, 2014.
4) X C Nguyen, K Miheaye, M G Kim, H Newman, D H Yoo, H Y Cho, Cees de Regt, J K Kim and W K Lee. A Study on Small Scale Associated Gas FLNG Utilizing Small Scale LNG Carriers to Near-by Onshore LNG Plant, Proceedings of the ASME 2016 35th International Conference on Ocean, Offshore and Arctic Engineering, June 19-24, Busan, South Korea, OMAE2016-55152, 2016.
5) W H Zhao, J M Yang, Z Q Hu and Y F Wei. Recent developments on the hydrodynamics of floating liquid natural gas (FLNG), Ocean Engineering, 38, pp. 1555-1567, 2011.
6) Watts P. On a method of reducing the rolling of ships at sea, Transactions of the (Royal) Institution of Naval Architects, Vol. 24, pp. 165-191, 1883.
7) Watts P. The Use of Water-Chambers for Reducing the Rolling of Ships at Sea, Transactions of the (Royal) Institution of Naval Architects, Vol. 26, pp. 30-49, 1885.
8) JJ van den Bosch and JH Vugts. Roll Damping by Free-Surface Tanks, Shipbuilding Laboratory of the Technological University, Delft, Report No. 134, 1965.
9) JJ van den Bosch and JH Vugts. On Roll Damping by Free-Surface Tanks, RINA, 1966.
10) Dodge FT. The New "Dynamic Behavior of Liquids in Moving Containers", Southwest Research Institute, 2000.
11) Komatsu K. Sloshing – Liquid Motion and Tank Shell Vibration –, 2015. (in Japanese)
12) S Yamashita. Motions of a floating body with a liquid storage tank, Transactions of the West-Japan Society of Naval Architects, 61, pp. 155–165, 1981. (in Japanese)
13) Molin B, Remy F, Rigaud S and C de Jouette. LNG-FPSO's: frequency domain, coupled analysis of support and liquid cargo motions, Proceedings of IMAM conference, 2002.
14) Malenica Š, Zalar M and Chen X B. Dynamic coupling of seakeeping and sloshing, 13th ISOPE Conference 23–28, Honolulu, USA, 2003.
15) Zalar M, Diebold L, Baudin E, Henry J, Chen X B. Sloshing Effects Accounting for Dynamic Coupling Between Vessel and Tank Liquid Motion, Proceedings of the 26th International Conference on Offshore Mechanics and Arctic Engineering, June 10-15, San Diego, California, USA, OMAE2007-29544, 2007.

16) Y Cao and F Zhang. Effects of Fluid Motions in Liquid Tanks on Vessel Motions Using a Simple Panel Method, Journal of Offshore Mechanics and Arctic Engineering, Vol. 138, 2016.
17) G F Clauss, D Testa, F Sprenger. Coupling Effects Between Tank Sloshing and Motions of A LNG Carrier, Proceedings of the 29th International Conference on Ocean, Offshore and Arctic Engineering, June 6-11, Shanghai, China, OMAE2010-20077, 2010.
18) Z Q Hu, S Y Wang, G Chen, S H Chai and Y T Jin. The effects of LNG-tank sloshing on the global motions of FLNG system, International Journal of Naval Architecture and Ocean Engineering, 9, pp. 114-125, 2017.
19) Journée J M J. Liquid Cargo and Its Effect on Ship Motions, Six International Conference on Stability of Ships and Ocean Structures, pp. 137-150, Varna, Bulgaria, September 22-27, 1997.
20) Rognebakke OF and Faltinsen OM. Coupling of sloshing and ship motions, Journal of Ship Research, 47(3), pp. 208–221, 2003.
21) Lee S J, Kim M H, Lee D H, Kim J W and Kim Y H. The effects of LNG tank sloshing on the global motions of LNG carriers, Ocean Engineering, 34, pp. 10–20, 2007.
22) Lee S J. The effects of LNG-sloshing on the global responses of LNG-carriers, PhD thesis, Texas A&M University, 2008.
23) Lee S J, Kim M H. The Effects of Inner-Liquid Motion on LNG Vessel Responses, Journal of Offshore Mechanics and Arctic Engineering, Vol. 132, 2010.
24) X Wang and M Arai. Research on computational method of coupled ship motions and sloshing, Journal of the Japan Society of Naval Architects and Ocean Engineers, 14, pp. 97-104, 2011.
25) X Wang and M Arai. A Study on Coupling Effect Between Seakeeping and Sloshing for Membrane-Type LNG Carrier, International Journal of Offshore and Polar Engineering, Vol. 21, No. 4, pp. 256-263, 2011.
26) X Wang. Coupled Analysis of Ship Motions and Tank Sloshing of LNG Carriers — Study of a Time-domain Numerical Method and its Application, PhD thesis, Yokohama National University, 2012.
27) X Wang and M Arai. A numerical study on coupled sloshing and ship motions of a liquefied natural gas carrier in regular and irregular waves, Journal of Engineering for the Maritime Environment, 229(1), pp. 3-13, 2015.
28) T Kawahashi, M Arai, X Wang, L Y Cheng, K Nishimoto and A Nakashima. Study on the influence of sloshing for the motion of FLNG in waves, Conference Proceedings of Asian-Pacific Technical Exchange and Advisory Meeting on Marine Structures, pp. 218-224, Oct. 10 - 13, Mokpo, Rep. of Korea, 2016.
29) T Kawahashi, M Arai, X Wang, L Y Cheng, K Nishimoto, A Nakashima. A Study on the Influence of Sloshing with Partial Filled Tank on FLNG Motion in Waves, Conference Proceedings of the Japan Society of Naval Architects and Ocean Engineers, No. 25, pp. 443-447, Hiroshima, Japan, 2017. (in Japanese)

30) K S Kim, M H Kim and J C Park. Simulation of Multiliquid-Layer Sloshing With Vessel Motion by Using Moving Particle Semi-Implicit Method, Journal of Offshore Mechanics and Arctic Engineering, Vol. 137, 2015.
31) T P Rocha, R Dotta, D P Vieira, P C Mello, E B Malta and K Nishimoto. Experimental investigation on the influence of liquid cargo in floating vessels motions, Offshore Technology Conference, OTC-26203-MS, 2015.
32) M Arai, Cheng LY and Y Inoue. 3D numerical simulation of impact load due to liquid cargo sloshing, Journal of the Japan Society of Naval Architects and Ocean Engineers, 171, pp. 177-184, 1992.
33) ANSYS Aqwa Theory Manual. USA, 2013.
34) Lee CH. WAMIT Theory Manual, Department of Ocean Engineering, Massachusetts Institute of Technology, MIT Report No. 95-2, 1995.
35) Faltinsen OM and Timokha AN. Sloshing, Cambridge University Press, 2009.
36) Gyeong JL. Moment of inertia of liquid in a tank, International Journal of Naval Architecture and Ocean Engineering, 6, pp. 132-150, 2014

9.2 Other References (Not Cited)

37) DNV Classification Notes No.30.9. Sloshing Analysis of LNG Membrane Tanks, 2014.
38) DNV Recommended Practice C205. Environmental Conditions and Environmental Loads, 2007.
39) A Nakashima and M Arai. The Mechanical Model representing Liquid Cargo Effects in FLNG Motion, Conference Proceedings of Asian-Pacific Technical Exchange and Advisory Meeting on Marine Structures, pp. 50-57, Oct. 10 - 13, Mokpo, Rep. of Korea, 2016.
40) A Nakashima and M Arai. Influence of Liquid Cargo on FLNG Motion, Conference Proceedings of Design and Construction of LNG Ships, The Royal Institution of Naval Architects, pp. 65-74, 26-27 October, London, UK, 2016.

Appendix 1 Details of Mathematical Expression in Chapter 2.2

A1.1 Preservation of Static Properties

To preserve the static properties of the liquid, the sum of all masses must be same as the liquid mass m_T, and their centres must be kept at the same elevation. These constraints are expressed analytically by:

$$m_0 + \sum_{n-1}^{\infty} m_n = m_T, \quad -m_0 H_0 + \sum_{n-1}^{\infty} m_n H_n = 0$$

Duplication of the natural frequencies requires:

$$m_n \omega_n^2 = K_n$$

where ω_n is the slosh natural frequency of the n-th mode. This is a first relation that shows how to choose the spring constant and spring-mass.

A1.2 Force and Moment by Linear Displacement

When the tank is excited at angular frequency ω by a small time-varying linear displacement X_0 along the x axis, the spring masses deflect by a distance x_n relative to the tank walls as a result of tank motion. The forced horizontal motion and the spring masses deflections are defined as follows:

$$X(t) = -iX_0 \exp(i\omega t) = X_0 \sin(\omega t) - iX_0 \cos(\omega t)$$

$$x_n(t) = x_n \exp(i\omega t) = x_n \cos(\omega t) + ix_n \sin(\omega t)$$

The equation of motion for each spring-mass system without damping is expressed as:

$$m_n \ddot{x}_n + K_n x_n = -m_n \ddot{X}$$

$$\left(-\omega^2 m_n + K_n\right) x_n \exp(i\omega t) = -i\omega^2 m_n X_0 \exp(i\omega t)$$

$$x_n = \frac{-i\omega^2 m_n X_0}{-\omega^2 m_n + K_n} = \frac{-i\omega^2 m_n X_0}{\left(\omega_n^2 - \omega^2\right) m_n} = \frac{-i\omega^2 X_0}{\omega_n^2 - \omega^2}$$

The net force exerted on the tank in the X_0 direction is given by the reversed inertia forces of the moving masses:

$$F_x = -m_0\ddot{X} - \sum_{n=1}^{\infty} m_n\left(\ddot{X} + \ddot{x}_n\right) = \left\{-i\omega^2 m_0 X_0 + \omega^2 \sum_{n=1}^{\infty} m_n\left(-iX_0 + x_n\right)\right\}\exp(i\omega t)$$

$$= \left\{-i\omega^2 m_0 X_0 + \omega^2 \sum_{n=1}^{\infty} m_n\left(-iX_0 - i\frac{\omega^2 X_0}{\omega_n^2 - \omega^2}\right)\right\}\exp(i\omega t)$$

$$= -iX_0\omega^2 \exp(i\omega t)\left\{m_0 + \sum_{n=1}^{\infty} m_n\left(1 + \frac{\omega^2}{\omega_n^2 - \omega^2}\right)\right\}$$

$$= -im_T X_0\omega^2 \exp(i\omega t)\left\{1 + \sum_{n=1}^{\infty}\frac{m_n}{m_T}\frac{\omega^2}{\omega_n^2 - \omega^2}\right\}$$

Likewise, the net moment exerted on the tank is given by:

$$M_y = -\sum_{n=1}^{\infty} m_n H_n \ddot{x}_n + g\sum_{n=1}^{\infty} m_n x_n$$

$$= -\sum_{n=1}^{\infty} m_n\left(H_n\ddot{x}_n - gx_n\right) = \sum_{n=1}^{\infty} m_n\left(\omega^2 H_n + g\right)x_n \exp(i\omega t)$$

$$= -im_T X_0\omega^2 \exp(i\omega t)\left\{\sum_{n=1}^{\infty}\frac{m_n}{m_T}\frac{\omega^2 H_n + g}{\omega_n^2 - \omega^2}\right\}$$

$$= -im_T hX_0\omega^2 \exp(i\omega t)\left\{\sum_{n=1}^{\infty}\frac{m_n}{m_T}\left(\frac{H_n}{h} + \frac{g}{h\omega^2}\right)\frac{\omega^2}{\omega_n^2 - \omega^2}\right\}$$

$$= -im_T hX_0\omega^2 \exp(i\omega t)\left\{\sum_{n=1}^{\infty}\frac{m_n}{m_T}\left(\frac{H_n}{h} + \frac{g}{h\omega^2}\frac{\omega^2}{\omega_n^2}\frac{\omega_n^2}{\omega^2}\right)\frac{\omega^2}{\omega_n^2 - \omega^2}\right\}$$

$$= -im_T hX_0\omega^2 \exp(i\omega t)\left\{\sum_{n=1}^{\infty}\frac{m_n}{m_T}\left(\frac{H_n}{h}\frac{\omega^2}{\omega_n^2 - \omega^2} + \frac{g}{h\omega_n^2}\frac{\omega_n^2}{\omega_n^2 - \omega^2}\right)\right\}$$

$$= -im_T hX_0\omega^2 \exp(i\omega t)\left\{\sum_{n=1}^{\infty}\frac{m_n}{m_T}\left[\frac{H_n}{h}\frac{\omega^2}{\omega_n^2 - \omega^2} + \frac{g}{h\omega_n^2}\left(1 + \frac{\omega^2}{\omega_n^2 - \omega^2}\right)\right]\right\}$$

$$= -im_T hX_0\omega^2 \exp(i\omega t)\left\{\sum_{n=1}^{\infty}\frac{m_n}{m_T}\frac{g}{h\omega_n^2}+\sum_{n=1}^{\infty}\frac{m_n}{m_T}\left(\frac{H_n}{h}+\frac{g}{h\omega_n^2}\right)\frac{\omega^2}{\omega_n^2-\omega^2}\right\}$$

A1.3 Force and Moment by Angular Rotation

When the tank is excited at angular frequency ω by a small time-varying angular rotation α_0 about an axis through the COG, the spring masses also deflect by a distance $x_n$relative to the tank walls as a result of tank motion.

The forced angular motion and the spring masses deflections are defined as follows:

$$\alpha(t) = -i\alpha_0 \exp(i\omega t) = \alpha_0 \sin(\omega t) - i\alpha_0 \cos(\omega t)$$

$$x_n(t) = x_n \exp(i\omega t) = x_n \cos(\omega t) + ix_n \sin(\omega t)$$

The equation of motion for each spring-mass system is expressed as:

$$m_n\ddot{x}_n + K_n x_n = -m_n H_n\ddot{\alpha} + m_n g\alpha$$

$$\left(-\omega^2 m_n + K_n\right)x_n \exp(i\omega t) = -im_n\left(\omega^2 H_n + g\right)\alpha_0 \exp(i\omega t)$$

$$x_n = \frac{-im_n\left(\omega^2 H_n + g\right)\alpha_0}{-\omega^2 m_n + K_n} = \frac{-im_n\left(\omega^2 H_n + g\right)\alpha_0}{\left(\omega_n^2 - \omega^2\right)m_n} = \frac{-i\left(\omega^2 H_n + g\right)\alpha_0}{\omega_n^2 - \omega^2}$$

The net force exerted on the tank is given by the reversed inertia forces of the moving masses:

$$F_x = -\sum_{n=1}^{\infty} m_n\ddot{x}_n = \omega^2\sum_{n=1}^{\infty} m_n x_n \exp(i\omega t) = \omega^2\sum_{n=1}^{\infty} m_n \frac{-i\left(\omega^2 H_n + g\right)\alpha_0}{\omega_n^2 - \omega^2}\exp(i\omega t)$$

$$= -i\alpha_0\omega^2 \exp(i\omega t)\sum_{n=1}^{\infty} m_n \frac{\omega^2 H_n + g}{\omega_n^2 - \omega^2}$$

$$= -im_T h\alpha_0\omega^2 \exp(i\omega t)\left\{\sum_{n=1}^{\infty}\frac{m_n}{m_T}\left(\frac{H_n}{h}+\frac{g}{h\omega^2}\right)\frac{\omega^2}{\omega_n^2-\omega^2}\right\}$$

$$= -im_T h\alpha_0\omega^2 \exp(i\omega t)\left\{\sum_{n=1}^{\infty}\frac{m_n}{m_T}\frac{g}{h\omega_n^2}+\sum_{n=1}^{\infty}\frac{m_n}{m_T}\left(\frac{H_n}{h}+\frac{g}{h\omega_n^2}\right)\frac{\omega^2}{\omega_n^2-\omega^2}\right\}$$

Likewise, the net moment exerted on the tank is given by;

$$M_y = -\left(I_0 + m_0 H_0^2\right)\ddot{\alpha} - \sum_{n=1}^{\infty} m_n H_n \left(\ddot{x}_n + H_n \ddot{\alpha}\right) + g\sum_{n=1}^{\infty} m_n x_n$$

$$= -\left(I_0 + m_0 H_0^2 + \sum_{n=1}^{\infty} m_n H_n^2\right)\ddot{\alpha} - \sum_{n=1}^{\infty} m_n \left(H_n \ddot{x}_n - g x_n\right)$$

$$= -i\alpha_0 \omega^2 \exp(i\omega t)\left(I_0 + m_0 H_0^2 + \sum_{n=1}^{\infty} m_n H_n^2\right) + \sum_{n=1}^{\infty} m_n \left(\omega^2 H_n + g\right) x_n \exp(i\omega t)$$

$$= -i\alpha_0 \omega^2 \exp(i\omega t)\left(I_0 + m_0 H_0^2 + \sum_{n=1}^{\infty} m_n H_n^2\right) + \sum_{n=1}^{\infty} m_n \left(\omega^2 H_n + g\right) \frac{-i\left(\omega^2 H_n + g\right)\alpha_0}{\omega_n^2 - \omega^2} \exp(i\omega t)$$

$$= -i\alpha_0 \omega^2 \exp(i\omega t)\left\{\left(I_0 + m_0 H_0^2 + \sum_{n=1}^{\infty} m_n H_n^2\right) + \sum_{n=1}^{\infty} m_n \left(H_n + \frac{g}{\omega^2}\right)^2 \frac{\omega^2}{\omega_n^2 - \omega^2}\right\}$$

$$= -i m_T h^2 \alpha_0 \omega^2 \exp(i\omega t)\left\{\frac{I_y}{m_T h^2} + \sum_{n=1}^{\infty} \frac{m_n}{m_T}\left(\frac{H_n}{h} + \frac{g}{h\omega^2}\right)^2 \frac{\omega^2}{\omega_n^2 - \omega^2}\right\}$$

$$= -i m_T h^2 \alpha_0 \omega^2 \exp(i\omega t)\left\{\frac{I_y}{m_T h^2} + \sum_{n=1}^{\infty} \frac{m_n}{m_T}\left(\frac{H_n^2}{h^2} + \frac{2H_n g}{h^2\omega^2} + \frac{g^2}{h^2\omega^4}\right) \frac{\omega^2}{\omega_n^2 - \omega^2}\right\}$$

$$I_y = I_0 + m_0 H_0^2 + \sum_{n=1}^{\infty} m_n H_n^2$$

The third and fourth terms in the parentheses are further expanded as:

$$\sum_{n=1}^{\infty} \frac{m_n}{m_T} \frac{2H_n g}{h^2\omega^2} \frac{\omega^2}{\omega_n^2 - \omega^2} = \sum_{n=1}^{\infty} \frac{m_n}{m_T} \frac{2H_n g}{h^2\omega^2} \frac{\omega_n^2}{\omega_n^2} \frac{\omega^2}{\omega_n^2 - \omega^2} = \sum_{n=1}^{\infty} \frac{m_n}{m_T} \frac{2H_n}{h} \frac{g}{h\omega_n^2} \frac{\omega_n^2}{\omega_n^2 - \omega^2}$$

$$= \sum_{n=1}^{\infty} \frac{m_n}{m_T} \frac{2H_n}{h} \frac{g}{h\omega_n^2}\left(1 + \frac{\omega^2}{\omega_n^2 - \omega^2}\right) = \sum_{n=1}^{\infty}\left(\frac{m_n}{m_T} \frac{g}{h\omega_n^2} \frac{2H_n}{h} + \frac{m_n}{m_T} \frac{g}{h\omega_n^2} \frac{2H_n}{h} \frac{\omega^2}{\omega_n^2 - \omega^2}\right)$$

$$\sum_{n=1}^{\infty} \frac{m_n}{m_T} \frac{g^2}{h^2\omega^4} \frac{\omega^2}{\omega_n^2 - \omega^2} = \sum_{n=1}^{\infty} \frac{m_n}{m_T} \frac{g^2}{h^2\omega^4} \frac{\omega_n^2}{\omega_n^2} \frac{\omega^2}{\omega_n^2 - \omega^2} = \sum_{n=1}^{\infty} \frac{m_n}{m_T} \frac{g}{h\omega_n^2} \frac{g}{h\omega^2} \frac{\omega_n^2}{\omega_n^2 - \omega^2}$$

$$=\sum_{n=1}^{\infty}\frac{m_n}{m_T}\frac{g}{h\omega_n^2}\frac{g}{h\omega^2}\left(1+\frac{\omega^2}{\omega_n^2-\omega^2}\right)=\sum_{n=1}^{\infty}\left(\frac{m_n}{m_T}\frac{g}{h\omega_n^2}\frac{g}{h\omega^2}+\frac{m_n}{m_T}\frac{g}{h\omega_n^2}\frac{g}{h\omega^2}\frac{\omega^2}{\omega_n^2-\omega^2}\right)$$

$$=\sum_{n=1}^{\infty}\left(\frac{m_n}{m_T}\frac{g}{h\omega_n^2}\frac{g}{h\omega^2}+\frac{m_n}{m_T}\frac{g}{h\omega_n^2}\frac{g}{h\omega_n^2}\frac{\omega_n^2}{\omega_n^2-\omega^2}\right)$$

$$=\sum_{n=1}^{\infty}\left(\frac{m_n}{m_T}\frac{g}{h\omega_n^2}\frac{g}{h\omega^2}+\frac{m_n}{m_T}\frac{g}{h\omega_n^2}\frac{g}{h\omega_n^2}+\frac{m_n}{m_T}\frac{g}{h\omega_n^2}\frac{g}{h\omega_n^2}\frac{\omega^2}{\omega_n^2-\omega^2}\right)$$

As a result, the net moment is finally expressed as:

$$M_y=-im_Th^2\alpha_0\omega^2\exp(i\omega t)\left\{\begin{array}{l}\dfrac{I_y}{m_Th^2}+\displaystyle\sum_{n=1}^{\infty}\frac{m_n}{m_T}\frac{g}{h\omega_n^2}\frac{g}{h\omega^2}\\ \qquad+\displaystyle\sum_{n=1}^{\infty}\frac{m_n}{m_T}\frac{g}{h\omega_n^2}\left(\frac{2H_n}{h}+\frac{g}{h\omega_n^2}\right)\\ \qquad\qquad+\displaystyle\sum_{n=1}^{\infty}\frac{m_n}{m_T}\left(\frac{H_n}{h}+\frac{g}{h\omega_n^2}\right)^2\frac{\omega^2}{\omega_n^2-\omega^2}\end{array}\right\}$$

A1.4 Linear Damping

It is reasonable to assume that it can be represented accurately by equivalent linear viscous damping when the damping is small. The equation of motion for horizontal motion with linear viscous damping is expressed as follows:

$$m_n\ddot{x}_n+C_n\dot{x}_n+K_nx_n=-m_n\ddot{X}$$

$$x_n=\frac{-i\omega^2X_0}{\omega_n^2-\omega^2+i2\gamma_n\omega_n\omega},\quad \gamma_n=\frac{C_n}{2m_n\omega_n}$$

The equation of motion for angular motion with linear viscous damping is expressed as follows:

$$m_n\ddot{x}_n+C_n\dot{x}_n+K_nx_n=-m_nH_n\ddot{\alpha}+m_ng\alpha$$

$$x_n=\frac{-i\left(\omega^2H_n+g\right)\alpha_0}{\omega_n^2-\omega^2+i2\gamma_n\omega_n\omega},\quad \gamma_n=\frac{C_n}{2m_n\omega_n}$$

As a result, force and moment due to horizontal motion and angular motion is obtained as below:

$$F_x = -im_T X_0 \omega^2 \exp(i\omega t)\left\{1+\sum_{n=1}^{\infty}\frac{m_n}{m_T}\frac{\omega^2}{\omega_n^2-\omega^2+i2\gamma_n\omega_n\omega}\right\}$$
$$-im_T h\alpha_0\omega^2\exp(i\omega t)\left\{\sum_{n=1}^{\infty}\frac{m_n}{m_T}\frac{g}{h\omega_n^2}+\sum_{n=1}^{\infty}\frac{m_n}{m_T}\left(\frac{H_n}{h}+\frac{g}{h\omega_n^2}\right)\frac{\omega^2}{\omega_n^2-\omega^2+i2\gamma_n\omega_n\omega}\right\}$$

$$M_y = -im_T hX_0\omega^2\exp(i\omega t)\left\{\sum_{n=1}^{\infty}\frac{m_n}{m_T}\frac{g}{h\omega_n^2}+\sum_{n=1}^{\infty}\frac{m_n}{m_T}\left(\frac{H_n}{h}+\frac{g}{h\omega_n^2}\right)\frac{\omega^2}{\omega_n^2-\omega^2+i2\gamma_n\omega_n\omega}\right\}$$
$$-im_T h^2\alpha_0\omega^2\exp(i\omega t)\left\{\begin{array}{l}\dfrac{I_y}{m_T h^2}+\displaystyle\sum_{n=1}^{\infty}\frac{m_n}{m_T}\frac{g}{h\omega_n^2}\frac{g}{h\omega^2}+\sum_{n=1}^{\infty}\frac{m_n}{m_T}\frac{2g}{h\omega_n^2}\left(\frac{H_n}{h}+\frac{g}{2h\omega_n^2}\right)\\ \quad+\displaystyle\sum_{n=1}^{\infty}\frac{m_n}{m_T}\left(\frac{H_n}{h}+\frac{g}{h\omega_n^2}\right)^2\frac{\omega^2}{\omega_n^2-\omega^2+i2\gamma_n\omega_n\omega}\end{array}\right\}$$

The term, $\frac{\omega^2}{\omega_n^2-\omega^2+i2\gamma_n\omega_n\omega}$ consist of a real and an imaginary number which are expressed as below:

$$\frac{\omega^2}{\omega_n^2-\omega^2+i2\gamma_n\omega_n\omega}=\frac{\omega^2}{\omega_n^2-\omega^2+i2\gamma_n\omega_n\omega}\times\frac{\omega_n^2-\omega^2-i2\gamma_n\omega_n\omega}{\omega_n^2-\omega^2-i2\gamma_n\omega_n\omega}$$
$$=\frac{\omega^2\left(\omega_n^2-\omega^2\right)}{\left(\omega_n^2-\omega^2\right)^2+\left(2\gamma_n\omega_n\omega\right)^2}+i\frac{-\omega^2\left(2\gamma_n\omega_n\omega\right)}{\left(\omega_n^2-\omega^2\right)^2+\left(2\gamma_n\omega_n\omega\right)^2}$$

$$\mathrm{Re}\left[\frac{\omega^2}{\omega_n^2-\omega^2+i2\gamma_n\omega_n\omega}\right]=\frac{\omega^2\left(\omega_n^2-\omega^2\right)}{\left(\omega_n^2-\omega^2\right)^2+\left(2\gamma_n\omega_n\omega\right)^2}$$

$$\mathrm{Im}\left[\frac{\omega^2}{\omega_n^2-\omega^2+i2\gamma_n\omega_n\omega}\right]=\frac{-\omega^2\left(2\gamma_n\omega_n\omega\right)}{\left(\omega_n^2-\omega^2\right)^2+\left(2\gamma_n\omega_n\omega\right)^2}$$

The damping is the energy dissipation of a real liquid. The energy dissipation occurs at the walls and free surface as a result of viscous boundary layers and within the interior of liquid as a result of viscous stresses. For small tanks, dissipation at boundary layers dominates, whereas for large tanks, the dissipation within the interior of liquid may be dominant.

The energy dissipation by wave propagation at far distance does not contribute to the energy dissipation mechanism of liquid cargo in the tank unlike the ones from the surrounding water. Damping solely viscous in nature is quite small even for a moderately large tank and for tanks with dimension of 1 m or so the damping ratio generally equals to 1% or less. For large tanks adopted in

FLNG or LNGC, damping is much smaller. Therefore, the effect of damping from liquid cargo on floating motion is quite small and negligible.

To achieve large damping ratio, a series of baffles shall be attached to the tank walls/bottom. However, the damping of liquid cargo is still small. Even with baffles, the damping ratio is seldom greater than 5% of the critical damping.

Appendix 2 Details of Mathematical Expression in Chapter 2.4

A2.1 Force and Moment by Linear Displacement

The horizontal force and moment in the rectangular tank excited horizontally are obtained by integrating the liquid pressure over the tank wall area.

$$F_x = \int_{-h/2}^{h/2+\delta}\int_{-b/2}^{b/2} p\big|_{x=a/2}\,dydz - \int_{-h/2}^{h/2-\delta}\int_{-b/2}^{b/2} p\big|_{x=-a/2}\,dydz = 2b\int_{-h/2}^{h/2} p\big|_{x=a/2}\,dz$$

$$= -i2b\int_{-h/2}^{h/2} \rho X_0\omega^2 \exp(i\omega t)\left\{\frac{a}{2} + \sum_{n=1}^{\infty}\frac{\omega^2}{\omega_n^2-\omega^2}\frac{4a}{\pi^2(2n-1)^2}\frac{\cosh\left[\lambda_n\left(z+h/2\right)\right]}{\cosh(\lambda_n h)}\right\}dz$$

$$= -i2\rho bX_0\omega^2 \exp(i\omega t)\int_{-h/2}^{h/2}\left\{\frac{a}{2} + \sum_{n=1}^{\infty}\frac{\omega^2}{\omega_n^2-\omega^2}\frac{4a}{\pi^2(2n-1)^2}\frac{\cosh\left[\lambda_n\left(z+h/2\right)\right]}{\cosh(\lambda_n h)}\right\}dz$$

$$= -i\rho abX_0\omega^2 \exp(i\omega t)\times$$
$$\left\{h + \sum_{n=1}^{\infty}\frac{\omega^2}{\omega_n^2-\omega^2}\frac{8}{\pi^2(2n-1)^2}\frac{1}{\cosh(\lambda_n h)}\int_{-h/2}^{h/2}\cosh\left[\lambda_n\left(z+h/2\right)\right]dz\right\}$$

$$= -i\rho abX_0\omega^2 \exp(i\omega t)\times$$
$$\left\{h + \sum_{n=1}^{\infty}\frac{\omega^2}{\omega_n^2-\omega^2}\frac{8}{\pi^2(2n-1)^2}\frac{1}{\cosh(\lambda_n h)}\frac{a}{\pi}\sinh(\lambda_n h)\right\}$$

$$= -im_T X_0\omega^2 \exp(i\omega t)\times$$
$$\left\{1 + \sum_{n=1}^{\infty}\frac{8(a/h)\tanh(\lambda_n h)}{\pi^3(2n-1)^3}\frac{\omega^2}{\omega_n^2-\omega^2}\right\},\quad m_T = \rho abh$$

$$M_y = \int_{-h/2}^{h/2+\delta}\int_{-b/2}^{b/2} zp\big|_{x=a/2}\,dydz - \int_{-h/2}^{h/2-\delta}\int_{-b/2}^{b/2} zp\big|_{x=-a/2}\,dydz + \int_{-a/2}^{a/2}\int_{-b/2}^{b/2} xp\big|_{z=-h/2}\,dydx$$

$$= 2b\int_{-h/2}^{h/2} zp\big|_{x=a/2}\,dz + b\int_{-a/2}^{a/2} xp\big|_{z=-h/2}\,dx$$

$$M_{y1} = 2b\int_{-h/2}^{h/2} zp\big|_{x=-a/2}\,dz$$

$$= -i2\rho bX_0\omega^2\exp(i\omega t)\times$$
$$\left\{\int_{-h/2}^{h/2}\frac{a}{2}z\,dz + \sum_{n=1}^{\infty}\frac{\omega^2}{\omega_n^2-\omega^2}\frac{4a}{\pi^2(2n-1)^2\cosh(\lambda_n h)}\int_{-h/2}^{h/2} z\cosh\left[\lambda_n\left(z+h/2\right)\right]dz\right\}$$

$$= -i2\rho bX_0\omega^2\exp(i\omega t)\times$$
$$\left\{\sum_{n=1}^{\infty}\frac{\omega^2}{\omega_n^2-\omega^2}\frac{4a}{\pi^2(2n-1)^2\cosh(\lambda_n h)}\left[\frac{h}{2\lambda_n}\sinh(\lambda_n h)-\frac{1}{\lambda_n^2}\left(\cosh(\lambda_n h)-1\right)\right]\right\}$$

$$= -im_T hX_0\omega^2\exp(i\omega t)\times$$
$$\sum_{n=1}^{\infty}\left\{\left[\frac{4a\tanh(\lambda_n h)}{\pi^3(2n-1)^3 h}-\frac{8}{\pi^4(2n-1)^4}\left(\frac{a}{h}\right)^2\left(1-\frac{1}{\cosh(\lambda_n h)}\right)\right]\frac{\omega^2}{\omega_n^2-\omega^2}\right\}$$

$$M_{y2} = b\int_{-a/2}^{a/2} xp\big|_{z=-h/2}\,dx$$

$$= -i\rho bX_0\omega^2\exp(i\omega t)\times$$
$$\left\{\int_{-a/2}^{a/2}x^2dx + \sum_{n=1}^{\infty}\frac{\omega^2}{\omega_n^2-\omega^2}\frac{4a(-1)^{n-1}}{\pi^2(2n-1)^2\cosh(\lambda_n h)}\int_{-h/2}^{h/2} x\sin(\lambda_n x)dx\right\}$$

$$= -i\rho bX_0\omega^2\exp(i\omega t)\times$$
$$\left\{\frac{a^3}{12}+\sum_{n=1}^{\infty}\frac{\omega^2}{\omega_n^2-\omega^2}\frac{4a}{\pi^2(2n-1)^4\cosh(\lambda_n h)}\frac{2a^2}{\pi^2}\right\}$$

$$= -im_T hX_0\omega^2\exp(i\omega t)\times$$
$$\left\{\frac{1}{12}\left(\frac{a}{h}\right)^2+\sum_{n=1}^{\infty}\frac{8}{\pi^4(2n-1)^4}\left(\frac{a}{h}\right)^2\frac{1}{\cosh(\lambda_n h)}\frac{\omega^2}{\omega_n^2-\omega^2}\right\}$$

$$M_y = M_{y1} + M_{y2}$$

$$= -im_T hX_0\omega^2 \exp(i\omega t)\times \left[\frac{1}{12}\left(\frac{a}{h}\right)^2 + \sum_{n-1}^{\infty}\left\{\left[\frac{4a\tanh(\lambda_n h)}{\pi^3(2n-1)^3 h} - \frac{8}{\pi^4(2n-1)^4}\left(\frac{a}{h}\right)^2\left(1-\frac{1}{\cosh(\lambda_n h)}\right) + \frac{8}{\pi^4(2n-1)^4}\left(\frac{a}{h}\right)^2\frac{1}{\cosh(\lambda_n h)}\right]\frac{\omega^2}{\omega_n^2-\omega^2}\right\}\right]$$

$$= -im_T hX_0\omega^2 \exp(i\omega t)\times \left[\frac{1}{12}\left(\frac{a}{h}\right)^2 + \sum_{n-1}^{\infty}\left\{\left[\frac{4a\tanh(\lambda_n h)}{\pi^3(2n-1)^3 h} - \frac{8}{\pi^4(2n-1)^4}\left(\frac{a}{h}\right)^2\left(1-\frac{2}{\cosh(\lambda_n h)}\right)\right]\frac{\omega^2}{\omega_n^2-\omega^2}\right\}\right]$$

The relationship below is introduced into the formula:

$$1-\frac{2}{\cosh(\lambda_n h)} = 2\left(1-\frac{1}{\cosh(\lambda_n h)}\right) - 1 = 2\tanh(\lambda_n h)\tanh\left(\frac{\lambda_n h}{2}\right) - 1$$

$$\omega_n^2 = g\lambda_n \tanh(\lambda_n h), \quad \lambda_n = \frac{(2n-1)\pi}{a}$$

Then, the formula of the moment is obtained as:

$$M_y = -im_T hX_0\omega^2 \exp(i\omega t)\times \left[\frac{1}{12}\left(\frac{a}{h}\right)^2 + \sum_{n-1}^{\infty}\left\{\left[\frac{4a\tanh(\lambda_n h)}{\pi^3(2n-1)^3 h} - \frac{8}{\pi^4(2n-1)^4}\left(\frac{a}{h}\right)^2\left(2\tanh(\lambda_n h)\tanh\left(\frac{\lambda_n h}{2}\right)-1\right)\right]\frac{\omega^2}{\omega_n^2-\omega^2}\right\}\right]$$

$$= -im_T hX_0\omega^2 \exp(i\omega t)\times \left[\frac{1}{12}\left(\frac{a}{h}\right)^2 + \sum_{n-1}^{\infty}\left\{\frac{8\,(a/h)\tanh(\lambda_n h)}{\pi^3(2n-1)^3}\left[\frac{1}{2} - \frac{2\,(a/h)}{\pi(2n-1)}\tanh\left(\frac{\lambda_n h}{2}\right) + \frac{(a/h)}{\pi(2n-1)}\frac{1}{\tanh(\lambda_n h)}\right]\frac{\omega^2}{\omega_n^2-\omega^2}\right\}\right]$$

$$= -im_T hX_0\omega^2 \exp(i\omega t)\times \left[\frac{1}{12}\left(\frac{a}{h}\right)^2 + \sum_{n-1}^{\infty}\left\{\frac{8\,(a/h)\tanh(\lambda_n h)}{\pi^3(2n-1)^3}\left[\frac{1}{2} - \frac{2\,(a/h)}{\pi(2n-1)}\tanh\left(\frac{\lambda_n h}{2}\right) + \frac{g}{h\omega_n^2}\right]\frac{\omega^2}{\omega_n^2-\omega^2}\right\}\right]$$

Appendix 3 Correction of The New "Dynamic Behavior of Liquids in Moving Containers"

This appendix shows notes for correction of the text named The New "Dynamic Behavior of Liquids in Moving Containers" which was referred in the mathematical expression of the mechanical model and the analytical solution for the rectangular tank (chapters 2.2 and 2.4, Appendices 1 and 2).

Horizontal motion parallel to the *x* axis. For this case, the tank displacement is expressed as $X(t) = -iX_o\exp(i\Omega t)$. This choice makes the real displacement equal to $X_o\sin\Omega t$. The velocity components of the tank walls are $v = w = 0$ and $u = iX_o\Omega\exp(i\Omega t)$. Thus, the boundary conditions at the wetted surfaces of the tank are expressed as:

$$n\cdot\nabla\Phi = iX_o\Omega e^{i\Omega t} \quad \text{at wetted surfaces} \tag{1.8}$$

To be corrected $X_0\Omega\exp(i\Omega t)$

OK $\Phi_X(t) = X(t) = -iX_0\exp(i\Omega t)$

This is correct.

Forced motion - oscillatory translation of the tank

The free (eigenfunction) slosh modes are the basis for constructing a solution when the tank is forced to oscillate. For a first example, the tank is assume to oscillate along the x axis. For a rectangular tank, the boundary condition Eq. (1.8) therefore reduces to:

$$\frac{\partial\Phi}{\partial x} = \Omega X_o e^{i\Omega t} \quad \text{for} \quad x = \pm a/2; \qquad \frac{\partial\Phi}{\partial y} = 0 \quad \text{for} \quad y = \pm b/2 \tag{1.22}$$

$$\Phi(x,z,t) = -Ae^{i\Omega t}\left\{x + \sum_{n=1}^{\infty}\frac{4a(-1)^{n-1}}{\pi^2(2n-1)^2}\left(\frac{\Omega^2}{\omega_n^2-\Omega^2}\right)\sin\left[(2n-1)\pi\frac{x}{a}\right]\times \frac{\cosh\left[(2n-1)\pi(z/a+h/2a)\right]}{\cosh\left[(2n-1)\pi(h/a)\right]}\right\} \tag{1.26}$$

To be corrected $\Omega X_0\exp(i\Omega t)$

Forces and torques. Proceeding as before to integrate the liquid pressure distribution on the walls and bottom, the x-component of the force exerted on the tank is found to be:

$$\frac{F_{xo}}{-i\Omega^2 m_{liq} h\alpha_o} = \left\{ \frac{1}{12}\left(\frac{a}{h}\right)^2 + 8\left(\frac{a}{h}\right)\sum_{n=1}^{\infty} \frac{\tanh[(2n-1)\pi h/a]}{(2n-1)^3\pi^3}\left[\frac{1}{2} - \frac{\tanh[(2n-1)\pi h/2a]}{(2n-1)\pi h/2a}\right] + \right.$$

$$\left. \frac{g}{h\omega_n^2}\left(\frac{\Omega^2}{\omega_n^2 - \Omega^2}\right)\right\}$$

To be corrected α_0

To be corrected $\frac{g}{2h\omega_n^2}$

Equation (1.34) shows that the *force* for a pitching oscillation is the same as the *torque* for a lateral oscillation [Eq. (1.30)] when the amplitude X_o of the translation is replaced by $h\alpha_o$. The torque exerted on the tank is given by:

$$\frac{M_{yo}}{im_{liq}h^3\alpha_o\Omega^2} = \left\{ \frac{I_y}{m_{liq}h^2} + 16\left(\frac{a}{h}\right)\sum_{n=1}^{\infty} \frac{\tanh[(2n-1)\pi h/a]}{(2n-1)^3\pi^3}\left(\frac{g}{h\omega_n^2}\right)\left[\frac{1}{2} + \frac{g}{h\omega_n^2} + \right.\right.$$

$$\left. - \frac{\tanh[(2n-1)\pi h/2a]}{(2n-1)\pi h/2a}\right] + 8\left(\frac{a}{h}\right)\sum_{n=1}^{\infty} \frac{\tanh[(2n-1)\pi h/a]}{(2n-1)^3\pi^3}\left[\frac{g}{h\omega_n^2}\right]\left[\frac{1}{2} + \frac{g}{h\omega_n^2} + \right.$$

To be deleted

(cont'd)

To be corrected $-im_{liq}h^2\alpha_0\Omega^2$

$$\left. \left. - \frac{\tanh[(2n-1)\pi h/2a]}{[(2n-1)\pi h/2a]}\right]^2 \left\{ \left(\frac{\Omega^2}{\omega_n^2 - \Omega^2}\right) + \frac{1}{12}\left(\frac{a}{h}\right)^2\left(\frac{g}{h\Omega^2}\right)\right\}\right\} \qquad (1.35)$$

Figure 3.2 shows the model and the symbols used in the analysis. The derivation of the model equations given below is independent of tank shape and fill level. The system of springs, masses, etc., is supposed to "fit" inside the actual tank and replace the liquid. For clarity, only two spring-masses are shown, but there is in fact one spring-mass for each slosh mode. The spring masses do not have a moment of inertia, so any needed moment of inertia I_0 is assigned to the rigidly-attached mass m_0. The center of mass of the system is at the same height above the bottom of the tank as the liquid, and the locations H_n of the masses are referenced to the center of mass. The width of the tank is $2a$. Gravity g or an equivalent thrust-induced acceleration acts along the axis of the tank. The tank is excited by a small time-varying linear displacement X_o and angular rotation α_o about an axis through the center of mass. The spring masses deflect a distance x_n relative to the tank walls as a result of the tank motion.

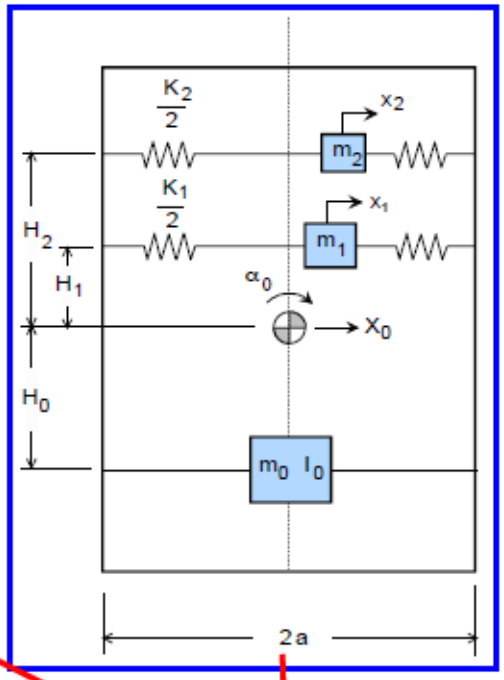

Figure 3.2. Schematic of equivalent mechanical model for lateral sloshing

To be corrected a

Static properties. To preserve the static properties of the liquid, the sum of all the masses must be the same as the liquid mass m_{liq}, and the center of mass of the model must be at the same elevation as the liquid. These constraints are expressed analytically by:

$$m_0 + \sum m_n = m_{liq} \tag{3.1}$$

$$m_0 H_0 + \sum m_n H_n = 0 \tag{3.2}$$

To be corrected H_0^2

To be corrected H_n

Likewise, the net torque exerted on the tank is given by:

$$-M = (I_0 + m_0 H_0)\ddot{\alpha}_0 + \sum m_n h_n (\ddot{x}_n + H_n \ddot{\alpha}_0) - g \sum m_n x_n \tag{3.5}$$

where the last term is the torque caused by the offset of each spring-mass from the tank centerline. (Some terms have already been cancelled out of this equation.) The equation of motion for each of the spring-masses is expressed as:

$$m_n (\ddot{X}_0 + \ddot{x}_n + H_n \ddot{\alpha}_0) + K_n x_n - m_n g \alpha_0 = 0 \tag{3.6}$$

Just as was done in Chapter 1, the tank accelerations are assumed to be oscillatory at frequency Ω. The components of the tank motion are therefore given by $-X_o \exp(i\Omega t)$ and $-i\alpha_o \exp(i\Omega t)$, and Eq. (3.6) can expressed as:

$$x_n = -\frac{i\Omega^2 X_0}{\omega_n^2 - \Omega^2} - \left(\frac{H_n + g/\Omega^2}{\omega_n^2 - \Omega^2} \right) i\Omega^2 \alpha_0 \tag{3.7}$$

To be corrected $-iX_0 \exp(i\Omega t)$

where Eq. (3.3) has also been used to eliminate K_n. With these equations, the amplitudes of the force and torque on the tank can be expressed analytically as:

$$\frac{F_{amp}}{i\Omega^2 m_{liq}} = -\left[1 + \sum \frac{m_n}{m_{liq}} \left(\frac{\Omega^2}{\omega_n^2 - \Omega^2} \right) \right] X_0 - \alpha_0 \sum \frac{m_n}{m_{liq}} \left(\frac{H_n \Omega^2 + g}{\omega_n^2 - \Omega^2} \right) \tag{3.8}$$

$$\frac{M_{amp}}{i\Omega^2} = -\alpha_0 \left[I_0 + m_0 H_0^2 + \sum m_n H_n^2 + m_{liq} \sum \frac{m_n}{m_{liq}} \left(\frac{H_n^2 \Omega^2 + 2 H_n g + g h^2 / \omega_n^2}{\omega_n^2 - \Omega^2} \right) \right]$$

$$- m_{liq} X_0 \sum \frac{m_n}{m_{liq}} \left(\frac{H_n \Omega^2 + g}{\omega_n^2 - \Omega^2} \right) \tag{3.9}$$

To be corrected g^2/Ω^2

To allow easy comparison to the model force comparison, the slosh force expression is re-written in a slightly different by using the following identities:

$$\frac{1}{\omega_n^2 - \Omega^2} = 1 + \frac{\Omega^2}{\omega_n^2 - \Omega^2} \qquad \text{and} \qquad 8 \sum \frac{\tanh[(2n-1)\pi h/a]}{\pi^5 (2n-1)^5} = \frac{1}{12} \frac{a}{h}$$

To be corrected ω_n^2

To be corrected $\sum_{n=1}^{\infty} \frac{8}{\pi^4 (2n-1)^4} = \frac{1}{12}$

Appendix 4 Parameters for Prismatic Tank Model

The dynamic behaviour of liquid in tank is represented by the mechanical model. The parameters of mechanical model for the rectangular tank can be obtained analytically.
This appendix shows that the analytical solution for rectangular tank can be expanded to a prismatic tank with slight modification.

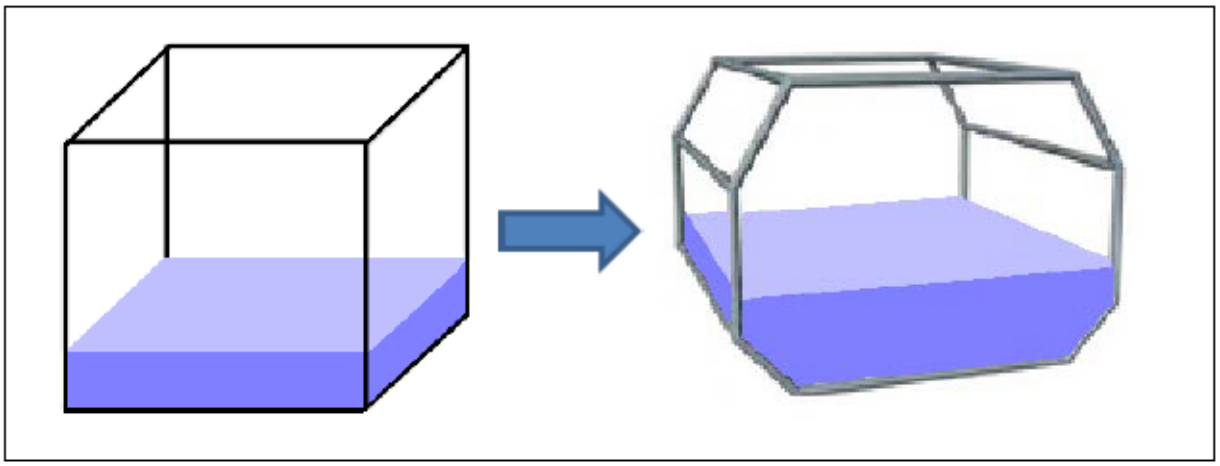

Figure A4.1. Rectangular Tank to Prismatic Tank

A4.1 Force and Moment by Dynamic Behaviour of Liquid in Tank

The force amplitude along x-axis and the moment amplitude about y-axis (passing through COG of liquid in tank) caused by the dynamic behaviour of liquid in tank excited horizontally and rotationally around y-axis are represented as following formula:

$$\frac{F_{x\_amp}}{m_T\omega^2} = X_0\left\{1+\sum_{n=1}^{\infty}\frac{m_n}{m_T}\frac{\omega^2}{\omega_n^2-\omega^2}\right\}+h\alpha_0\left\{\sum_{n=1}^{\infty}\frac{m_n}{m_T}\frac{g}{h\omega_n^2}+\sum_{n=1}^{\infty}\frac{m_n}{m_T}\left(\frac{H_n}{h}+\frac{g}{h\omega_n^2}\right)\frac{\omega^2}{\omega_n^2-\omega^2}\right\}$$

$$\frac{M_{y\_amp}}{m_T h\omega^2} = X_0\left\{\sum_{n=1}^{\infty}\frac{m_n}{m_T}\frac{g}{h\omega_n^2}+\sum_{n=1}^{\infty}\frac{m_n}{m_T}\left(\frac{H_n}{h}+\frac{g}{h\omega_n^2}\right)\frac{\omega^2}{\omega_n^2-\omega^2}\right\}$$
$$+h\alpha_0\left\{\begin{array}{r}\dfrac{I_y}{m_T h^2}+\displaystyle\sum_{n=1}^{\infty}\frac{m_n}{m_T}\frac{g}{h\omega_n^2}\frac{g}{h\omega^2}+\sum_{n=1}^{\infty}\frac{m_n}{m_T}\frac{g}{h\omega_n^2}\left(\frac{2H_n}{h}+\frac{g}{h\omega_n^2}\right)\\ +\displaystyle\sum_{n=1}^{\infty}\frac{m_n}{m_T}\left(\frac{H_n}{h}+\frac{g}{h\omega_n^2}\right)^2\frac{\omega^2}{\omega_n^2-\omega^2}\end{array}\right\}$$

A4.2 Mechanical Model Parameters of Rectangular Tank

The mechanical model parameters of a rectangular tank are obtained analytically.

$$\omega_n^2 = g\lambda_n \tanh(\lambda_n h), \quad \lambda_n = \frac{(2n-1)\pi}{a}$$

$$\frac{m_n}{m_T} = \frac{8a}{h}\frac{\tanh(\lambda_n h)}{\pi^3(2n-1)^3}, \quad \frac{H_n}{h} = \frac{1}{2} - \frac{2(a/h)}{\pi(2n-1)}\tanh\left(\frac{\lambda_n h}{2}\right)$$

$$I_R = \frac{1}{12}m_T\left(a^2+h^2\right), \quad I_d = \frac{1}{12}m_T\left(a^2+h^2\right)\left\{\frac{4}{1+(h/a)^2} - \frac{768a/h}{\pi^5\left[1+(h/a)^2\right]}\sum_{n=1}^{\infty}\frac{\tanh\left[(2n-1)\pi h/2a\right]}{(2n-1)^5}\right\}$$

$$m_T = \rho\, abh$$

A4.3 Modification of tank model parameters from Rectangular to Prismatic

The parameters of mechanical model of a prismatic tank can be obtained from that of a rectangular one by applying slight modifications as shown below.

1. Free Surface Width

For a rectangular tank, free surface width is equal to its width and does not vary with liquid depth. However, free surface width of a prismatic tank varies with liquid depth; hence *a* is replaced by *a(h)*.

$$\omega_n^2 = g\lambda_n \tanh(\lambda_n h), \quad \lambda_n = \frac{(2n-1)\pi}{a(h)}$$

$$\frac{m_n}{m_T} = \frac{8a(h)}{h}\frac{\tanh(\lambda_n h)}{\pi^3(2n-1)^3}, \quad \frac{H_n}{h} = \frac{1}{2} - \frac{2(a(h)/h)}{\pi(2n-1)}\tanh\left(\frac{\lambda_n h}{2}\right)$$

2. Liquid Mass

Liquid mass shall be obtained from prismatic volume of the tank.

$$m_T = \rho\left(abh - V_{chamfer}\right)$$

3. Mass Inertia

Mass inertia of rigid cargo of a prismatic tank is smaller than that of a rectangular one. It shall be calculated based on the dimensions of tank such as overall width, liquid height and chamfer dimensions.

The mass inertia of free rotating liquid is subtracted and as a result, the mass inertia of liquid cargo becomes significantly smaller than that of rigid cargo.

The ratio of mass inertia is decreased when the ratio of width and liquid depth is close to 1. The red line shown in Figure A4.2 denotes probable ratio of mass inertia of a prismatic tank. It is smaller than that of a rectangular tank due to chamfer and larger than that of a hexagonal one.
The effect of reduction in mass inertia due to liquid cargo, however, is small comparing with the total force and moment. Therefore, analytical formula for rectangular tank can be used.

$$I_R = \frac{1}{12} m_T \left(a(h)^2 + h^2 \right)$$

$$I_d = \frac{1}{12} m_T \left(a(h)^2 + h^2 \right) \left\{ \frac{4}{1 + (h/a(h))^2} - \frac{768\, a/h}{\pi^5 \left[1 + (h/a(h))^2 \right]} \sum_{n=1}^{\infty} \frac{\tanh\left[(2n-1)\pi h / 2a(h) \right]}{(2n-1)^5} \right\}$$

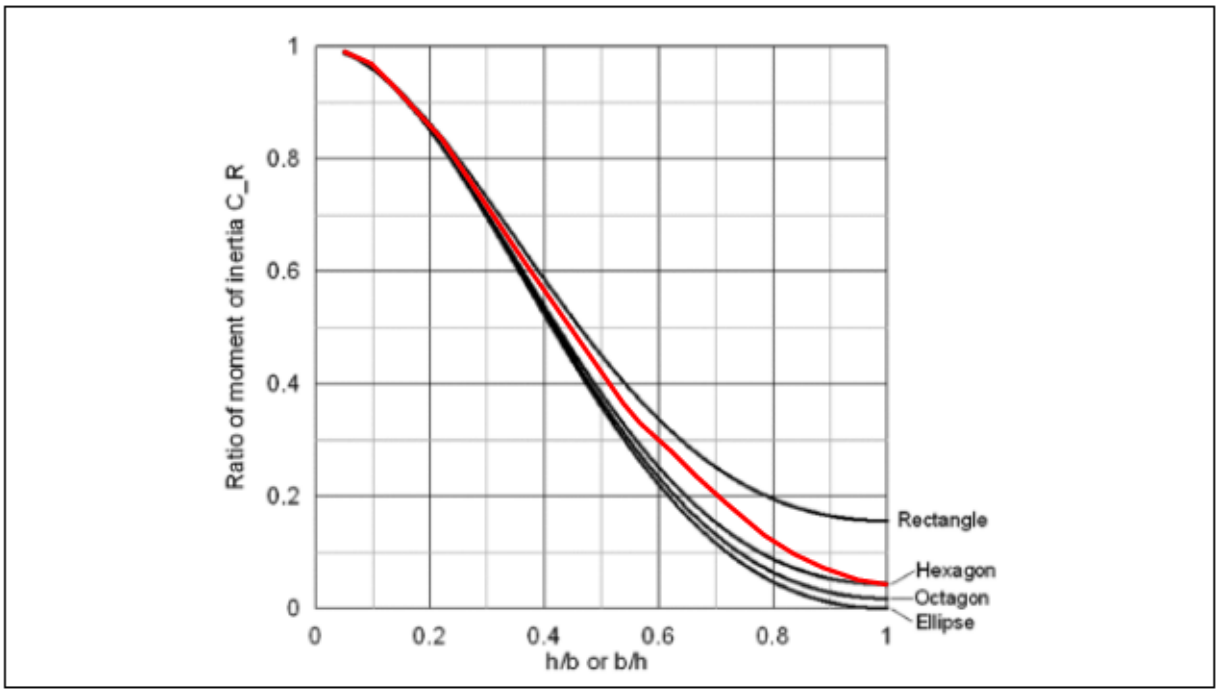

Figure A4.2. Ratio of Moment of Inertia of Various Shapes

A4.4 Sloshing Natural Frequency of Prismatic Tank

According to "Sloshing" by Faltinsen and Timokha [35], the sloshing natural frequency of the i-th mode of a prismatic tank with chamfered bottom is given by the equations (1) and (2) in Figure A4.3. Eq. (1) gives the sloshing natural frequency of a rectangular tank and Eq. (2) gives a correction factor and $\omega'_{r,i}$ is the corrected sloshing natural frequency of a prismatic tank.

However, following points shall be kept in mind in order to use the correction factor properly.

1. Correction factor is valid only for free surface width equals to B_T.
2. Correction factor of chamfered top is not obtained.
3. Correction factor is generally close to 1.

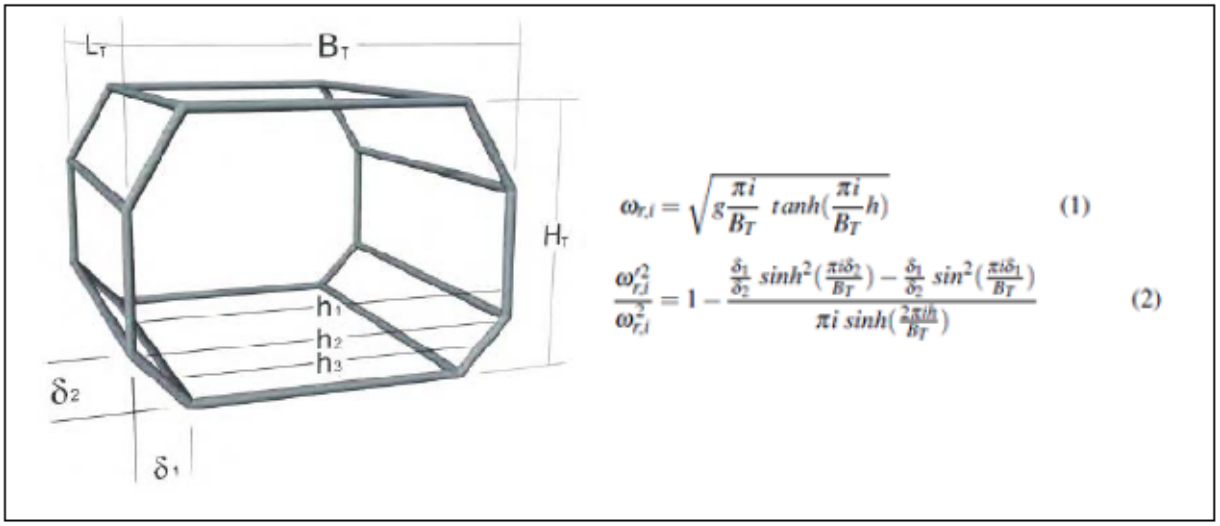

Figure A4.3. Corrected Sloshing Natural Frequency of Prismatic Tank

In addition, the sloshing natural frequency of a prismatic tank can be approximated using the equation of sloshing natural frequency of a rectangular tank with varying free surface width. Therefore, in practice, the correction factor of Eq. (2) can be omitted to obtain the sloshing natural frequency of a prismatic tank.

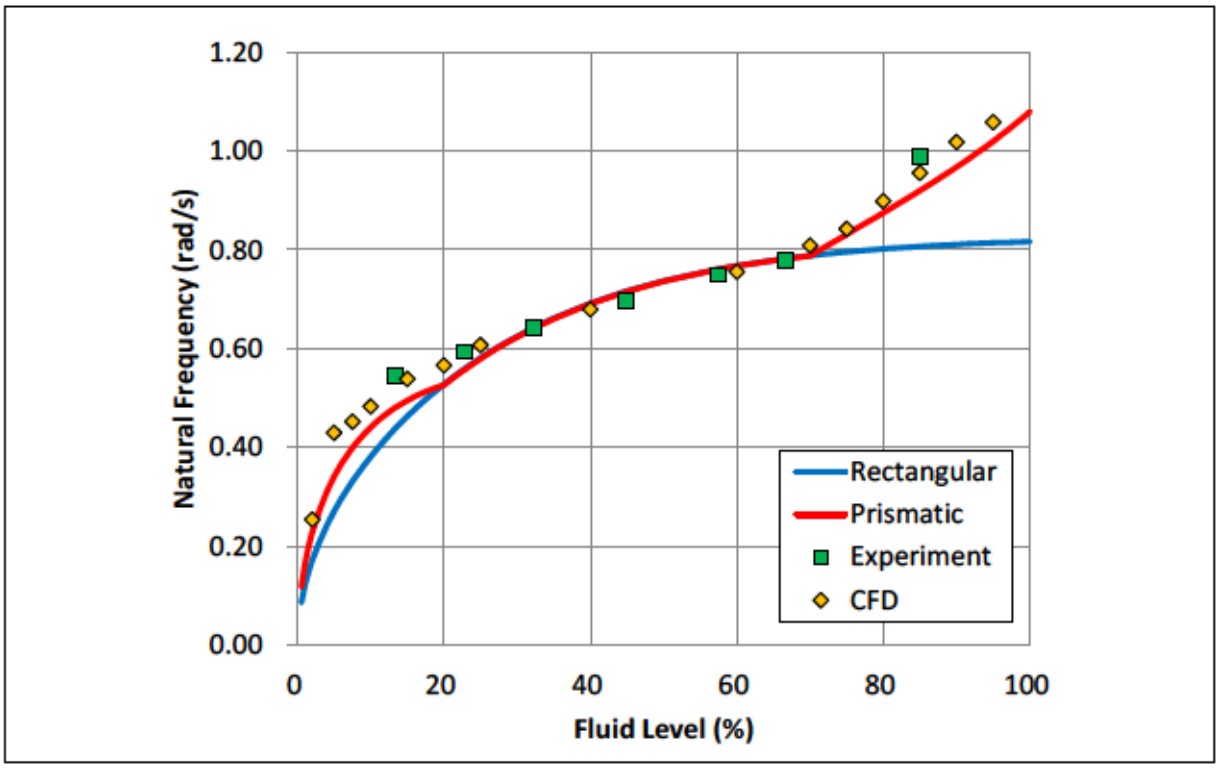

Figure A4.4. Sloshing Natural Frequency of Prismatic Tank

The Eq. (2) is obtained as an asymptotic formula in "Sloshing" for a two-dimensional prismatic tank with the chamfered bottom by Faltinsen and Timokha [35]. The assumptions of the asymptotic formula are as follows:

1) target liquid domain is geometrically close to the original liquid domain,
2) target liquid domain is contained within the original liquid domain,
3) the mean free surface of the target liquid domain is same as that of the original liquid domain

When the mean free surface is located at the bottom of chamfer, the original liquid domain Q_0 shall be redefined, whereas when it is located at the top of chamfer, the asymptotic formula is not applicable due to the assumption 2) mentioned above.

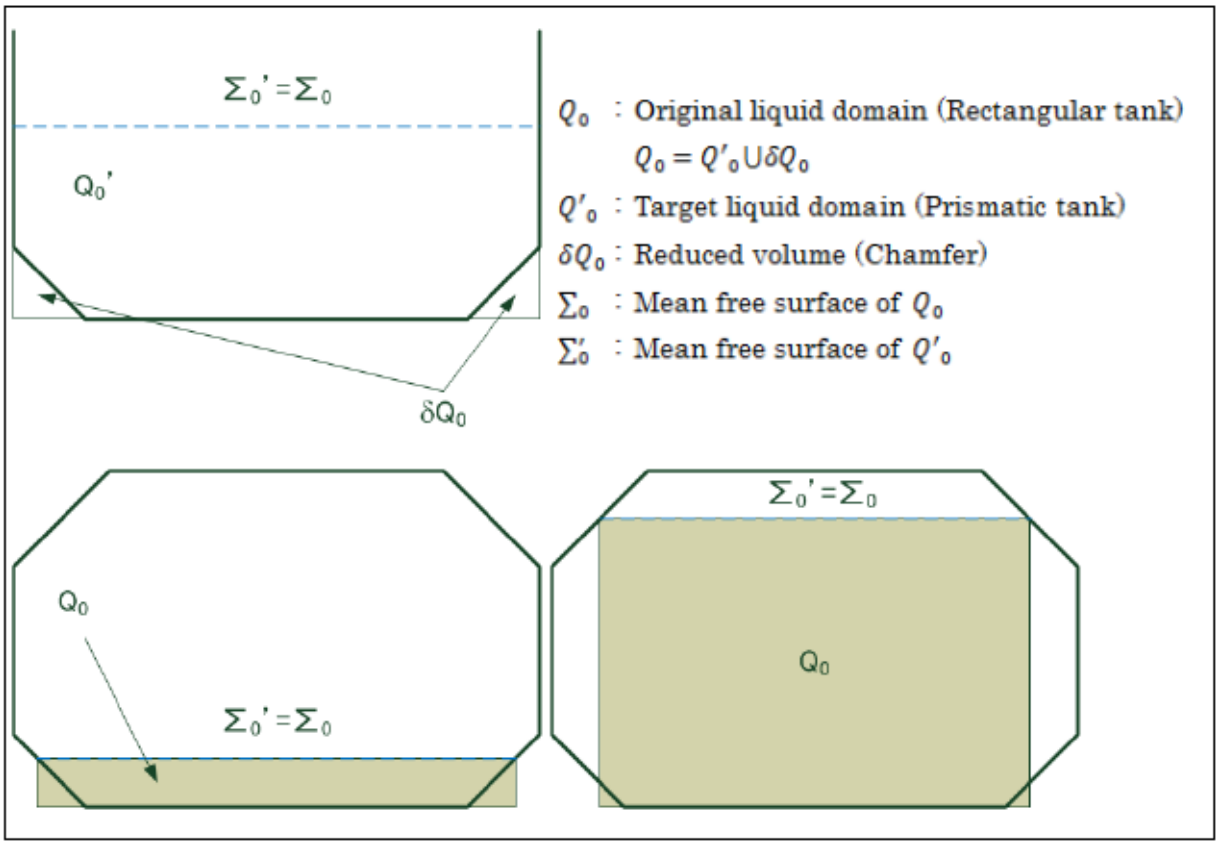

Figure A4.5. Assumptions of Asymptotic Formula

The sloshing natural frequency and correction factor for a prismatic tank with dimensions as shown in Figure A4.6 are obtained and plotted. The sloshing natural frequencies obtained by experiment and CFD are also plotted.

The sloshing natural frequency is mostly related to the free surface width. The contribution of the correction factor is negligible.

The correction factor takes the minimum value, when the free surface is located at the up end of the chamfered bottom (20% fluid level in this case); however, the relative error is less than 0.4 %. This is also pointed in "Sloshing" by Faltinsen and Timokha [35].

The sloshing natural frequencies of a prismatic tank obtained by experiment and CFD are agreed well with that of the one calculated by the following equations.

$$\omega_n^2 = g\lambda_n \tanh(\lambda_n h), \quad \lambda_n = \frac{(2n-1)\pi}{a(h)}$$

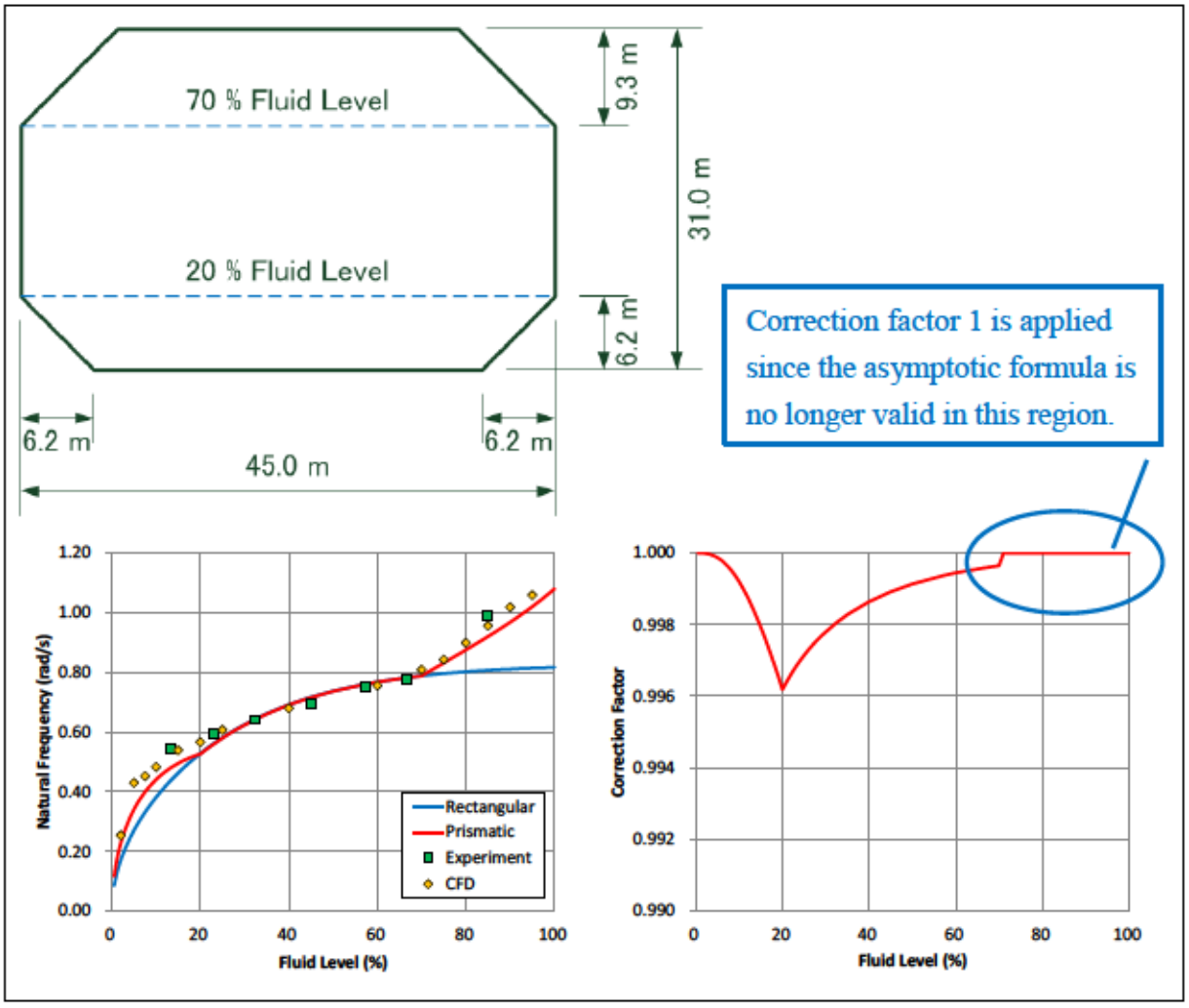

Figure A4.6. Sloshing Natural Frequency and Correction Factor for Prismatic Tank

A4.5 Moment of Inertia of Liquid in Tank

Gyeong[36] demonstrated the reduction in mass inertia due to freely rotating liquid for shapes, rectangular, ellipse, hexagon and octagon with various aspect ratios. The octagon case is close to that of a prismatic one. This is a good reference for consideration of mass inertia of a prismatic tank. However, it is essential to note that the term 'h' refers to overall height of the tank, not the height of liquid.

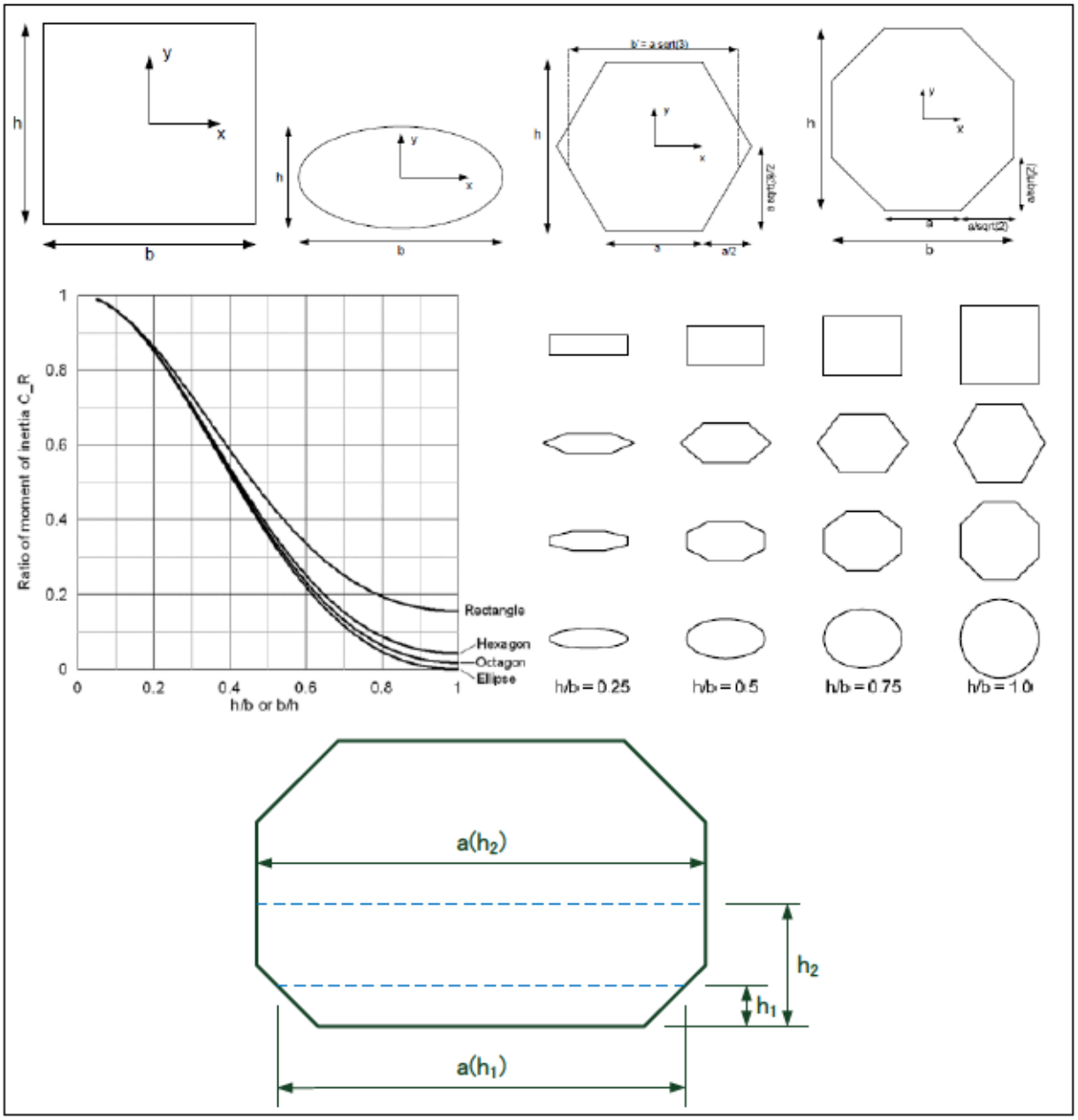

Figure A4.7. Moment of Inertia of Liquid in Tank

Appendix 5 Parameters for Arbitrarily Shaped Tank Model

In many cases, determination by analytical solution is neither practical nor possible. In such circumstances, determination either by numerical calculation or experimental measurement is the only available option.

For practical applications, modes at higher order (n > 2) are usually of little concern, since the magnitudes of slosh mass for these modes are very small compared to the fundamental mode. It is sufficient to consider only the first, lowest-frequency slosh mass. The procedure for determination of parameters of a tank model is to excite it by simple harmonic motion using both horizontal and rotating oscillation over a range of frequencies that encompasses the first sloshing natural frequency, calculate or measure the resulting force and moment responses as a function of excitation frequency, and fit a model to suit the force and moment calculated in the previous step. The slosh mass, associated height and mass inertia of disk are calculated by following equations. As shown in the equations below, slosh mass is determined from calculated or measured horizontal force against horizontal oscillation. Slosh mass height is determined from moment against horizontal oscillation or by horizontal force against rotating oscillation. Mass inertia of free rotating liquid is determined from moment against rotating oscillation. These are summarized in Table A5.1.

$$m_1 = \left(\frac{F_{x\_amp}}{\omega^2 X_0} - m_T \right) \left(\frac{\omega_1^2 - \omega^2}{\omega^2} \right)$$

$$H_1 = \left(\frac{M_{y\_amp}}{m_1 \omega^2 X_0} - \frac{g}{\omega_1^2} \right) \left(\frac{\omega_1^2 - \omega^2}{\omega^2} \right) - \frac{g}{\omega_1^2} \quad \text{or} \quad H_1 = \left(\frac{F_{x\_amp}}{m_1 \omega^2 \alpha_0} - \frac{g}{\omega_1^2} \right) \left(\frac{\omega_1^2 - \omega^2}{\omega^2} \right) - \frac{g}{\omega_1^2}$$

$$I_d = I_R + \frac{m_1 g^2}{\omega_1^2 \omega^2} + \frac{m_1 g}{\omega_1^2} \left(2H_1 + \frac{g}{\omega_1^2} \right) + m_1 \left(H_1 + \frac{g}{\omega_1^2} \right)^2 \frac{\omega^2}{\omega_1^2 - \omega^2} - \frac{M_{y\_amp}}{\omega^2 \alpha_0}$$

Remaining parameters, spring constant, fixed mass and height are determined as below:

$$K_1 = m_1 \omega_1^2, \quad m_0 = m_T - m_1, \quad H_0 = \frac{m_1}{m_0} H_1$$

Table A5.1. Determination of Parameters for Arbitrarily Shaped Tank Model

Applied oscillation		Horizontal oscillation, X_0		Rotating oscillation, α_0	
Calculation or Measurement		H force	Moment	H force	Moment
Slosh mass	m_1	O			
Slosh mass height	H_1		O	O	
Mass inertia of free rotating liquid	I_d				O

Appendix 6 Details of Tank Liquid Force Matrix

Details of the matrix transferring the coordinate of the tank liquid force from its local origin to COG are provided here.

$$\mathbf{F_{TG}} = \begin{bmatrix} 0 & -\mathbf{F_T^{L11}V} \\ \mathbf{VF_T^{L11}} & \mathbf{VF_T^{L12}} - \mathbf{F_T^{L21}V} - \mathbf{VF_T^{L11}V} \end{bmatrix}$$

$$-\mathbf{F_T^{L11}V} = -m_T\omega^2 \times \begin{bmatrix} 0 & -(1+A_x)(z_{TG}-z_G) & (1+A_x)(y_{TG}-y_G) \\ (1+A_y)(z_{TG}-z_G) & 0 & -(1+A_y)(x_{TG}-x_G) \\ -(y_{TG}-y_G) & x_{TG}-x_G & 0 \end{bmatrix}$$

$$\mathbf{VF_T^{L11}} = m_T\omega^2 \times \begin{bmatrix} 0 & -(1+A_y)(z_{TG}-z_G) & y_{TG}-y_G \\ (1+A_x)(z_{TG}-z_G) & 0 & -(x_{TG}-x_G) \\ -(1+A_x)(y_{TG}-y_G) & (1+A_y)(x_{TG}-x_G) & 0 \end{bmatrix}$$

$$\mathbf{VF_T^{L12}} = m_T\omega^2 \times \begin{bmatrix} hB_y(z_{TG}-z_G) & 0 & 0 \\ 0 & hB_x(z_{TG}-z_G) & 0 \\ -hB_y(x_{TG}-x_G) & -hB_x(y_{TG}-y_G) & 0 \end{bmatrix}$$

$$-\mathbf{F_T^{L21}V} = -m_T\omega^2 \times \begin{bmatrix} -hB_y(z_{TG}-z_G) & 0 & hB_y(x_{TG}-x_G) \\ 0 & -hB_x(z_{TG}-z_G) & hB_x(y_{TG}-y_G) \\ 0 & 0 & 0 \end{bmatrix}$$

$$-\mathbf{VF_T^{L11}V} = -m_T\omega^2 \times \begin{bmatrix} a^{11} & a^{12} & a^{13} \\ a^{21} & a^{22} & a^{23} \\ a^{31} & a^{32} & a^{33} \end{bmatrix}$$

$$\begin{aligned} a^{11} &= -\left[(y_{TG}-y_G)^2 + (z_{TG}-z_G)^2\right] - A_y(z_{TG}-z_G)^2 \\ a^{22} &= -\left[(x_{TG}-x_G)^2 + (z_{TG}-z_G)^2\right] - A_x(z_{TG}-z_G)^2 \\ a^{33} &= -\left[(x_{TG}-x_G)^2 + (y_{TG}-y_G)^2\right] - A_x(y_{TG}-y_G)^2 - A_y(x_{TG}-x_G)^2 \end{aligned}$$

$$\begin{aligned} a^{12} &= a^{21} = (x_{TG}-x_G)(y_{TG}-y_G) \\ a^{13} &= a^{31} = (1+A_y)(x_{TG}-x_G)(z_{TG}-z_G) \\ a^{23} &= a^{32} = (1+A_x)(y_{TG}-y_G)(z_{TG}-z_G) \end{aligned}$$

$$\mathbf{VF_T^{L12}} - \mathbf{F_T^{L21}V} - \mathbf{VF_T^{L11}V} = m_T\omega^2 \times \begin{bmatrix} b^{11} & b^{12} & b^{13} \\ b^{21} & b^{22} & b^{23} \\ b^{31} & b^{32} & b^{33} \end{bmatrix}$$

$$b^{11} = 2hB_y(z_{TG} - z_G) + \left[(y_{TG} - y_G)^2 + (z_{TG} - z_G)^2\right] + A_y(z_{TG} - z_G)^2$$
$$b^{22} = 2hB_x(z_{TG} - z_G) + \left[(x_{TG} - x_G)^2 + (z_{TG} - z_G)^2\right] + A_x(z_{TG} - z_G)^2$$
$$b^{33} = \left[(x_{TG} - x_G)^2 + (y_{TG} - y_G)^2\right] + A_x(y_{TG} - y_G)^2 + A_y(x_{TG} - x_G)^2$$

$$b^{12} = b^{21} = -(x_{TG} - x_G)(y_{TG} - y_G)$$
$$b^{13} = b^{31} = -hB_y(x_{TG} - x_G) - (1 + A_y)(x_{TG} - x_G)(z_{TG} - z_G)$$
$$b^{23} = b^{32} = -hB_x(y_{TG} - y_G) - (1 + A_x)(y_{TG} - y_G)(z_{TG} - z_G)$$

The forces induced by liquid cargo relative to the COG of the floating body are expressed as below:

$$\mathbf{F_T^L} + \mathbf{F_{TG}} = \omega^2 \mathbf{M_{LA\_G}} + \mathbf{C_{L\_G}}$$
$$= \omega^2 \begin{pmatrix} M^{11} & 0 & 0 & 0 & M^{15} & M^{16} \\ 0 & M^{22} & 0 & M^{24} & 0 & M^{26} \\ 0 & 0 & M^{33} & M^{34} & M^{35} & 0 \\ 0 & M^{42} & M^{43} & M^{44} & M^{45} & M^{46} \\ M^{51} & 0 & M^{53} & M^{54} & M^{55} & M^{56} \\ M^{61} & M^{62} & 0 & M^{64} & M^{65} & M^{66} \end{pmatrix} + \begin{pmatrix} 0 & 0 & 0 & 0 & 0 & 0 \\ 0 & 0 & 0 & 0 & 0 & 0 \\ 0 & 0 & 0 & 0 & 0 & 0 \\ 0 & 0 & 0 & C^{44} & 0 & 0 \\ 0 & 0 & 0 & 0 & C^{55} & 0 \\ 0 & 0 & 0 & 0 & 0 & 0 \end{pmatrix}$$

$$M^{11} = m_T(1 + A_x) = m_T + m_T A_x$$

$$M^{22} = m_T(1 + A_y) = m_T + m_T A_y$$

$$M^{33} = m_T$$

$$M^{15} = M^{51} = m_T hB_x + m_T(1 + A_x)(z_{TG} - z_G) = m_T(z_{TG} - z_G) + m_T\left[A_x(z_{TG} - z_G) + hB_x\right]$$

$$M^{16} = M^{61} = -m_T(1 + A_x)(y_{TG} - y_G) = -m_T(y_{TG} - y_G) - m_T A_x(y_{TG} - y_G)$$

$$M^{24} = M^{42} = -m_T hB_y - m_T(1 + A_y)(z_{TG} - z_G) = -m_T(z_{TG} - z_G) - m_T\left[A_y(z_{TG} - z_G) + hB_y\right]$$

$$M^{26} = M^{62} = m_T(1+A_y)(x_{TG}-x_G) = m_T(x_{TG}-x_G) + m_T A_y(x_{TG}-x_G)$$

$$M^{34} = M^{43} = m_T(y_{TG}-y_G)$$

$$M^{35} = M^{53} = -m_T(x_{TG}-x_G)$$

$$\begin{aligned} M^{44} &= I_x + m_T h^2 C_y + m_T\left\{2hB_y(z_{TG}-z_G) + \left[(y_{TG}-y_G)^2 + (z_{TG}-z_G)^2\right] + A_y(z_{TG}-z_G)^2\right\} \\ &= (I_{xR}-I_{xd}) + m_T\left[(y_{TG}-y_G)^2 + (z_{TG}-z_G)^2\right] + m_T h^2 C_y + 2m_T hB_y(z_{TG}-z_G) + m_T A_y(z_{TG}-z_G)^2 \\ &= I_{xR} + m_T\left[(y_{TG}-y_G)^2 + (z_{TG}-z_G)^2\right] - I_{xd} + m_T h^2 C_y + 2m_T hB_y(z_{TG}-z_G) + m_T A_y(z_{TG}-z_G)^2 \end{aligned}$$

$$C^{44} = m_T h^2 D_y$$

$$\begin{aligned} M^{55} &= I_y + m_T h^2 C_x + m_T\left\{2hB_x(z_{TG}-z_G) + \left[(x_{TG}-x_G)^2 + (z_{TG}-z_G)^2\right] + A_x(z_{TG}-z_G)^2\right\} \\ &= (I_{yR}-I_{yd}) + m_T\left[(x_{TG}-x_G)^2 + (z_{TG}-z_G)^2\right] + m_T h^2 C_x + 2m_T hB_x(z_{TG}-z_G) + m_T A_x(z_{TG}-z_G)^2 \\ &= I_{yR} + m_T\left[(x_{TG}-x_G)^2 + (z_{TG}-z_G)^2\right] - I_{yd} + m_T h^2 C_x + 2m_T hB_x(z_{TG}-z_G) + m_T A_x(z_{TG}-z_G)^2 \end{aligned}$$

$$C^{55} = m_T h^2 D_x$$

$$M^{66} = m_T\left[(x_{TG}-x_G)^2 + (y_{TG}-y_G)^2\right] + m_T A_x(y_{TG}-y_G)^2 + m_T A_y(x_{TG}-x_G)^2$$

$$M^{45} = M^{54} = -m_T(x_{TG}-x_G)(y_{TG}-y_G)$$

$$\begin{aligned} M^{46} = M^{64} &= -m_T hB_y(x_{TG}-x_G) - m_T(1+A_y)(x_{TG}-x_G)(z_{TG}-z_G) \\ &= -m_T(x_{TG}-x_G)(z_{TG}-z_G) - m_T(x_{TG}-x_G)\left[A_y(z_{TG}-z_G) + hB_y\right] \end{aligned}$$

$$\begin{aligned} M^{56} = M^{65} &= -m_T hB_x(y_{TG}-y_G) - m_T(1+A_x)(y_{TG}-y_G)(z_{TG}-z_G) \\ &= -m_T(y_{TG}-y_G)(z_{TG}-z_G) - m_T(y_{TG}-y_G)\left[A_x(z_{TG}-z_G) + hB_x\right] \end{aligned}$$

The sum of the mass matrices of the floating body (excluding liquid cargo) and liquid cargo is further calculated as below:

$$\mathbf{M}_{\mathbf{B\_G}} + \sum \mathbf{M}_{\mathbf{LA\_G}} = \begin{pmatrix} M^{11} & 0 & 0 & 0 & M^{15} & M^{16} \\ 0 & M^{22} & 0 & M^{24} & 0 & M^{26} \\ 0 & 0 & M^{33} & M^{34} & M^{35} & 0 \\ 0 & M^{42} & M^{43} & M^{44} & M^{45} & M^{46} \\ M^{51} & 0 & M^{53} & M^{54} & M^{55} & M^{56} \\ M^{61} & M^{62} & 0 & M^{64} & M^{65} & M^{66} \end{pmatrix} = \mathbf{M}_{\mathbf{G}} + \sum \mathbf{M}_{\mathbf{L\_G}}$$

$$M^{11} = M_B + \sum \left(m_T + m_T A_x \right) = M + \sum m_T A_x$$

$$M^{22} = M_B + \sum \left(m_T + m_T A_y \right) = M + \sum m_T A_y$$

$$M^{33} = M_B + \sum m_T = M$$

$$\begin{aligned} M^{15} = M^{51} &= M_B (z_{BG} - z_G) + \sum m_T (z_{TG} - z_G) + \sum m_T \left[A_x (z_{TG} - z_G) + hB_x \right] \\ &= \left(M_B z_{BG} + \sum m_T z_{TG} \right) - \left(M_B + \sum m_T \right) z_G + \sum m_T \left[A_x (z_{TG} - z_G) + hB_x \right] \\ &= 0 + \sum m_T \left[A_x (z_{TG} - z_G) + hB_x \right] \end{aligned}$$

$$\begin{aligned} M^{16} = M^{61} &= -M_B (y_{BG} - y_G) - \sum m_T (y_{TG} - y_G) - \sum m_T A_x (y_{TG} - y_G) \\ &= -\left(M_B y_{BG} + \sum m_T y_{TG} \right) + \left(M_B + \sum m_T \right) y_G - \sum m_T A_x (y_{TG} - y_G) \\ &= 0 - \sum m_T A_x (y_{TG} - y_G) \end{aligned}$$

$$\begin{aligned} M^{24} = M^{42} &= -M_B (z_{BG} - z_G) - \sum m_T (z_{TG} - z_G) - \sum m_T \left[A_y (z_{TG} - z_G) + hB_y \right] \\ &= -\left(M_B z_{BG} + \sum m_T z_{TG} \right) - \left(M_B + \sum m_T \right) z_G - \sum m_T \left[A_y (z_{TG} - z_G) + hB_y \right] \\ &= 0 - \sum m_T \left[A_y (z_{TG} - z_G) + hB_y \right] \end{aligned}$$

$$\begin{aligned} M^{26} = M^{62} &= M_B (x_{BG} - x_G) + \sum m_T (x_{TG} - x_G) + \sum m_T A_y (x_{TG} - x_G) \\ &= \left(M_B x_{BG} + \sum m_T x_{TG} \right) - \left(M_B + \sum m_T \right) x_G + \sum m_T A_y (x_{TG} - x_G) \\ &= 0 + \sum m_T A_y (x_{TG} - x_G) \end{aligned}$$

$$M^{34} = M^{43} = M_B (y_{BG} - y_G) + \sum m_T (y_{TG} - y_G) = \left(M_B y_{BG} + \sum m_T y_{TG} \right) - \left(M_B + \sum m_T \right) y_G = 0$$

$$M^{35} = M^{53} = -M_B(x_{BG} - x_G) - \sum m_T(x_{TG} - x_G) = -(M_B x_{BG} + \sum m_T x_{TG}) + (M_B + \sum m_T)x_G = 0$$

$$\begin{aligned} M^{44} &= I^G_{B11} + \sum I_{xR} + \sum m_T\left[(y_{TG} - y_G)^2 + (z_{TG} - z_G)^2\right] \\ &\quad + \sum\left[-I_{xd} + m_T h^2 C_y + 2m_T h B_y(z_{TG} - z_G) + m_T A_y(z_{TG} - z_G)^2\right] \\ &= I^G_{11} + \sum\left[-I_{xd} + m_T h^2 C_y + 2m_T h B_y(z_{TG} - z_G) + m_T A_y(z_{TG} - z_G)^2\right] \end{aligned}$$

$$\begin{aligned} M^{55} &= I^G_{B22} + \sum I_{yR} + \sum m_T\left[(x_{TG} - x_G)^2 + (z_{TG} - z_G)^2\right] \\ &\quad + \sum\left[-I_{yd} + m_T h^2 C_x + 2m_T h B_x(z_{TG} - z_G) + m_T A_x(z_{TG} - z_G)^2\right] \\ &= I^G_{22} + \sum\left[-I_{yd} + m_T h^2 C_x + 2m_T h B_x(z_{TG} - z_G) + m_T A_x(z_{TG} - z_G)^2\right] \end{aligned}$$

$$\begin{aligned} M^{66} &= I^G_{B33} + \sum m_T\left[(x_{TG} - x_G)^2 + (y_{TG} - y_G)^2\right] + \sum m_T A_x(y_{TG} - y_G)^2 + \sum m_T A_y(x_{TG} - x_G)^2 \\ &= I^G_{33} + \sum m_T A_x(y_{TG} - y_G)^2 + \sum m_T A_y(x_{TG} - x_G)^2 \end{aligned}$$

$$M^{45} = M^{54} = I^G_{B12} - \sum m_T(x_{TG} - x_G)(y_{TG} - y_G) = I^G_{12}$$

$$\begin{aligned} M^{46} = M^{64} &= I^G_{B13} - \sum m_T(x_{TG} - x_G)(z_{TG} - z_G) - \sum m_T(x_{TG} - x_G)\left[A_y(z_{TG} - z_G) + hB_y\right] \\ &= I^G_{13} - \sum m_T(x_{TG} - x_G)\left[A_y(z_{TG} - z_G) + hB_y\right] \end{aligned}$$

$$\begin{aligned} M^{56} = M^{65} &= I^G_{B23} - \sum m_T(y_{TG} - y_G)(z_{TG} - z_G) - \sum m_T(y_{TG} - y_G)\left[A_x(z_{TG} - z_G) + hB_x\right] \\ &= I^G_{23} - \sum m_T(y_{TG} - y_G)\left[A_x(z_{TG} - z_G) + hB_x\right] \end{aligned}$$

Appendix 7 Velocity Potential of Incoming Wave and Phase Definition

There is no firm rule to define the direction of wave propagation and wave condition of the reference origin (t=0, x=0) of velocity potential. Definition generally depends on the application of the velocity potential. Hence, it is imperative that the readers understand them carefully.
The wave propagation is defined by the combination of signs of ωt (variable of time) and kx (variable of location). When the signs are the same e.g. both positive and both negative, wave propagates in the negative x direction.
For the floating motion applications in offshore industry, same signs are not usually adopted, so that the wave propagation is in the positive x direction.

$A\cos(\omega t + kx)$ $A\cos(\omega t - kx)$

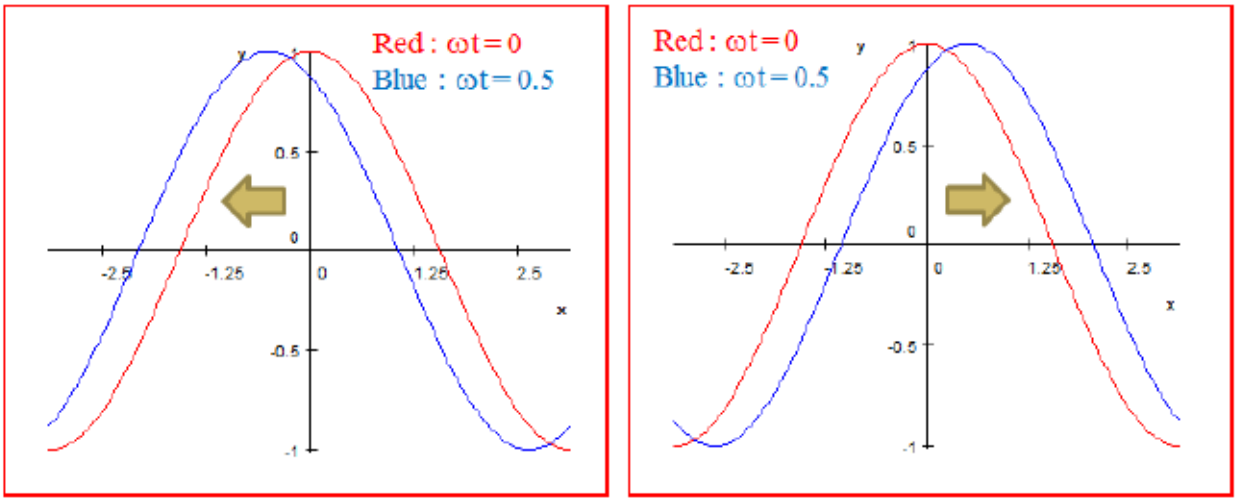

Figure A7.1. Direction of Wave Propagation

The velocity potential of the incoming wave is expressed as below:

$$\Phi_1 = \mathrm{Re}\left\{ \frac{i\,gA}{\omega} \frac{\cosh k(z+h)}{\cosh kh} \exp(i\,\omega t) \exp(-i\,kx) \right\} = \mathrm{Re}\left\{ \frac{\boxed{i}^{1}\,gA}{\omega} \frac{\cosh k(z+h)}{\cosh kh} \exp[\boxed{i}^{2}(\omega t - kx)] \right\}$$

The wave condition of the reference origin is determined by the combination of "1" and "2" indicated in the formula above. "1" can take *1*, *–1*, *i* or *–i* and "2" can take *i* or *–i*.

In cases 1 and 4, the wave crest is at the location x=0 at a time t=0. In cases 5 and 6, the water surface elevation is the mean elevation at the location x=0 at a time t=0 and the water surface elevation will become lower in the next step.

Table A7.1. Combination of "1" and "2"

Case	1	2	Wave	Direction	Phase
1	+i	+i	$A\cos(\omega t - kx)$	To positive x	0
2	+i	−i	$-A\cos(\omega t - kx)$	To positive x	+180
3	−i	+i	$-A\cos(\omega t - kx)$	To positive x	+180
4	−i	−i	$A\cos(\omega t - kx)$	To positive x	0
5	+1	+i	$A\sin(\omega t - kx)$	To positive x	−90
6	+1	−i	$A\sin(\omega t - kx)$	To positive x	−90
7	−1	+i	$-A\sin(\omega t - kx)$	To positive x	+90
8	−1	−i	$-A\sin(\omega t - kx)$	To positive x	+90

Examples of incoming wave velocity potential from the papers and theory manuals are shown here.

Example 1

Case 1 is adopted in WAMIT and WADAM.

$$\Phi^{(1)}(\mathrm{x},t) = Re\sum_j \phi_j(\mathrm{x})e^{i\omega_j t}$$

$$\phi_I = \frac{igA}{\omega}Z(\kappa z)e^{-i\kappa(x\cos\beta + y\sin\beta)}\ Z(\kappa z) = \frac{\cosh(\kappa(z+h))}{\cosh(\kappa h)}$$

Example 2

Case 4 is adopted in AQWA. The equation of velocity potential is slightly different from that of case 1 above; however, both equations are identical.

$$\Phi_I(\vec{X},t) = \varphi_I(\vec{X})e^{-i\omega t}$$
$$= -\frac{iga_w\cosh[k(Z+d)]}{\omega\cosh(kd)}e^{i[-\omega t + k(X\cos\chi + Y\sin\chi) + \alpha}$$

Example 3

Case 8

$$\phi^{(i)} = -\frac{g\,H}{2\sigma}\ \frac{\cosh k\,(d+z)}{\cosh kd}\ e^{i\,(kx-\sigma t)}$$

Case 1

$$\Phi_I = \mathrm{Re}\left\{ \frac{i\,gA}{\omega}\frac{\cosh k(z+h)}{\cosh kh}\exp(-i\,kx)\exp(i\,\omega t)\right\} = \mathrm{Re}\left\{ \frac{i\,gA}{\omega}\frac{\cosh k(z+h)}{\cosh kh}\exp[i\,(\omega t - kx)]\right\}$$

$$\begin{aligned}\eta &= -\frac{1}{g}\frac{\partial \Phi_I}{\partial t}\bigg|_{z=0} = -\frac{1}{g}\frac{\partial}{\partial t}\mathrm{Re}\left[\frac{igA}{\omega}\frac{\cosh k(0+h)}{\cosh kh}\exp[i\,(\omega t - kx)]\right] \\ &= \mathrm{Re}\left[-\frac{1}{g}\frac{igA}{\omega}i\omega\exp[i\,(\omega t - kx)]\right] = \mathrm{Re}\left[A\exp[i\,(\omega t - kx)]\right] \\ &= \mathrm{Re}\left[A\left[\cos(\omega t - kx) + i\sin(\omega t - kx)\right]\right] = A\cos(\omega t - kx)\end{aligned}$$

Case 2

$$\Phi_I = \mathrm{Re}\left\{ \frac{i\,gA}{\omega}\frac{\cosh k(z+h)}{\cosh kh}\exp[-i\,(\omega t - kx)]\right\}$$

$$\begin{aligned}\eta &= -\frac{1}{g}\frac{\partial \Phi_I}{\partial t}\bigg|_{z=0} = -\frac{1}{g}\frac{\partial}{\partial t}\mathrm{Re}\left[\frac{igA}{\omega}\frac{\cosh k(0+h)}{\cosh kh}\exp[-i\,(\omega t - kx)]\right] \\ &= \mathrm{Re}\left[-\frac{1}{g}\frac{igA}{\omega}(-i\omega)\exp[-i\,(\omega t - kx)]\right] = \mathrm{Re}\left[-A\exp[-i\,(\omega t - kx)]\right] \\ &= \mathrm{Re}\left[-A\left[\cos(\omega t - kx) - i\sin(\omega t - kx)\right]\right] = -A\cos(\omega t - kx)\end{aligned}$$

Case 3

$$\Phi_I = \mathrm{Re}\left\{ \frac{-i\,gA}{\omega}\frac{\cosh k(z+h)}{\cosh kh}\exp[i\,(\omega t - kx)]\right\}$$

$$\begin{aligned}\eta &= -\frac{1}{g}\frac{\partial \Phi_I}{\partial t}\bigg|_{z=0} = -\frac{1}{g}\frac{\partial}{\partial t}\mathrm{Re}\left[\frac{-igA}{\omega}\frac{\cosh k(0+h)}{\cosh kh}\exp[i\,(\omega t - kx)]\right] \\ &= \mathrm{Re}\left[-\frac{1}{g}\frac{-igA}{\omega}i\omega\exp[i\,(\omega t - kx)]\right] = \mathrm{Re}\left[-A\exp[i\,(\omega t - kx)]\right] \\ &= \mathrm{Re}\left[-A\left[\cos(\omega t - kx) + i\sin(\omega t - kx)\right]\right] = -A\cos(\omega t - kx)\end{aligned}$$

Case 4

$$\Phi_I = \mathrm{Re}\left\{ \frac{-i\,gA}{\omega}\frac{\cosh k(z+h)}{\cosh kh}\exp[-i\,(\omega t - kx)] \right\}$$

$$\eta = -\frac{1}{g}\frac{\partial \Phi_I}{\partial t}\bigg|_{z=0} = -\frac{1}{g}\frac{\partial}{\partial t}\mathrm{Re}\left[\frac{-igA}{\omega}\frac{\cosh k(0+h)}{\cosh kh}\exp[-i\,(\omega t - kx)] \right]$$
$$= \mathrm{Re}\left[-\frac{1}{g}\frac{-igA}{\omega}(-i\omega)\exp[-i\,(\omega t - kx)] \right] = \mathrm{Re}\left[A\exp[-i\,(\omega t - kx)] \right]$$
$$= \mathrm{Re}\left[A\left[\cos(\omega t - kx) - i\sin(\omega t - kx) \right] \right] = A\cos(\omega t - kx)$$

Case 5

$$\Phi_I = \mathrm{Re}\left\{ \frac{gA}{\omega}\frac{\cosh k(z+h)}{\cosh kh}\exp[i\,(\omega t - kx)] \right\}$$

$$\eta = -\frac{1}{g}\frac{\partial \Phi_I}{\partial t}\bigg|_{z=0} = -\frac{1}{g}\frac{\partial}{\partial t}\mathrm{Re}\left[\frac{gA}{\omega}\frac{\cosh k(0+h)}{\cosh kh}\exp[i\,(\omega t - kx)] \right]$$
$$= \mathrm{Re}\left[-\frac{1}{g}\frac{gA}{\omega}i\omega\exp[i\,(\omega t - kx)] \right] = \mathrm{Re}\left[-iA\exp[i\,(\omega t - kx)] \right]$$
$$= \mathrm{Re}\left[-iA\left[\cos(\omega t - kx) + i\sin(\omega t - kx) \right] \right] = A\sin(\omega t - kx)$$

Case 6

$$\Phi_I = \mathrm{Re}\left\{ \frac{gA}{\omega}\frac{\cosh k(z+h)}{\cosh kh}\exp[-i\,(\omega t - kx)] \right\}$$

$$\eta = -\frac{1}{g}\frac{\partial \Phi_I}{\partial t}\bigg|_{z=0} = -\frac{1}{g}\frac{\partial}{\partial t}\mathrm{Re}\left[\frac{gA}{\omega}\frac{\cosh k(0+h)}{\cosh kh}\exp[-i\,(\omega t - kx)] \right]$$
$$= \mathrm{Re}\left[-\frac{1}{g}\frac{gA}{\omega}(-i\,\omega)\exp[-i\,(\omega t - kx)] \right] = \mathrm{Re}\left[iA\exp[-i\,(\omega t - kx)] \right]$$
$$= \mathrm{Re}\left[iA\left[\cos(\omega t - kx) - i\sin(\omega t - kx) \right] \right] = A\sin(\omega t - kx)$$

Case 7

$$\Phi_I = \mathrm{Re}\left\{ -\frac{gA}{\omega}\frac{\cosh k(z+h)}{\cosh kh}\exp[i\,(\omega t - kx)]\right\}$$

$$\eta = -\frac{1}{g}\frac{\partial \Phi_I}{\partial t}\bigg|_{z=0} = -\frac{1}{g}\frac{\partial}{\partial t}\mathrm{Re}\left[-\frac{gA}{\omega}\frac{\cosh k(0+h)}{\cosh kh}\exp[i\,(\omega t - kx)]\right]$$
$$= \mathrm{Re}\left[\frac{1}{g}\frac{gA}{\omega} i\omega \exp[i\,(\omega t - kx)]\right] = \mathrm{Re}\left[iA\exp[i\,(\omega t - kx)]\right]$$
$$= \mathrm{Re}\left[iA\left[\cos(\omega t - kx) + i\sin(\omega t - kx)\right]\right] = -A\sin(\omega t - kx)$$

Case 8

$$\Phi_I = \mathrm{Re}\left\{ -\frac{gA}{\omega}\frac{\cosh k(z+h)}{\cosh kh}\exp[-i\,(\omega t - kx)]\right\}$$

$$\eta = -\frac{1}{g}\frac{\partial \Phi_I}{\partial t}\bigg|_{z=0} = -\frac{1}{g}\frac{\partial}{\partial t}\mathrm{Re}\left[-\frac{gA}{\omega}\frac{\cosh k(0+h)}{\cosh kh}\exp[-i\,(\omega t - kx)]\right]$$
$$= \mathrm{Re}\left[\frac{1}{g}\frac{gA}{\omega}(-i\,\omega)\exp[-i\,(\omega t - kx)]\right] = \mathrm{Re}\left[-iA\exp[-i\,(\omega t - kx)]\right]$$
$$= \mathrm{Re}\left[-iA\left[\cos(\omega t - kx) - i\sin(\omega t - kx)\right]\right] = -A\sin(\omega t - kx)$$

Appendix 8 Matrix Transformation to Arbitrary Reference Point

A8.1 Coordinate Transformation Matrix

The arbitrary matrix $\mathbf{A_G}$ transferring the coordinates from COG of the floating body to its origin (0, 0, 0) is shown here. The coordinate origin is used as the motion reference point and can be defined at any location.

$$\mathbf{A_{GO}} = \begin{bmatrix} 0 & -\mathbf{A_G^{11}V} \\ \mathbf{VA_G^{11}} & \mathbf{VA_G^{12}} - \mathbf{A_G^{21}V} - \mathbf{VA_G^{11}V} \end{bmatrix}$$

where,

$$\mathbf{A_G} = \begin{bmatrix} \mathbf{A_G^{11}} & \mathbf{A_G^{12}} \\ \mathbf{A_G^{21}} & \mathbf{A_G^{22}} \end{bmatrix} \qquad \mathbf{V} = \begin{bmatrix} 0 & -z_G & y_G \\ z_G & 0 & -x_G \\ -y_G & x_G & 0 \end{bmatrix}$$

A8.2 Mass Matrix without Liquid Cargo

The mass matrix of the floating body relative to its COG and the coordinate transformation matrix are detailed as below:

$$\mathbf{M_G} = \begin{pmatrix} M & 0 & 0 & 0 & 0 & 0 \\ 0 & M & 0 & 0 & 0 & 0 \\ 0 & 0 & M & 0 & 0 & 0 \\ 0 & 0 & 0 & I_{11}^G & I_{12}^G & I_{13}^G \\ 0 & 0 & 0 & I_{21}^G & I_{22}^G & I_{23}^G \\ 0 & 0 & 0 & I_{31}^G & I_{32}^G & I_{33}^G \end{pmatrix}$$

$$-\mathbf{A_G^{11}V} = -\begin{bmatrix} 0 & -Mz_G & My_G \\ Mz_G & 0 & -Mx_G \\ -My_G & Mx_G & 0 \end{bmatrix} \qquad \mathbf{VA_G^{11}} = \begin{bmatrix} 0 & -Mz_G & My_G \\ Mz_G & 0 & -Mx_G \\ -My_G & Mx_G & 0 \end{bmatrix}$$

$$\mathbf{VA_G^{12}} - \mathbf{A_G^{21}V} - \mathbf{VA_G^{11}V} = \begin{bmatrix} M\left(y_G^2 + z_G^2\right) & -Mx_G y_G & -Mx_G z_G \\ -Mx_G y_G & M\left(x_G^2 + z_G^2\right) & -My_G z_G \\ -Mx_G z_G & -My_G z_G & M\left(x_G^2 + y_G^2\right) \end{bmatrix}$$

The mass matrix of the floating body relative to the reference point is obtained as below:

$$\mathbf{M_O} = \mathbf{M_G} + \mathbf{A_{GO}}$$

$$= \begin{pmatrix} M & 0 & 0 & 0 & Mz_G & -My_G \\ 0 & M & 0 & -Mz_G & 0 & Mx_G \\ 0 & 0 & M & My_G & -Mx_G & 0 \\ 0 & -Mz_G & My_G & I_{11}^G + M\left(y_G^2 + z_G^2\right) & I_{12}^G - Mx_G y_G & I_{13}^G - Mx_G z_G \\ Mz_G & 0 & -Mx_G & I_{21}^G - Mx_G y_G & I_{22}^G + M\left(x_G^2 + z_G^2\right) & I_{23}^G - My_G z_G \\ -My_G & Mx_G & 0 & I_{31}^G - Mx_G z_G & I_{32}^G - My_G z_G & I_{33}^G + M\left(x_G^2 + y_G^2\right) \end{pmatrix}$$

$$= \begin{pmatrix} M & 0 & 0 & 0 & Mz_G & -My_G \\ 0 & M & 0 & -Mz_G & 0 & Mx_G \\ 0 & 0 & M & My_G & -Mx_G & 0 \\ 0 & -Mz_G & My_G & I_{11}^O & I_{12}^O & I_{13}^O \\ Mz_G & 0 & -Mx_G & I_{21}^O & I_{22}^O & I_{23}^O \\ -My_G & Mx_G & 0 & I_{31}^O & I_{32}^O & I_{33}^O \end{pmatrix}$$

$$I_{11}^O = \iiint_M \left[y^2 + z^2\right] dm \qquad I_{12}^O = I_{21}^O = -\iiint_M xy\, dm$$

$$I_{22}^O = \iiint_M \left[x^2 + z^2\right] dm \qquad I_{13}^O = I_{31}^O = -\iiint_M xz\, dm$$

$$I_{33}^O = \iiint_M \left[x^2 + y^2\right] dm \qquad I_{23}^O = I_{32}^O = -\iiint_M yz\, dm$$

$$I_{11}^G + M\left(y_G^2 + z_G^2\right) = \iiint_M \left[(y - y_G)^2 + (z - z_G)^2\right] dm + M\left(y_G^2 + z_G^2\right)$$

$$= \iiint_M \left[y^2 + z^2\right] dm - 2y_G \iiint_M y\, dm - 2z_G \iiint_M z\, dm + \left(y_G^2 + z_G^2\right) \iiint_M dm + M\left(y_G^2 + z_G^2\right)$$

$$= \iiint_M \left[y^2 + z^2\right] dm - 2My_G^2 - 2Mz_G^2 + M\left(y_G^2 + z_G^2\right) + M\left(y_G^2 + z_G^2\right) = I_{11}^O$$

$$I_{12}^G - Mx_G y_G = -\iiint_M (x - x_G)(y - y_G)\, dm - Mx_G y_G$$

$$= -\iiint_M xy\, dm + y_G \iiint_M x\, dm + x_G \iiint_M y\, dm - x_G y_G \iiint_M dm - Mx_G y_G$$

$$= -\iiint_M xy\, dm + Mx_G y_G + Mx_G y_G - Mx_G y_G - Mx_G y_G = I_{12}^O$$

A8.3 Mass Matrix with Liquid Cargo

The mass matrix of the floating body (excluding liquid cargo) relative to its COG (including liquid cargo) and the coordinate transformation matrix are described below:

$$\mathbf{M_{B\_G}}=\begin{pmatrix} M_B & 0 & 0 & 0 & M_B(z_{BG}-z_G) & -M_B(y_{BG}-y_G) \\ 0 & M_B & 0 & -M_B(z_{BG}-z_G) & 0 & M_B(x_{BG}-x_G) \\ 0 & 0 & M_B & M_B(y_{BG}-y_G) & -M_B(x_{BG}-x_G) & 0 \\ 0 & -M_B(z_{BG}-z_G) & M_B(y_{BG}-y_G) & I^G_{B11} & I^G_{B12} & I^G_{B13} \\ M_B(z_{BG}-z_G) & 0 & -M_B(x_{BG}-x_G) & I^G_{B21} & I^G_{B22} & I^G_{B23} \\ -M_B(y_{BG}-y_G) & M_B(x_{BG}-x_G) & 0 & I^G_{B31} & I^G_{B32} & I^G_{B33} \end{pmatrix}$$

$$-\mathbf{A_G^{11}V}=-\begin{bmatrix} 0 & -M_Bz_G & M_By_G \\ M_Bz_G & 0 & -M_Bx_G \\ -M_By_G & M_Bx_G & 0 \end{bmatrix} \qquad \mathbf{VA_G^{11}}=\begin{bmatrix} 0 & -M_Bz_G & M_By_G \\ M_Bz_G & 0 & -M_Bx_G \\ -M_By_G & M_Bx_G & 0 \end{bmatrix}$$

$$\mathbf{VA_G^{12}}-\mathbf{A_G^{21}V}-\mathbf{VA_G^{11}V}=M_B\times\begin{bmatrix} c^{11} & c^{12} & c^{13} \\ c^{21} & c^{22} & c^{23} \\ c^{31} & c^{32} & c^{33} \end{bmatrix}$$

$$c^{11}=2y_{BG}y_G-y_G^2+2z_{BG}z_G-z_G^2 \qquad c^{12}=c^{21}=-x_{BG}y_G-x_Gy_{BG}+x_Gy_G$$
$$c^{22}=2x_{BG}x_G-x_G^2+2z_{BG}z_G-z_G^2 \qquad c^{13}=c^{31}=-x_{BG}z_G-x_Gz_{BG}+x_Gz_G$$
$$c^{33}=2x_{BG}x_G-x_G^2+2y_{BG}y_G-y_G^2 \qquad c^{23}=c^{32}=-y_{BG}z_G-y_Gz_{BG}+y_Gz_G$$

The mass matrix of the floating body (excluding liquid cargo) relative to the reference point is obtained as below:

$$\mathbf{M_{B\_O}}=\mathbf{M_{B\_G}}+\mathbf{A_{GO}}$$
$$=\begin{pmatrix} M_B & 0 & 0 & 0 & M_Bz_{BG} & -M_By_{BG} \\ 0 & M_B & 0 & -M_Bz_{BG} & 0 & M_Bx_{BG} \\ 0 & 0 & M_B & M_By_{BG} & -M_Bx_{BG} & 0 \\ 0 & -M_Bz_{BG} & M_By_{BG} & I^O_{B11} & I^O_{B12} & I^O_{B13} \\ M_Bz_{BG} & 0 & -M_Bx_{BG} & I^O_{B21} & I^O_{B22} & I^O_{B23} \\ -M_By_{BG} & M_Bx_{BG} & 0 & I^O_{B31} & I^O_{B32} & I^O_{B33} \end{pmatrix}$$

$$I^O_{B11}=\iiint_{M_B}\left[(y-y_{BG})^2+(z-z_{BG})^2\right]dm+M_B\left[{y_{BG}}^2+{z_{BG}}^2\right]=\iiint_{M_B}\left[y^2+z^2\right]dm$$
$$I^O_{B22}=\iiint_{M_B}\left[(x-x_{BG})^2+(z-z_{BG})^2\right]dm+M_B\left[{x_{BG}}^2+{z_{BG}}^2\right]=\iiint_{M_B}\left[x^2+z^2\right]dm$$
$$I^O_{B33}=\iiint_{M_B}\left[(x-x_{BG})^2+(y-y_{BG})^2\right]dm+M_B\left[{x_{BG}}^2+{y_{BG}}^2\right]=\iiint_{M_B}\left[x^2+y^2\right]dm$$

$$I^O_{B12} = I^O_{B21} = -\iiint_{M_B} (x - x_{BG})(y - y_{BG})\, dm - M_B[x_{BG} y_{BG}] = -\iiint_{M_B} xy\, dm$$
$$I^O_{B13} = I^O_{B31} = -\iiint_{M_B} (x - x_{BG})(z - z_{BG})\, dm - M_B[x_{BG} z_{BG}] = -\iiint_{M_B} xz\, dm$$
$$I^O_{B23} = I^O_{B32} = -\iiint_{M_B} (y - y_{BG})(z - z_{BG})\, dm - M_B[y_{BG} z_{BG}] = -\iiint_{M_B} yz\, dm$$

A8.4 Hydrostatic Restoring Matrix

The hydrostatic restoring matrix of the floating body relative to its COG and the coordinate transformation matrix are described below:

$$\mathbf{C_G} = g\times \begin{pmatrix} 0 & 0 & 0 & 0 & 0 & 0 \\ 0 & 0 & 0 & 0 & 0 & 0 \\ 0 & 0 & \rho A_{wp} & \rho A_{wp}(y_f - y_G) & -\rho A_{wp}(x_f - x_G) & 0 \\ 0 & 0 & \rho A_{wp}(y_f - y_G) & \rho(S^G_{11} + V_w z_b) - Mz_G & \rho S^G_{12} & -\rho V_w x_b + Mx_G \\ 0 & 0 & -\rho A_{wp}(x_f - x_G) & \rho S^G_{21} & \rho(S^G_{22} + V_w z_b) - Mz_G & -\rho V_w y_b + My_G \\ 0 & 0 & 0 & 0 & 0 & 0 \end{pmatrix}$$

$$-\mathbf{A^{11}_G V} = -\rho g A_{wp} \begin{bmatrix} 0 & 0 & 0 \\ 0 & 0 & 0 \\ -y_G & x_G & 0 \end{bmatrix} \qquad \mathbf{VA^{11}_G} = \rho g A_{wp} \begin{bmatrix} 0 & 0 & y_G \\ 0 & 0 & -x_G \\ 0 & 0 & 0 \end{bmatrix}$$

$$\mathbf{VA^{12}_G} - \mathbf{A^{21}_G V} - \mathbf{VA^{11}_G V} = \rho g A_{wp} \begin{bmatrix} 2y_f y_G - y_G^2 & -y_f x_G - x_f y_G + x_G y_G & 0 \\ -y_f x_G - x_f y_G + x_G y_G & 2x_f x_G - x_G^2 & 0 \\ 0 & 0 & 0 \end{bmatrix}$$

The hydrostatic restoring matrix relative to the reference point is obtained as below:

$$\mathbf{C_O} = \mathbf{C_G} + \mathbf{A_{GO}} = g\times \begin{pmatrix} 0 & 0 & 0 & 0 & 0 & 0 \\ 0 & 0 & 0 & 0 & 0 & 0 \\ 0 & 0 & \rho A_{wp} & \rho A_{wp} y_f & -\rho A_{wp} x_f & 0 \\ 0 & 0 & \rho A_{wp} y_f & \rho(S^O_{11} + V_w z_b) - Mz_G & \rho S^O_{12} & -\rho V_w x_b + Mx_G \\ 0 & 0 & -\rho A_{wp} x_f & \rho S^O_{21} & \rho(S^O_{22} + V_w z_b) - Mz_G & -\rho V_w y_b + My_G \\ 0 & 0 & 0 & 0 & 0 & 0 \end{pmatrix}$$

$$S^O_{11} = \iint_{A_{wp}} y^2\, da \quad S^O_{22} = \iint_{A_{wp}} x^2\, da \quad S^O_{12} = S^O_{21} = -\iint_{A_{wp}} xy\, da$$

$$S_{11}^{G} + A_{wp}\left(2y_f y_G - y_G^2\right) = \iint_{A_{wp}} (y - y_G)^2 \, da + A_{wp}\left(2y_f y_G - y_G^2\right)$$
$$= \iint_{A_{wp}} y^2 \, da - 2y_G \iint_{A_{wp}} y \, da + y_G^2 \iint_{A_{wp}} da + A_{wp}\left(2y_f y_G - y_G^2\right)$$
$$= \iint_{A_{wp}} y^2 \, da - 2A_{wp} y_f y_G + A_{wp} y_G^2 + A_{wp}\left(2y_f y_G - y_G^2\right) = S_{11}^{O}$$

$$S_{12}^{G} + A_{wp}\left(-y_f x_G - x_f y_G + x_G y_G\right) = -\iint_{A_{wp}} (x - x_G)(y - y_G) \, da + A_{wp}\left(-y_f x_G - x_f y_G + x_G y_G\right)$$
$$= -\iint_{A_{wp}} xy \, da + x_G \iint_{A_{wp}} y \, da + y_G \iint_{A_{wp}} x \, da - x_G y_G \iint_{A_{wp}} da + A_{wp}\left(-y_f x_G - x_f y_G + x_G y_G\right)$$
$$= -\iint_{A_{wp}} xy \, da + A_{wp} y_f x_G + A_{wp} x_f y_G - A_{wp} x_G y_G + A_{wp}\left(-y_f x_G - x_f y_G + x_G y_G\right) = S_{12}^{O}$$

A8.5 Tank Liquid Force Matrix

The tank liquid force matrix, $\mathbf{F_T^L}$ to transfer the coordinate from its local origin to the coordinate origin (0, 0, 0) is shown below.

$$\mathbf{F_{TO}} = \begin{bmatrix} 0 & -\mathbf{F_T^{L11}V} \\ \mathbf{VF_T^{L11}} & \mathbf{VF_T^{L12}} - \mathbf{F_T^{L21}V} - \mathbf{VF_T^{L11}V} \end{bmatrix}$$

where,

$$\mathbf{F_T^L} = \begin{bmatrix} \mathbf{F_T^{L11}} & \mathbf{F_T^{L12}} \\ \mathbf{F_T^{L21}} & \mathbf{F_T^{L22}} \end{bmatrix} \qquad \mathbf{V} = \begin{bmatrix} 0 & -z_{TG} & y_{TG} \\ z_{TG} & 0 & -x_{TG} \\ -y_{TG} & x_{TG} & 0 \end{bmatrix}$$

The tank liquid force matrix relative to local tank origin and the coordinate transformation matrix are detailed below:

$$\mathbf{F_T^L} = m_T \omega^2 \times$$
$$\begin{pmatrix} 1+A_x & 0 & 0 & 0 & hB_x & 0 \\ 0 & 1+A_y & 0 & -hB_y & 0 & 0 \\ 0 & 0 & 1 & 0 & 0 & 0 \\ 0 & -hB_y & 0 & \dfrac{I_x}{m_T} + h^2 C_y + D_y \dfrac{h^2}{\omega^2} & 0 & 0 \\ hB_x & 0 & 0 & 0 & \dfrac{I_y}{m_T} + h^2 C_x + D_x \dfrac{h^2}{\omega^2} & 0 \\ 0 & 0 & 0 & 0 & 0 & 0 \end{pmatrix}$$

$$-\mathbf{F_T^{L11}V} = -m_T\omega^2 \times \begin{bmatrix} 0 & -(1+A_x)z_{TG} & (1+A_x)y_{TG} \\ (1+A_y)z_{TG} & 0 & -(1+A_y)x_{TG} \\ -y_{TG} & x_{TG} & 0 \end{bmatrix}$$

$$\mathbf{VF_T^{L11}} = m_T\omega^2 \times \begin{bmatrix} 0 & -(1+A_y)z_{TG} & y_{TG} \\ (1+A_x)z_{TG} & 0 & -x_{TG} \\ -(1+A_x)y_{TG} & (1+A_y)x_{TG} & 0 \end{bmatrix}$$

$$\mathbf{VF_T^{L12}} - \mathbf{F_T^{L21}V} - \mathbf{VF_T^{L11}V} = m_T\omega^2 \times \begin{bmatrix} d^{11} & d^{12} & d^{13} \\ d^{21} & d^{22} & d^{23} \\ d^{31} & d^{32} & d^{33} \end{bmatrix}$$

$$\begin{aligned} d^{11} &= 2hB_y z_{TG} + \left[{y_{TG}}^2 + {z_{TG}}^2\right] + A_y {z_{TG}}^2 & d^{12} &= d^{21} = -x_{TG}y_{TG} \\ d^{22} &= 2hB_x z_{TG} + \left[{x_{TG}}^2 + {z_{TG}}^2\right] + A_x {z_{TG}}^2 & d^{13} &= d^{31} = -hB_y x_{TG} - (1+A_y)x_{TG}z_{TG} \\ d^{33} &= \left[{x_{TG}}^2 + {y_{TG}}^2\right] + A_x {y_{TG}}^2 + A_y {x_{TG}}^2 & d^{23} &= d^{32} = -hB_x y_{TG} - (1+A_x)y_{TG}z_{TG} \end{aligned}$$

The forces induced by liquid cargo relative to the reference point are expressed as below:

$$\mathbf{F_T^L} + \mathbf{F_{TO}} = \omega^2 \mathbf{M_{LA\_O}} + \mathbf{C_{L\_O}}$$

$$= \omega^2 \begin{pmatrix} M^{11} & 0 & 0 & 0 & M^{15} & M^{16} \\ 0 & M^{22} & 0 & M^{24} & 0 & M^{26} \\ 0 & 0 & M^{33} & M^{34} & M^{35} & 0 \\ 0 & M^{42} & M^{43} & M^{44} & M^{45} & M^{46} \\ M^{51} & 0 & M^{53} & M^{54} & M^{55} & M^{56} \\ M^{61} & M^{62} & 0 & M^{64} & M^{65} & M^{66} \end{pmatrix} + \begin{pmatrix} 0 & 0 & 0 & 0 & 0 & 0 \\ 0 & 0 & 0 & 0 & 0 & 0 \\ 0 & 0 & 0 & 0 & 0 & 0 \\ 0 & 0 & 0 & C^{44} & 0 & 0 \\ 0 & 0 & 0 & 0 & C^{55} & 0 \\ 0 & 0 & 0 & 0 & 0 & 0 \end{pmatrix}$$

$$M^{11} = m_T(1+A_x) = m_T + m_T A_x$$

$$M^{22} = m_T(1+A_y) = m_T + m_T A_y$$

$$M^{33} = m_T$$

$$M^{15} = M^{51} = m_T hB_x + m_T(1+A_x)z_{TG} = m_T z_{TG} + m_T\left[A_x z_{TG} + hB_x\right]$$

$$M^{16} = M^{61} = -m_T(1+A_x)y_{TG} = -m_T y_{TG} - m_T A_x y_{TG}$$

$$M^{24} = M^{42} = -m_T h B_y - m_T (1 + A_y) z_{TG} = -m_T z_{TG} - m_T \left[A_y z_{TG} + h B_y \right]$$

$$M^{26} = M^{62} = m_T (1 + A_y) x_{TG} = m_T x_{TG} + m_T A_y x_{TG}$$

$$M^{34} = M^{43} = m_T \, y_{TG}$$

$$M^{35} = M^{53} = -m_T \, x_{TG}$$

$$\begin{aligned} M^{44} &= I_x + m_T h^2 C_y + m_T \left\{ 2 h B_y z_{TG} + \left[{y_{TG}}^2 + {z_{TG}}^2 \right] + A_y {z_{TG}}^2 \right\} \\ &= (I_{xR} - I_{xd}) + m_T \left[{y_{TG}}^2 + {z_{TG}}^2 \right] + m_T h^2 C_y + 2 m_T h B_y z_{TG} + m_T A_y {z_{TG}}^2 \\ &= I_{xR} + m_T \left[{y_{TG}}^2 + {z_{TG}}^2 \right] - I_{xd} + m_T h^2 C_y + 2 m_T h B_y z_{TG} + m_T A_y {z_{TG}}^2 \end{aligned}$$

$$C^{44} = m_T h^2 D_y$$

$$\begin{aligned} M^{55} &= I_y + m_T h^2 C_x + m_T \left\{ 2 h B_x z_{TG} + \left[{x_{TG}}^2 + {z_{TG}}^2 \right] + A_x {z_{TG}}^2 \right\} \\ &= (I_{yR} - I_{yd}) + m_T \left[{x_{TG}}^2 + {z_{TG}}^2 \right] + m_T h^2 C_x + 2 m_T h B_x z_{TG} + m_T A_x {z_{TG}}^2 \\ &= I_{yR} + m_T \left[{x_{TG}}^2 + {z_{TG}}^2 \right] - I_{yd} + m_T h^2 C_x + 2 m_T h B_x z_{TG} + m_T A_x {z_{TG}}^2 \end{aligned}$$

$$C^{55} = m_T h^2 D_x$$

$$M^{66} = m_T \left[{x_{TG}}^2 + {y_{TG}}^2 \right] + m_T A_x {y_{TG}}^2 + m_T A_y {x_{TG}}^2$$

$$M^{45} = M^{54} = -m_T x_{TG} y_{TG}$$

$$\begin{aligned} M^{46} = M^{64} &= -m_T h B_y x_{TG} - m_T (1 + A_y) x_{TG} z_{TG} \\ &= -m_T x_{TG} z_{TG} - m_T x_{TG} \left[A_y z_{TG} + h B_y \right] \end{aligned}$$

$$\begin{aligned} M^{56} = M^{65} &= -m_T h B_x y_{TG} - m_T (1 + A_x) y_{TG} z_{TG} \\ &= -m_T y_{TG} z_{TG} - m_T y_{TG} \left[A_x z_{TG} + h B_x \right] \end{aligned}$$

A8.6 Equation of Floating Body Motion

The floating body motion relative to the reference point is described by the following equation in frequency domain.

$$\left[-\omega^2\left(\mathbf{M_O}+\mathbf{M_{A\_O}}\right)+i\omega\mathbf{B_O}+\mathbf{C_O}\right]\cdot\mathbf{X_O}=\mathbf{F_O^{DI}}$$

And the equation of the floating body motion coupled with the liquid cargo effects is obtained as follows:

$$\left[-\omega^2\left(\mathbf{M_{B\_O}}+\mathbf{M_{A\_O}}+\sum\mathbf{M_{LA\_O}}\right)+i\omega\mathbf{B_O}+\mathbf{C_O}-\sum\mathbf{C_{L\_O}}\right]\cdot\mathbf{X_O}=\mathbf{F_O^{DI}}$$

or

$$\left[-\omega^2\left(\mathbf{M_O}+\mathbf{M_{A\_O}}+\sum\mathbf{M_{L\_O}}\right)+i\omega\mathbf{B_O}+\mathbf{C_O}-\sum\mathbf{C_{L\_O}}\right]\cdot\mathbf{X_O}=\mathbf{F_O^{DI}}$$

Appendix 9 Non-dimensional Form of Sway and Roll Motion

The expression of sway and roll motion mentioned in the thesis is identical to the one from the reference as shown in Table A9.1.
This is useful for comparing the sway and roll motion obtained by the author's method with those in the reference; however, it is not convenient for comparing with other results.

Table A9.1. Axis of Sway and Roll Motion

	Barge (Molin et al.)	FLNG (Rocha et al.)
Chapter	5.2 and 6.2	5.3 and 6.3
Horizontal Axis	Angular frequency (radian/sec)	Period (sec)
Vertical Axis for Sway	Sway per unit wave (m/m)	Sway per unit wave (m/m)
Vertical Axis for Roll	Roll per unit vave (radian/m)	Roll per unit vave (degree/m)

This appendix reproduces the sway and roll motion in the non-dimensional form as below:

1. Horizontal Axis

$$\sigma = \omega\sqrt{\frac{B}{g}}$$

2. Vertical Axis for Sway (not different)

$$x_2' = \frac{x_{G2}}{w_a}$$

3. Vertical Axis for Roll

$$x_4' = \frac{x_{G4}}{kw_a}$$

where, w_a is the incident wave amplitude, B is the breadth of the floating body, g is the gravity constant and k is the wave number.

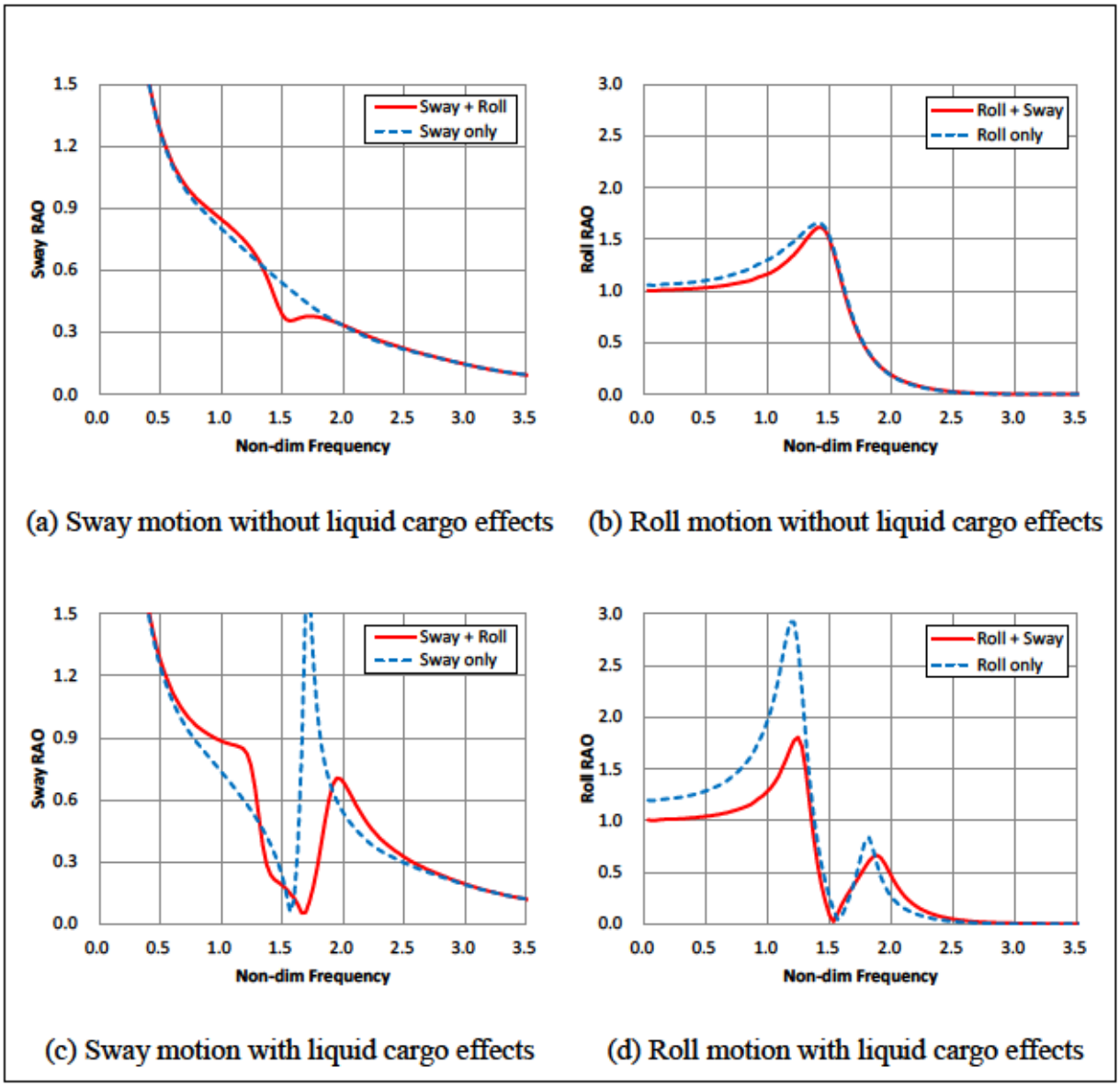

Figure A9.1. RAO of Sway and Roll motion for Barge Case 1

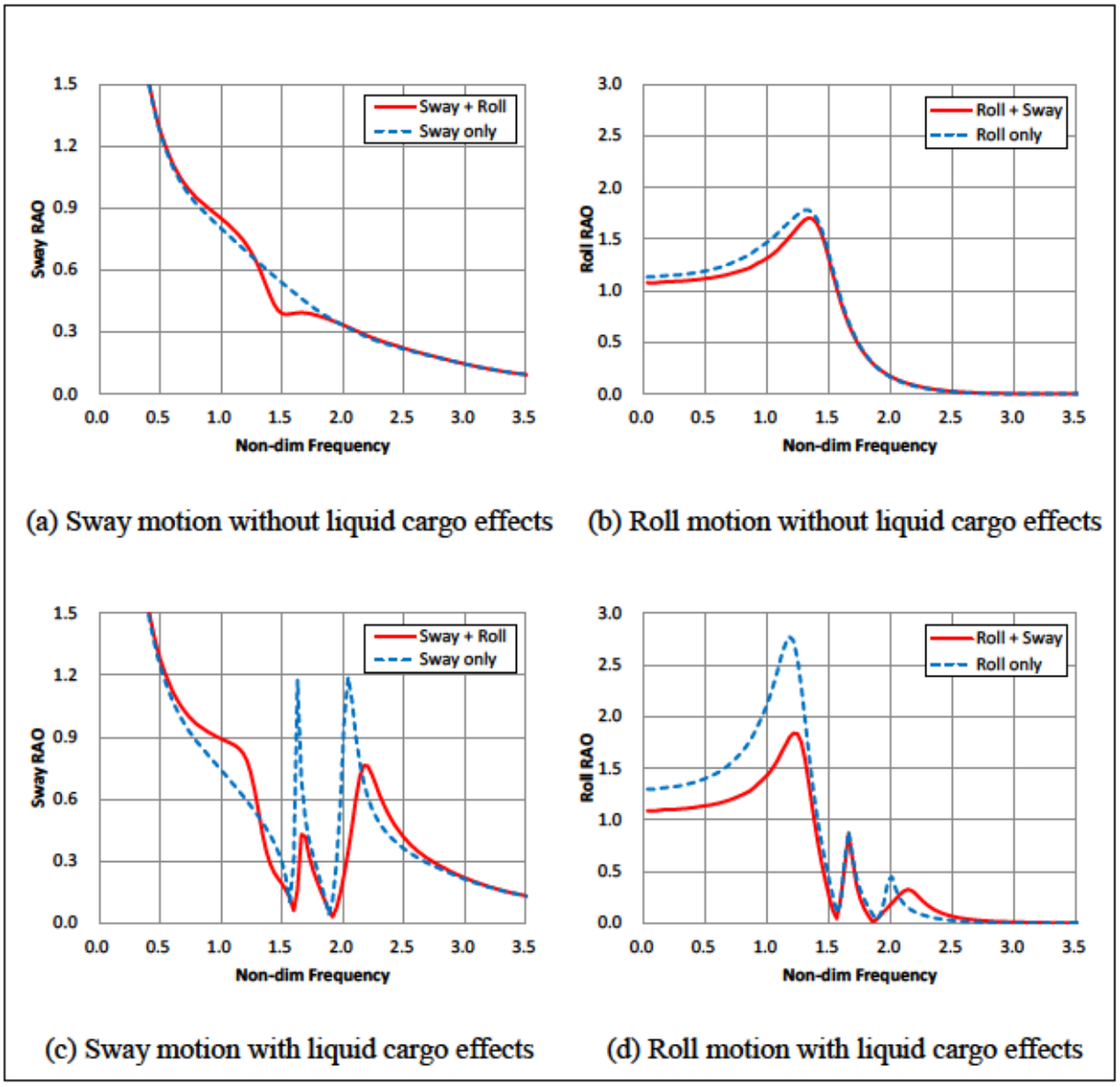

Figure A9.2. RAO of Sway and Roll motion for Barge Case 2

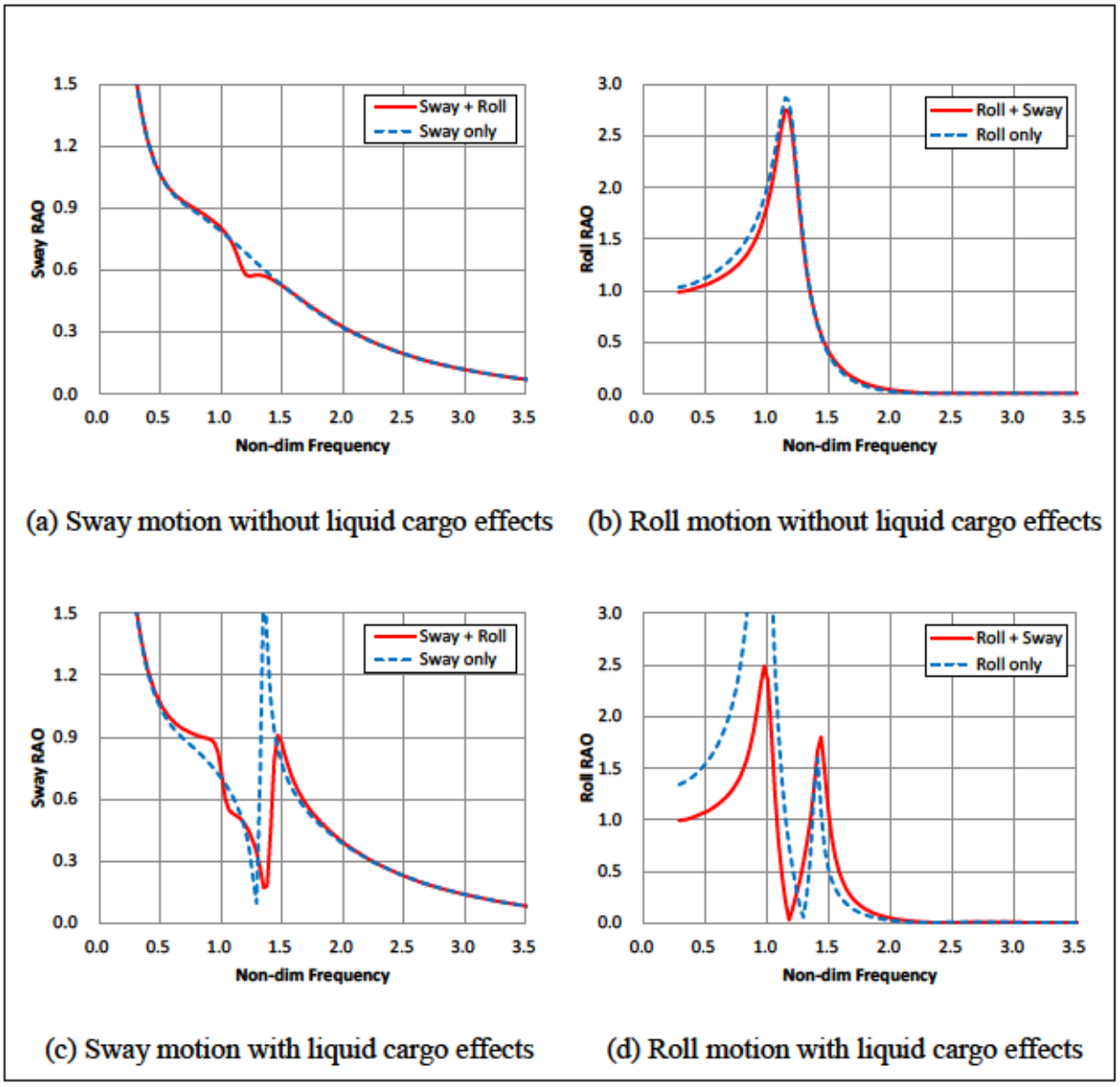

Figure A9.3. RAO of Sway and Roll motion for FLNG LC of 15%

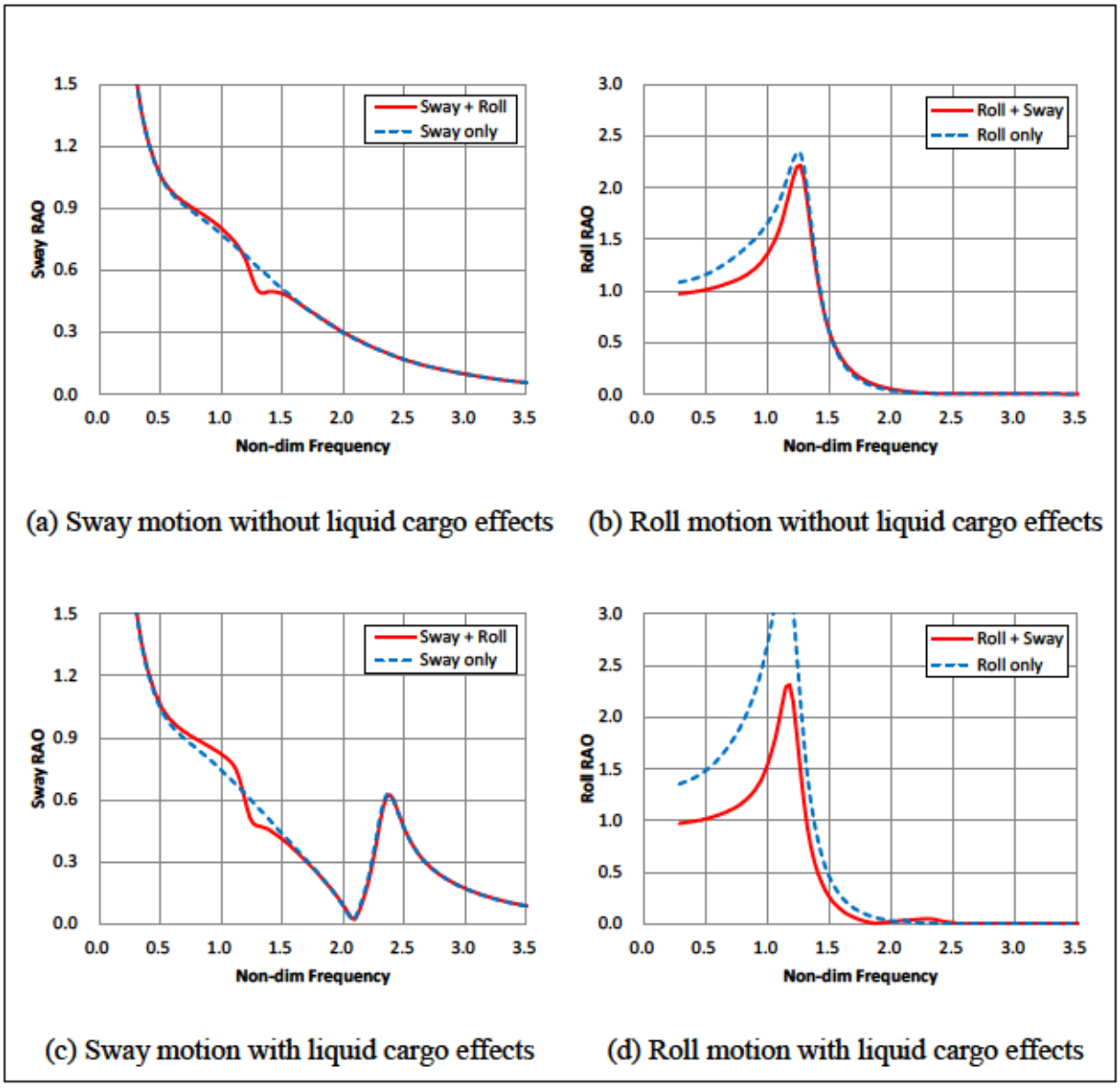

Figure A9.4. RAO of Sway and Roll motion for FLNG LC of 50%

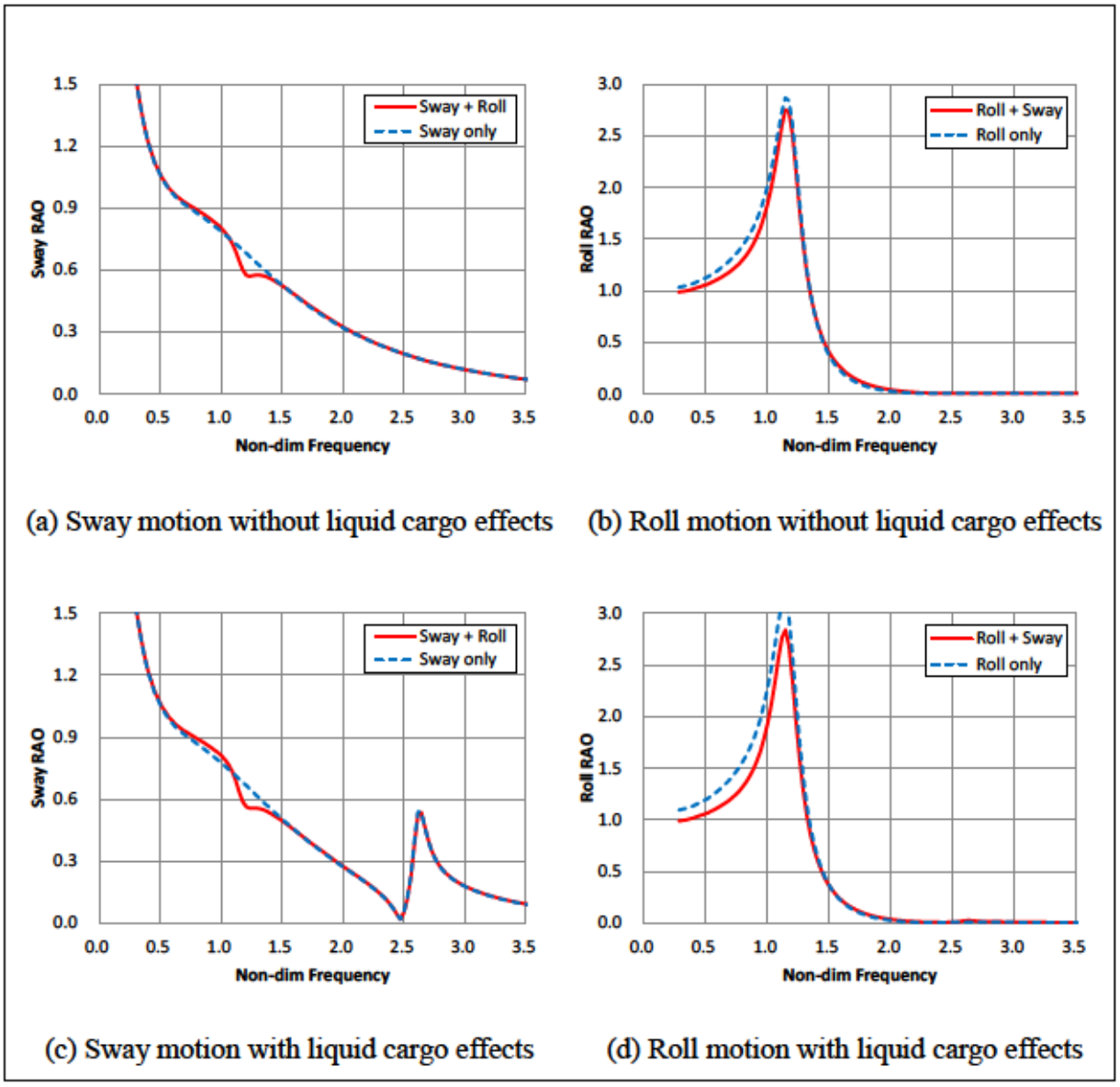

Figure A9.5. RAO of Sway and Roll motion for FLNG LC of 15% Double-row Case

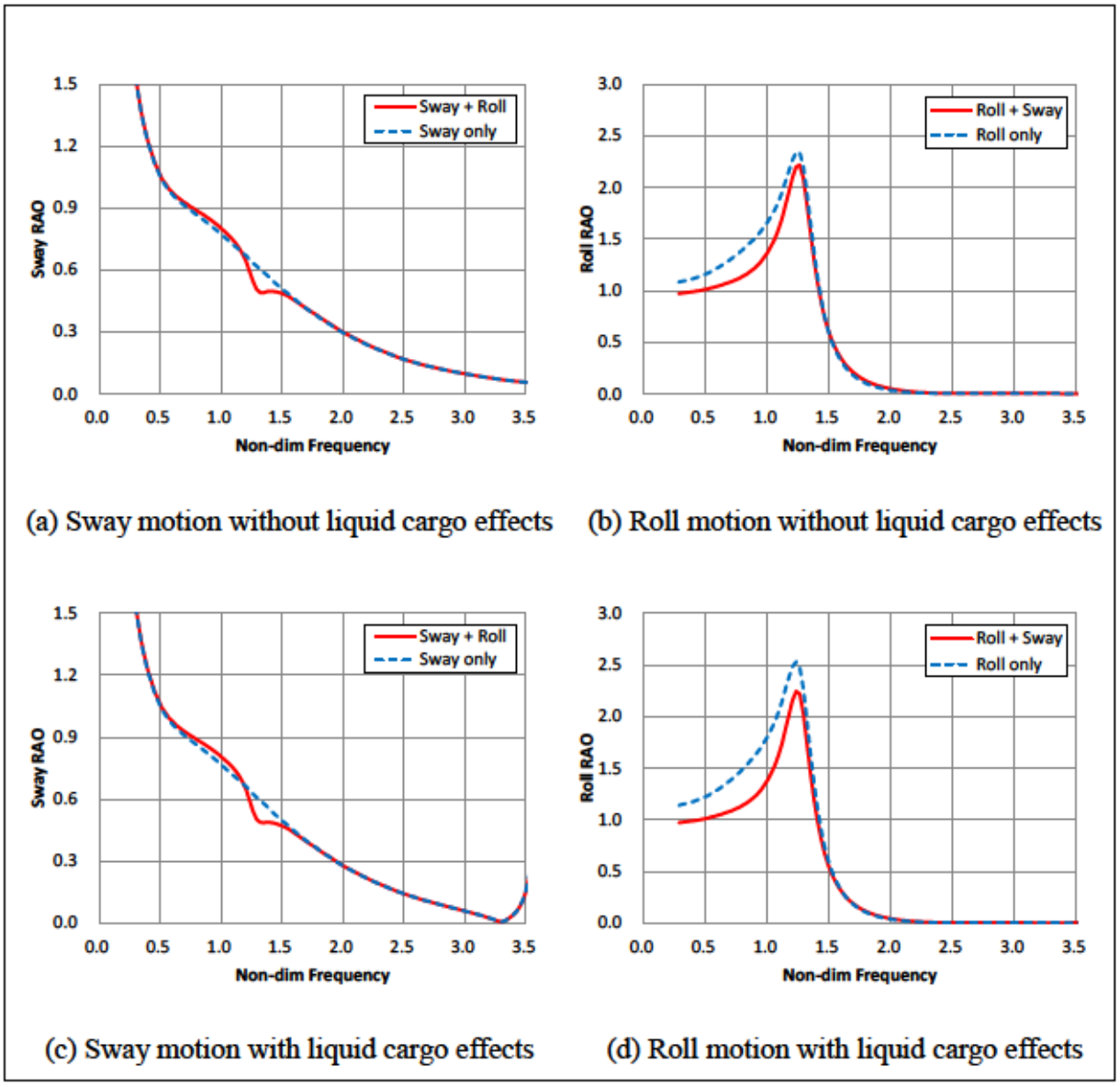

Figure A9.6. RAO of Sway and Roll motion for FLNG LC of 50% Double-row Case

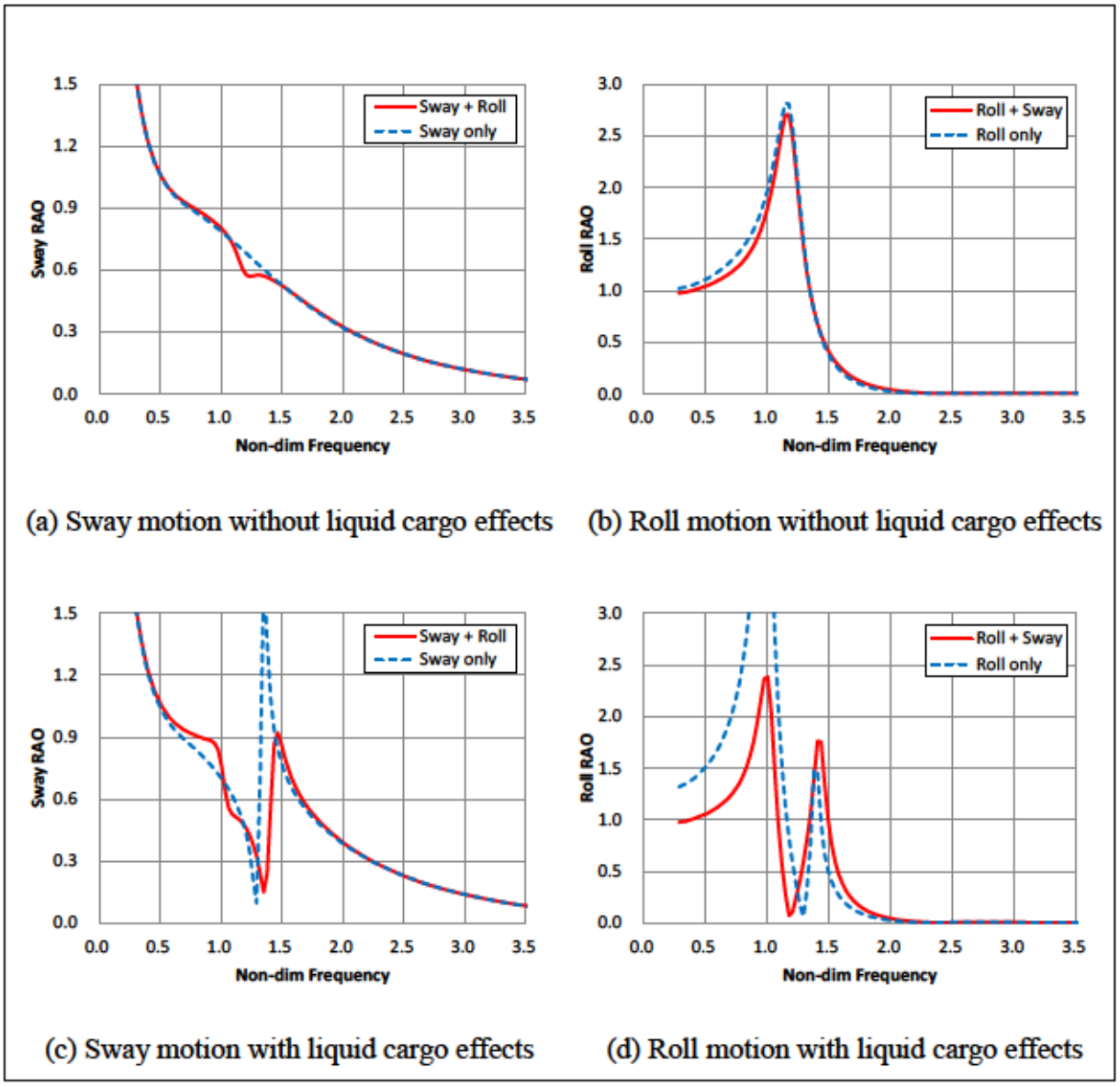

Figure A9.7. RAO of Sway and Roll motion for FLNG LC of 15% Lower Case

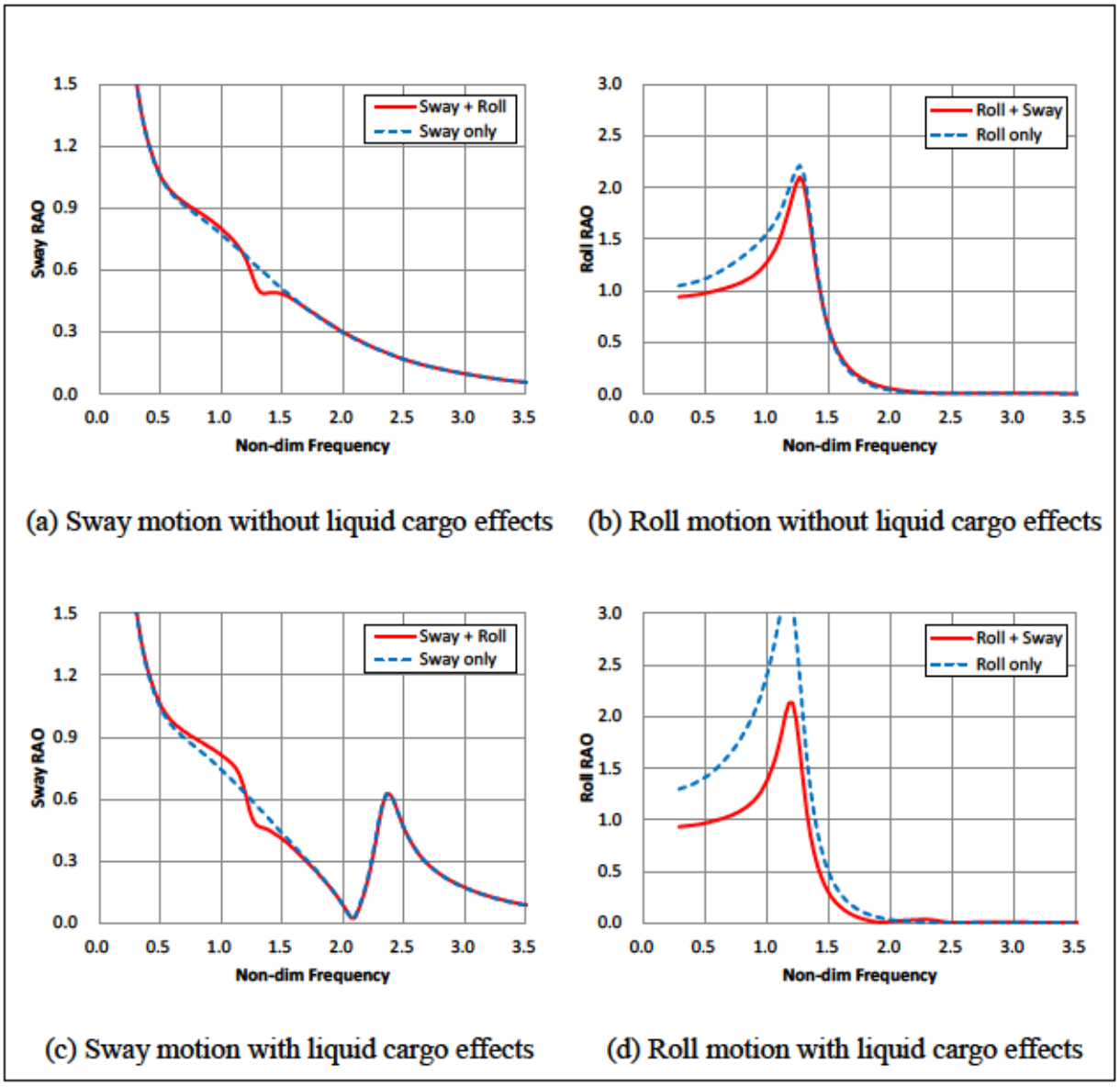

Figure A9.8. RAO of Sway and Roll motion for FLNG LC of 50% Lower Case

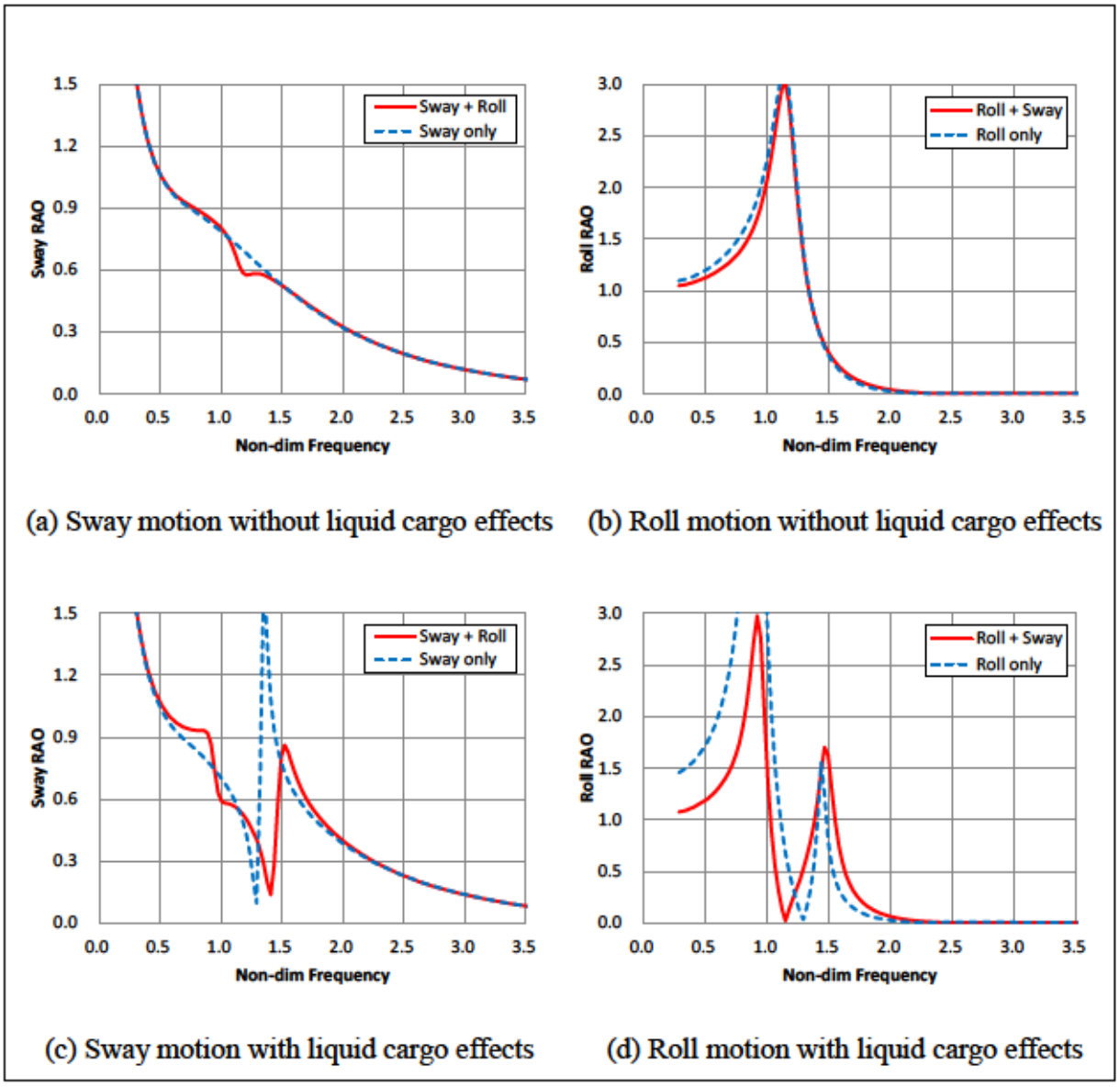

Figure A9.9. RAO of Sway and Roll motion for FLNG LC of 15% Higher Case

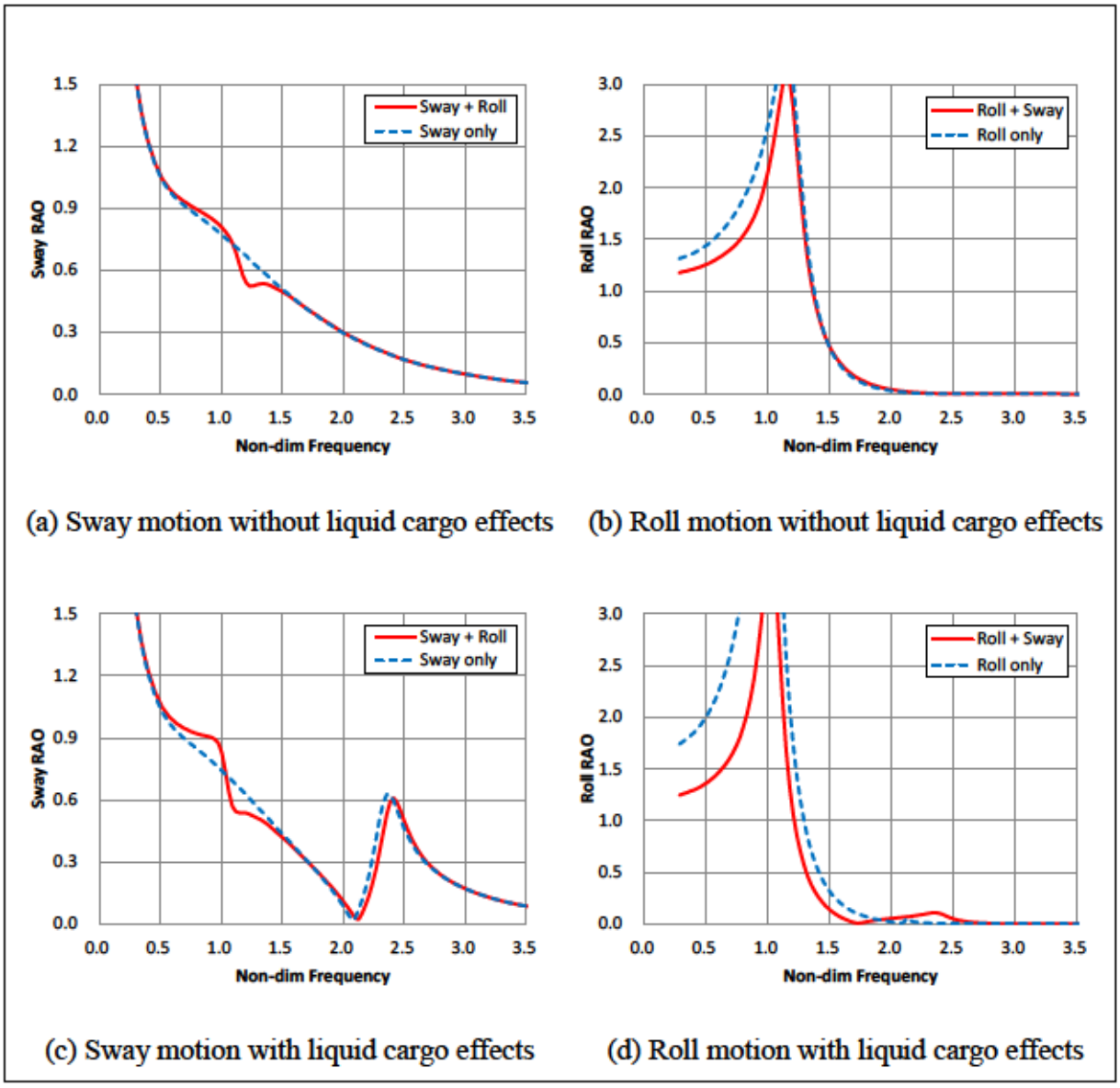

Figure A9.10. RAO of Sway and Roll motion for FLNG LC of 50% Higher Case

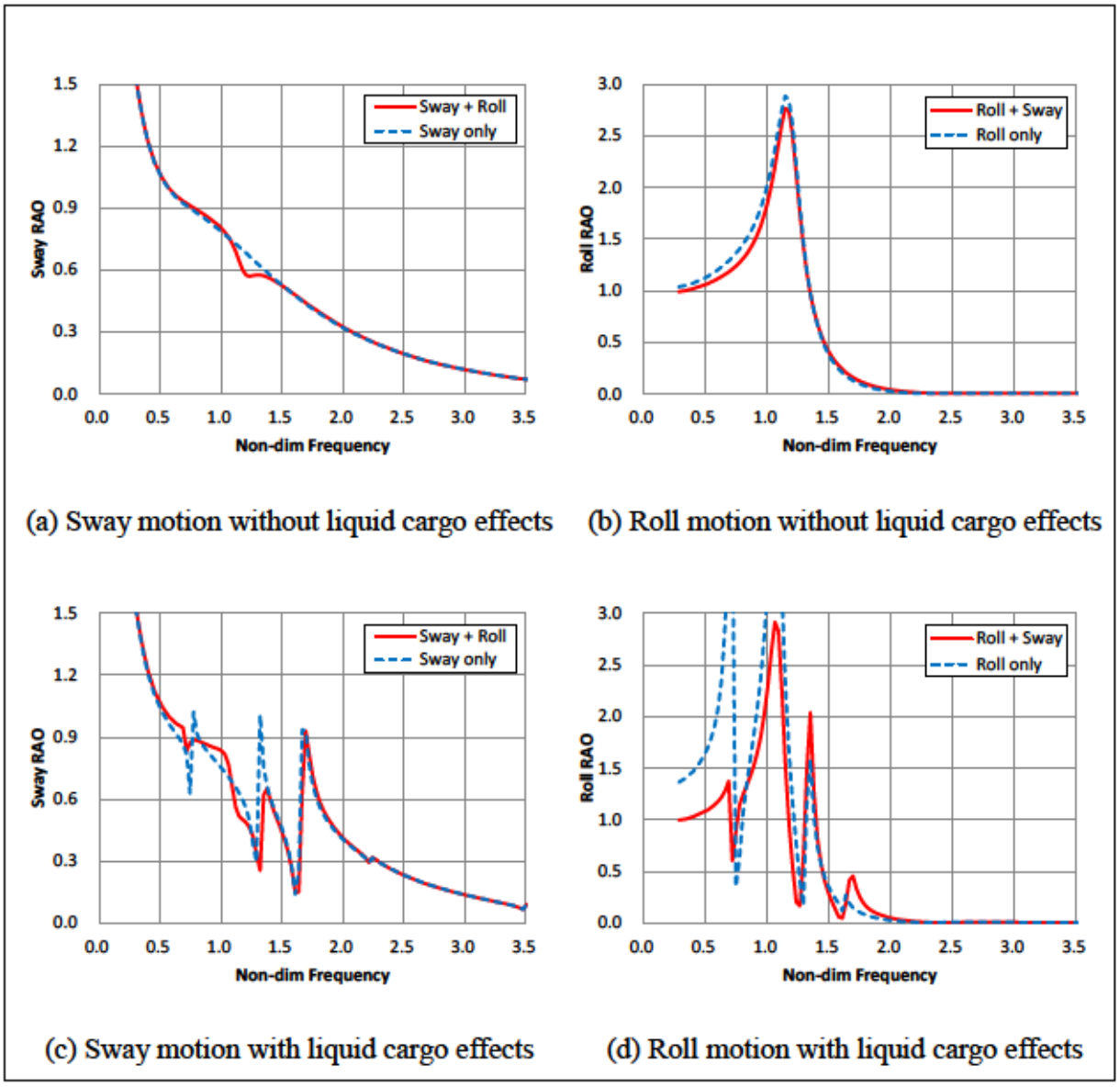

Figure A9.11. RAO of Sway and Roll motion for FLNG Draft 12.22 m Tank Operation Case 1

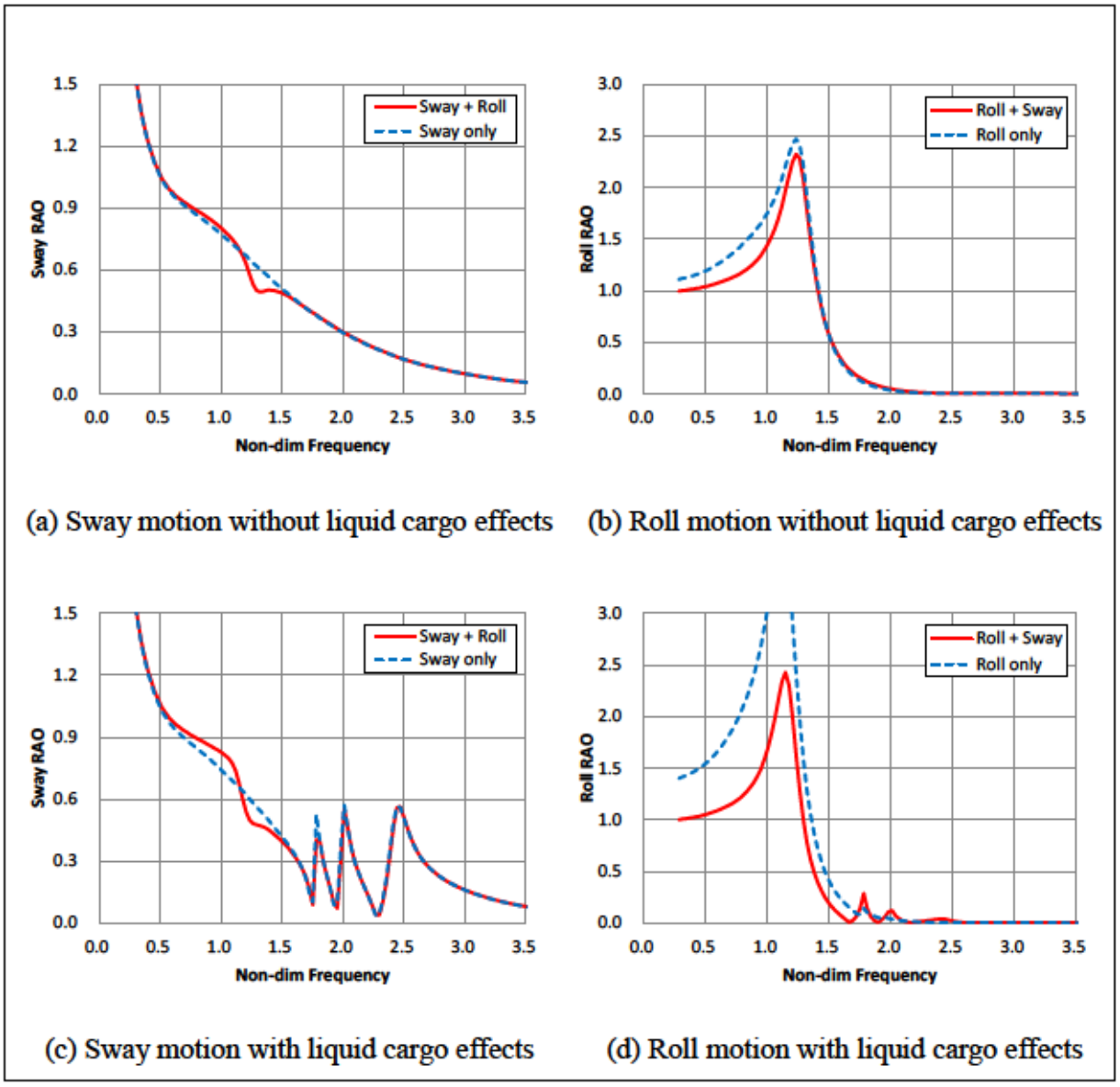

Figure A9.12. RAO of Sway and Roll motion for FLNG Draft 16.60 m Tank Operation Case 1

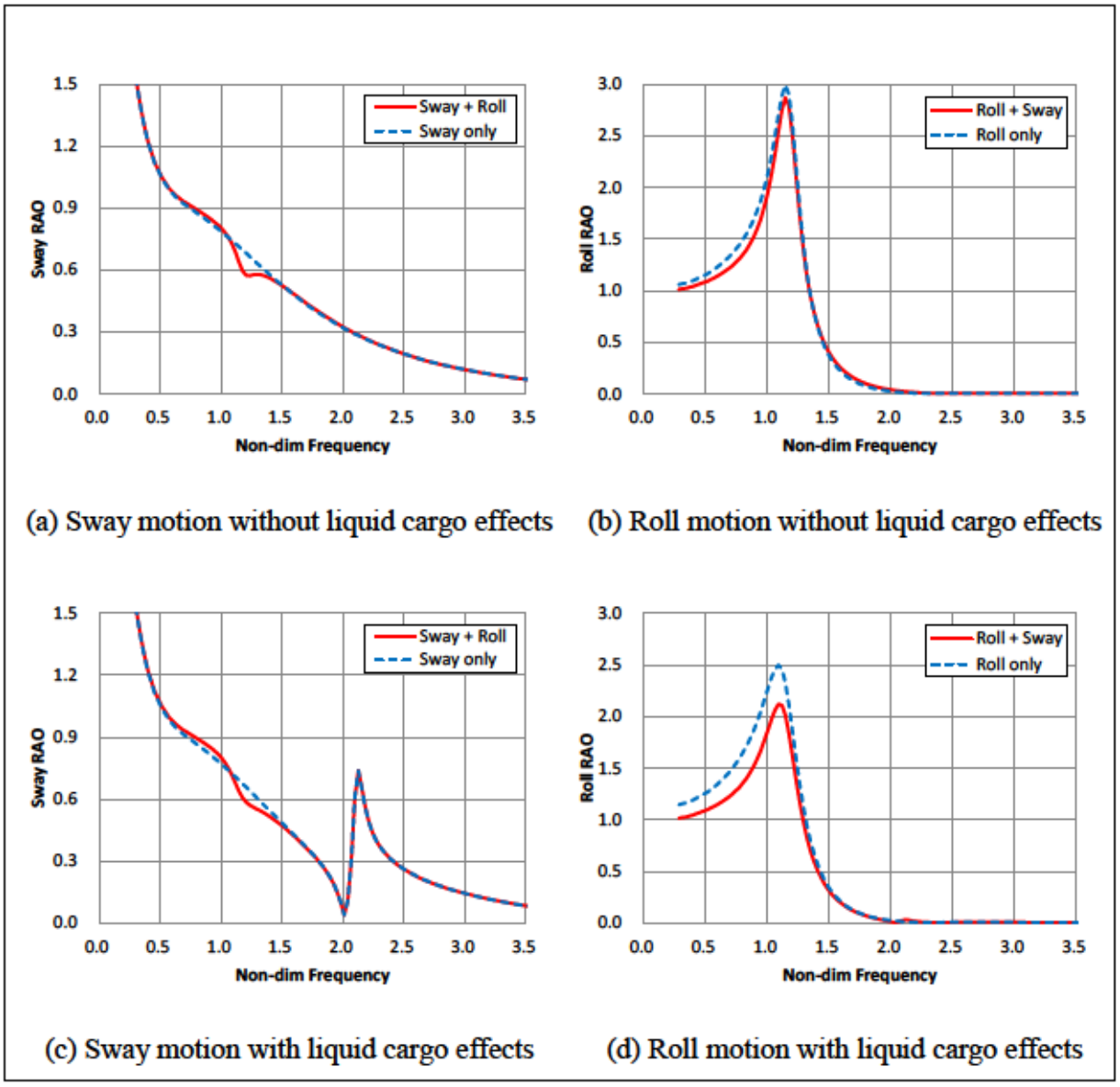

Figure A9.13. RAO of Sway and Roll motion for FLNG Draft 12.22 m Tank Operation Case 2

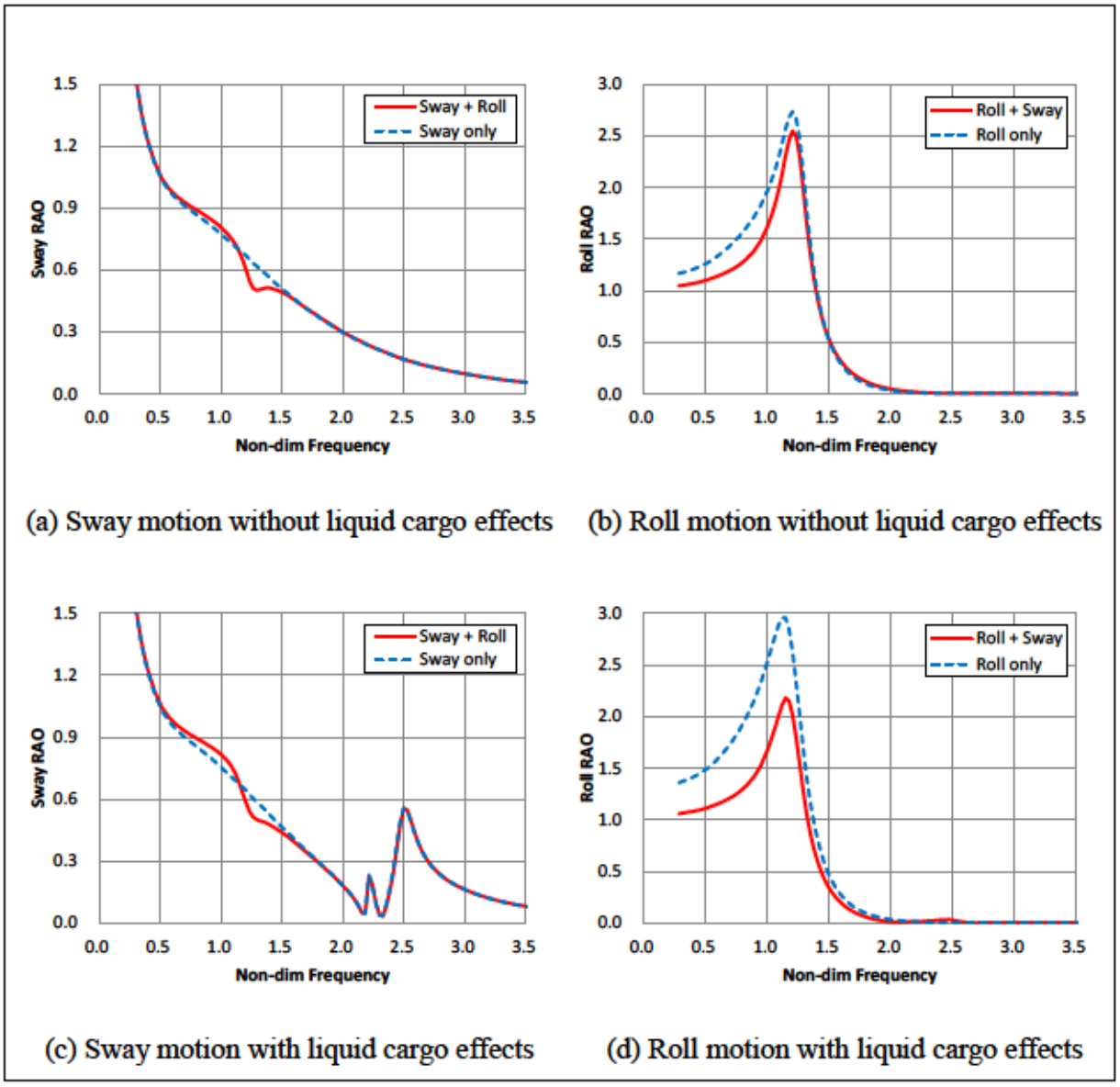

Figure A9.14. RAO of Sway and Roll motion for FLNG Draft 16.60 m Tank Operation Case 2